Driver Alertness Monitoring using Steering, Lane Keeping and Eye Tracking Data under Real Driving Conditions

Von der Fakultät Informatik, Elektrotechnik und Informationstechnik
der Universität Stuttgart
zur Erlangung der Würde eines Doktor-Ingenieurs (Dr.-Ing.)
genehmigte Abhandlung

vorgelegt von
Fabian Friedrichs
aus Ludwigsburg

Hauptberichter:	Prof. Dr.-Ing. Bin Yang
Mitberichter:	Prof. Dr.-Ing. Klaus Dietmayer
Tag der Einreichung:	14. Dezember 2018
Tag der mündlichen Prüfung:	26. Juni 2019

Institut für Signalverarbeitung und Systemtheorie
der Universität Stuttgart

2020

Contents

Abstract

Since humans operate trains, vehicles, aircrafts and industrial machinery, *fatigue* has always been one of the major causes of accidents. Experts assert that sleepiness is among the major causes of severe road accidents. In-vehicle fatigue detection has been a research topic since the early 80's. Most approaches are based on driving simulator studies, but do not properly work under real driving conditions.

The Mercedes-Benz ATTENTION ASSIST is the first highly sophisticated series equipment driver assistance system on the market that detects early signs of fatigue. Seven years of research and development with an unparalleled demand of resources were necessary for its series introduction in 2009 for passenger cars and 2012 for busses. The system analyzes the driving behavior and issues a warning to sleepy drivers. Essentially, this system extracts a single *measure* (so-called *feature*), the *steering event rate* by detecting a characteristic pattern in the steering wheel angle signal. This pattern is principally described by a steering pause followed by a sudden correction. Various challenges had to be tackled for the series-production readiness, such as handling individual driving styles and external influences from the road, traffic and weather. Fuzzy logic, driving style detection, road condition detection, change of driver detection, fixed-point parameter optimization and sensor surveillance were some of the side results from this thesis that were essential for the system's maturity.

Simply issuing warnings to sleepy drivers is faintly "experiencable" nor transparent. Thus, the next version 2.0 of the system was the introduction of the more vivid ATTENTION LEVEL, which is a permanently available bargraph monitoring the current driving performance. The algorithm is another result of this thesis and was introduced 2013 in the new S-Class.

Fatigue is very difficult to grasp since a ground truth reference does not exist. Thus, the presented findings about camera-based driver monitoring are included as fatigue reference for algorithm training. Concurrently, the presented results build the basis for eye-monitoring cameras of the future generation of such systems. The driver monitoring camera will also play a key role in "automated driving" since it is necessary to know if the driver looks to the road while the vehicle is driving and if he is alert enough to take back control over the vehicle in complex situations. All these improvements represent major steps towards the paradigm of *crash free driving*.

In order to develop and improve the ATTENTION ASSIST, the central goal of the present work was the development of pattern detection and classification algorithms to detect fatigue from driving sensors. One major approach to achieve a sufficiently high detection rate while maintaining the false alarm rate at a minimum was the incorporation of further patterns with sleepiness-associative ability. Features reported in literature were assessed as well as improved extraction techniques. Various new features were proposed for their applicability under real-road conditions. The mentioned steering pattern detection is the most important feature and was further optimized.

Essential series sensor signals, available in most today's vehicles were considered, such as steering wheel angle, lateral and longitudinal acceleration, yaw rate, wheel rotation rate, acceleration pedal, wheel suspension level, and vehicle operation. Another focus was on the

lateral control using camera-based lane data. Under real driving conditions, the effects of sleepiness on the driving performance are very small and severely obscured by external influences such as road condition, curvature, cross-wind, vehicle speed, traffic, steering parameters etc. Furthermore, drivers also have very different individual driving styles. Short-term distraction from vehicle operation also has a big impact on the driving behavior. Proposals are given on how to incorporate such factors. Since lane features require an optional tracking camera, a proposal is made on how to estimate some lane deviation features from only inertial sensory by means of an extended Kalman filter. Every feature is related to a number of parameters and implementation details. A highly accelerated method for parameter optimization of the large amount of data is presented and applied to the most promising features.

The alpha-spindle rate from the Electroencephalogram (EEG) and Electrooculogram (EOG) were assessed for their performance under real driving conditions. In contrast to the majority of results in literature, EEG was not observed to contribute any useful information to the fatigue reference (except for two drives with microsleeps). Generally, the subjective self-assessments according to the Karolinska Sleepiness Scale and a three level warning acceptance question were consequently used. Various correlation measures and statistical test were used to assess the correlation of features with the reference.

This thesis is based on a database with over 27,000 drives that accumulate to over 1.5 mio km of real-road drives. In addition, various supervised real-road driving studies were conducted that involve advanced fatigue levels.

The fusion of features is performed by different classifiers like Artificial Neural Networks (ANN) and Support Vector Machines (SVM).

Fair classification results are achieved with ANN and SVM using cross-validation. A selection of the most potential and independent features is given based on automatic SFFS feature selection. Classical machine learning methods are used in order to yield maximal system transparency and since the algorithms are targeted to run in present control units. The potential of using end-to-end deep learning algorithms is discussed. Whereas its application to CAN-signals is problematic, there is a high potential for driver-camera based approaches. Finally, features were implemented in a real-time demonstrator using an own CAN-interface framework.

While various findings are already rolled out in ATTENTION ASSIST 1.0, 2.0 and ATTENTION LEVEL, it was shown that further improvements are possible by incorporating a selection of steering- and lane-based features and sophisticated classifiers. The problem can only be solved on a system level considering all topics discussed in this thesis. After decades of research, it must be recognized that the limitations of indirect methods have been reached. Especially in view of emerging automated driving, direct methods like eye-tracking must be considered and have shown the greatest potential.

Zusammenfassung

Seit der Bedienung von Fahrzeugen, Zügen, Flugzeugen und industriellen Maschinen durch Menschen stellt *Müdigkeit* eine der Hauptursachen für Unfälle dar. Experten versichern, dass Müdigkeit eine der Hauptursachen für schwere Verkehrsunfälle ist. Seit den 80er Jahren ist Müdigkeit am Steuer ein Forschungsthema. Die meisten Ansätze basieren auf Fahrsimulatorstudien, die unter realen Fahrbedingungen jedoch nicht funktionieren.

Der Mercedes-Benz ATTENTION ASSIST ist das erste und fortschrittlichste Seriensystem auf dem Markt, das frühe Anzeichen von Müdigkeit zuverlässig erkennt. Sieben Jahre Forschung und Entwicklung sowie ein beispielloser Bedarf an Ressourcen waren für die Serieneinführung 2009 im PKW und 2012 im Reisebus notwendig. Das System analysiert das Fahrverhalten und warnt müde Fahrer. Im Wesentlichen extrahiert das System ein Maß (sog. *Merkmal*) für die Häufigkeit von Lenkereignissen indem charakteristische Muster im Lenkwinkelsignal detektiert werden. Die Muster können vereinfacht durch eine Lenkpause gefolgt von einer plötzlichen Lenkkorrektur beschrieben werden. Für die Serienreife mussten vielerlei Hürden überwunden werden, wie beispielsweise der Umgang mit fahrerindividuellen Fahrstilen, Umwelteinflüssen von der Straße, Verkehr und Wetter. Fuzzy-Logik, Fahrstilerkennung, Straßenzustandserkennung, Fahrerwechsel, Festkomma - Parameteroptimierung und Sensorüberwachung waren einige der Ergebnisse aus dieser Dissertation, die für den Reifegrad des Systems essenziell waren.

Die schlichte Ausgabe eine Warnung ist weder sehr erlebbar noch transparent. Daher wurde in der Folgeversion 2.0 des Systems das dynamischere ATTENTION LEVEL eingeführt, das eine permanent verfügbare Balkenanzeige anzeigt, die der aktuell ermittelten Fahrtüchtigkeit entspricht. Der Algorithmus ist ein weiteres Ergebnis dieser Arbeit und wurde 2013 in der neuen W222 S-Klasse eingeführt.

Müdigkeit ist sehr schwer zu greifen, da als Referenz keine "absolute Wahrheit" existiert. Aus diesem Grund wurden die hier vorgestellten Ergebnisse der auf Fahrerkameradaten basierenden Fahrerzustandsbeobachtung als Müdigkeitsreferenz zum Training der Algorithmen mitverwendet. Gleichzeitig bilden die Ergebnisse die Basis für die Fahrerkamera in der zukünftigen Generation des Systems. Die Fahrerkamera wird auch eine wichtige Rolle beim "hochautomatisierten Fahren" spielen, da es notwendig ist zu wissen ob der Fahrer während der Fahrt auf die Straße schaut und ob er in komplexen Situationen aufmerksam genug ist, um die Kontrolle zu übernehmen. Alle diese Verbesserungen repräsentieren einen wesentlichen Schritt in Richtung der Vision vom *unfallfreien Fahren*.

Um den ATTENTION ASSIST zu entwickeln und zu verbessern bestand das zentrale Ziel der hier vorgestellten Arbeit in der Entwicklung von Mustererkennungs- und Klassifikationsalgorithmen die Müdigkeit anhand von Fahrzeugsensoren erkennen. Ein wesentlicher Ansatz um eine genügend hohe Erkennungsrate zu erreichen und dabei die Falschalarmraten minimal zu halten war der Einbezug von weiteren Mustern mit müdigkeitsbezogenen Eigenschaften. Merkmale aus der Literatur wurden untersucht ebenso wie verbesserte Extraktionsmethoden. Zahlreiche neue Merkmale wurden für den Einsatz unter realen Fahrbedingungen vorgeschlagen. Das oben genannte Lenkmuster ist das wichtigste Merkmal und wurde weiter optimiert.

Die wichtigsten Signale der Seriensensorik, die heute in den meisten Fahrzeugen verfügbar sind wurden verwendet, wie zum Beispiel Lenkwinkelsensor, Quer- und Längsbeschleunigung, Gierrate, Raddrehzahl, Gaspedalweg, Fahrwerkfederwege und Fahrzeugbedienung. Ein weiterer Fokus bestand in der Querregelung unter Verwendung von kamerabasierten Spurdaten. Unter realen Fahrbedingungen sind die Einflüsse von Müdigkeit auf das Fahrvermögen sehr klein und stark durch externe Einflüsse überlagert, wie beispielsweise Straßenzustand, Kurvigkeit, Seitenwind, Geschwindigkeit, Verkehr, Lenkungsparameter usw. Weiterhin unterscheiden sich Fahrer durch sehr individuelle Fahrstile. Kurzzeitige Ablenkung durch Fahrzeugbedienhandlungen haben ebenso einen starken Einfluss auf das Fahrverhalten. Es werden Vorschläge gemacht um diese Faktoren mit zu berücksichtigen. Da Spurmerkmale eine Kamera benötigen die nur als Sonderausstattung erhältlich ist, wird ein Vorschlag gemacht wie einige der Spurmerkmale mittels Inertialsensorik und einem erweiterten Kalman Filter geschätzt werden können. Jedes Merkmal ist mit einer Vielzahl von Parametern und Implementierungsdetails verknüpft. Eine beschleunigte Methode zur Parameteroptimierung zur Bewältigung der riesigen Datenmenge wird vorgestellt und für die vielversprechendsten Merkmale angewendet.

Die Alpha-Spindelrate aus dem Elektroenzephalogramm (EEG) und Elektrookulogramm (EOG) wurden hinsichtlich ihrer Eignung als Referenz unter realen Fahrbedingungen bewertet. Ausgenommen von wenigen Ausnahmen, konnte im Gegensatz zu den Ergebnissen in der Literatur nicht beobachtet werden, dass EEG einen wertvollen Beitrag als Müdigkeitsreferenz liefert. Die subjektive Selbsteinschätzung nach der Karolinska Müdigkeitsskala und einer dreistufigen Warnungsakzeptanzfrage wurde daher durchgängig als Referenz verwendet. Verschiedene Korrelationsmaße und statistische Test wurden herangezogen um die Korrelation von Merkmalen mit der Referenz zu bewerten.

Diese Dissertation basiert auf einer Datenbank mit über 27.000 Fahrten deren Fahrleistung über 1.5 mio km reale Fahrdaten umfasst. Zusätzlich wurden überwachte Fahrversuche mit fortgeschrittenen Müdigkeitsstadien durchgeführt.

Brauchbare Klassifikationsergebnisse werden mit künstlichen neuronalen Netzwerken (ANN) und Support Vektor Machines (SVM) und Kreuzvalidierung erreicht. Eine Auswahl der unabhängigsten Merkmale mit dem höchsten Potential wird vorgestellt, basierend auf automatischer Merkmalselektion mittels SFFS. Es werden Mathoden aus dem klassischen maschinellen Lernen verwendet, um maximale Transparenz über das System zu erhalten und weil die Algorithmen in aktuellen Steuergeräten eingesetzt werden. Abschließend wurden diese Merkmale in einem Echtzeitsystem mit einem eigenen CAN-Interface implementiert. Der Einsatz von end-to-end deep learning wird dirkutiert. Während die Anwendung auf CAN-Signale problematisch ist, gibt es ein hohes Potential bei Fahrerkamera-basierten Ansätzen.

Während viele der Erkenntnisse bereits in ATTENTION ASSIST 1.0, 2.0 und ATTENTION LEVEL eingeflossen sind, wurde gezeigt, dass weitere Verbesserung durch Einbezug einer Auswahl von Lenkwinkel- und Spurbasierten Merkmalen und Klassifikatoren erzielt werden kann. Das Problem kann nur auf der Systemebene gelöst werden indem alle in dieser Dissertation angesprochenen Themen berücksichtigt werden. Nach Jahrzehnten der Forschung muss akzeptiert werden, dass die Grenzen der indirekten Methoden erreicht sind. Insbesondere in Betracht auf automatisiertes Fahren sind direkte Methoden wie Lidschlagerkennung notwendig und zeigen das höchste Potential.

Acknowledgement

This work was partially conducted at the *University of Stuttgart* at the *Institute of Signal Processing and System Theory* under the supervision of Professor Dr.-Ing. Bin Yang. First and foremost, I would like to express my gratitude for his scientific supervision in assistance and guidance, his advices, feedback, inspiration and especially his outstanding support in reviewing papers and preparing conferences. I also would like to thank Professor Dr.-Ing. Klaus Dietmayer from the *University of Ulm* for taking over the assessment of this thesis.

This project was also conducted at the *Daimler AG* R&D facility in Sindelfingen, where I got access to vehicles, resources and an unparalleled amount of data. I'm grateful for the experience, trust and involvement in the algorithm development for the series introduction of the ATTENTION ASSIST. In the Active Safety department, I gratefully acknowledge the support of Dr. Jörg Breuer, Dr. Uwe Petersen and Dr. Werner Bernzen for their confidence in me to start this project. Similarly, my thanks go to Dr. Michael Wagner, Elisabeth Hentschel, Dr. Frauke Driewer, Dr. Doris Schmidt, and the entire project team for the extensive scientific exchange and the pleasant atmosphere. Again, I would like to thank Dr. Breuer to create a trainee position during the 2010 crisis that also allowed me continued access to project resources. My special thanks go to Reinhold Schneckenburger for the exchange about external influences and the algorithm core functionality. Furthermore, I would like to thank Wiebke Müller, Istvan Bognar, Jens Meyn, Erik Rechtlich and Björn Westphal for organizing the test drives and the support on vehicle software updates, measurement equipment, CAN interface, data conversions, and evaluations of the measurements.

My thanks also go to all my former students who worked with me and under my supervision. I greatly value their tremendous effort, especially Christiane Gärtner, Alexander Fürsich and Özgür Akin who now became colleagues. The working atmosphere made the countless night experiments less straining and I am grateful for the ten excursion drives to Papenburg, Idiada (Spain) and Arjeplog (Sweden). These are the situations in which reliable and pleasant colleagues are priceless. I thank the countless test subjects for their participation in the extremely exhausting simulator and night experiments.

Especially, I thank my successors Peter Hermanndstädter, Parisa Ebrahim and co-doctorate students Michael Miksch, Michael Simon, Andreas Sonnleitner, and Eike Schmidt for the countless discussions, the cooperation and the scientific exchange on EEG. I thank Dr. Klaus-Peter Kuhn, Dr. Wolfgang Stolzmann and Andreas Pröttel from research.

I would like to thank my parents for letting me use their empty flat as office during months of vacations and over-hours. Most of all, I thank my son Milo for the indescribable joy, happiness and energy he gives me. At the same time I would like to express my deep regret for the trouble I've caused everyone around me with this journey.

List of Tables

List of Figures

Symbols and Abbreviations

Notation

x	Scalar
$\mathbf{x}$	Vector
$\underline{\tau}$	Parameter
A	Matrix
I	Identity matrix
$\hat{x}$	Estimate
C	Set of numbers
$\mathbb{R}, \mathbb{N}, \mathbb{Z}$	Set of real, natural, integer numbers

Mathematic Operations

x^*	Complex conjugated
$\equiv$	"Is defined by" (also congruency, equivalent, identity)
$\sim$	"Is distributed as"
$\lvert\mathbf{x}\rvert$	Magnitude
$\lvert X\rvert$	Determinant of matrix X
$\lVert\mathbf{x}\rVert$	Euclidean norm
$\bar{\mathbf{x}}$	Arithmetic mean
$\mathrm{sat}_l^u(x)$	Saturation of x to the minimum l and maximum u, i.e. $\max(l, \min(x, u))$
$\lceil x \rceil$	Ceiling operation (round up)
$\lfloor x \rfloor$	Floor operation (truncate x after radix point)
$\vee, \wedge$	Logical OR, AND boolean conjunction (bitwise)
X^{-1}	Inverse of matrix X
X^T	Transpose of matrix X
X^+	Pseudo-inverse of matrix X

Symbols and Special Functions

$\mathcal{F}_i$	Feature i in feature matrix F
$\mathcal{M}_i$	Measure i with $\mathcal{M}_i \in \{F, \mathrm{KSS}\}$
$\mathcal{O}(\cdot)$	Landau-symbol or Big-O Notation for computational complexity estimation
$\mathrm{P}(\cdot)$	Probability of an event
$\mathcal{N}(\boldsymbol{\mu}, Q)$	Normal distribution with mean $\boldsymbol{\mu}$ and covariance matrix Q

$\mathcal{B}(n,\pi)$	Binomial distribution with n trials and success probability $\pi \in [0,1]$ in each trial
$\mathcal{U}(a,b)$	Uniform distribution from a to b
$\arg\min_a(C(x))$	Element a of $x \in C$ for which C is minimum
$\arg\max_a(C(x))$	Element a of $x \in C$ for which C is maximum
$\mathrm{mod}(a,b)$	Modulo-operator that returns the remainder of the division a/b (i.e. $\lfloor \frac{a}{b} \rfloor$)
$\mathrm{sign}(\cdot)$	Sign-operator: $\mathrm{sign}(x) = \frac{x}{\lvert x \rvert}$
$\mathrm{E}(\cdot)$	Expected or mean value of a random variable or signal
$\mathrm{Var}(\cdot)$	Variance of a random variable or signal
$\mathrm{Std}(\cdot)$	Standard deviation of a random variable or signal
$\mathrm{Cov}(\mathbf{x},\mathbf{y})$	Covariance of the vectors $\mathbf{x}$ and $\mathbf{y}$
$\Sigma(\mathbf{X})$	Covariance matrix of row vectors in matrix X
$\mathrm{MSE}(\mathbf{x},\mathbf{y})$	Mean squared error between two vectors $\mathbf{x}$ and $\mathbf{y}$
$\mathrm{IQR}(\cdot)$	Interquartile range of a signal
$\mathrm{FD}(\mathbf{x},\mathbf{y})$	Fisher distance between two measures $\mathbf{x}$ and $\mathbf{y}$
$\mathrm{MDA}(\cdot)$	Multiple dimension analysis Fischer metric between measures
$\mathrm{MA}(\cdot)$	Moving Average
$\mathrm{EWVAR}_N(\cdot)$	Exponentially weighted moving variance filter applied to signal for window size N
$\mathrm{EWMA}_N(\cdot)$	Exponentially weighted moving average filter applied to signal for window size N
$\mathrm{EwmaN}_N(\cdot)$	Exponentially weighted moving average filter applied to the last N non-zero events
$\mathrm{FIR}_b(\cdot)$	non-recursive finite impulse response filter application to a signal with coefficients b
$\mathrm{IIR}_{a,b}(\cdot)$	recursive infinite impulse response filter application to a signal with coefficients b, and recursive coefficients a
NaN	Not any Number (NaN)

Vehicle Parameters

d_{whl}	Wheel circumference $[m]$
l	Wheel base $[m]$
SR	Steering ratio $[-]$
SG	Self-steering gradient $[-]$
v_{ch}	Characteristic lower velocity $[m/s]$

Vehicle Dynamics and Sensors

$\psi, \dot{\psi}, \ddot{\psi}$	Yaw angle $[°]$, yaw rate $[°/s]$ and yaw acceleration $[°/s^2]$
CG	Center of gravity of the vehicle
ICR	Instant center of rotation
x_{veh}, y_{veh}	Longitudinal and lateral coordinate origin of vehicle $[m]$
$n_{FL/\,FR/\,RL/\,RR}$	Wheel rotation rate sensor (Front/Rear, Left/Right) $[1/s]$
v_{veh}	Vehicle longitudinal speed from wheel rotation rate sensors n $[m/s]$
$a_{x,whl}$	Longitudinal acceleration from wheel rotation rate sensors n $[m/s^2]$
$a_{x,SC}$	Longitudinal acceleration from accelerometer in sensor cluster $[m/s^2]$
$a_{y,SC}$	Lateral acceleration from accelerometer in sensor cluster $[m/s^2]$
$a_{y,stw}$	Lateral acceleration from the single-track model (cf. Sec. 6.3) $[m/s^2]$
$a_{y,stw,subj}$	Subjective perceived lateral acceleration from $a_{y,stw}$ and v_{veh} $[m/s^2]$
δ_A	Ackerman steering angle $\delta_A = \delta_S \cdot SR$ $[°]$
δ_S	Steering wheel angle $[°]$
$\dot{\delta}_S$	Steering wheel angle velocity (differentiated by DISPOfilter) $[°/s]$
y_L	Lateral lane position $[m]$
R	Curve radius $(1/\kappa)$ $[m]$
κ	Curvature $(1/R)$ $[1/m]$
J_z	Vehicles inertia torque $[kg\,m^2]$
β	Sideslip angle $[°]$

Kalman Filter and Extended Kalman Filter (EKF)

$\mathbf{A}$	State transition matrix $(n \times n)$
$\mathbf{B}$	Control input transition matrix $(n \times o)$
$\mathbf{P}$	Covariance of the state vector estimate
$\mathbf{H}$	Measurement transition matrix $(m \times n)$
$\mathbf{Q}$	Process noise covariance
$\mathbf{R}$	Measurement noise covariance
$\mathbf{x}(k)$	State vector at instant k
$\mathbf{m}(k)$	Measurement vector at instant k
$\mathbf{z}(k)$	Initial states at instant k
$\mathbf{w}(k)$	Model/process noise with covariance matrix $\mathbf{W}$
$\mathbf{v}(k)$	Measurement noise with covariance matrix $\mathbf{V}$
$\mathbf{J}(\mathbf{f})$	Jacobi matrix of function $\mathbf{f}$
δ_{nk}	Dirac delta distribution (or "impulse") $\begin{cases} 1 & \text{if } n = k \\ 0 & \text{otherwise} \end{cases}$

General

T_s, F_s	Cycle time $\frac{1}{F_s}$ [s] and cycle frequency $\frac{1}{T_s}$ [Hz]
$F_{s,f}$	Sampling rate of features (0.5 Hz) [Hz]
λ_μ	Forgetting factor of exponentially weighted moving average EWMA [–]
λ_{σ^2}	Forgetting factor of exponentially weighted moving variance EWVAR [–]
N_μ	Window size of exponentially weighted moving average EWMA [–]
N_{σ^2}	Window size of exponentially weighted moving variance EWVAR [–]
ρ_S, ρ_P	Spearman and Pearson correlation coefficient [–]
β_i	Regression coefficients in regression analysis [–]
ε	Residual error [–]

Eye-tracking and EYE Features

$e_{l,r}$	Eye closure left/right [%]
x, y, z	3D head position [m]
φ, ψ, γ	3D head rotation [m]
$c_{l,r}$	Confidence of eye signals left/right [%]
c_h	Confidence of 3D head signals [%]
τ	GPS time [s]
λ	GPS longitude [°]
θ	GPS latitude [°]
v_{GPS}	GPS vehicle speed [m/s]

Abbreviations

ABS ..... Anti-lock Braking System
ACC ..... Adaptive Cruise Control
ADAS ..... Advanced Driver Assistance System
ADC ..... Analog Digital Converter
AD ..... Aftermarket Device
ALDW ..... Advanced Lane Departure Warning
ALSTM-FCN . Attention Long Short Term Memory Fully Convolutional Network
ALU ..... Arithmetic Logic Unit
ANN ..... Artificial Neural Network
ASIC ..... Application-Specific Integrated Circuit
CAN ..... Controller Area Network
CCP ..... CAN Calibration Protocol
CNN ..... Convolutional Neural Network
COMAND .... Mercedes-Benz Head-Unit
CPU ..... Central Processing Unit
DBC ..... Database CAN (encoding definition file)
DFT ..... Discrete Fourier Transform
DGPS ..... Differential Global Positioning System
DISPO ..... Digital Smoothing Polynomial
DL ..... Deep Learning
DNN ..... Deep Neural Network
DSP ..... Digital Signal Processor
DWL ..... Desired KSS Warning Level
ECG ..... Electrocardiogram
ECU ..... Electronic Control Unit
EEG ..... Electroencephalogram
EEPROM ..... Electrically Erasable Programmable Read-Only Memory
EKF ..... Extended Kalman Filter
EMG ..... Electromyogram
EM ..... Expectation Maximization algorithm
EOG ..... Electrooculogram
ESC ..... Electronic Stability Control (also ESP)
ESP ..... Electronic Stability Program (also ESC)
EWIQR ..... Exponentially Weighted Interquartile Range
EWMA ..... Exponentially Weighted Moving Average
EWVAR ..... Exponentially Weighted Moving Variance
FFT ..... Fast Fourier Transform
GPS ..... Global Positioning System
GPU ..... Graphics Processing Unit
GRS80 ..... Geodic Reference System 1980
GUI ..... Graphical User Interface

HMI	Human Machine Interface
ICA	Independent Component Analysis
IQR	Interquartile Range
KNFE	Kundennahe Fahrerprobung (Customer-near driving experiments)
KSS	Karolinska Sleepiness Scale
LIDAR	Light Detection and Rating
LIN	Local Interconnect Network
LSB	Least Significant Bit
LSTM	Long Short Term Memory Neural Network
LTE+	Long Term Evolution (4th mobile phone generation)
MEMS	Micro-Electro-Mechanical System
MLE	Maximum Likelyhood Estimation
ML	Machine Learning
MSE	Mean Squared Error
NHTSA	National Highway Traffic Safety Administration
OTA	Over-the-Air
PCA	Principal Component Analysis
PLCD	Permanentmagnetic Linear Contactless Displacement
PPG	Photoplethysmography
RAM	Random Access Memory
RMS	Root Mean Square
RNN	Rrecurrent Neural Network
RPM	Rotations Per Minute
SNR	Signal-to-Noise Ratio
SOC	Systen-on-a-Chip
SPI	Serial Peripheral Interface
SQL	Structured Query Language
STW	Steering Wheel Angle
SVM	Support Vector Machine
TLC	Time To Lane Crossing
TTC	Time To Collision
USB	Universal Serial Bus
WGS84	World Geodic System 1984
XCP	Universal (X) Measurement and Calibration Protocol
ZC	Zero Crossing
LDA	Linear Discriminant Analysis
UTM	Universal Transverse Mercator

Chapter 1.

Introduction

1.1. Chapter Overview

Chapter 1: Introduction The current chapter will introduce the topic of assistance systems that detect sleepiness from the driving style. It will provide an overview of the state-of-the-art in literature and competitor systems while pointing out the new aspects of the present work. Countermeasures and warning strategies against sleepiness behind the steering wheel will be presented and further ideas will be proposed.

Chapter 2: Sensors and Data Acquisition In this chapter, in-vehicle and supplementary sensors used for the driving data acquisition, their principles and derived signals will be presented. Another major part of this chapter is the measurement equipment, data conversion and validation process, the SQL database and everything related to it. This basic process is very extensive but indispensable and not trivial.

Chapter 3: Evaluation of Driver State References This chapter will explain the definitions of *sleepiness*, *drowsiness*, *fatigue*, *vigilance*, and their distinction against *distraction* (Ch. 3.1). Common approaches to directly and indirectly measure sleepiness will be presented and compared. Physiological measures from brain activity and eyelid closure are thoroughly investigated in order to obtain a reliable reference. Developing a system to detect sleepiness is impossible without a good reference, thus merging the different measures into a single reference was investigated.

Chapter 4: Extraction of Features for Driver State Detection The features in literature are described and own ideas based on steering angle, lane data and other sensors are proposed. Moreover, preprocessing of sensor signals and signal processing methods commonly used for many features are presented. The basic principles behind the features are explained as well as the various signals they are based on. Another important topic of this thesis is the systematic optimization of the countless parameters involved in the different features. Processing the large amount of data requires smart strategies to optimize the features within manageable time. Approaches to efficiently cope with these problems will be presented here exemplarily for the most promising features.

Chapter 5: External Factors and Driver Influences This chapter will structure all influences that have an impact on the driving behavior into three groups: *external*, *situation based* and *driver-related* influences. External influences such as vehicle speed, road condition, curves or cross-wind have impacts on the driving behavior that is generally stronger than sleepiness. Situation based factors like daytime, monotony, and traffic density are *a priori* probabilities that make general statements rather than considering individual persons. Furthermore, every driver has an individual driving style that needs

to be adapted. Analyzing, understanding and considering these influences during the feature extraction will be subject of this chapter.

Chapter 6: Approximation of Lane-based Features from Inertial Sensors This chapter will describe how some of the features obtained from the lane-tracking camera sensor unit can be approximated using inertial sensors. The advantage is that inertial sensors are standard equipment in contrast to the lane-tracking camera and inertial sensors do not suffer from poor vision conditions. The relevant theory of vehicle dynamics and Kalman filters will be presented here.

Chapter 7: Result of Assessment of Features This chapter will introduce various different methods to assess the correlation of single or multiple features with the sleepiness reference. Metrics as well as graphical illustrations are presented and compared. Since many measures are based on similar patterns and sensors, a grouping of features is proposed.

Chapter 8: Classification of Features The subject of this chapter will outline the fusion of features by means of classification. The information fusion either on a signal level, feature level, or on a decision level will be discussed. The benefits of transforming the feature space to lower dimensions using principle component analysis or Fisher transform will be explained. Classification of distraction using the same features and methods will be another side-topic of this chapter. It is based on an extensive experiment with 45 real-road drives and defined distraction tasks.

Chapter 9: Conclusion This chapter will present the classification results. A real-time framework and demonstration system will be introduced in order to assess the performance online in the vehicle. A conclusion will be given, as well as potential for future work and open issues.

Chapter A: Appendix This chapter contains documentation and mathematical background of important theory this thesis is based on.

1.2. Motivation

1.2.1. History of Safety

Since Karl Benz's patent application of the Motorwagon over 125 years ago[1] the number of vehicles has been steadily increasing. While the number of vehicles in Germany had grown to 3.7 Mio in 1939 (DESTATIS, 2011a), it dropped below 200.000 vehicles as a consequence of World War II. Fig. 1.1 shows the number of injured persons and persons killed within 30 days after a traffic accident. After the fatalities reached their maximum of 21.332 persons killed in 1970, both, the total number of injured and killed persons decreased. Fig. 1.2 shows the number of vehicles per person on the road in Germany. It can be seen that today, about 70% of all 82 Mio Germans have a car. The figure also sets the total number of crashes, injured persons and fatalities in relation to the registered vehicles. The proportion of accidents per car is steadily diminishing, whereas accident prevention becomes more and more difficult every year. Even with this positive development, we have to consider that still ten persons die and about 1000 get injured every day in Germany alone. The number of crashes without injury is even increasing.

[1] Patent 37435 of the Benz Patent-Motorwagon by Karl Benz, applied on January 29, 1886 (Benz & Co, 1886)

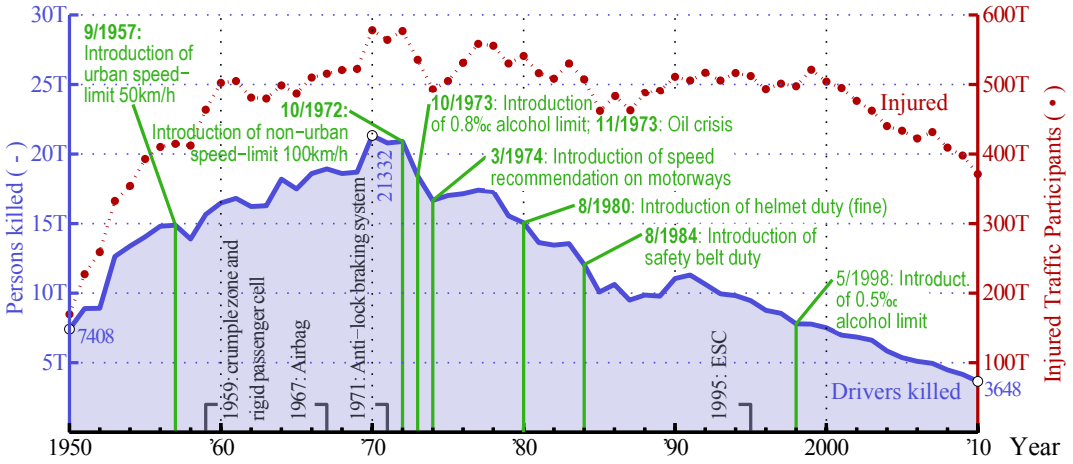

Figure 1.1.: Persons killed and injured in traffic accidents in Germany
(Own drawing, data from *Statistisches Bundesamt*, Wiesbaden DESTATIS, 2011a, 2.1)

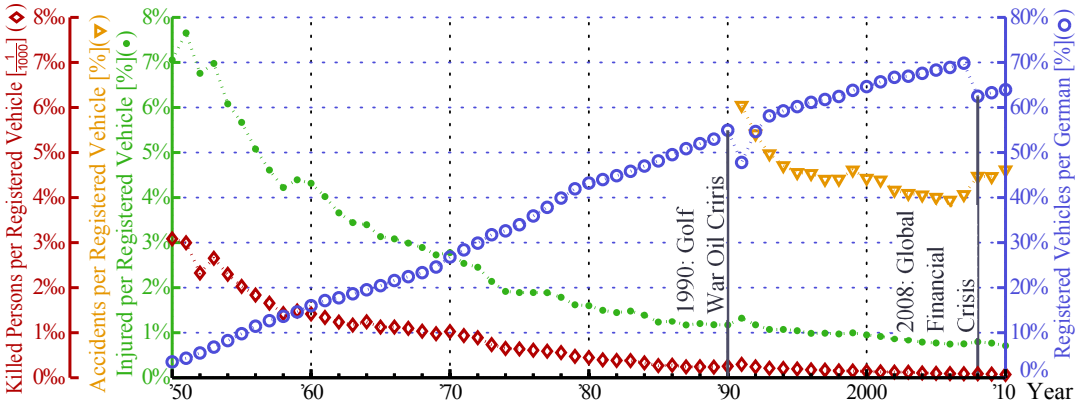

Figure 1.2.: Injured persons and fatalities set into relation with registered vehicles (Own drawing, data from *Verkehrsunfälle Zeitreihen, Statistisches Bundesamt* DESTATIS, 2011b, 2.1/2)

1.2.2. Safety Systems

Various factors account for the continuous reduction of traffic accidents or their impact. Fig. 1.1 indicates how the number of fatalities could be reduced over the years, thanks to a series of new and strickter regulations, such as traffic signs, road improvements, police enforcements, and better medical infrastructure. Beside these regulations, Fig. 1.1 shows the introduction of important safety innovations. Generally, these safety systems are classified into *active* and *passive safety* systems. According to "Milestones in vehicle safety" (Daimler COM/M, 2009), active safety comprises all systems and technologies that *prevent* accidents whereas passive safety technologies *reduce the consequences* for the passengers.

Passive Safety: The safety belt, invented by Gustave-Désiré Leveau in 1903, was one of the first and most important safety inventions (Leveau, 1903). Its German patent application of Bohlin (1961) was selected by the German patent office as one of the eight most valuable inventions for mankind within the last 100 years and is expected to having saved over 1 mio lives (Hell, 2010). A pioneer in the field of passive safety was Barényi (1952) at Mercedes-Benz Sindelfingen who invented the crumple zone and rigid passenger cell in 1939,

that was first introduced in 1959 (Daimler COM/M, 2009). Another major invention from Mercedes-Benz was the airbag in 1967, introduced in Germany with the S-Class (W126) in 1981 (Daimler COM/M, 2009). The passenger airbag, sidebag, windowbag and recently also the kneebag followed (Mercedes-Benz, 2012; auto.de, 2009).

Active Safety: One of the early active safety systems is the electronic active braking system "Sure Brake", introduced by Chrysler in 1971 (Heißing, 2011; Angermann, 2011). In 1978, Bosch introduced the first fully electronic Active Braking System (ABS), launched with the Mercedes-Benz S-Class (W116) (Daimler COM/M, 2009; Angermann, 2011). With the S 600 Coupé (C140), Mercedes-Benz introduced the first electronic stability program (ESP® or ESC) in 1995, supplied by Bosch (Heißing, 2011). If the steering direction does not fit to the vehicle motion (i.e. for large sideslip angles β), the ESP corrects the vehicle trajectory in the direction of steering by braking a single rear wheel. In 1996, Mercedes-Benz also introduced the Brake Assistant as standard equipment for passenger cars (Daimler COM/M, 2009). In 1997 Mercedes-Benz presented the emergency call TELEAID (SOS/Emergency Call, called *mbrace* in the USA) that automatically or manually submits the GPS position and relevant vehicle and crash information (Dietsche and Jäger, 2003; Mercedes-Benz USA, 2012). Similar systems are Onstar, also introduced in 1997 and provided by GM (onstar.com, 2013), and BMW ConnectedDrive introduced in 2011 (BMW, 2011). Blind spot monitoring systems such as the BLIS from Volvo and the BSM (radar-based) from Mercedes-Benz monitor vehicles in the blind spot (Volvo Cars, 2007a). PRE-SAFE®, introduced by Mercedes in 2002, is a system that takes actions to protect passengers shortly before an accident (Daimler COM/M, 2009). Since 2006, the PRE-SAFE brake can automatically decelerate the car if a dangerous situation is detected ahead. One of the latest PRE-SAFE based innovations in 2009 is the braking bag, an airbag below the vehicle front that can achieve twice the deceleration of a full brake (Daimler COM/M, 2009). Based on camera vision, the Advanced Lane Departure Warning Assist (ALDW) and Protection (LDP) support the driver in lane keeping by warnings or active control. The speed limit assist, night view and adaptive curve light are just a few other systems that are based on camera.

One of the latest innovations from Mercedes-Benz is the ATTENTION ASSIST, introduced with the E-Class (W212 and 207) in 2009 which is subject of the present work. It detects fatigue based on the driving behavior and issues a visual and acoustic warning to the driver.

1.2.3. Drowsiness related Accidents

According to the *German Federal Agency for Statistics* (DESTATIS, 2011a), the main reason for road accidents with injuries in 2010 were speeding (10.7%), mistakes while turning/maneuvering/reversing (10.2%), right of way violation (9.7%), insufficient clearance distance (8.1%) followed by wrong road use (4.7%). Alcohol plays an important role, especially in severe accidents (DESTATIS, 2013a,b). Slippery road (from ice, snow, or rain), fog, or venison on road are the main non-driver related accident reasons. In Germany, only 4.2% of the accidents are related to technical defects (2.9% related to tire and 1.3% to brake deficiencies). Fig. 1.3 shows that the majority of accidents are caused by the driver and only a minor part by vehicle failure or road condition. The “100-Car Study", conducted by the VTTI for the *National Highway Traffic Safety Administration (NHTSA)* in 2006 (Martin, 2006), found that about 80% of accidents and 65% of near-crashes involved within three seconds before the event some form of driver inattention, at least as a second reason. According to Volvo, even up to 90% of all traffic accidents are caused by driver distraction (Volvo Cars, 2007b). Cell phone use and *drowsiness* were beneath the primary causes for reduced alertness.

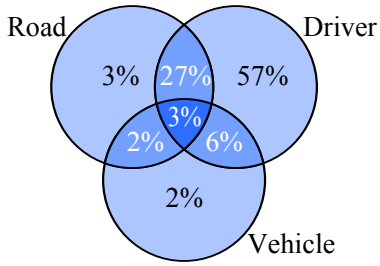

Figure 1.3.: Proportion of accidents by one or several reasons. The driver is accountable for most traffic accidents (Source: Volvo Cars, 2007b)

Drowsy Driving: When interrogating test subjects and other people about drowsy driving, it was surprising that many of them could tell about their own personal experience or even accidents. In most stories nothing happened because they woke up from hitting a traffic cone, short before the guardrail, or from driving into a field. However, some cases ended in more severe accidents. It is not possible to prove that a driver was sleepy, since fatigue cannot be measured as easily as alcohol consumption (e.g. by breathalyzer or blood test). Thus, many drivers do not admit that sleepiness or distraction was responsible for the accident. Drowsy driving is prohibited by law and is persecuted by the police. The insurance withdraws meeting the cost of a drowsiness related crash as it is regarded as reckless induced (BGH, 2002) since falling asleep is always preceded by fatigue signs (BGH, 1969). This also applies to co-passengers if they are aware of the driver's condition (Doppelklicker, 2011). This may be the main reason why drowsy driving is assumed to be significantly under-reported in police crash investigations. The German Federal Agency for Statistics (DESTATIS, 2011b) published that only about 1% of the accidents are related to sleepiness. According to Lyznicki et al. (1998), driver fatigue is the causative factor in 1 to 3% of all US motor vehicle crashes. However, experts assume that about 24 to 33% of the severe accidents are related to drowsiness (Daimler, 2008; Duncker, 2007; Künzel, 2008; Fertner, 2009; Schneider, 2006; Batista, 2007). According to the earlier mentioned 100-Car Study, drowsiness increases the driver's risk of having a crash or near-crash by at least a factor of four. In fatal accidents it is assumed that driver fatigue is more prevalent than either alcohol or drugs, especially for truck drivers (Knipling and Wang, 1994).

Fig. 1.4 shows a picture from press releases that report about accidents with only one vehicle involved and where the accident cause was not clearly determined. Many of the so called "single-car crashes" occur late at night and have fatal consequences, especially when the driver falls asleep and does not react to avoid the crash. In most cases, one can only assume that fatigue was the cause. For instance, during a microsleep phase of two seconds, a vehicle that drives with 140 km/h travels a distance of almost 80 meters without control. What many people do not consider is that not only the microsleep, but also the early phases of fatigue can increase the risk of having an accident significantly. Fig. 1.5 shows the decrease in reaction time after driving duration. Studies show that after just four hours of non-stop driving, drivers' reaction times can be up to 50% slower. Thus, the risk of an accident doubles during this time. And the risk increases more than eight-times after just six hours of non-stop driving. According to NOVA (2002) and Daimler (2008), 24 hours without sleep can be compared have an influence comparable to one per mill of alcohol. The combination of fatigue and even small doses of alcohol can be much more dangerous than the sum of both influences (Reyner, 2005; Mara, 1999; Oberman, 2006, P. 218). Due to their reduced judgment, sleepy drivers are often not aware of their condition. They overestimate themselves or do not admit

Figure 1.4.: So called "single-car crash" - accidents with only one vehicle involved that occur at night are most probably related to fatigue (Source: Furtwängler, 2013).

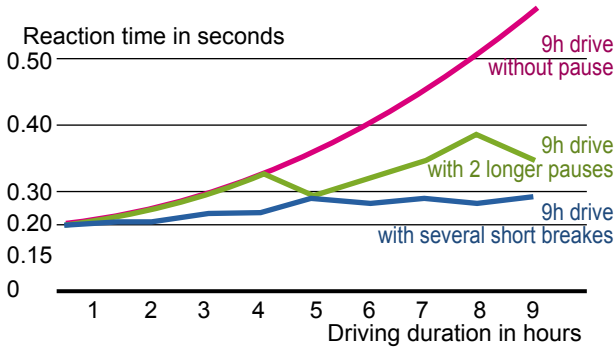

Figure 1.5.: Decreasing reaction time after increasing driving duration (so called "Time-on-Task") (Source of numbers: Mara, 1999, Fig. 2)

to "give up" the fight against their sleep pressure. Time pressure can also be a factor that keeps drivers away from having a pause. The risk of falling asleep is at its greatest on long-distance journeys in the dark or in monotonous conditions. This is when drivers are most likely to suffer a lapse in attention. Young people under 30 are four times more endangered than elder groups (Knipling and Wang, 1995). Especially young males are involved in drowsy-driving crashes five times more likely than females (Wang and Knipling, 1996).

1.2.4. Perspective of Mobility and Safety Systems

Above, German statistics were exemplarily used and can be transfered to the situation in other countries. Clearly, it is very important to consider the worldwide developments. In countries like the USA, Australia or France, drowsy driving is an even bigger problem, as they have very long monotonous roads through areas with low population density. There are more than one billion vehicles and trucks on the roads worldwide (Die Welt.de, 2008) and a growth of almost 20% is predicted within the next seven years. The growth in North America is expected to be the lowest with only 8% and 15% in Europe, driven by Eastern Europe. While the automotive growth is nearly saturated in North America and Europe, the industry in the BRICS countries[2] is booming. With 20% growth within the last years, China is one of the fastest growing markets worldwide. Since only 2% of the Chinese population

[2]BRICS stands for the emerging market countries: **B**rasil, **R**ussia, **I**ndia, **C**hina and **S**outh Africa

have a car, it is expected that the growth will continue (Bleich, 2009, P. 57). In addition, the nowadays very dense road infrastructure and the related industry will not disappear all of a sudden. At the same time, the protection standards in the BRICS are not very evolved. With 142 485 deaths in 2011, India has the most road fatalities in the world (Government of India, 2011) followed by China with 68 000 in 2009 (NPC China, 2010) due to the high population. It is getting more and more difficult to further reduce the number of severe accidents while keeping the traffic efficient. Autonomous driving is certainly a major step towards the paradigm of efficient and "crash free driving" (Daimler COM/M, 2009). Berger and Rumpe (2008) conclude from the Darpa Urban Challenge that autonomous driving is generally possible, but many open questions are still to be solved. According to Wagoner (GM CEO) (Wagoner, 2008) autopilots could become reality in 2020 or within the next years, so Ralf Herrtwich, head of ADAS at Mercedes-Benz (Heuer, 2013). An autopilot has to know even more that the driver is not sleeping when it needs to hand over the vehicle control to the driver in situations that cannot be handled automatically. And until the question is not solved of who is responsible if the autopilot causes an accident, the driver will remain in charge of the steering wheel.

Briefly worded, we can expect that the concept of personal mobility will remain the same for many years, which makes it crucial to introduce new advanced driver assistance systems (ADAS) for the reduction of the prohibitive high number of accidents. Thus, research in the field of driver monitoring has the highest potential with regards to crash reduction.

1.3. Driver State Warning Systems and their Human Machine Interface (HMI)

Until today, safety systems were focusing on either intervention after a driver made a mistake or on reducing the impact of a crash. In the precedent vehicles, there were virtually no systems focusing on the driver. The aim of Advanced Driver Monitoring Systems (ADAS) is to detect the onset of sleepiness by analyzing the driving style or physiological indicators of the driver. People who are skeptical about the concept of a driver monitoring system often argue that they do not need to be told when they are tired. They think that they are always aware of their condition by themselves. But the danger of reduced vigilance is often underestimated. 41% of the drivers interrogated in a recent study by the *AAA Foundation for Traffic Safety* admit to having fallen asleep behind the wheel at some point (TRUEcar, 2010). But just because nothing happened in the past doesn't mean that it will turn out well every time in the future. Since drivers obviously underestimate the risk and do not act adequately, it makes sense to develop systems that support the driver.

Depending on the accuracy with which the driver's vigilance level can be estimated, it needs to be discussed what to do with this driver state information in the first place. For the acceptance of the system, it is essential not to infantilize the driver. Today, most drivers would probably not accept a system that takes over control and automatically drives to the road shoulder, brakes and locks the vehicle if sleepiness was detected. (This might be more appropriate if a cardiac flatline was detected). So the most expedient feedback strategy is to issue an acoustic and visual warning to the driver suggesting to have a pause. Issuing false warnings too often risks that the driver might later neglect a correct warning. As well, it is important not to store any data about a driver's state that could be used against him after an accident. A system that is switched off by the driver for such reasons is useless. As long as

the detection rate doesn't approach 100%, the driver cannot completely rely on the system. He has to know that the assistance system can only support him and that he is always responsible for his safety himself. When feeling tired, he has to make a pause even though there has not been any warning.

Fig. 1.15(a) and 1.15(b) show pictures of the ATTENTION ASSIST warning and status icon introduced 2009 in the Mercedes-Benz E-Class and then spread to all vehicles and tour buses. As a next, more "experiencable" step, a bargraph is displayed that is permanently available in the instrument cluster (Fig. 1.16(a)) and Fig. 1.6(b) depicts the ATTENTION LEVEL of the version 2.0 launched in the W222 S-Class. The level is based on the algorithms developed in this thesis. Fig. 1.6(a) shows a picture of how the *Human Machine Interface* (HMI) of such a bargraph could further look like. Fig. 1.6(b) shows how the history of the past 15 to 30 minutes could further illustrate the degrading trend of the driving performance. A positive

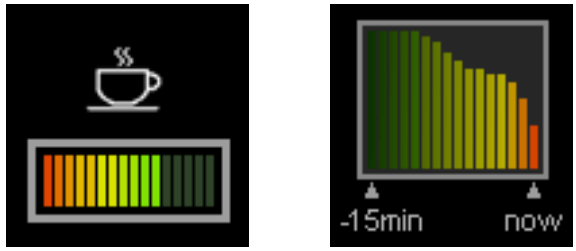

(a) Bargraph of driving performance (b) Bargraph with history

Figure 1.6.: Proposal for two HMI concepts with a permanently available bargraph and a bargraph with history could be displayed to drivers (own drawing)

side effect of permanently displaying a bargraph is that it reminds the driver to remain aware of his fitness. Simply displaying a status icon of the system already addresses this topic as a safety issue and brings the topic into drivers' minds. Fig. 1.7 shows three frames of an animated eye that closes with increasing sleepiness. It is more self-explaining than a bargraph or a status icon and color displays are nowadays available in many upper class vehicles. This might suit best for a camera based drowsiness detection system.

(a) Opened eye for *awake* (b) Half closed eye for *sleepy* (c) Closed eye for *very sleepy*

Figure 1.7.: Another proposed example of a more self-explaining HMI concept for a high resolution color display (own drawing)

Another possibility of using the information about the driver's fitness is to adapt the sensitivity of other driver assistance systems. As an example, the Time-To-Collision (TTC) threshold for braking warnings and autonomous braking could be lowered with reduced driver vigilance. Also, the ALDW could be adjusted to be more sensitive with increasing fatigue. For instance, there were test subjects that often exceeded the lane and obtained wrong warnings while they were awake. But as soon as they became sleepy, the immediate feedback of lane

departure before entering a dangerous situation became very valuable. These improved HMI concepts lead to the major goals of the research on driver monitoring systems:

- Estimating a reliable measure of fatigue with multiple levels
- Determining the time instant of suggesting a pause

1.4. Countermeasures against Sleepiness behind the Wheel

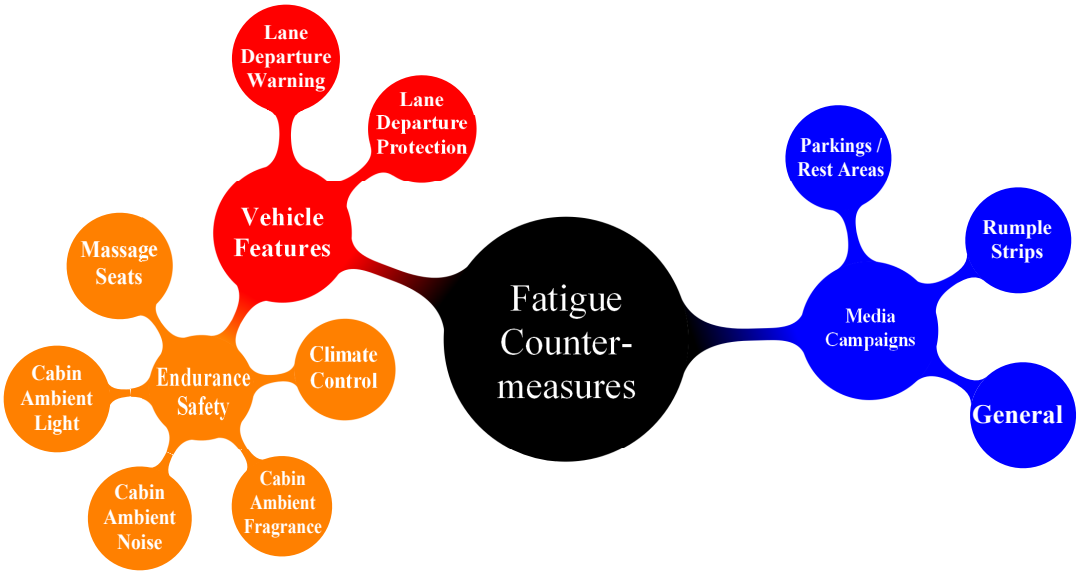

Figure 1.8.: Mindmap of countermeasures to reduce fatigue-related accidents (own drawing)

Fig. 1.8 shows a mindmap of countermeasures against fatigue. The 2010 study of the *AAA Foundation for Traffic Safety* showed that most of the drowsiness related accidents could have been prevented (AAA, 2013). But what could be done for the prevention? The most important prevention is a responsible behavior of the drivers, like planning to get sufficient sleep before a long drive and limiting drives between midnight and 6 a.m. (Mara, 1999). As soon as a driver becomes sleepy, a sensible measure would be to let a co-passenger drive or stop to take a nap. But not everybody is that reasonable, especially if one is in a hurry. Thus, an important strategy against drowsiness related crashes are *media campaigns* to make drivers aware of the risks (Nordbakke and Sagberg, 2007; van Wees et al., 2004; Hell, 2001). Beside press articles and advertising, many book and movie authors use a drowsiness related accident as a reason for a fatal life-changing incident [3]. Fig. 1.9 shows motorway panels that address drowsy driving.

Fig. 1.10(a) shows *rumple strips*, which are another countermeasure to alert inattentive drivers (Elango, 2002). Rumble strips are edge- or centerline grooves, cut or rolled in the pavement that emit an audible rumbling when encountered by vehicle tires. They are most effective if the road shoulder is wide enough. According to the FHWA Safety, shoulder rumble strips can reduce overall crashes by 14 to 17%. In particular, centerline rumble strips may reduce run-off-road crashes by up to 41% and head-on crashes by up to 68% (FHWA, 2012). According to the National Highway Traffic Safety Administration (NHTSA) (Mara, 1999), rumble

[3] Movies that address sleepiness and distraction-related accidents: Mr. Bean, I Robot, 50 first dates, etc.

(a) US campaign (Source: wikipedia)

(b) French campaign meaning "Sleeping or Driving" (own photograph)

(c) South African campaign "Stay Alert - Stay Alive" (own photograph)

Figure 1.9.: US, French and South African motorway signs against drowsy driving

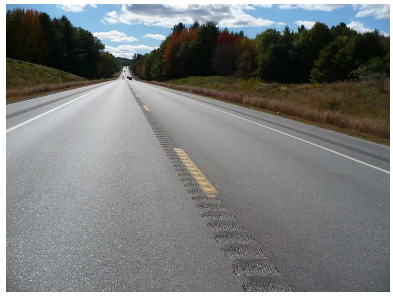

(a) Centerline rumple strips in the US (Source: wikimedia)

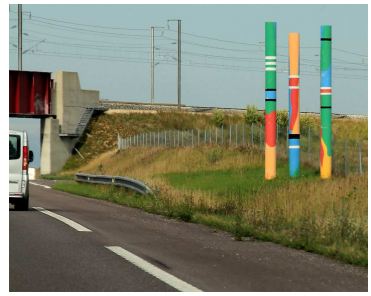

(b) Road arts on french motorways as "novelty" to occupy drivers (own photograph)

Figure 1.10.: Countermeasures against drowsy driving in the US and France

strips can reduce drive-off-the-road crashes by 30 to 50%. Besides the high construction and maintenance cost, rumple strips have some disadvantages, which are still evaluated in Germany (Rieckmann, 2010). For instance, it can be very disturbing if a lane is shifted to the side within construction sites, so that cars permanently have to drive on the rumble strips. Rumple strips are by far not installed on all road markings which speaks for in-vehicle ADAS.

Advanced Lane Departure Warning (ALDW): Lane markings are tracked by a lane tracking camera and a warning is issued when the lane is exceeded. ALDW has the advantages that it works for all lane markings and its warning sensitivity can be adjusted. Altmüller (2007) investigated how undesired ALDW warnings can be distinguished from desired warnings. ALDW systems are very robust nowadays as long as the lane markings are good, which is not always the case. And like all camera based systems, the ALDW performance suffers from bad vision conditions. ALDW is focusing on preventing lane exceeding due to distraction but also helps to prevent accidents by "dozing-off". However, drifting off the road due to sleepiness happens in a very late stadium of fatigue and a pause should be made earlier.

When the driver is overwhelmed by his fatigue or when he becomes aware of his sleepiness through a warning system, how can he make it to the next parking lot or hotel? Are there ways to prolong the driver's fitness or even bring him back to a fit condition in which an immediate pause is not necessary? The dissertation of Greschner (2011) is focusing on this question, especially looking for effective countermeasures that are operating fast and long lasting. It turned out that the repeated pressing of a button and vibrations in the safety belt did not or almost not improve the fitness.

In their studies, Reyner and Horne (1998); Horne and Reyner (1999) demonstrate that cold air and listening to the car radio did not have significant effects on drifting over lane markings, although there was a trend for the radio to initially reduce such incidents and cold air also had some effect. The study of Greschner (2011) confirms the weak and short influence of listening to the car radio. Unfortunately, exercise and stretching is also of little use.

Studies by (Scott, 2009; Philip and Taillard, 2006; Sagaspe et al., 2007; Horne and Reyner, 1999; Anund et al., 2008; Mara, 1999) all came to the conclusion that stopping for a caffeine containing drink, such as one or two cups of coffee and a short nap for about 15 to 20 minutes, are the most effective short-term countermeasures for alleviating sleepiness. Based on two driving simulator studies, Reyner and Horne (2000) concluded that a caffeine dose of 200mg (feasibly taken via 2 to 3 cups of coffee, energy drinks or caffeine tablets (Anund et al., 2008; Mets et al., 2011)) effectively reduces early morning driver sleepiness for 30 min to two hours, depending on the sleep deprivation. In order to measure sleepiness, the subjective sleepiness rating, EEG α-band power and lane driftings were used. According to Scott (2009), up to two cups of coffee can increase alertness for several hours, but it takes on average 20 to 30 min to take effect. Thus, it is recommended to drink the coffee at the beginning of a break before taking a nap. (Scott, 2009) also proposes to take a break every two hours on a long journey. Caffeine can prolong the driver's fitness only to a certain extend and cannot replace sleep over a longer period (Mara, 1999). In a more recent study, Sagaspe et al. (2007) considered the age of drivers and came to the conclusion that coffee significantly improves performance only in young and middle-aged participants. Napping is more efficient in younger than in older participants, so they proposed that the countermeasures should be adapted to the age of the drivers. Mets et al. (2011) found that Red Bull® Energy Drink also significantly improves driving performance compared to Placebo drinks and reduces driver sleepiness during prolonged highway driving during the 3rd and 4th hour of driving (which is not surprising since energy drinks contain caffeine).

Drory (1985) examined the effects of different rest levels and secondary-tasks on performance and fatigue of sixty male truck drivers engaged in a seven hour simulated driving task. The results showed that performance and perceived fatigue were significantly higher when a secondary task involving voice communication was added to the basic driving task, yet an added vigilance task had less effect. An extra 30 minute rest period in the middle of the experimental session significantly alleviated the reported experience of fatigue but did not affect the performance. In contrast to the distraction of a telephone conversation during normal driving, Greschner (2011) concluded from his experimental study that a phone talk of 15 min has a very significant positive influence on the driver alertness.

It is commonly known and confirmed by accident statistics (Greschner, 2011, Fig. 1) and (Altmüller, 2007) that talking to co-passengers keeps the driver more alert than driving alone or when all passengers are sleeping. It helps to prevent from psychological underload (e.g. due to monotony), and exhausted drivers become better aware of their fatigue.

Altmüller (2007) concludes from Gillberg et al. (1996) that sleep is the only remedy against fatigue related from stress overload, physical exhaustion or sleep deprivation while psychological underload might be threated differently.

Exposing the driver to light was investigated as a countermeasure against fatigue. Blue light increasingly suppresses melatonin for higher light intensity and length of exposure.

The photopigments in the human eye mediate circadian photoreception that promote sleepiness (Greschner, 2011; Brainard and Hanifin, 2001, Ch. 3.2). Becker (2008) investigated light-induced melatonin suppression on 37 females and 35 males. He identified 446 to 477 nm as the most potent wavelength region. For continuous insolation to bright light with over 2000 Lux, the melatonin level was reduced while the temperature and performance was higher compared to subjects that were exposed to moderate light below 100 Lux. Own investigations at Daimler have not shown significant improvement of the degree of fatigue.

In the questionnaire used in this thesis during night experiments, some of the test subjects answered that they drive faster to raise the adrenalin level and to get out of the monotony. In fact, in the measurements recorded in this thesis, there was a significant correlation between the subjective self-ratings of sleepiness and vehicle velocity on monotonous motorways.

An effective but maybe too radical countermeasure tested during some specific drives within this project was cold water or ice in the neck or face (advisably not while driving). The short-term increase of alertness is quite obvious as exposure to cold water or ice increases the heart rate, blood pressure and adrenalin level (Houben et al., 1982). It would be interesting to investigate this countermeasure more thoroughly even if it is not practicable.

Grace and Steward (2001) emitted peppermint as an alerting stimulus combined with a buzzer alarm as a warning, but with little additional impact. The Daimler patents (Jellentrup et al., 2009; Jellentrup and Rothe, 2009) propose to combine the ATTENTION ASSIST warning by emitting the smell of coffee or fresh cookies to motivate the driver to have a break.

1.5. Approaches to Detect Drowsiness in the Vehicle

Drowsy drivers exhibit specific observable patterns including eye gaze, eyelid movement, head movement, and facial expression (Barr and Howarth, 2006).

Fig. 1.11 provides an overview over various approaches to *directly* or *indirectly* detect reduced vigilance in a driving context.

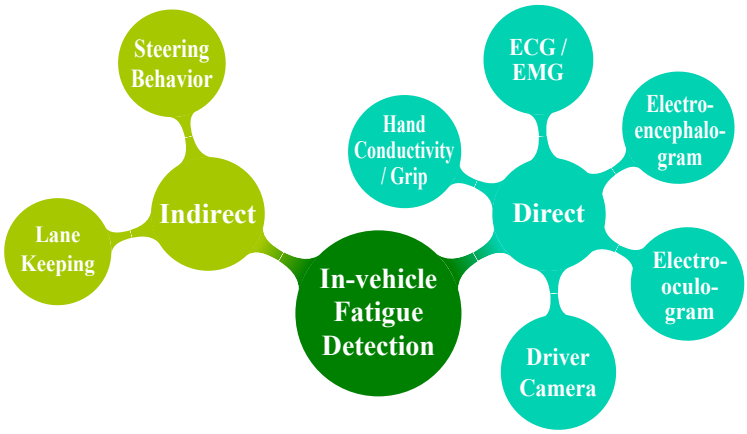

Figure 1.11.: Mindmap of in-vehicle approaches to reduce fatigue-related accidents (own drawing)

Since there is not an objective criteria for fatigue, some of the direct approaches are used as "ground truth" reference. Ch. 3 will further investigate promising measures that are suitable

as fatigue reference in combination with subjective self-ratings. Fatigue can be rated by a majority voting of experts or self-rated by the driver.

Direct approaches measure vigilance immediately from the driver. For instance, the brain, muscle or heart activity can be measured by Electroenzephalography (EEG), Electromyogram (EMG) or Electrocardiogram (ECG). Wiring the driver with electrodes is not practicable for series applications, so that there are approaches to estimate the ECG by radar in the vehicle cabin (Mahler, 2005). The eye lid movement is another indicator for fatigue and can be observed by electrodes around the eyes in the Electrooculogram (EOG) or by attaching spindles directly to the eye lids (Hargutt and Krüger, 2000). A less intrusive way is to capture the eye lid movements by an eye-tracking camera. In the past, the acceptance of a camera pointing directly at the driver was too low for a series application. More recently, internal studies show that the acceptance for such eye-tracking "sensors" has increased. Measuring the hand grip force or the humidity directly on the steering wheel is a weak indicator for the driver fitness and cannot be used as standalone features.

In comparison, *indirect* methods evaluate secondary effects such as impaired driving accuracy. The idea behind indirect approaches is to consider the *driver-vehicle-road* scenario (Fig. 1.12) as a control system in which the driver has to constantly adjust the lateral and longitudinal position. Reduced vigilance results in a decrease of control accuracy which can be represented by different driver model parameter. The driver has to constantly react to external influences induced by the road or traffic. The vehicle translates the actions with a certain phase delay into movements. The error that the driver makes within this control

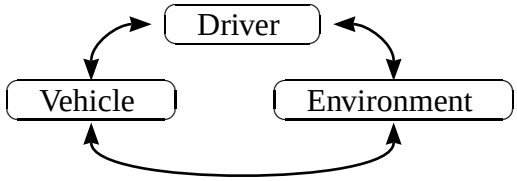

Figure 1.12.: Driver within a control system

loop is partially correlated with his short-term attention, his fitness and fatigue level, but unfortunately also to other influences such as varying driving styles, road condition, traffic influences and many others. Thus, the long term lane keeping performance, steering behavior or reaction time to external events can be used as indirect indicators for reduced vigilance. These approaches will be investigated in Ch. 4. The external influences will be discussed in Ch. 5.

Due to their non-intrusiveness and lower costs, indirect methods are more suitable for series applications. Therefore, it is more attractive for car manufacturers to focus on indirect methods using in-vehicle sensors that are already available for the Electronic Stability Control (ESC) and other standard equipment systems.

1.6. Drowsiness Detection Systems on the Market

The first prevention driver assistance systems on the market focusing on fatigued drivers were the Volvo *Driver Alert Control* (Volvo Cars, 2007b; Ritter, 2007) introduced in 2007, as special equipment, and the Mercedes-Benz ATTENTION ASSIST in 2009 as series equipment (Daimler, 2008; Daimler COM/M, 2009). The ATTENTION ASSIST is running on ESC platforms from Bosch, Delphi and TRW that have all different architectures. In 2010, Bosch

and VW introduced a fatigue detection system in the VW Passat, also as series equipment, working similarly to the ATTENTION ASSIST (von Jan et al., 2005). Nowadays, many automotive OEMs work on fatigue detection systems.

The Mitsubishi's *Driver's Attention Monitoring System* (MDAS-III) from Mitsubishi-Fuso (2012) is available for heavy duty trucks and large tourist buses based on a white-line-recognition camera, steering wheel sensor and various sensors to monitor the attention level. It calculates the degree of monotony by evaluating the clutch, auxiliary brake and signal lights. The system also emits a fragrance during monotonous driving in order to maintain attention without discomfort (Mitsubishi, 2012).

Volvo Driver Alert Control

The *Volvo Driver Alert Control* (DAC) detects drowsiness or unintended lane exceeding while driving. The system turns on at 65 km/h and remains active until the speed falls below 60 km/h. The first version of the DAC was introduced in 2007 in the X60 as special equipment package in combination with lane departure warning. Rather than assessing the human behavior directly, DAC monitors the driving behavior directly. DAC determines whether the vehicle is driven in a controlled or uncontrolled way. Therefore, the system uses signals from the lane tracking camera along with steering movements and constantly compares erratic behavior to the normal driving style (Volvo Cars, 2012). The DAC runs on a Delphi platform and uses only three signals (lane position, yaw rate, and vehicle speed). When DAC detects

Figure 1.13.: Volvo Driver Alert showing a bargraph (Source: Autokiste.de, 2007)

signs of fatigue or a lack in concentration, an audible warning is emitted. At the same time, a message is displayed on the instrument panel suggesting a break (Volvo Cars, 2012). In addition, a bargraph with five levels is provided, as shown in Fig. 1.13 for more experiencability. The sensitivity can be adapted via personalization properties. The system is quite simple, dynamic and therefore transparent. Manipulating the bargraph and provoking a warning is easy. This brings experiencability whereas reduces the detection accuracy.

Mercedes-Benz Attention Assist

In 2009, Mercedes Benz introduced the ATTENTION ASSIST with the new E- and S-Class as series equipment. Today, the system is spread to the entire product portfolio as series equipment. The system is a milestone in the history of safety systems as shown in the latest cover of the Daimler brochure "Milestones in Vehicle Safety" in Fig. 1.14. Mercedes-Benz has developed the innovative system, which can detect the onset of driver fatigue or a lack in concentration and prompts them a proposal to take a break before it is too late. The system was designed to detect the transition from awakeness to drowsiness while driving and issues an acoustical and visual warning suggesting a brake. Fig. 1.15 depicts the warning in the instrument cluster of the first version in the E- and S-Class. Fig. 1.16(a) depicts the

Figure 1.14.: ATTENTION ASSIST as cover of Daimler *milestones in vehicle safety. The vision of Crash Free Driving.* (Source: 5836/1622/00/0609 Daimler COM/M, 2009)

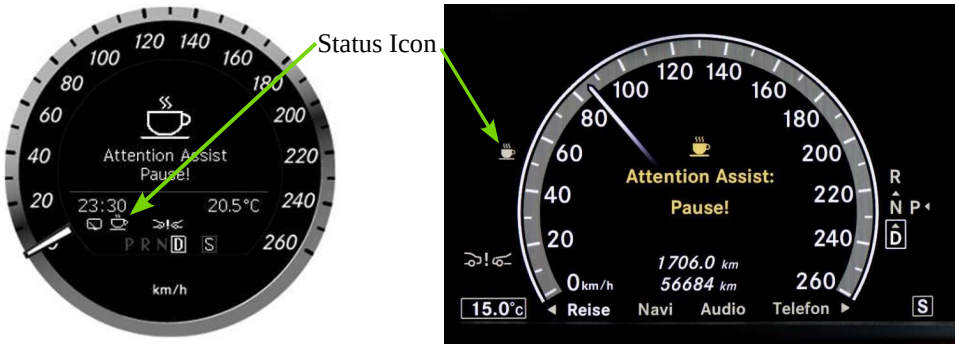

(a) E-Class 2008 (b) S-Class 2009

Figure 1.15.: ATTENTION ASSIST warning in the E- and S-Class

ATTENTION LEVEL in the instrument cluster of the version 2.0 launched in the W222 S-Class that illustrates an early stage of the algorithms developed in this thesis.

(a) Attention Level (b) HMI and warning concept

Figure 1.16.: ATTENTION LEVEL and warning concept in the W222 (Source: Mercedes-Benz MBRSA, 2013)

As shown in Fig. 1.17, over 80 signals are evaluated and more than 200 parameters are involved. At the heart of this system is a highly sensitive steering wheel sensor which allows an extremely precise monitoring of the steering wheel movements and the steering speed. Since tired drivers have difficulties in accurately following the lane, they make small steering mistakes that are often corrected in a fast and characteristic way. The frequency and intensity as well as five other measures represent the basic measure for fatigue. Extensive data analyses of over 1000 drivers have proven that these mistakes already occur in an early onset of sleepiness, long before the dangerous micro-sleep. The ATTENTION ASSIST observes the driver's steering behavior and, during the first few minutes of every trip, determines a driver specific profile that is then continuously compared with the actual steering data. Besides analyzing

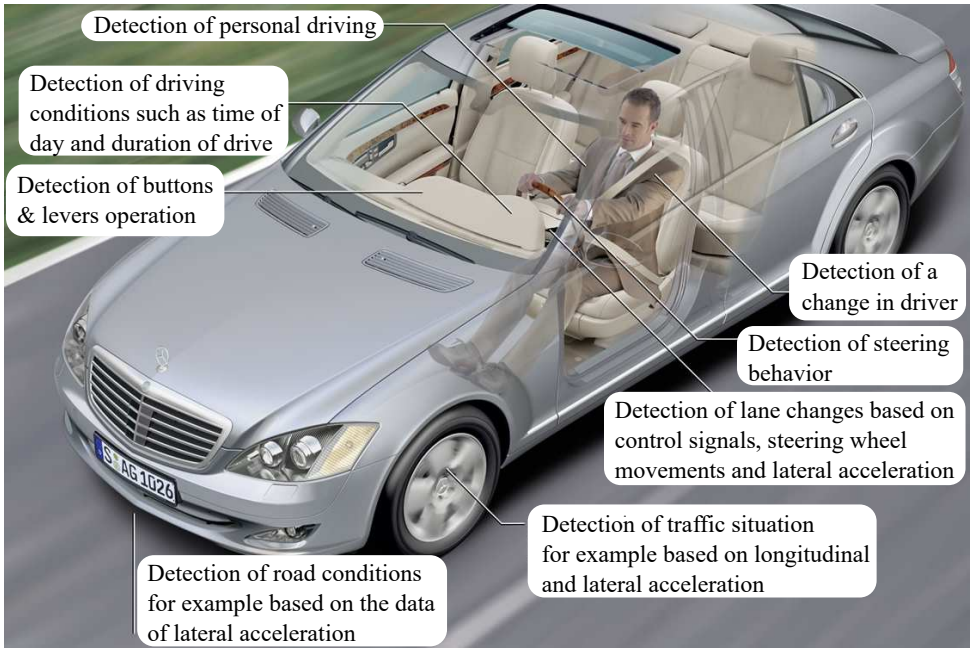

Figure 1.17.: The signals that the ATTENTION ASSIST is using (Mercedes-Benz, 2008)

the steering behavior, the system permanently adapts to the actual steering style that may vary because of external influences, speed or road types. The system is active at speeds between 80 and 180 km/h. The road condition and cross-wind are detected and taken into account. Operations on buttons, levers, headunits as well as phone calls, etc. are also detected and taken into account in the same way as overtaking or lane changing maneuvers. The dynamic of the driving style (i.e. sporty or monotonous) is also incorporated. Also the daytime and driving duration are taken into account. The system is reseted with engine restart or when a driver change is detected. Fuzzy logic was introduced in order to improve the system's performance and to reduce fixed-point scaling artifacts. Many of the results presented in this thesis were integrated in this system.

The current system is optimized to issue a warning to the driver in the right moment. However, many drivers will rarely experience this moment, as it can take a while until such a state is reached. In order to provide more transparency and make the system more experiencable, a bargraph would be the next step as presented in Fig. 1.6(a).

1.7. State-of-the Art and Literature Review

Monitoring the driver behavior is a research topic reaching back to the 90s and many studies have been conducted over the last decades. Most studies were based on data from driving simulators since in-vehicle drowsiness experiments require a tremendous amount of effort.

Knipling and Wang (1994) found that driving duration and time of day (Circadian) are correlated with fatigue and can be used for detection. Ueno et al. (1994) used image processing technology to analyze images of the driver's face to estimate drowsiness. Using simulator data and Artificial Neural Networks (ANN), Sayed (2001); Eskandarian and Mortazavi (2007) found that steering activity, among other variables, correlate well with drowsiness. They achieved an accuracy of 89% for the class *awake* and 85% for *drowsy*. Knipling and

Wang (1994); Fairbanks et al. (1995); Wierwille (1996a); Wierwille et al. (1996); Wierwille (1996b) proposed a set of features based on driving simulator data. Their potential features are included and further improved in this project. In his dissertation, Altmüller (2007) analyzed the deadband rate in the steering velocity, based on 44 simulator drives. The deadband is a phase in which the driver is not steering due to a lack of awareness. These features are included in this thesis and analyzed using real road data. Batavia (1999) used real world data to optimize a driver aware lane departure system.

Schmitz (2004) proposed improvements to suppress warnings for intended lane departures based on simulator results that are verified in two field studies. Kozak and Pohl (2006) did the same, however based on 32 truck simulator drives.

Berglund (2007); Kanstrup (2006); Mattsson (2007) used multiple regression on in-vehicle steering and lane data variables to accurately (87%) classify drowsiness, based on 22 truck simulator drives. Whereas Löfgren (2007) was focusing on lane data, Wigh (2007) was evaluating lane-based features such as time-to-lane crossing at Daimler.

Forsman and Vilaa (2012) performed a driving simulator study with twelve participants and 87 different driving metrics focusing on the detection of moderate drowsiness levels. She confirms that steering wheel variability provides a cost-effective and easy-to-install alternative for in-vehicle drowsy driver detection at moderate fatigue levels.

1.8. Goals of this Thesis

The general goal of this thesis is to improve online fatigue level estimation algorithms for the application in drowsiness detection systems such as the Mercedes-Benz ATTENTION ASSIST. For this reason, it is mandatory to use sensor data that are suitable for in-vehicle use and preferably based on available standard equipment sensors. The detection accuracy of the system should be as high as possible while keeping the false alarm rate at a minimum. The algorithms should be robust and reliable under any road condition and for any type of driver.

The main focus of this thesis is on the study, implementation and evaluation of the fatigue related features in literature. Moreover, own ideas and approaches will be proposed. This also involves the data acquisition and handling of over one million kilometers of real road test data and night experiments.

In order to reach the goals, an adequate reference for sleepiness has to be found and used to represent the ground truth for optimization. For the effectiveness of the system, the aim is to provide a warning that is plausible with regards to the *subjective* self-assessment of the driver on the one hand, and that prevents accidents by providing *objective* feedback to the driver about his impaired driving performance at the other hand. Rather than the detection of short term distraction, the focus of this thesis is on middle and long term lack of concentration or alertness. At the same time, the onset of fatigue should be detected *early* enough so that there remains enough time for the driver to reach the next parking area. The later the system detects arising fatigue, the more severe is the risk of having an accident. Thus, if the early onset of fatigue was not detected, it is important to at least detect the later phases of sleepiness, especially when micro-sleep occurs.

Whereas the current system only displays a warning with an acoustic warning signal, the next generation is intended to output an online bargraph that constantly monitors the driver. Providing a permanently available bargraph of the actual driver state demands the estimation of a continuous-valued measure of the driver's vigilance level. This drowsiness level is also valuable for adapting the sensitivity of other driver assistance systems such as lane departure and collision warning systems.

In addition, there are other demands of series production to fulfill. The number of variants and the effort for the application of the system to individual vehicle types must be manageable. Furthermore, it is important to keep the system simple to conquer its complexity and reduce the risk of software errors. Algorithms that are targeted to run on the ESC controller unit must run in real-time and in fixed-point with a very limited demand of resources.

1.9. New Contributions of this Thesis

The contributions of this thesis to the field of driver state monitoring are as follows:

Signals and Data
Unparalleled amount of real-world driving data: Compared to any other previous work, this thesis is based on an unparalleled amount of real world driving data. Most studies in literature, as for instance (Altmüller, 2007; Knipling and Wang, 1994; Batavia, 1999; Kozak and Pohl, 2006; Schmitz, 2004; Ueno et al., 1994; Wigh, 2007) are evaluated on a comparatively smaller amount of simulator drives or sometimes on-road measurements under restricted lab conditions. As discussed in Sec. 2.1, it makes a huge difference if test drives are recorded in a simulator or on real roads.
Fusion of sensor signals: This thesis deals with the problem of handling mixed, asynchronous CAN data in which signals are sometimes unavailable. The lane position is often unavailable due to bad lane markings or vision issues. The lane position and vehicle level signals are not available in all vehicles. Fail-safe considerations and fall-back strategies of faulty or missing signals are made. Online sensor fault monitoring algorithms for sensor blindspots and hysteresis are proposed that run in fixed-point with very low resource consumption. Methods for the plausibility check of signals by the use of redundancy, expert knowledge and physical vehicle models are implemented.

Fatigue References
Assessment of EEG, Camera and Self-estimation: The subjective self-estimation, camera-based eye-tracking and EEG brain activity are critically evaluated for their validity in real driving environments. External measures like eye-tracking and EEG suffer from negative influences during regular road drives. Hence, the Karolinska Sleepiness Scale (KSS) is primarily used since the driver must accept the warnings and when thoroughly recorded, it is more reliable than any other recorded measure. But since the subjective understanding of the KSS scale differs amongst drivers, a *desired warning level* was introduced. In addition, a *warning acceptance question* was interrogated for cross-validation of the KSS.

Features
New and improved features: In addition to promising fatigue measures (so called features) found in literature, new features are proposed. Their suitability for working under real driving conditions is evaluated thoroughly on an amount of real world measurements of over 1.5 million kilometers. For instance, a feature similar to *Degree-of-Interaction* is proposed but

without the need of the steering wheel torque. In comparison to (Mattsson, 2007), an alternative method for detecting zig-zag events is given.
Incorporation of a-priori measures: A-priori measures (such as daytime, "time-on-task", light condition) have been considered separately during the training of the classifiers. This makes the assessment of features more sensitive to the actual driver state rather than using the probability of being sleepy in the actual driving situation alone.
Application of new signal processing methods: In order to improve the performance of the features and their extraction efficiency, new signal processing methods are proposed for this application (e.g. EWMA , EWVAR , EWIQR , DISPO,...) (cf. Ch. 4).
Also, a convenient and resource-efficient online-estimation of steering velocity percentiles is proposed using an array of EWMA filters.
Feature extraction using Fuzzy logic: This was introduced to detect steering corrections more reliably and to reduce fixed-float differences.
Adaptive window size of filters: Drowsiness increases rather slowly, so the correlation between features and drowsiness is better for smoothing with large window sizes. A major problem in previous work was the large window sizes of 10-30 minutes that make the system nonreactive to quick fatigue level changes. Compared to Sayed (2001), for instance, an adaptive window size is used to be more dynamic in drowsiness supporting situations.
Accelerated optimization of feature parameters: Convex parameter optimization of single features and global parameter optimization algorithms are applied. For feature extraction, computation cost reduction of over factor 100 is achieved by scaling all pre-processed signals to the tightest data type, loading the 60 GB into the RAM and applying efficient matrix operations.

Lane Data
Features from advanced lane-departure camera: In addition to sensor data from steering angle, acceleration and yaw-rate, a portion of the investigated features is based on data from the *Advanced Lane Departure Warning (ALDW)* system. This *advanced* LDW provides additional signals, is calibrated more accurately and has higher availability compared to individually built-in aftermarket sensors from previous studies.
Estimation of lane-based features by inertial sensors and extended Kalman filter (EKF): For the extraction of some features based on lane-tracking camera, it is proposed to only use inertial motion sensors in combination with an EKF. The performance between original lane features and the estimated coupled motion pendants are compared.

External Factors
Compensation of external factors: Moreover, external factors like road condition, cross-wind, traffic density and vehicle operations are examined. A novel adaptive notch-filter is used to suppress vibration noise from unbalanced wheel mass. A new sensitive detection of road bumps is presented using the temporal delay between front and rear wheels. As in no other previous publications, vehicle level signals from the air suspension or Active Body Control (ABC) sensor are evaluated to estimate measures for the road condition. A comparison to the other methods is given.
Compensation of individual driving styles: Adaption to the large variety of individual driving styles is crucial and handled by *baselining*. Different methods are compared.
Compensation of vehicle parameters: There is a large number of vehicle properties like steering ratio, steering resistance and torque, vehicle mass etc. on which the detection depends. Cross-wind detection, for instance, is very sensitive to vehicle parameters. Such vehicle dependencies are incorporated in this thesis.

Classification
Fusion of features by classification The fusion of the features is discussed on the physical, feature, and decision level. With other words, modeling expert knowledge on feature extraction level, feature selection and classification are compared. The performance of a combination of features is assessed by classifiers and dimension reduction techniques. Classification methods for modeling expert knowledge are examined by using Hidden Markov Models (HMM).
Real-time online demonstrator and novel CAN-interface: Approved algorithms are implemented with very limited pixed-point resources in real-time in the ESC of all today's Mercedes-Benz cars. More sophisticated features were implemented in an own Matlab MEX C++ CAN-Interface with a visualization GUI for in-vehicle online assessment.

1.10. Challenges of in-vehicle Fatigue Detection

Clearly, a major challenge about drowsiness detection is the amount of data needed for the development and everything that is related to the data recording and handling. Since the driver's state generally decreases slowly over many minutes or even hours, very long measurements are needed. At the same time, fatigue related patterns occur within seconds and require a sufficiently high sampling frequency. Thus, not only the 2 TB of data, but also the long duration of the measurements makes them difficult to record, handle, and analyze. Also, the driving behavior must not be influenced by the touchscreen KSS entries or immediate feedback of driving performance. Furthermore, it makes a big difference when the driver has lane departure warnings or lane keeping available and switched on.

Also, a big issue was driving until the onset of sleepiness, but making sure that the risk of having an accident is not higher than for normal traffic. So, every drive with involved fatigue required at least a co-driver and sometimes a second set of pedals. These preventions made it possible that not one single critical situation occurred during the entire project.

Another difficulty was the large number of signals that have to be processed. Whereas many signal processing fields are focusing one a few channels, the features in this thesis are based on over 200 signals that all need to be validated. They all have different characteristics and each signal originates from different vehicle types with different sensors and controller unit manufacturers with different software. The computer devices for measurement in the vehicle are very complex, sensitive to faults, and often suffer from miss-configuration. The driving simulator, the various prototype vehicles, the measurement equipment, the 10.000 hours of driving, the man power for data acquisition, and the research over one decade costed millions of Euros.

Finally, the most difficult challenge was to uncover the information about the driver's condition. The driver hat to be observed within countless hours and in various situations to discover and cluster promising patterns and to come up with ideas how to automatically detect them. Every driver drives differently and even one driver can change his behavior depending on his/her condition, his/her mood, or the situation. So the observed patterns are covered by many factors that severely overlay the weak fatigue patterns.

Even after all these considerations, the classification results did not reach the results obtained in a driving simulator. It is still not clear, if online fatigue detection will ever work with very high accuracy under all circumstances.

Chapter 2.

Sensors and Data Acquisition

2.1. Driving Experiments

A prerequisite for obtaining results on fatigue detection is a sufficiently large amount of recorded data with high quality. But even a large amount of data is useless without a reliable reference and good transparency of what happened during the drives. It is very important to know under which conditions the drives have been recorded, for instance, to know the speed profile, road type, weather and driver type. Fig. 2.1 shows a map of valid drives in Europe. Different experiment scenarios have been designed to record data that represent regular driving. These experiment types are described in the following section.

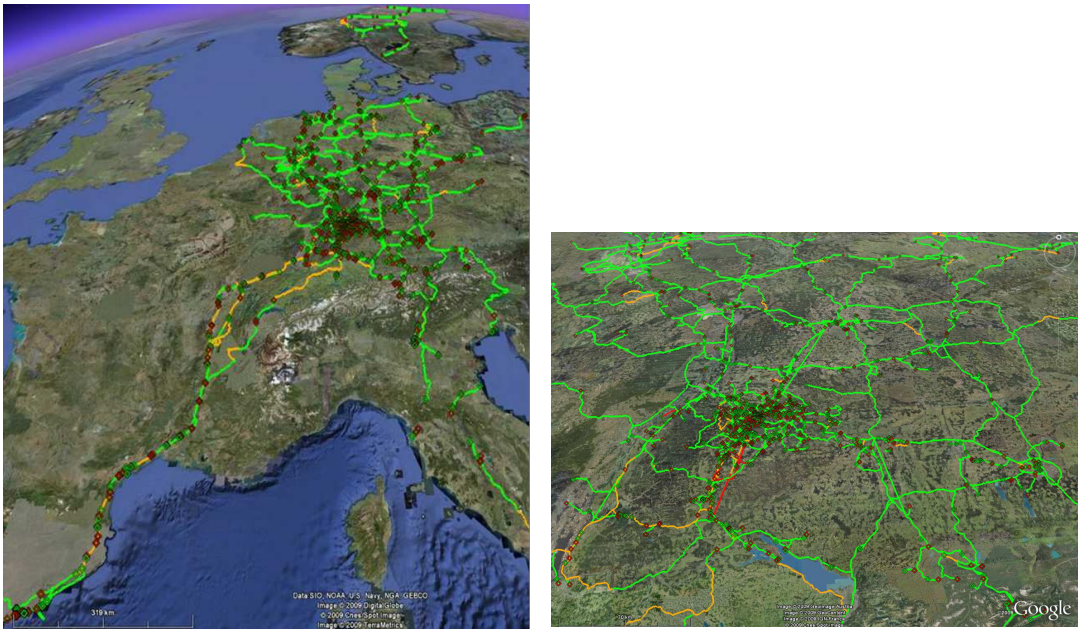

Figure 2.1.: Map of drives: begin / end of drives are indicated with a green / red dot. Green lines indicate *awake* driving sections, orange lines indicate *acceptable* and red lines *drowsy* drives (see Ch. 3.3).

Night experiments: Drives with provoked fatigue levels were typically performed on monotonous motorway sections with very low traffic and limited speed from about 120 to 140 km/h. This was the most important scenario since most of these drives involved a certain extend of fatigue. In addition to the subjective KSS self-rating, the driver's vigilance level

was constantly monitored by eye-tracking cameras and partially by EEG. For these drives, the self-assessments of the fatigue level were most accurate thanks to the supervision by the co-driver. Drivers were carefully monitored by specially trained supervisors, capable to intervene from the passenger seat with a second set of pedals (Schmidt, 2009). The supervisor made notes about the driver's vigilance, the driving performance, and happenings that could later be of interest. As it is usual for driving on public roads, the driver was always responsible for driving safety. The drivers had to stop as soon as they had concerns about safety. The supervisor also had soft and hard criteria to interrupt the drive. For instance, entering the KSS level 9 one time or entering level 8 two times were hard criteria to interrupt the drive. In none of the drives, interaction of the co-driver was necessary. Allowing more fatigue than this was not possible on public roads. A questionnaire had to be filled out by the driver before and after the ride to determine irregularities and to collect driver characteristics. More night drives with fatigue have been recorded on the closed 12km test track in Papenburg. However, these drives were not realistic enough and thus not considered here.

Customer Near Driving (KNFE) and Free Driving: Daily routine driving profiles comprise the majority of drives in this thesis. Random persons obtain a vehicle to drive to their individual destination. These drives are without any restrictions and do not specifically pursue the goal of becoming tired. It is just desired to drive over 1600 km, thus, the vehicles are often used to drive long distances on motorways that are more probable to contain fatigue than other drives. All drivers get instructions, especially on how to estimate their level of fatigue using the KSS. They were instructed to interrupt the drive when they felt tired, no matter if they get a warning or not. Still, some drivers did not reliably enter their KSS fatigue level, so that a validation process was needed (see Sec. A.7.3). The only thing the driver had to do was to enter his/her sleepiness level every 15 minutes and fill out a touch screen questionnaire before and after every drive. In addition, warnings must be rated as *false*, *acceptable*, or *correct*. Drivers are not always used to the vehicle, so they sometimes test vehicle dynamics or driver assistance systems. Some drivers tried to provoke an ATTENTION ASSIST warning without being tired. Such drives are not suitable for training and, thus, excluded from the present study.

Driving Simulator: Simulator studies are the safest and easiest way to record advanced fatigue levels. Especially falling asleep can only be recorded in a driving simulator. Recording data in the driving simulator in Fig. 2.2 was part of previous project phases. Anyway, in the scope of this thesis and the diploma thesis of Akin (2007), 30 simulator drives had to be recorded to evaluate the latest eye-tracking system by letting the drivers fall asleep behind the wheel.

There are big differences between data from regular everyday driving situations compared to data from simulator drives. As reported in (Belz, 2000; Belz et al., 2004; Berka et al., 2005), fatigue develops differently in a driving simulator compared to real drives. According to (Philip and Sagaspe, 2005), the line crossings are of higher amplitude in the simulated condition. Fig. 2.2 shows an advanced moving-base driving simulator compared to a drive in a real vehicle. Especially psychological factors and external influences have a significant impact on the driving performance. One of the most essential differences is the driver's awareness of being in a situation, in which his life depends on his fitness. In a simulator, drivers go much closer to the limit of falling asleep, which is much too late for practical applications. This is confirmed by the fact that most of the 30 test persons have fallen asleep in the simulator experiment conducted for this thesis. As drives on public roads must be

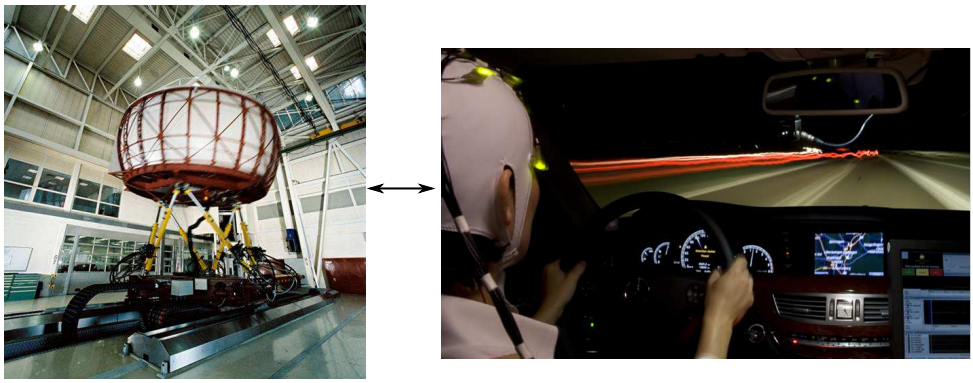

Figure 2.2.: There are important differences between driving in a simulator compared to real driving conditions. This is why many fatigue detection approaches that worked well in a simulator fail on real roads.

interrupted in an early phase of sleepiness, the drowsiness related patterns are more rare and not very significant. Subjects that are monitored by a supervisor drive more strained and calmer. A lot of "noise" is introduced by different road types, lane markings, traffic density, curvature, speed profiles, driving styles, and vehicle types. The lane quality varies severely and is affected by weather. In reality, realistic roads are never perfectly even. Such noise cannot be simulated by even the most advanced simulators.

Proving Grounds: Driving experiments with safety concerns cannot be performed on public roads. Private proving grounds like Papenburg in Germany or Idiada in Spain are not representative for regular motorway drives. However, these testing areas are very suitable for testing the detection of road bumps or the application of vehicle and system parameters. Therefore, testing the detection of fatigue patterns like zig-zag driving, lane exceeding, and monotonous or sporty driving was tested on these proving grounds. Fig. A.1 shows a map of the commonly used proving grounds Papenburg and Idiada.

Excursion Experiments: Long drives which are performed by experts who have a lot of expertise in estimating their fatigue level are excursion experiments. The driving behavior is well comparable to regular drives, since they are not limited to any kind of behavior, road or driving situation. There was always an experienced co-driver when fatigue was involved. In general, there are several vehicles driving in a group, which allows the comparison of vehicles and drivers.

2.2. Database

The present results are based on a large selection of the Mercedes-Benz drowsiness database. An unparalleled amount of data with over 27.000 drives and over 1.46 million kilometers were recorded. Over 11.170 of these drives were valid for simulation.

- about 13.000 hours of driving time
- all valid drives were over ten kilometers and lasted up to eleven hours
- over 18 night experiments
- 1.485 drivers who’s age ranged from 18 to 77 years, 87% males
- 84 different vehicles from C- to S-Class and SLK- to M-Class
- 12 different countries (Europe, Emirates, Japan, USA, Namibia, South Africa)

- all kind of roads (motorways, country roads, urban, gravel, testing ground, snow, ice)
- weather and temperatures ranged from -30 degree in Sweden to over +40 degree in the Death Valley, Dubai and Namibia.
- The drivers were generally experienced, whereas some drivers had little experience. 91% of the drivers were familiar with the actual vehicle type.

App. A.2 shows the filter criteria of *datasets* for different applications.

2.2.1. Touchscreen and Questionnaire

The KSS level was interrogated every 15 minutes through a touch screen display by a beep sound. Fig. 2.3 shows the questionnaire that the drivers had to answer before and after each drive. The actually entered value remained highlighted so that the driver could always confirm or update the last entry.

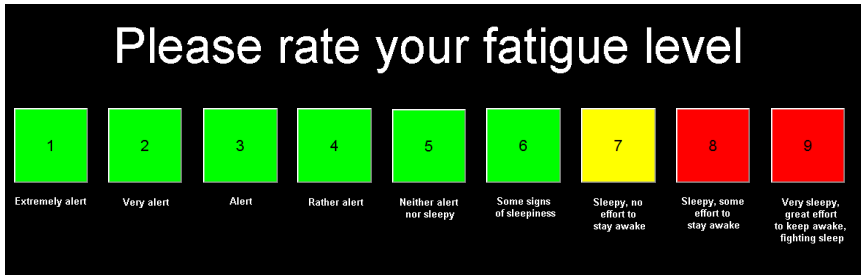

Figure 2.3.: MATLAB KSS input GUI for the driving simulator, similar to the touch screen in every vehicle

Before the drive, the driver had to answer the following questions:

- Full Name
- Gender
- Year of birth
- Driven distance in km per year (see statistic in Fig. 2.4(a))
- Most often driven vehicle brand and type
- Personally use manual or automatic transmission
  (44.2% used automatic and 55.8% manual transmission)
- Usual driving duration until having a break (see statistic in Fig. 2.4(b))
- Number of drives over four hours per month (see statistic in Fig. 2.4(c))

After the drive, the following questions had to be answered:

- Weather conditions (rain or fog, aquaplaning)
- Road condition (rills, road bumps)
- Occurrence of cross-wind
- Degree of distraction and reason (discussion, operation, thoughts)
- Desired KSS warning level: DWL
- Effectiveness of the warning (reason why driving was continued)
- Opinion on warning design

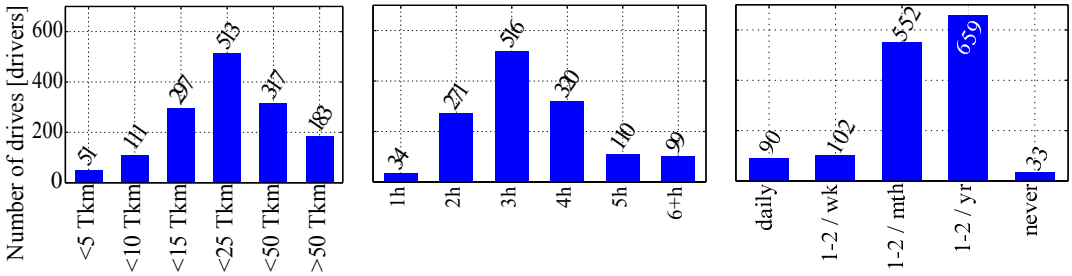

(a) Drivers' annual driven distance (b) Driving duration after which drivers have a break (c) Frequency of drives over 4 h

Figure 2.4.: Statistic over the driver's answers to the touchscreen questionnaire. Even if the recorded drivers drive many kilometers per year, they only have a few long drives over 4 h per year. Most drivers usually have a pause every 2 - 4 h whereas 19 % of the drivers drive 5 h and more without a break.

2.3. Sensors

Every sensor was attached over ADC, LIN- or SPI-bus to an *Electronic Controller Unit* (ECU) that translates the physical signals to CAN messages. Some of the sensor modules send multiple signals. The majority of the CAN signals in Tab. A.1 in App. A.3 are vehicle operation signals, such as turn indicators or steering wheel buttons that originate from every different discrete button or lever states. ALDW provides 29 signals as described in Tab. A.2. Signals from the ALDW lane keeping camera are investigated while longitudinal radar information is not used. Some reasons are that the driver's lateral vehicle control is permanently necessary while the longitudinal control depends on external driving situations and the limiter or (adaptive) cruise control might be active. The most important sensors are described in the following.

2.3.1. Vehicle Speed from Wheel Rotation Rate Sensor

The vehicle speed is measured by wheel rotation rate sensors ("wheelticks") that use a hall sensor and a magnet wheel with magnetically encoded pulses to detect partial rotations and the rotation direction. Depending on the vehicle drive train type, the *wheel rotations per minute* $WhlRPM$ at time instant n are calculated according to Eq. (2.1). If one of the used sensors is implausible, only the plausible sensor is taken. This, however, results in a speed deviation within curves.

$$WhlRPM[n] = \begin{cases} \left(WhlRPM_{FL}[n] + WhlRPM_{FR}[n]\right)/2 & \text{for rear wheel drive} \\ \left(WhlRPM_{RL}[n] + WhlRPM_{RR}[n]\right)/2 & \text{for front wheel drive} \end{cases} \tag{2.1}$$

The *vehicle speed* v_{veh} [km/h] at time interval n is then obtained using the *dynamic wheel circumference* d_{whl} in [m] according to Eq. (2.2). The wheel circumference grows with increasing speed, so the *dynamic* wheel circumference was chosen according to the speed range of interest. Too small or worn out tires cause a small deviation that cannot be detected so far. This parameter is an input of the algorithm stored as table in the ESC and is selected based on the vehicle variant code (SCN). The values originate from the tire suppliers.

$$v_{veh}[n] = WhlRPM[n] \cdot d_{whl} \cdot \frac{3.6\frac{km}{h} \cdot \frac{s}{m}}{60\frac{min}{s}} \tag{2.2}$$

2.3.2. Inertial Sensors

The yaw rotation and acceleration are measured by the sensor cluster in the vehicle's center of gravity or directly onboard in the ESC. A two-dimensional MEMS accelerometer (cf. A.5) measures the *longitudinal* and *lateral acceleration* a_x and a_y, each with the range $\pm 10.24 \frac{m}{s^2}$. The *yaw rate* $\dot{\psi}$ is measured by a MEMS gyroscope, while *yaw angle* and *acceleration* are calculated. To cope with mounting tolerances and road inclination, the sensor offsets are compensated online as explained in App. A.4.

Forces are generally related to the center of gravity of the vehicle. However, for cost reasons the additional sensor cluster module was integrated from the vehicle's center of mass into the ESC. While the yaw rate is independent from the mounting position, the measured accelerations are influenced by rotation and, thus, must be transformed to the vehicle's center of gravity as explained in App. A.4.

2.3.3. Steering Wheel Angle Sensor (STW)

The sensor for the *steering wheel angle* (STW) δ_S is one of the most important components of the fatigue detection system. In contrast to previous publications, a high precision steering wheel angle sensor with a resolution of 0.1° was used. This sensitivity is an enabling property for new innovations, for which the legacy ESC sensor $\delta_{S,ESC}$ has an insufficient resolution of 0.5° or 2°. However, the $\delta_{S,ESC}$ is better secured against failures since it is safety relevant for the ESC. Different vehicle classes have individual assembly requirements regarding packaging space on the steering column, so products from different suppliers are needed. Depending on the manufacturer, the sensor either works according to *optical* or *magnetical* principles as explained in App. A.5.

Depending on the vehicle and steering type (parameter/direct/vario steering), *steering angle* δ_A of the wheel is related to *steering wheel angle* δ_S by a speed dependent curve. For small steering wheel angles δ_S, this curve can be simplified to a *steering ratio* SR factor as described in Eq. (2.3).

$$\delta_A = \delta_S \cdot SR(v_{veh}, \delta_S) \approx \delta_S \cdot SR \tag{2.3}$$

In production assembly, the sensor mounting is affected by a tolerance and there is usually a 3% lateral road trend (for rain water drain), so an offset needs to be estimated and compensated for. For reasons of simplicity, the adaptive *steering wheel angle offset* $\delta_{S,offset}$ is already included in δ_S.

Sensor Aging

Due to the involved mechanics or optics, the steering wheel sensors suffer from aging. Sensors that were intensively exposed to extreme situations were available to analyze whether the sensor prototypes fulfill their specification.

For the precise quantitative assessment of sensor errors, a steering robot (see Fig. 2.5) and a steering wheel angle sensor with 0.0001° accuracy were installed in the cockpit.

The coded discs of optical sensors can suffer from dust that results in "blind spots" of the signal, so that certain quantization values occur less often or never while adjacent values are repeated too often. With the steering robot, perfectly linear triangle movements from -30° to +30° were repeatedly recorded, so that every quantization value was distributed uniformly.

Figure 2.5.: Steering robot SR60 from Anthony Best Dynamics (Source: Anthony Best Dynamics, 2012) to validate steering wheel angle sensor

Fig. 2.6 shows a *discrete histogram* of the steering wheel angle and the reference signal. Fig. 2.7 shows the recorded trapezodial and a zoom of the signal in the time-domain where the gaps and increased occurences can be seen.

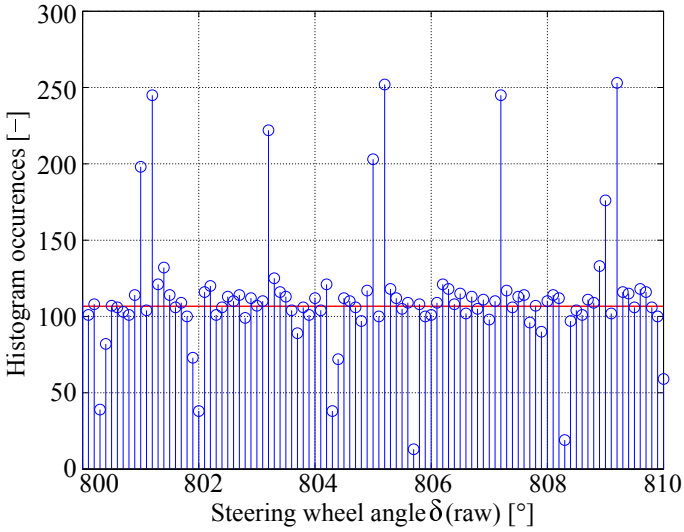

Figure 2.6.: "Blind Spots" in which dust covers a slot of the sensor disc

As Fig. 2.8 shows, aging of the gearing can further result in a *hysteresis* of several samples and non-linearity. To detect such a "backlash" across the relevant sensor range, the large linear triangles were superposed with sines, each with an amplitude of 2°. The backlash could be detected as a plateau at inflection points by comparing of the reference and worn-out sensor signals. Non-linearities could also be detected this way.

Simulations with artificial blind spots have shown that the Digital Polynomial Smoothing and Differentiation Filter (DISPO) (cf. 4.1.1) can cope with up to two blind spots equivalent to 0.2° without significantly affecting the detection rate. Larger blind spots do not allow to detect some fast steering corrections and have a severe impact on the detection rate. An efficient online algorithm was implemented that detects sensor defects from large gaps by exploiting the fact that adjacent quantization values are equally probable. During the beginning of a

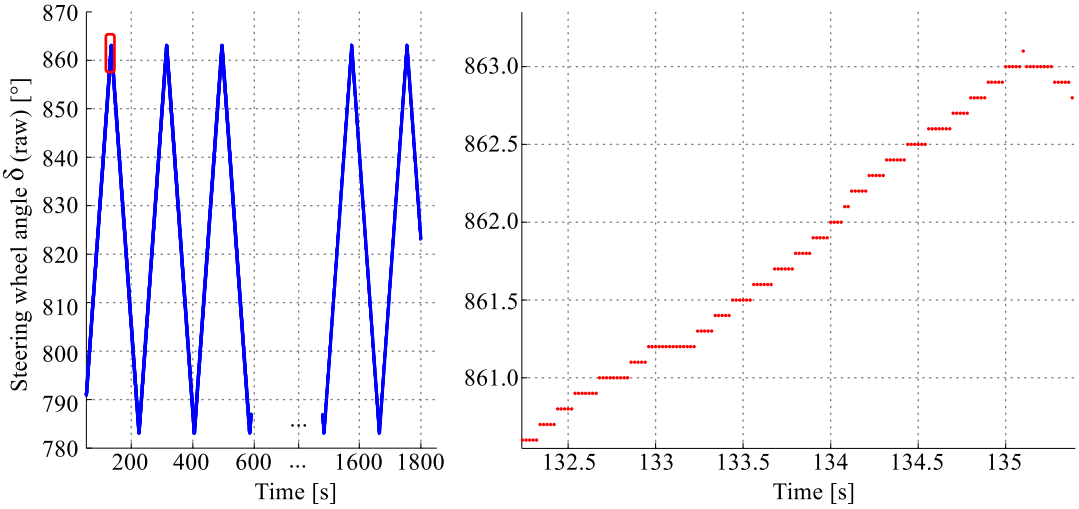

Figure 2.7.: "Blind Spots" in the time-domain

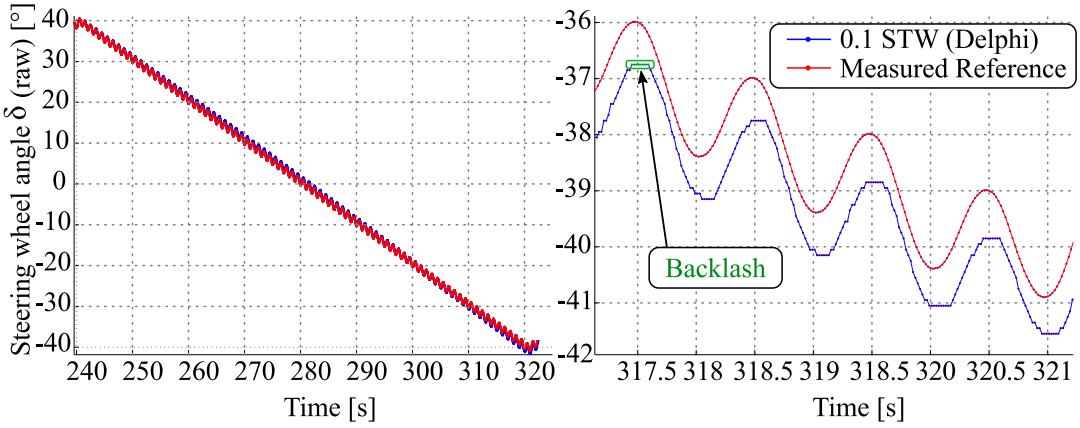

Figure 2.8.: Hysteresis (backlash) in the steering wheel angle sensor

drive, a range of ten adjacent sensor points around the ±10° region of interest is randomly selected. An EWMA filter for every point determines if the occurrence of one or more points is significantly lower after a minimum number of occurrences. If such blind spots are detected by the ESC algorithm after a number of drives, an error code is stored with the instruction to replace the sensor during the next service visit.

Online detection of a backlash is much more difficult since it is not known how long the steering wheel is really stopped at inflection points. Only absence of a hysteresis could be detected, but is not discussed here.

2.3.4. Advanced Lane Departure Warning (ALDW) Assistance Systems

The driver assistance systems *Advanced Lane Departure Warning* (ALDW) and *Lane Departure Protection* (LDP) help to prevent lane exceeding by distraction or late phases of fatigue and micro-sleeps. The systems detect lane markings based on the images of a multiple purpose camera which is available as special equipment. The quality of the lane detection depends on the quality of the lane markings as well as the light conditions and environmental influences like rain or fog (also cf. (Kozak and Pohl, 2006)). Data of a calibrated ALDW

have been used which provided over 35 signals with high accuracy. Tab. A.2 in App. A.3 lists the CAN signals for the system.

2.3.5. Global Positioning System (GPS) Sensor

Global Positioning System (GPS) data are obtained over the regular built-in series GPS sensor through the head unit as well as over an additional USB GPS device (Weiss, 2011). The head-unit additionally provides GPS signals matched with vehicle speed and map data. The signals are listed in Tab. A.1.

2.3.6. Rain and Light Sensor

The rain and light sensor uses an optical photo sensor matrix to detect rain and light through the reflections on the windshield. The reflection coefficient of the front window is measured by a matrix of photo resistors and IR-emitters. Rain is detected as a change of this coefficient while the absolute illumination level is measured at the same time by photo resistors.

2.4. Co-passenger Observations during Night Experiments, Excursions and Free drives

When looking at recorded driving data, it easily becomes clear that the transparency of what happened during the drive is very low, especially if no video was recorded. Aware driving as co-passenger or by one-self provides much more transparency of the actual driving and sleepiness context. *Online* observation of different drivers and driving situations is crucial for identifying fatigue related patterns. Roughly spoken, the intensity of driving patterns, as for instance steering correction, can be experienced live. Some qualitatively noticeable and prominent examples will be discussed here.

Thus, after every night or excursion drive of three to ten hours, plenty of notes were recorded over specific observations, the performance of fatigue measures, and sometimes new ideas for features emerged. Thereby, the focus was particularly on patterns that can realistically and robustly work in practice and in real-time.

For instance, the beginning of a curve after a straight road section was notably often paralleled with steering corrections, quite independently of the driver's state. The consequence is that steering events are subsequently suppressed that result from curve entries.

Moreover, it was observed that the driving performance correlated quite well with a certain pattern for one or a group of drivers whereas other patterns correlated with other drivers. Especially one driver (ID 473) reliably started to approach or exceed the lanes with increasing fatigue levels. The ALDW system, made him aware of his exceedances and was very valuable for this driver. This observation underlined the approach to combine driver clustering and fatigue detection.

It was reported that especially in the free or unsupervised driving, some drivers were not very motivated to drive properly in specific situations. Such a sloppy driving style is generally characterized by loose lane keeping on empty roads, lane exceedances or lane changes without the use of the turn indicator. For instance, in France, where the maximum speed is limited to 130 km/h and where the roads are often very empty, the driver tend to drive in a similar "sloppy" way as with fatigue. The differentiation between unmotivated and fatigue-related

driving style is often very difficult. However, it is plausible to objectively be monitored of such impaired driving performance.

Furthermore, some drivers realized that they have the tendency to drive more to the right, when another car is overtaking. At the other hand, they tend to drive more to the left when driving on the middle or lefter lanes if cars on the right lane are present. This effect is increasing with higher speeds. This was the motivation to compensate driver and situation dependent lateral lane offsets for lane features.

Changes in the driving situation, e.g. during construction sites, tunnels, weather changes, can wake up a driver out of a monotonous fatigue. However, long tunnels can be very monotonous again after some time. It is very clear to see that the driving and especially steering behavior becomes much more hectic within construction sites. For this reason, situation changes were suppressed in the algorithm until driving parameters adapted to the new situation.

Depending on the motivation and experience of the drivers in estimating their KSS fatigue level, some expert drivers were precisely aware of their actual KSS level, with even higher resolution than the scale allows. In this attentive focus, it was observed that the sleepiness level varies much faster than the 15 min long interrogation interval that only summarizes the average level. For this purpose the supervising co-pilot noted additional information about the driver's fatigue level and sometimes revised KSS entries. This also supported the motivation to investigate other fatigue references.

Also, the different reasons for fatigue, whether it is caused by monotony or exhaustion became very experiencable. It was observed that the restrictions "no music", "no talking", "no cold air" have a huge impact on the time until drivers were getting sleepy. Fatigue is very rare on regular roads but traffic accidents are also very rare when we consider that the average driver has an accident every ≈ 400.000 km (Martin, 2006). *Driving condition safety* of the E- and S-Class are very good, for instance due to low noise, precise steering and comfortable seats. Studies from Mercedes-Benz show that these factors significantly support the driver to remain alert for an extended time. For instance, most of the twelve hours drives from Stuttgart to Barcelona in the S-Class allowed subjects to work afterwards or even continue driving. Small, sporty cars are louder and require more steering corrections which is much more exhausting. For this purpose, it was necessary to apply parameters for every vehicle independently with a sufficiently high number of drives. These observations indicate that a driver will be longer "fit" under real circumstances than under the monotonous night experiments. These findings build a basis for the implementation of new and iteratively improved features. The repeated driving experiments were also crucial for the assessment of changed features.

Chapter 3.

Evaluation of Driver State References

During the development of fatigue detection algorithms, the key importance of a good fatigue reference became clear. The performance of the fatigue detection can only be as good as the reference according to which it is optimized. The major problem is to find a "true" reference, also referred to as *ground truth*. However, there is no such objective ground truth for fatigue as there is for alphabetic character recognition, for instance. The behavior of the detection system follows the properties of the reference. For instance, a reference that has a low temporal resolution, will not allow the development of a system that is more dynamic than the reference. For this reason, it is very important that the reference meets the requirements of the system behavior. At the same time, the amount of effort to measure the reference has to be manageable. There are various approaches to measure fatigue in a driving environment. The most promising, non-intrusive and practicable ones will be evaluated in this chapter.

3.1. Terminology and Physiology of Fatigue

Fatigue (from lat. *Defatigatio*) is a discomfort evolving from preceding exertion, disease, suppressed need for sleep or sleep deprivation. In general, it is an imbalance between exertion and rest, due to physical or mental overstrain, induced by lifestyle. Fatigue is marked out as lack of energy, mental or physical exhaustion. Fatigue in a driving context can have different reasons and has various facets and phases. According to Altmüller (2007, page 6), fatigue can have the following reasons:

- Stress overload: too much mental demand that can not be handled provokes drowsiness
- Physical exhaustion: hard physical or mental work can lead to a strong desire to rest
- Sleep deprivation: bad or extended lack of sleep can cause a high pressure to sleep
- Psychological underload or monotonous situations can provoke sleepiness. A lack of motivation can also play a role.

For adolescent persons, fatigue is normal to a certain degree. It is caused by growth, lack of sleep and social or scholar burdens. Oron-Gilad et al. (2007) state that fatigue is influenced by two factors: the driver's initial state before starting the drive and the characteristics of the drive. Both factors have a cumulative property. "Active" fatigue is caused by lack of sleep, and does not necessarily prevent "passive" fatigue (inherent boredom) caused by monotonous driving situations. The sources of active fatigue are homeostatic factors that relate to the neurobiological need to sleep. The longer the wakefulness cycle, the more difficult it is to resist the pressure to sleep (Dinges et al., 1987). Homeostatic factors govern circadian factors to regulate the timing of sleepiness and wakefulness (Mara, 1999). Countermeasures are not very effective if drowsiness is caused by exhaustion. In contrast, fatigue caused by monotony can be overcome by different activating countermeasures.

First of all, we need to define the terminology in regards to fatigue. A definition of the notion can be found in (Brown, 1994; Blanco and Bocanegra, 2009):

Exhaustion Lack of energy and concentration after prolonged execution of working tasks. When a driver is extremely exhausted and deprived of sleep, even caffeine or short pauses do not help any more.

Fatigue The difficulty to remain awake (Philip and Sagaspe, 2005). It is influenced by the circadian rhythm and homeostatic variables (Schmidt, 2009, 1.1). The alertness can be medically and psychologically divided in several stages. These range from unconscious coma to highest excitation (e.g. shock). Fatigue, as perceivable physiological necessity for sleep stands in inverse relationship to alertness and vigilance. Fatigue is a rather slowly changing inner degree of exhaustion and rather a temporal smooth average of vigilance variations.

Sleepiness Physical sleep pressure that a person perceives. In (Philip and Sagaspe, 2005), it is defined as the difficulty to remain awake. It is influenced by circadian and homeostatic variables (Schmidt, 2009). Sleepiness is describing the late phase of *fatigue*, i.e. the fight against sleep which is often accompanied by *microsleep*.

Vigilance (lat. *vigilantia*: wakefulness, sharpness). In physiology and psychology, wakefulness denotes a state of permanent alertness. Wakefulness is a partial aspect of consciousness. Vigilance describes the neuro-physiological level of excitation that modulates the willingness of a person to take action. *Vigilance variations* are referred to as temporal variations in performance. A shock can, for instance, change the vigilance state immediately to wide-awake while the basic fatigue level remains.

Hyper- and Hypovigilance *Hypervigilance* is a medical term for augmented wakefulness and the opposite of Hypovigilance, which stands for increased sleepiness.

Attention The ability of a person to consciously or instinctively orientate (e.g. taking controlled action) as a reaction to different sensory or mental inputs. Attention can be short, mid or long-term and is strongly moderated by simultaneous secondary tasks such as distraction by mental thoughts or side-tasks.

Microsleep Short gaps of unawareness from 0.5 to 2 seconds while the eyes are generally closed. A certain kind of microsleep happens with the eye wide open ("looked-but-failed-to-see" phenomenon (Herslund and Jorgensen, 2003)). When driving on a straight motorway while not having control of the car or taking any action for two seconds, in most cases nothing happens. However, it is often too late to take action in time when driving in a curve or when approaching a preceding vehicle, a construction site or when a reaction to an unforeseen obstacle is needed.

Highway Hypnosis Sleep-inducing ("narcotic") impact of a monotonous driving situation. Prolonged driving in monotonous situations can favor fatigue.

Knowing that one is approaching the target destination has a motivating, arousing effect. It was often observed that this is the case especially for sleepiness induced by monotony.

Fatigue during the night drives recorded in this thesis is mostly induced by exhaustion from a regular work day as well as by monotony since drivers were not allowed to talk or listen to the radio. Otherwise, the experiment would have taken much longer.

There are many aspects related to the physiology of fatigue. In this thesis, the cause or reason for fatigue is of little interest in contrast to the driving performance which is directly related

to the risk of having an accident. Thus, the terms **fatigue**, **drowsiness**, and **tiredness** are used in a similar way to describe the driver's driving performance across the entire range. **Sleepiness** is generally used for the later phase close to falling asleep. The term **microsleep** is used to describe the latest phase and highest degree of fatigue.

3.2. Phases of Fatigue

There is a broad variety of approaches to detect fatigue within a driving context. Before discussing these approaches, it needs to be considered that fatigue consists of different phases to which the approaches are sensitive to. These phases are depicted in Fig. 3.1. A driver monitoring system has to be sensitive enough to detect sleepiness *early before* dangerous situations arise, i.e. phase II.

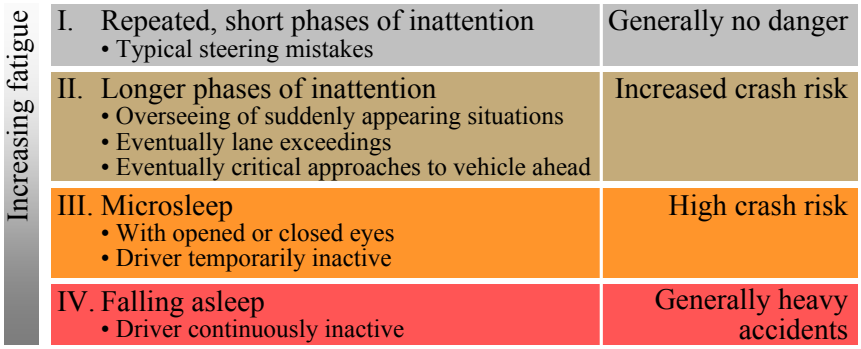

Figure 3.1.: Phases and effects of drowsiness while driving (Source: Daimler, 2007)

3.3. Drowsiness Reference

As mentioned before, the development and optimization of vehicle data based algorithms to detect driver impairment demands a solid reference.

Inattention and drowsiness both similarly result in decreased driving performance whereas most references are rather sensitive to either one of them. An overview over the different approaches to detect fatigue in general was introduced in Sec. 1.5. Since the often used self-rating according to the KSS scale has certain shortcomings, as summarized in (Schmidt, 2009), this chapter compares alternative drowsiness references in a driving context. Especially, a better temporal resolution is of central interest for the development of a drowsiness detection system.

The utilization of *subjective* scales generally has several drawbacks like intra- and inter-individual variation or intrusive influences on the driver. Thus, an *objective* driver alertness metric is desirable if the performance should be sufficiently high and robust.

Different measures were investigated as drowsiness reference:

- Subjective ratings of the driver's fatigue level
- Eye-tracking camera to record blinking behavior and gaze direction
- Electrooculogram (EOG) to electrically monitor eye blinking behavior
- Electroencephalogram (EEG) to measure electric brain activity

In this thesis, EEG, EOG and eye-tracker equipment were only available in certain night experiments as these methods are very impractical and it was not feasible to wire drivers on every drive.

As recording units become more and more mature, camera-based approaches are potential candidates for serial online driver monitoring, including distraction recognition. PERCLOS, introduced by (Hargutt, 2001), is one of the most common measures for drowsiness in literature. In this chapter, an advanced measure of driver impairment is proposed that incorporates eye opening frequency, driver adaptive baselining, head movements, distraction and overtaking suppression.

3.3.1. Subjective Self-ratings and Expert-ratings

Subjective ratings of the driver's fatigue level according to the KSS scale can be conducted in multiple ways:

Online by the driver: aware drivers are "experts" on how they feel and which mistakes they make. However, their judgment may be subjective and impaired by reduced awareness e.g. by sleepiness.

Online expert rating by the co-driver: the passenger can remain awake and attentively observe a sleepy driver. The co-driver perspective allows to directly monitor the driver's behavior, facial expression and gestures while keeping an eye on the driving performance and situations.

Offline expert majority voting: a group of experts may retrospectively assess the driver's fatigue level e.g. by watching video recordings of the driver and the road. Behavioral patterns as eyelid and body movements, yawing, and head nodding (cf. Gallay and Schleicher (2002)) can also be seen in the video, yet not as good as actually being in the car. The video additionally allows to rewind questionable situations. The advantage of the majority voting is that multiple persons can repeatedly estimate multiple drivers which reduces subjective variations. Results from (Wierwille and Ellsworth, 1994) indicate that this is the most reliable and consistent method to estimate fatigue.

The disadvantage of subjective scales is that everyone perceives and understands fatigue and the scales in different ways which makes the self-ratings very difficult to compare. Also the opinion on the level from which a driver considers his fatigue as dangerous varies, i.e. some drivers are more courageous than others. In any case, it is very difficult to compare the fatigue level of different persons as everyone shows different behaviors and physiological patterns.

Unfortunately, expert ratings are much too laborious for the amount of data in this project. For practical reasons, it was decided to use the self-ratings of the drivers since these can even be made with only one person in the vehicle. In night studies, the co-passenger additionally noted the driver's fatigue patterns as well as situations in which the driver's self-rating did not match his/her opinion.

3.3.2. Karolinska Sleepiness Scale (KSS)

Besides the *Stanford Sleepiness Scale (SSS)* and the *Tiredness Symptoms Scale (TSS)* (see Akin, 2007), the most commonly used subjective self-estimation reference is the Karolinska Sleepiness Scale (KSS). This *interval scale* (Bleymüller and Gehlert, 2012) is shown in Tab. 3.1. The KSS was proposed in 1979 by Åkerstedt and Gillberg (1980) and his group.

It is a linear scale with nine levels, assuming that the difference between every level corresponds to the difference in the attention level. The scale ranges from the most awake state KSS 1 to the most sleepy state KSS 9. The next state after KSS 9 would be "asleep".

KSS	Description
1	Extremely alert
2	Very alert
3	Alert
4	Rather alert
5	Neither alert nor sleepy
6	Some signs of sleepiness
7	Sleepy, no effort to stay awake
8	Sleepy, some effort to stay awake
9	Very sleepy, great effort to keep awake, fighting sleep

Table 3.1.: Karolinska Sleepiness Scale (KSS) of Horne and Reyner (1995), modified by Svensson (2004). The colors represent the representation in the touchscreen.

The KSS was recorded during all drives and interrogated through a touchscreen every 15 minutes which was announced by a beep sound. The entries were supervised by the passenger (cf. Sec. 3.3.1). Fig. 2.3 (cf. Sec. 2.2.1) shows an image of the touchscreen display to enter the self-rating. The colors are supposed to suggest *no warning desired* (green), *warning may be issued, but does not have to* (yellow) and *warning required* (red). The use of three colors may already affect the linearity of the scale, e.g. some drivers hesitate to step to the next level, for instance from 7 to 8. However, the benefit of unifying different drivers outbalances this drawback. The colors resolve the region of interest sharper to distinguish whether a warning is required or not.

A large percentage (about 15%) of the drives were set as not valid because KSS entries were implausible or missing due to unmotivated drivers or misinterpretations of the scale. The 15 minutes were chosen as a trade-off between good temporal resolution and avoiding intrusive feedback. As a consequence, there is a certain temporal vagueness and it was not possible to record sudden drowsiness variations caused by different situations. Nevertheless, drivers could make a KSS entry at any time they felt that their level had changed. Sec. 3.3.6 discusses the temporal interpolation of the KSS.

Fig. 3.2 shows a histogram and average of the KSS entries over time-of-day and driving duration. It can be seen that the entries at night are on average four levels higher than during the day. The sudden increase from 21h00 to midnight stems from the continuous arising fatigue level during the night experiments staring in the evening. The average KSS also increases by one level after three and again after 5 hours of driving. Fig. 3.3 shows the KSS entries over age. The average KSS entries in the database are about one to two levels higher between 30 to 40 years in comparison to elder people. It was observed that elder people are more reasonable and tend to give up fighting against fatigue earlier.

In many night experiments, it was observed that drivers are quite well capable of realizing *relative* changes in their attention level but fail in repeatedly estimate their *absolute* level. They compare themself towards previous states while forgetting to focus on the absolute state. As for all subjective scales, the varying interpretation among different drivers is a major problem. The absolute value can vary between different drivers by one, or sometimes even

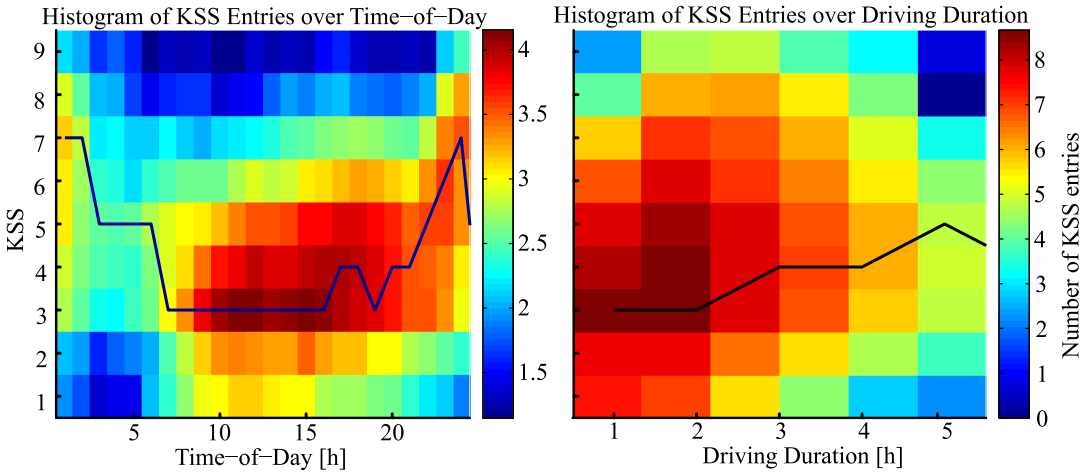

Figure 3.2.: KSS over time-of-day and driving duration

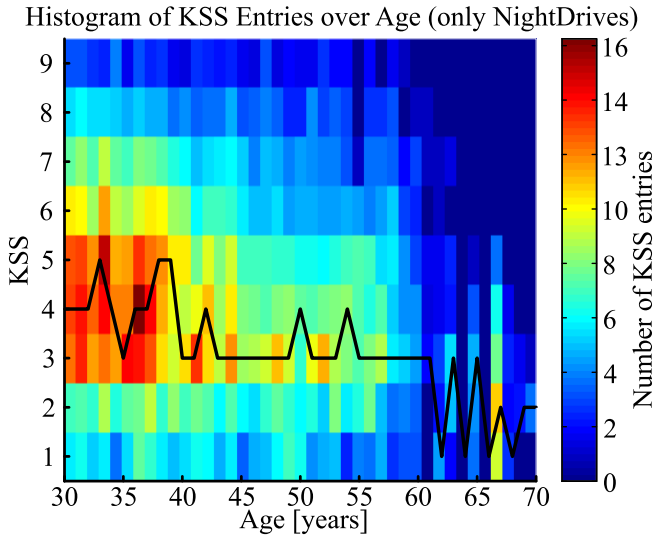

Figure 3.3.: KSS over age

two, levels in the here conducted experiments. Some drivers seem to be quite experienced and certain in rating their fatigue level while others seem to be very insecure.

Basically, the ultimate goal is to assess the safety risk from how well the driver handles the vehicle and not when he/she is tired. For these reasons, it appeared not to be sufficient to solely record the KSS level. Thus, a lot of effort was invested in this thesis in searching for practical and reliable alternatives.

3.3.3. Desired Warning Level (DWL)

The sensitivity to the instant, when to issue a warning to the driver is another major issue and differs among drivers. While some drivers would like to have an early warning as they stop the drive at the first signs of fatigue, others tend to fight the sleep longer. This strongly relates to the acceptance of the system and the system is worthless if it is switched off. Moreover, drivers sometimes realize after a drive that their self-rating was generally too high or too low. The strategy of the ATTENTION ASSIST is to issue an early warning based on the first signs of fatigue and to point out the increased risk of having an accident. Introduced in the

W222, the driver has the possibility to adjust the sensitivity of the system. For these reasons, a *Desired Warning Level* (DWL) was interrogated after every drive. This DWL declares at which KSS level the driver requires a warning to be obligatory. The default desired warning level was considered to be KSS 8. It was provided to drivers as an orientation and asked if they wanted to be warned earlier or later than this.

Tab. 3.2 shows the distribution of the desired warning level based on 10 135 drives.

KSS	Proportion
KSS 6	12.8%
KSS 7	29.4%
KSS 8	56.5%
KSS 9	1.3%

Table 3.2.: Distribution of the Desired Warning Level (DWL) entered by drivers after each drive

3.3.4. Warning Acceptance and Warning Assessment

After every warning that was issued by the ATTENTION ASSIST, a *warning assessment* had to be entered in the touchscreen, whether the warning was *right*, *acceptable* or *wrong*. In the night experiment 2010/03 with 91 drives, the warning acceptance was also interrogated every 15 minutes on how correct a warning would be in this moment. As it can be seen in Fig. 3.4, the warning acceptance does not always match the entered KSS, which indicates contradicting inputs.

Tab. 3.3 shows the confusion matrix on how well the warning acceptance question matches the KSS levels by defining classes under the consideration of the desired warning level (DWL) minus *one* and minus *two*. Tab. 3.4 shows the same confusion matrix but with the tighter definition of *acceptable* as DWL minus *one*.

The overall result shows that the tighter definition of *acceptable* as desired warning level minus one matches the warning acceptance question best. This complies with the button colors in the touchscreen in Fig. 2.3 and supports the class definition in the next Sec. 3.3.5. With these discrete KSS levels, a better class definition is not possible. Since these warning acceptance entries were only continuously interrogated during night experiment 2010/03, only this information can be used for the class definition using the KSS. However, the *warning assessment* of issued warnings provides additional transparency during the refinement of the system. For such transparency reasons and better correlation to alertness variations, the fine KSS resolution of nine levels can not be replaced by the warning assessment.

3.3.5. Definition of Classes *awake, acceptable* and *drowsy*

In regards to the classification algorithms, it is reasonable to define classes of when to issue a warning or not. Additionally, it makes sense to define an early phase, or a pre-warning phase in which the driver and the algorithm are in a "transition phase". This yields the three classes *awake*, *acceptable* and *drowsy* as defined in Tab. 3.5. This definition is based on the KSS entries (cf. Sec. 3.3.2) with and without the desired warning level (DWL) from Sec. 3.3.3 and corresponds to the warning assessment in Sec. 3.3.4.

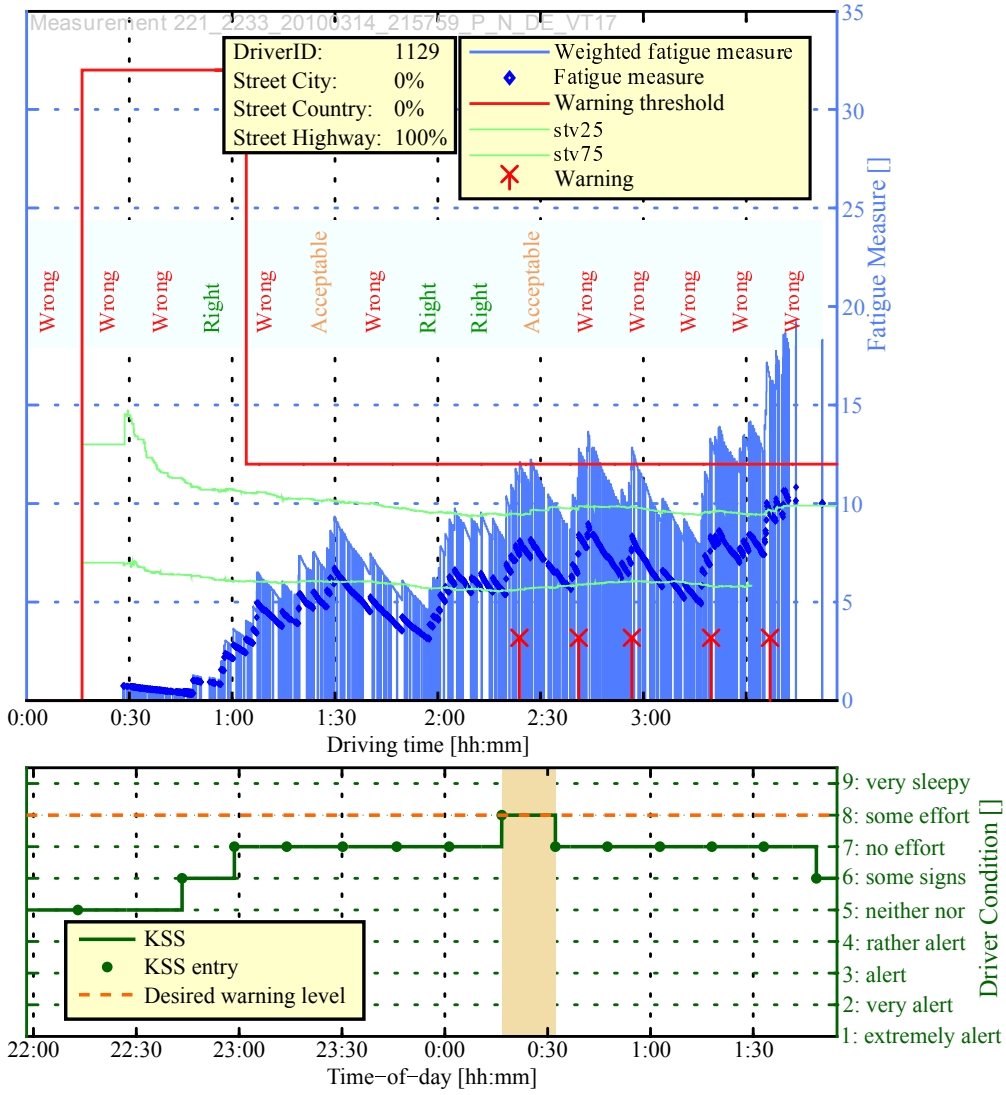

Figure 3.4.: The warning threshold, combined fatigue output and warnings of the ATTENTION ASSIST are shown in this standard toolchain figure. To counter-check the KSS (bottom), the driver is asked every 15 minutes if a warning would now be *wrong*, *acceptable* and *correct* (top). Drivers often contradict themselfs with their own statements. This driver assesses that his fatigue level is only above the warning threshold (DWL) between 2:17 h and 2:32 h of driving while he already assesses a warning to be correct after 0:50 h and 1:50 h of driving. He assesses the first ATTENTION ASSIST warning after 2:25 h during his KSS maximum only as *acceptable* and all later warnings to be *wrong*.

3.3.6. Interpolation of KSS Entries

Fatigue detection must work continuously. Thus, the fatigue reference is necessary more often than every 15 minutes. Moreover, for the calculation of the correlation, it is helpful to have the same sampling rate for all signals. For this reason, the KSS entries must be interpolated appropriately. The KSS is prompted retrospectively from the instant of interrogation back to the last interrogation. KSS entries are thus most accurate shortly before the moments of the entries. To be concise, the values in between regular KSS entries may severely vary

		KSS / desired warning level (DWL)		
		KSS ≥ DWL	KSS = DWL - **1** or KSS = DWL - **2**	KSS < DWL-**2**
Warning Assessment	Drowsy	80.7 %	17.6 %	1.7 %
	Acceptable	22.4 %	64.2 %	13.4 %
	Awake	1.5 %	33.0 %	63.5 %

Table 3.3.: Confusion matrix for warning acceptance and three classes based on KSS and DWL considering the desired warning level (DWL) minus *two* (average correct: 68.5% match)

		KSS / desired warning level (DWL)		
		KSS > DWL-**1**	KSS = DWL-**1**	KSS < DWL-**1**
Warning Assessment	Drowsy	80.7 %	15.1 %	4.2 %
	Acceptable	22.4 %	44.8 %	32.8 %
	Awake	1.5 %	13.4 %	85.9 %

Table 3.4.: Confusion matrix for warning acceptance and three classes based on KSS and DWL considering the desired warning level (DWL) minus *one* (average correct: 80.1% match)

Class	**with DWL**	**without DWL** (motivated by Wierwille and Ellsworth (1994))
Awake	KSS < DWL-1	KSS < 7
Acceptable	DWL-1 ≤ KSS < DWL	KSS = 7
Drowsy	DWL ≤ KSS	8 ≤ KSS

Table 3.5.: Definition of fatigue classes using the Karolinska Sleepiness Scale (KSS) with and without consideration of the desired warning level (DWL)

in any arbitrary way, which, however, were not recorded as additional KSS entries. This information is lost and cannot be recovered by interpolation. However, there are several approaches to fill the time gaps in between KSS entries.

It is obvious that a driver cannot estimate his future fatigue level. Hence, assuming that the driver follows the instructions and enters the KSS always retrospectively for the last 15 minutes, the interval to the *previous* KSS entry can be filled with the latest entry. The last entered value is highlighted in the touchscreen, so that the driver can always see what he/she has entered last. If the driver tries to *permanently* reflect his fatigue level on the touchscreen, filling up the gaps in between entries by holding the last KSS to the next entry would be correct. A trade-off between holding entries and retrospective filling would be the methods *nearest neighbor* or *linear* inter- and extrapolation. Linear interpolation produces *intermediate values* that cause a distribution between KSS values, that depend on the change frequency. This can be undesired, depending on the application. Fig. 3.5 shows the piecewise *cubic Hermite* interpolated KSS as an alternative to linear interpolation.
The correlation between fatigue measures and *discrete* KSS values is not optimal and would be better if the KSS quantization would be finer. The interpolation is more relevant for fast changing levels. The EEG spindle rate in Fig. 3.5 confirms that the fatigue level changes faster than the KSS entries. For instance, it can be seen that the first peaks of the EEG is not represented by the KSS. Sudden variations are also not always recorded and the absolute peak height does not match. Also the time instant of the peaks and minima appear to be slightly shifted. More frequent interrogation of the KSS would however have an intrusive

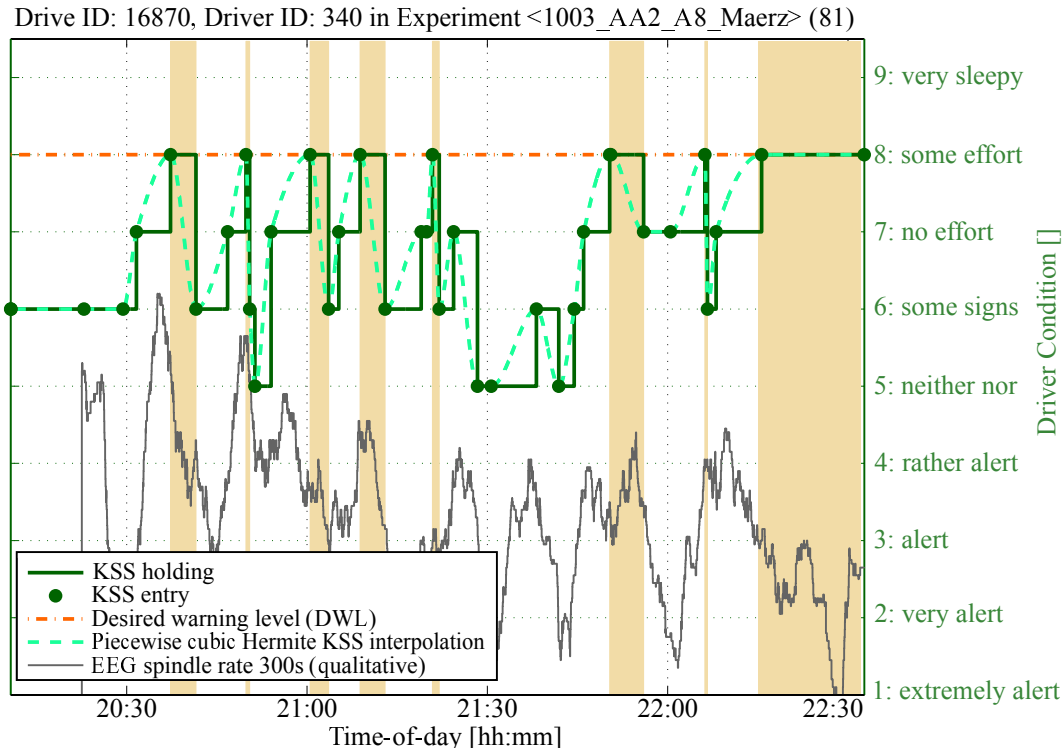

Figure 3.5.: KSS entries, interpolation by holding and piecewise cubic Hermite interpolation. In comparison, the character of the EEG spindle rate is much more similar to cubic interpolation than to KSS holding. However, the dynamic resolution of the EEG signal is still more agile than any KSS interpolation and the peaks are often not synchronous.

influence on the fatigue level of the driver. It must be mentioned that the selected drive is among the ones in which EEG performed best.

The KSS has the highest confidence at the time instants when KSS entries are made. Another approach is thus to just compare the KSS entries to the signal of interest by reducing it to these instants using *aggregation*. This means that the signal values within the time frame of KSS entries are summarized to a single value by using e.g. the *mean* or *maximum*. The latter has shown to be most appropriate for this application, because drivers tend to focus on the sleepiest, most dangerous situation peaks within the last time interval.

In this thesis, linear interpolation is generally used for correlation measures and the assessment of warning instants. Aggregation to the maximum is used for statistical significance tests as the values in between entries contain less information.

3.3.7. Temporal Smoothing Delay of Features and KSS

It was observed that vehicle data based features are delayed due to smoothing with window sizes of several minutes. The EEG spindle rate (cf. Sec. 3.4) in Fig. 3.5 gives an impression of this. EEG signals use a causal low-pass filter that has a window size of about six minutes. It is obvious that all smoothed signals are delayed depending on their window size. When comparing the phase delays of blinking based fatigue measures, which have a high temporal resolution, and KSS entries, it turned out that delaying the KSS by $\tau = 1.8$ min improves its correlation with the blinking based feature PERCLOS. One factor may be that sleepy phases

can occur before the driver becomes aware of them or is willing to admit his sleepiness. In any way, the goal remains to develop features which are reactive to the underlying ground truth. Smoothing with low phase delay is used to obtain good correlation results.

Advantages and Disadvantages of Self-assessment

Schmidt (2009) summarized that research on the self-assessment of vigilance came to contradicting results. Multiple studies showed that self-ratings are not accurate enough to function as reliable and valid indicators of driving performance and reaction time. For instance, Belz et al. (2004) evaluated driver performance in an extended-duration real-world environment of commercial motor vehicles. Without exception, the correlation analyses between KSS and minimum time-to-collision (TTC) and minimum/mean headway yielded that neither of them are valid indicators of driver fatigue. Philip and Sagaspe (2005) reported as well that the self-assessment of the subsequent performance in a reaction time task under prolonged daytime driving conditions was rather poor.

The findings of Baranski (2007) from a cognitive work study with 64 adults suggest that people can accurately assess their own cognitive performance after being deprived of one night of sleep. In a real car driving simulator study with 38 sleep-restricted young adults, Horne and Baulk (2004) found that subjective sleepiness, EEG activity, and lane drifting were highly correlated. Schmidt (2009) argues that drivers are well aware of their deteriorating vigilance, but that early warning signs are often ignored or misinterpreted.

Besides the above mentioned intra- and inter-individual variation, self-ratings are always intrusive, i.e. have an awaking impact. According to Schmidt (2009), the KSS poling has an aftereffect of about one minute in the EEG alpha spindle rate and about two minutes in the eye lid closure and can be neglected. Drivers have difficulties in rating their fitness, especially after more than three hours of continuous monotonous daytime driving with advanced degrees of fatigue. Schmidt has also shown that subjects that feel more awake after long drives, are not more powerful, but rather drive even worse, react slower and have more α-spindles.

Hargutt et al. (2005) investigate the intrusion influence of driver state and driving performance feedback systems. Really drowsy drivers gain small fitness improvements for about 5 to 15 minutes after an interrogation, so the influence is not too strong. Own experiments from (Schmidt, 2009, 2010) and qualitative observations in night experiments generally confirmed this finding.

On the other hand, advantages of interrogating the drivers about their sleepiness levels is very simple and thus relatively robust. If conscientiously used, the probability of intra-individual deviation is mostly limited to one or two KSS levels. Hence, self-ratings are still quite reliable and consistent compared to other automated methods. Despite the inter-individual variations, the drivers mostly know about their drowsiness and have to accept warnings of a drowsiness detection system.

Own observations have shown that at night, especially between midnight and 6 a.m. it is more difficult to estimate one's self-rating. The highway hypnosis and lack of situations that require action makes it difficult to estimate how tired one is. For instance, many drivers have difficulties to estimate their velocity when they have to brake behind a heading truck. Generally, drivers have more difficulties in rating their fatigue levels above KSS 7 and are often not aware that they already had small microsleep events.

3.4. Electrophysiological Measures

Electrophysiological measures that allow inference about drowsiness are, for instance:

- *Electroencephalogram* (EEG) is a commonly used method to directly estimate driver fatigue. Thereby, the electric brain activity is measured in the $\alpha-$ and β-band.
- *Electrooculogram* (EOG) records the eye and lid movement, discussed in Sec. 3.6.
- *Electromyogram* (EMG) records the muscular activity.
- *Electrocardiogram* (ECG) records the electrical heart activity, not just the heart rate.

Electrophysiological measures provide input signals for automatically obtained, direct estimation of a vigilance correlated reference. The ability of electrophysiological measures to predict fatigue was already published under laboratory conditions, but was not yet proven to work for real-road driving. This, however, is necessary to meet the requirements for the development of a series system.

As described by (Schmidt, 2009, 2010), electrophysiological measures are commonly used methods to directly estimate the fatigue level. Hereby, electrodes are attached to the head and body and filled by a conductive fluid to measure voltage differences in the μV domain. Very expensive multi-channel amplifiers are necessary. The synchronous oscillation of many neural brain cells is amplified and measured (see Kirchstein (2008)).

The setup of the electrodes is laborious and, thus, in this thesis only available for a selection of night experiments. Still, the amount of recorded real-road data exceeds previous publications by magnitudes, as for instance (Yeo et al., 2009; Jap et al., 2009; Pal and Chuang, 2008; Svensson, 2004; Thorslund, 2003; Lal and Craig, 2002; Hargutt and Krüger, 2000) who involve 13 to 52 subjects in driving simulators with much shorter driving distances. Fig. 3.6 shows the cap utilized in the real-road drives. Three LEDs with the colors red, orange and green indicate if the conductivity is sufficiently high.

Figure 3.6.: EEG cap used in vehicles

Distraction and fatigue both lead to impaired driving performance due to reduced attention on the driving task. EEG based parameters, however, measure the brain activity, which is high during distraction and low for fatigue. Thus, as confirmed by Simon (2012); Sonnleitner and Simon (2012); Sonnleitner (2012) distraction and fatigue can be distinguished well using EEG.

3.4.1. Evaluation of EEG and EOG as Drowsiness References

For the evaluation of the suitability of EEG and EOG as fatigue references, a night experiment with six drives (2009/09) and a night experiment (2010/03) with 91 drives was performed. Further data from other studies were available. Two S-Class and one E-Class vehicle were equipped with EEG measurement and eye tracking camera. Ten supervisors were trained to avoid systematic distortion due to subjective opinions of single supervisors. Tab. 3.6 shows the routes of the day and night drives.

	Day drives		Night drives	
Num. of Drives:	46	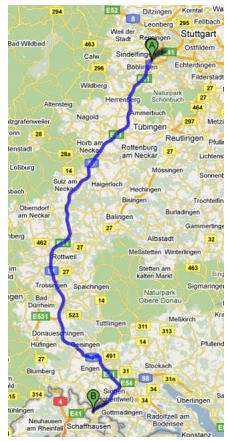	45	
Max. Route Distance:	276 km		434 km	
Total Distance:	11.605 km		13.046 km	
Duration:	2:33 h		4:12 h	
Total Duration:	124 h		181 h	

Table 3.6.: Setup of experiment 2010/03 to validate EEG and EOG as fatigue references

For the recording of EEG and EOG, certain additional steps have to be conducted before and after the drive. Attaching the electrodes to the head takes about 20 to 40 minutes until the impedance drops below 5 – 10kΩ. Doing so, every electrode must be filled with a conductive fluid (silver nitrate) to establish the proper connection to the head skin. After the drive, the cap must be washed and dried to get rid of the fluid as it would dry out and jam the electrodes. This process takes again another 10 minutes. The subject must wash at least once his/her hair immediately after the drive as the fluid gums up the hair after some time. Fig. 3.7 shows the cap with the injection of the fluid. Tab. 3.8(a) shows the different frequency bands of brain

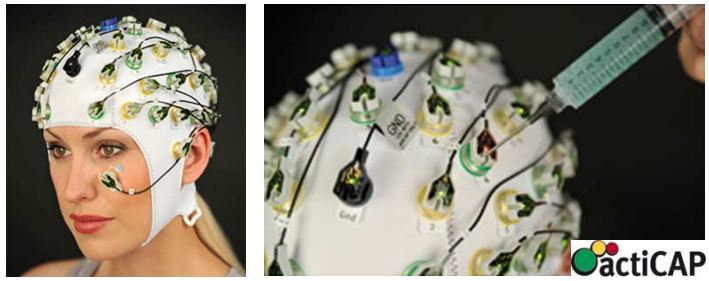

Figure 3.7.: EEG cap in the vehicle (Source: actiCAP)

waves. The alpha band is most related to fatigue and sleep.
An isolation amplifier (5-100 μV) is used for the measurement in every electrode (Fig. 3.8(b)) with a sampling frequency of 250 Hz (min 128 Hz; up to 1 kHz). The measurement can be evaluated against the average of all electrodes or against a single reference (behind the ears or at electrode C_z). Details can be found in (Sonnleitner, 2012).

Delta	0 - 4	Hz
Theta	4 - 8	Hz
Alpha	8 - 13	Hz
Beta	13 - 20	Hz

(a) EEG frequency bands

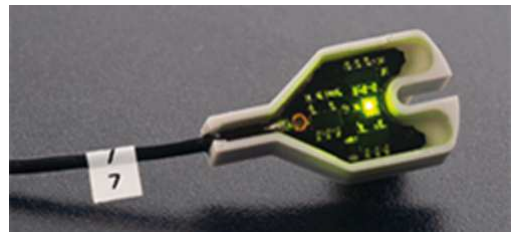

(b) Active electrode

Figure 3.8.: EEG measurement

The international 10/20 system was applied for the electrode placement, depicted in Fig. 3.9. Generally, 24 or 32 electrodes are used, whereas in this study a reduced set of only 16 electrodes and two reference electrodes were used. However, using it as a reference in regular drives is still not possible due to the high effort. In Fig. 3.9, the characters indicate the placement of the electrodes from the front to the back head. The number shows the lateral angle in relation to the middle line.

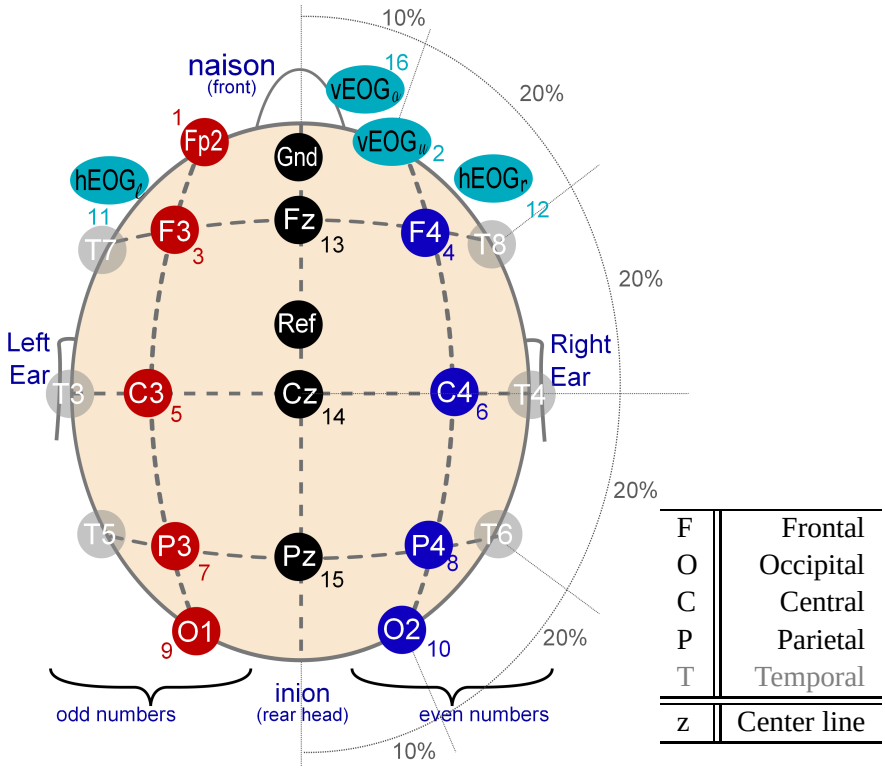

F	Frontal
O	Occipital
C	Central
P	Parietal
T	Temporal
z	Center line

Figure 3.9.: Placement of the EEG electrodes and table with abbreviation characters

Head and body movements produce heavy artifacts due to electric voltages produced in muscles and impedance changes in electrodes. These artifacts highly affect the signal quality. The head movement must be constrained and the inflexible head posture is little convenient for driving. The chin strap slightly pinches off the throat. It has to be assured that driving safety is never affected. There are several post-processing steps required to remove signal

artifacts. Artifacts and countermeasures are, for instance:

- Alternating current and power line hum is removed by a *Notch filter*
- Muscle tension like head movements, gnashing of teeth and chewing gum events are detected and suppressed
- Eye movements in the EEG signals are either compensated by *subtraction of EOG signals under consideration of the spatial distance* or by suppression of EOG Signals using *ICA* (as described in Sec. 3.5.1).

Fig. 3.10 shows EEG signals especially of the frontal electrodes (e.g. F3) that are distorted by EOG (red) and then after the EOG removal using ICA (blue).

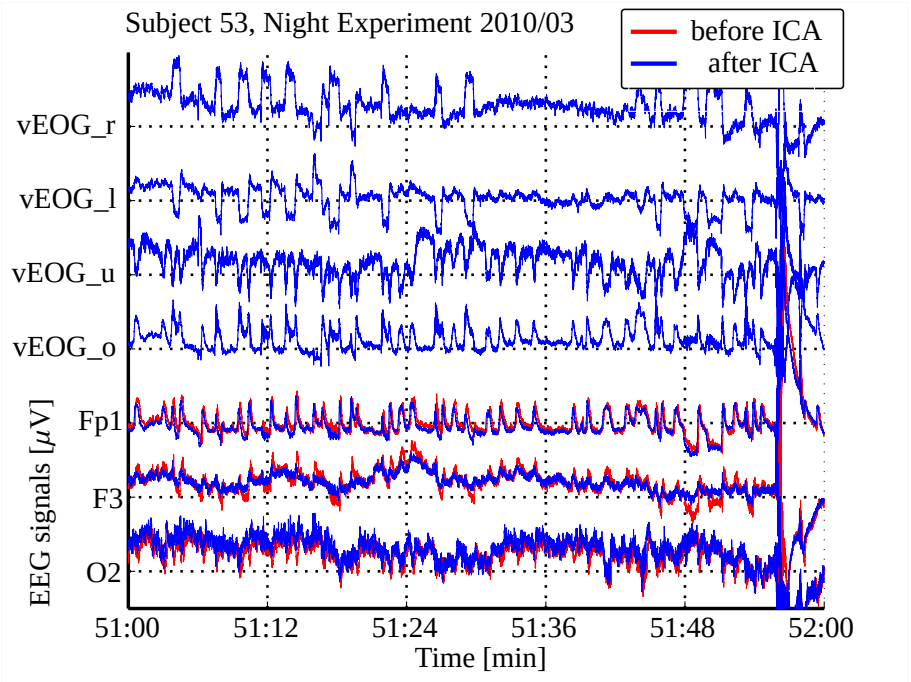

Figure 3.10.: EOG artifact removal in EEG signals before and after using ICA

Alpha spindle rate vs. Alpha band power Based on the data outlined in Sec. 3.4.1, Simon and Schmidt (2011) found that the *alpha spindle rate* and *intensity* is a more sensitive indicator than the alpha band power used in other publications. Fig. 3.11 shows the detection of alpha spindles. Windowing and FFT of $N = 1024$ points are applied to every EEG channel. Here, the overlap is set to $N - 1$ as the offline computation complexity is neglectable. For the detection of spindles in the alpha band, a $1/f$ curve (Fisher-Snedecor distribution) is fitted from the entire signal and used as threshold as shown in Fig. 3.12. The $1/f$ curve is multiplied by a factor and used as threshold to detect alpha spindles.

The detected spindles are filtered by a 60 or 300 second moving average filter. A proposed improvement is to use the EWMA and EWVAR filter as described in 4.1.2. The intensity and duration of the spindles yield separate features. Fig. 3.13 shows both most important features in the alpha band (8-13Hz) for the night drive of test subject 53.

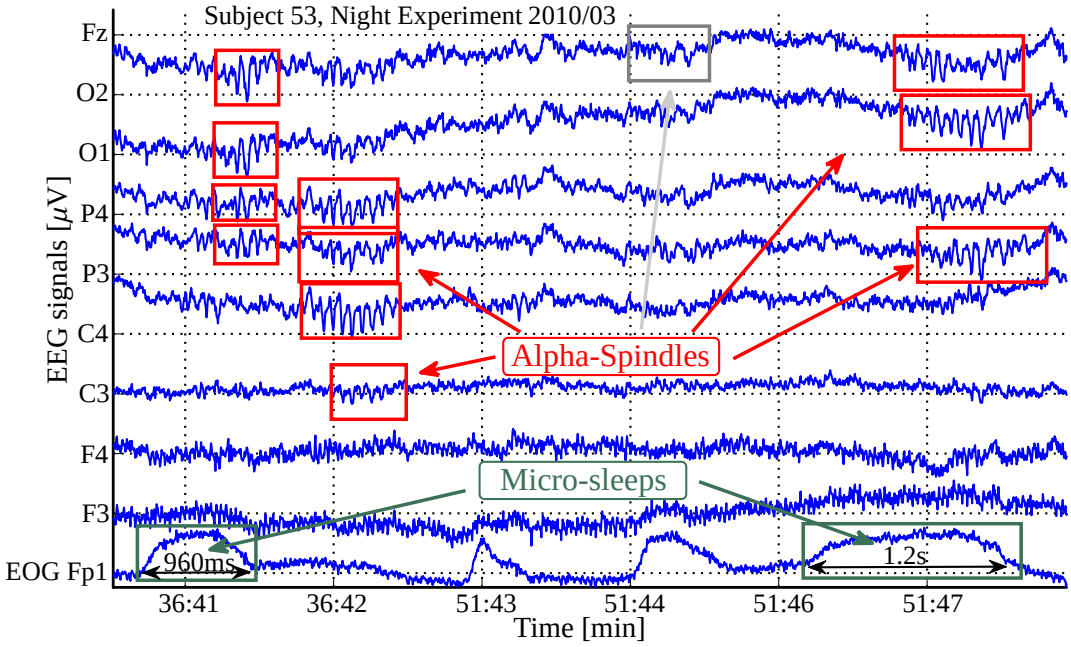

Figure 3.11.: Raw EEG signals in the time domain at KSS 9 with highlighted alpha spindles

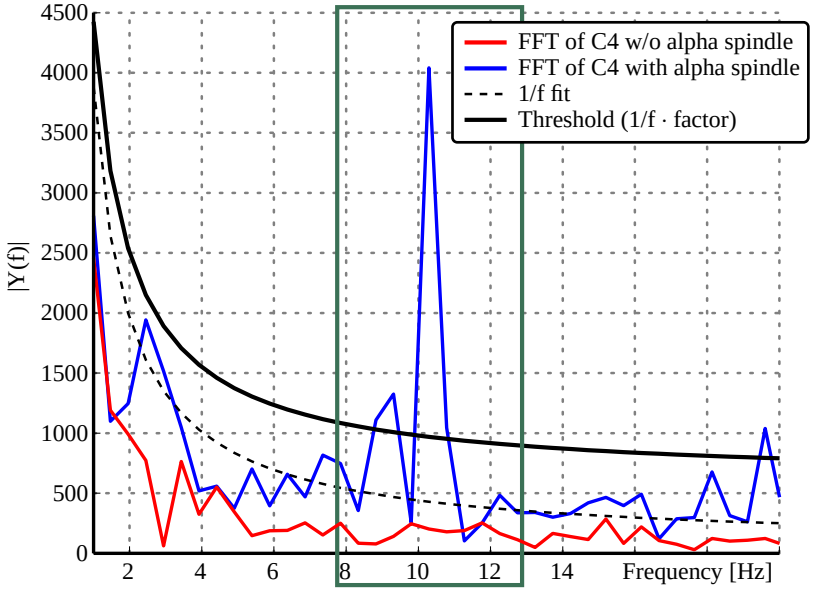

Figure 3.12.: Alpha spindle detection in the frequency domain using an adaptive $1/f$ curve threshold

Different approaches are then used for baselining:

- Warning threshold at $\mu + 3 \cdot \sigma$ (as for outlier detection)
- Normalization to the maximum after the first 20 minutes of active time
- Normalization to the last 10 minutes of the active time for subjects that terminated the drive due to fatigue. This can only be applied offline.

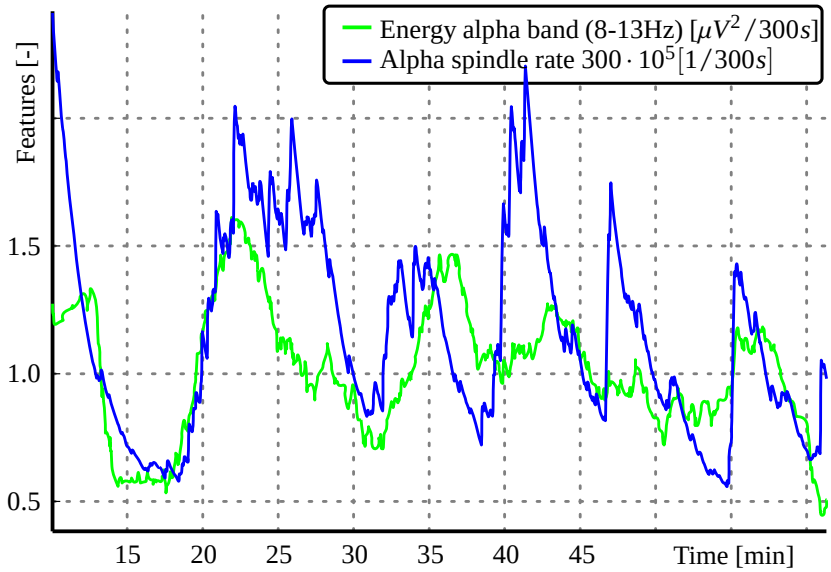

Figure 3.13.: Most important EEG features (Band power and 300s EWMA of spindle rate) in the alpha band

In literature, the summation signal and the occipital spindle rate suit best for the detection of fatigue. Here, an equivalent contribution of every channel was used.

Fig. 3.14 shows different measures of fatigue for driverID 156. The correlation of the signals can be seen quite well. Fig. 3.15 shows the two lane based features of fatigue, `ZIGZAGS`

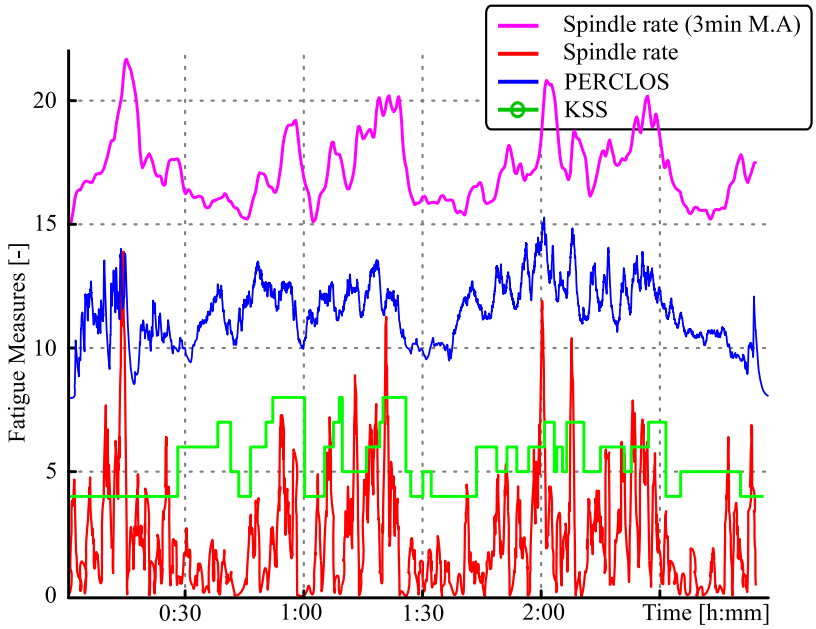

Figure 3.14.: KSS, EEG and PERCLOS have similar slopes and signal runs, but no simple functional relationship. The KSS is entered more often and more accurately here compared to the rest of the drives.

and LANEAPPROXADAPT (cf. 4.3), together with the EEG spindle rate. The similarity of the signals can be seen well, even though the relationship between both functions cannot be described by a simple functional relationship or correlation measures. Fig. 3.16 shows the EEG

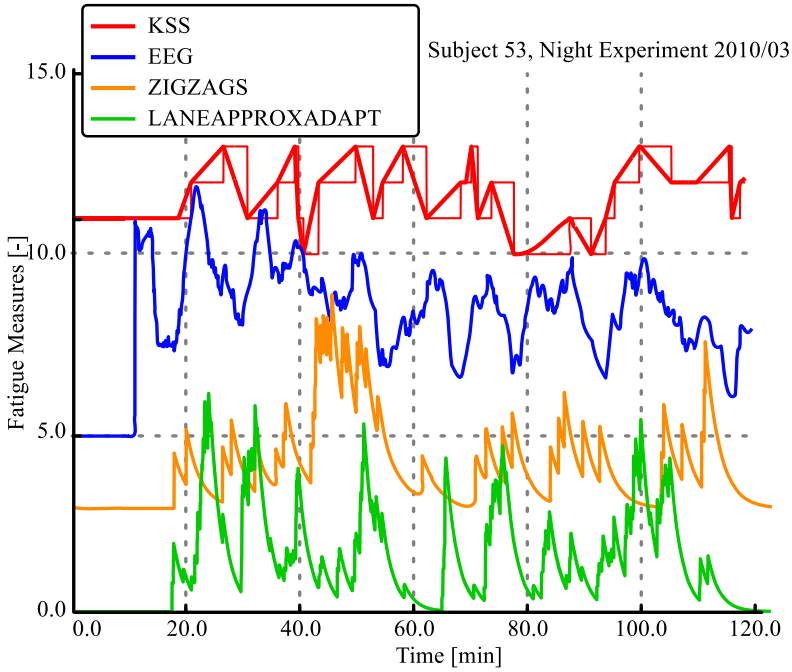

Figure 3.15.: KSS, EEG and lane based features ZIGZAGS and LANEAPPROXADAPT

spindle rate with annotations how external influences have an impact on the alpha spindle rate. The drops in the signal can be related to activating situations whereas the raising slopes can be matched with monotonous situations. Fig. 3.17 shows a histogram of Spearman correlation coefficients calculated between KSS and EEG for every drive. It can be seen that there is a positive correlation for the majority of drives. More statistical results on the presented methods and data can be found in (Simon, 2012; Sonnleitner, 2012; Schmidt, 2010).

3.4.2. Assessment of Electrophysiological-based Fatigue References

In literature, electrophysiological measures perform well for measuring fatigue in simulated environments. However, even the refined methods here could not reproduce this performance under real traffic driving conditions.

The validation of EEG is very difficult since there is no ground truth to reliably assess this reference. Only a few figures and results of drives and features could be presented here. Except for a few drivers, the signal runs reveal that the EEG measures are by far not plausible enough to serve as a reliable reference for the development of a series system. The KSS may have a bad temporal resolution and be wrong for one or two levels, but EEG based features widely behave completely arbitrary and implausible. Especially the absolute values severely vary between different drivers. They severely suffer from intra- and inter-individual variations and external influences. All observations indicate that EEG features rather relate to mental awareness or load than directly with fatigue. They appear to correlate with the attention to "novelty" from external situations.

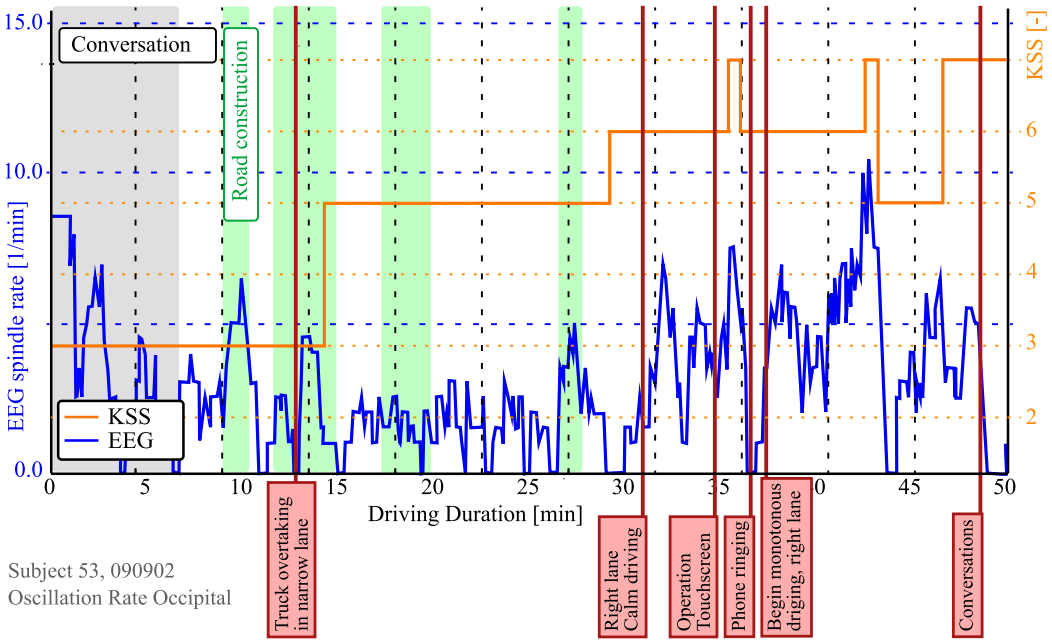

Figure 3.16.: EEG alpha spindle rate with annotations about external influences

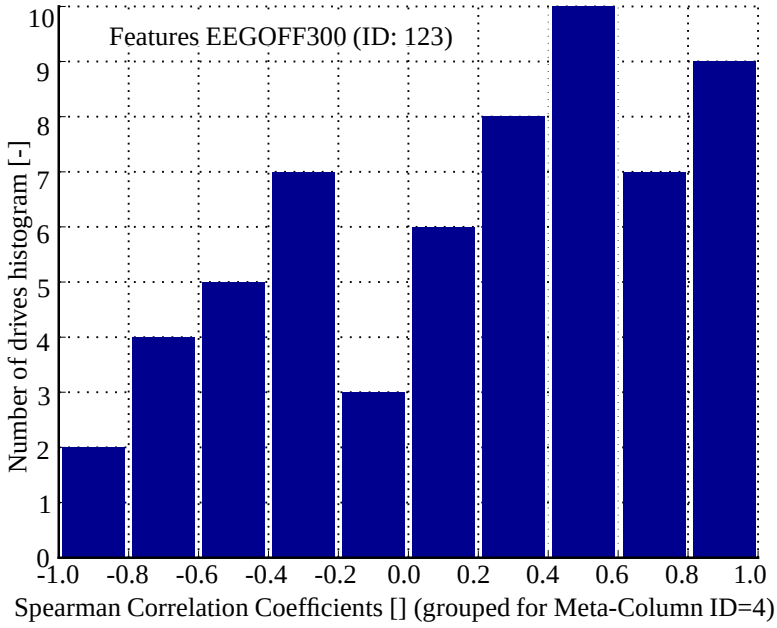

Figure 3.17.: Correlation histograms between KSS and EEG 300 seconds

A major deficiency of EEG is that it does not work for about 20% of the drivers since they have no alpha spindles. Thus, every subject must perform a pre-test to find out whether they produce alpha spindles or not. For some drives, the signals are corrupted due to insufficient contact conductivity of the reference electrodes.

Often, short-term attention can be seen from the EEG signal incline and decay, even if the

absolute amplitudes change over time. Also due to the high purchasing cost of EEG devices and the high effort for its recording, it was only used for a small percentage of the drives. In this scope, one must come to the conclusion that EEG does not provide any additional benefit that counterbalances the additional effort compared to the KSS. Yet, EEG provides additional transparency over short-term changes when manually evaluating the results.

3.5. Heart Rate Tracking from Driver Camera

The *cardiovascular pulse wave* (also called the blood volume pulse) can also be estimated by tiny skin color variations from a simple camera and Independent Component Analysis (ICA) on the RGB channels (see Poh and McDuff (2010)). This approach to estimate the heart rate has also been implemented in this thesis and turned out to well detect the heart rate under good light conditions. Yet, the performance under light conditions in real-world driving or at night with IR-Pods turned out to be not very robust. Since the heart rate has strong inter-individual variations and is not a reliable predictor for fatigue, this approach was not further investigated.

3.5.1. Independent Component Analysis (ICA)

Blind Source Separation (BSS) is a commonly used technique for noise removal from physiological data as for ECG (Chawla et al., 2008) and EEG recordings (Jung and Makeig, 2000). The *Independent Component Analysis* (ICA) (Comon, 1994; Hyvärinen and Oja, 2000) is one BSS method for uncovering independent source signals from a linear mixture of them, observed by several independent sensors. The basic principle behind ICA is the assumption that the source signals $\mathbf{s}(n) = [s_1(n), s_2(n), \ldots, s_N(n)]^{\mathrm{T}}$ are linearly combined to the observed signals, represented by $\mathbf{x}(n) = [x_1(n), x_2(n), \ldots, x_M(n)]^{\mathrm{T}}$ at time instant n. In conventional ICA, the number of recoverable sources cannot exceed the number of observations behind them. This linear mixing can be described as in Eq. (3.1) with the *mixture matrix* A of dimension M $\times$ N of the mixture coefficients $a_{i,j}$.

$$\mathbf{x}(n) = A\,\mathbf{s}(n) \tag{3.1}$$

The goal of ICA is to find a *separating matrix* W, which is the inverse of A for $M = N$ with the estimated output vector of $\hat{\mathbf{s}}(n)$:

$$\hat{\mathbf{s}}(n) = W\,\mathbf{x}(n) \tag{3.2}$$

It is known that the superposition of signals is always more Gaussian than the individual signals. Hence, a cost function that describes the Gaussianity must be defined and minimized by iterative variation of the separating matrix W. The *FastICA* library was available for this purpose. Fig. 3.18 shows the result of the heart rate estimation where $x(n)$ is the spatial average of the RGB channels in the facial region of interest. The three source signals $\hat{s}(n)$ are obtained after ICA and FFT is applied to the sources to search for the most plausible heart rate frequency. As side effects, detecting the heart rate from the driver-camera can also be used for other applications such as emergency stop during cardiac flatline or emotion detection.

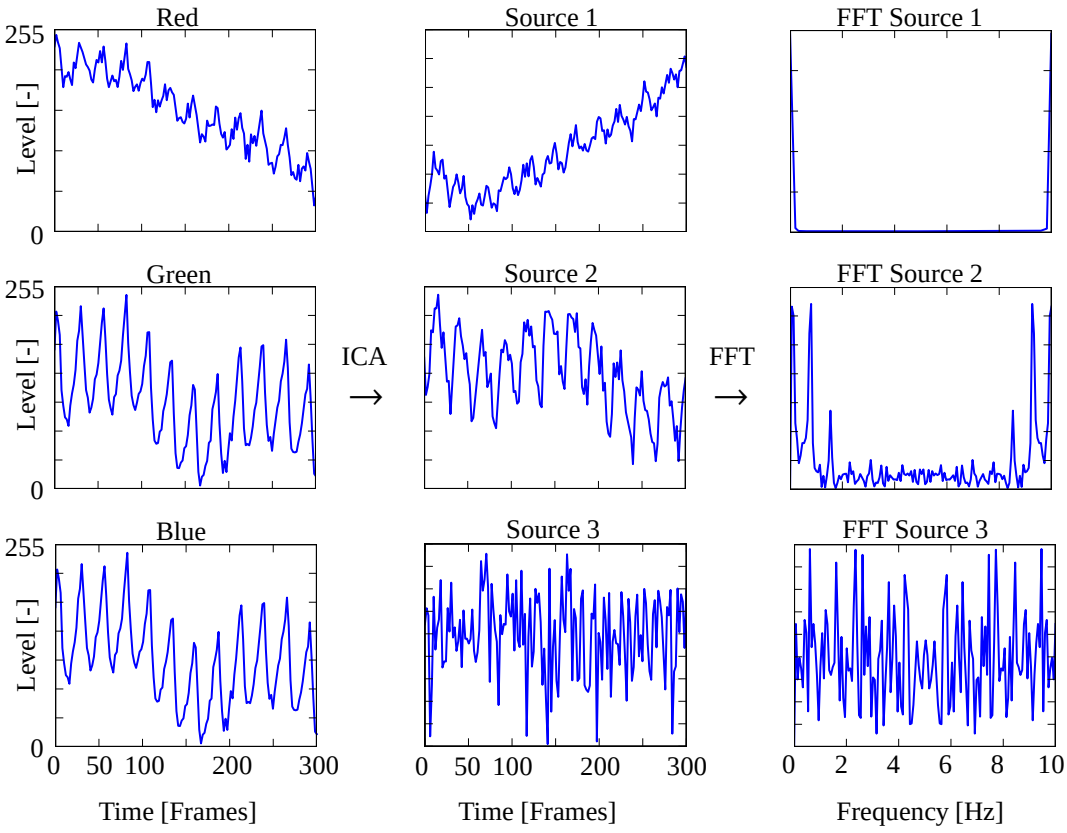

Figure 3.18.: ICA and FFT applied on the driver-camera RGB channels in order to extract the heart rate

3.6. Eye Blinking based Fatigue Reference and Features

Head- and eye-tracking driver-cameras allow another *direct* approach for fatigue detection that is not only suitable as *reference*, but also for *series application*. The target of this thesis was to use camera as reference as well as investigate its series capability. The blinking behavior based on eye-tracking cameras, as well as EOG was analyzed under real traffic driving conditions. Vision based approaches have the advantage that they are not intrusive as no wiring or interrogation of the driver is necessary.

Another major benefit of such eye-tracking systems is the detection of short- and mid-term distraction by the head-position, -rotation and gaze direction ("eyes-on-road"). EOG can also be used to roughly estimate the eye gaze direction.

A disadvantage of camera based detection of fatigue is that micro-sleep can occur with opened, staring eyes. Also, the robustness suffers from poor light conditions and with drivers who wear glasses. Intensive computation for image processing is required.

3.6.1. Evaluation of Eye-Tracking Camera Systems

In this thesis, the latest eye tracking devices *Anti-sleep* from SmartEye, *ESMA* from Denso and *DSS* 1.0 to 3.0 from SeeingMachines were evaluated and compared.

Anti-sleep: The data quality of the Anti-Sleep was almost comparable to the DSS, but required a regular PC, which was not practicable.

ESMA: The embedded ESMA system from Denso with CAN interface could not only detect the head, but also the gaze direction. The data quality, however, was generally quite poor.

DSS: The DSS 3.0 detects head rotations to the side with up to 90° quite robustly. A drawback of the DSS is that it has no direct CAN output for synchronous recording with the main measurement equipment. About 220 subjects across all ages were tested using the DSS 3.0 with the goal to provoke a micro-sleep and PERCLOS warning by looking tired. Only about five subjects with glasses and two with large beards were not sufficiently detected. From version 1.0 to 3.0, the DSS still has problems with persons wearing glasses. While the Denso system can record and process full videos, the DSS records only small eye extracts of micro-sleep events. More details can be found in (Akin, 2007).

The latest *Driver State Sensor* (DSS) from SeeingMachines (2007) was deployed for the experiments, since it showed the most confident data quality.

All systems provide the opening degree signal of both eyes, GPS and other signals such as confidence, head- and eye-signals, depending on the system. Manual conversion and synchronization via GPS time are required for micro-sleep detection and for matching lane changes with head rotations. In this thesis, an own face and eye-lid tracking algorithm was implemented, however, the performance did not compete with the DSS system. The contribution of this thesis was on camera signal *post*-processing and extraction of fatigue, which is at least as challenging as the image processing part.

The video-based drowsiness measures are explained in (Friedrichs and Yang, 2010a). Some popular features extracted from the eye signals were used and new ones are proposed. In addition, for some drives, eye blinking duration and opening duration were derived using EOG in order to evaluate the camera results.

3.6.2. Literature on Camera-based Driver Monitoring

Within the last years, a lot of effort has been made to investigate driver monitoring based on blinking behavior. The book of Moussa (2009) is focusing on the real-time implementation of designing a device for driver vigilance monitoring on a FPGA based multiprocessor platform. In (Sherry, 2000; Batista, 2007), the measure, referred to as PERCLOS (Knipling, 1998; Sayed, 2001) (cf. 3.6.7) was found to be the most reliable and valid determination of a driver's alertness level. PERCLOS is defined as the proportion of time within three minutes in which the eye is closed more than 70% (sometimes 80%). MEANCLOS on the other hand is the average degree of eye opening. Batista (2007) presents a framework for face localization and extraction of eyelid movement parameters. While focusing on facial detection algorithms, he also calculates the measures PERCLOS and AECS (cf. 3.6.7) without further investigating them. Hargutt (2001); Tietze and Hargutt (2001) attached electric spindles to the eyes in order to analyze vigilance and attention within a driving context. They stated that a combination of blinking related parameters is necessary for estimating every vigilance stage. They found out that the blink duration is related to sleepiness (Circadian, sleep deprivation and psychoactive drugs), and verified their results by conducting a driving simulator study with 12 participants. The baselining that they applied made the effects more stable. They described the blinking rate to depend on the work load and to relate to information

processing. The blinking rate, but not the blinking duration, increased with raising time-on-task and decreased during pauses. Picot (2010) recently proposed a fuzzy logic algorithm for drowsiness detection in high frame rate videos. In 60h of driving by 20 drivers, it detects 80% of the drowsiness states. Thorslund (2003) and Svensson (2004) used EOG to estimate the driver's alertness in relation to the subjective self-rating and EEG. Using simulator drives, Svensson reached a 70% correspondence with the self-rating and 56% with the EEG.

3.6.3. Driving Simulator Experiment

A simulator study with 21 test subjects was performed with the focus on evaluating the performance of the DSS 1.0 and the features derived from it. Details on the experiment design and results can be found in (Akin, 2007). Only 27.5% of the micro-sleeps were detected by the DSS 1.0. It was observed that many micro-sleep events occur with opened eyes but the eye gaze direction was not actively monitoring the scene any more. Drivers did not react to road signs or left the lanes. Another conclusion from this and further driving simulator experiments was that even in the most advanced driving simulator, there are severe differences towards real world driving. The night experiment was also very valuable to evaluate the driving performance in the simulator. As already stated by Wierwille (1996b), drivers are more tolerant to lane errors in a simulator than in a vehicle.

Own algorithms for blinking detection and feature extraction were implemented. Details can be found in (Teofilov, 2009).

3.6.4. Database with Eye-tracking Data

Three night experiments and some long free drives was performed with the latest DSS 3.0 camera. In total, 31 real traffic drives (eight with glasses) with valid self-ratings (KSS) and without measurement problems remained:

- 23 real traffic night study drives (7,054 km)
- eight free daytime drives (2,607 km)

The conduction of night experiments and regular drives is explained in (Friedrichs and Yang, 2010b; Schmidt, 2009).

3.6.5. Eye-tracking Hard-/Software

For the extraction of blinking parameters, the DSS with the latest algorithm version 3.0 from (SeeingMachines, 2007) was used which recorded the eye- and gaze direction. The IR-camera unit (640×480 pixels) was mounted in the instrument cluster.

For illumination, two IR-pods were installed on the A-column and over the head unit in a way that reflections on glasses could be minimized. Most glasses are transparent to IR light so that the eyes can be detected well. Here, the Denso system showed an approach to avoid reflections on glasses using precisely synchronized shutters.

For the validation of the signals and algorithms, an additional facial video was recorded and all signals could synchronously be played in a MATLAB GUI (Teofilov, 2009).

The pre-processed signals (Tab. 3.7) were recorded with up to 60 fps to an USB-drive of a portable computer unit. The GPS signals were obtained from an external USB device. The obtained eye blinking, head posture and gaze direction signals were quite good, especially

for drivers without glasses. The confidence measures showed quite well when the left/right eye-lid and head signals were not reliable.

Description	Signal	DSS Signal Name
Eye closure l/r	$e_{l,r}$	LEFT_ / RIGHT_EYE_CLOSE
Eye confidence l/r	$c_{l,r}$	LEFT_ / RIGHT_CLOS_CONF
3D head position	x,y,z	HPOS_FILT_X / Y / Z
3D head rotation	φ,ψ,γ	HROT_PITCH / _YAW / _ROLL
3D head confidence	c_h	HPOS_CONF
GPS time	τ	GPS_GMT_TIME
GPS longitude	λ	GPS_Longitude
GPS latitude	θ	GPS_Latitude
GPS vehicle speed	v	GPS_SPEED_KM_H

Table 3.7.: Used signals from the Driver State Sensor (DSS)

3.6.6. Processing of Eye Signals

This section presents several pre-processing steps that are needed for extracting individual drowsiness-related patterns from the raw signals. The recorded camera data are converted, synchronized and time offset is compensated for the vehicle CAN data using the interpolated GPS GMT-time and velocity signal which is sufficiently accurate. The detection of eye blinks works well for the camera frame rate of 60Hz, but the calculation of the eye-lid velocity becomes more inaccurate. Svensson (Svensson, 2004) stated that the sampling frequency should be high (at least 500Hz) when blinking related characteristics like blink duration are measured. The frame rate often dropped due to windows system resources and caused measurement gaps of up to half a second. These gaps were linearly interpolated in order to keep the timestamps synchronized.

For many features, the derivative and intensity are relevant. Thus, an EWVAR or EWMA filter is applied as described in Ch. 4.1.2. For the calculation of the eye-lid velocity, a DISPO filter was used as explained in Ch. 4.1.1.

Next, both eye signals e_l and e_r are combined to a single eye signal e_c by weighting and normalization with the confidence values c_l and c_r of both eyes.

The *system active signal* SAS_{eye} is defined to be active for a head yaw angle $|\psi| \leq 15°$ to suppress lane changes (i.e. 5-20% of the time, depending on driver and traffic) and for a sufficiently high confidence measure average $\bar{c} = (c_l + c_r)/2 \geq 55\%$. Furthermore, vehicle speed $v \leq 30$ km/h and lane changes using the turn indicator are suppressed. An average active time of about 70-90% remains for most drives while it is lower ($\approx$ 60%) for drivers with glasses.

Detection of Blinks

Another important pre-processing step is the detection of blinks. At first, blinking candidates are searched by applying an adaptive threshold to the eye signal e_c. Then the above described system active signal SAS_{eye} was applied. It is also important to suppress the blink during a head rotation or at the same moment as the combined confidence signal $\bar{c}$ drops below a threshold. 60 - 90% of the blinks have been detected, which is heavily depending on the situation and tracking state. Fig. 3.19 shows some examples of the blinking detection. A major problem are vertical looks to the dashboard, instrument cluster or head-unit. Looks

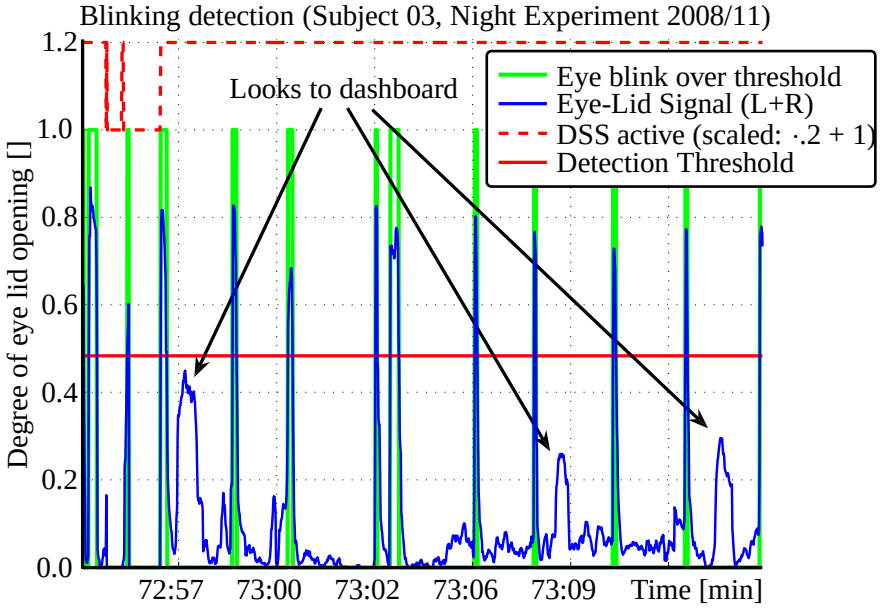

Figure 3.19.: Blinking and look to dashboard detection

to the dashboard can be detected well, since the iris is also lowered towards the dashboard or head-unit, while the iris turns up during an eye blink. Especially in the EOG that detects blinkings via eye ball movements, this property can be utilized well. In the video and signal validation GUI it was observed that eye-ball movements are coupled with movements of the eye-lid:

- Horizontal eye-ball movement: small influence on eye-lid
- Vertical eye-ball movement: relevant change in eye opening amplitude

Such eye movements often occur with short blinks. For this reason, a minimum blink duration of 130 ms was defined to neglect these looks. Then, each blinking candidate that fulfilled several other criteria (min/max duration, shape and minimum amplitude) was labeled as a valid eye blink.

Driver Adaption (Baselining)

An essential contribution to the feature performance is the adaption to the driver, referred to as *baselining*. The inter-individual variation between drivers has a severe impact on the features and overlays the drowsiness-related patterns. It is assumed that the drivers are usually awake during the first 15 minutes of a drive. The *mean* or *maximum* of a feature during this time is then used for normalization. The *maximum* has shown to yield the best results for most features. The *zero-mean unit-variance normalization* (in statistics also called *z-transform*) is the subtraction of the mean and division by the variance. This method was assessed, but finally used in a few cases only. Automatic parameter optimization has found the optimal time frame between 20 and 40 minutes, depending on the feature. 20 minutes is chosen for all features as a trade-off between quick and sufficiently robust adaption, since the active time is often below 50%.

3.6.7. Eye Feature Extraction

From the eye signals returned by the camera system, 23 features, as listed in Tab. 3.8, were extracted for drowsiness detection. The main feature groups are briefly described in this section. Features with superscript [1] are baselined and superscript [2] are own proposals.

ID	CLASS	Feature Name	Description
74	EYE	AECS	Average eye closure speed
75	EYE	APCV	Amplitude/velocity ratio
92	EYE	APCVBL[1,2]	APCV with regression
95	EYE	BLINKDURBL[1,2]	BLINKDUR baselined
78	EYE	BLINKFREQ	Blinking frequency
76	EYE	BLINKAMP[2]	Blink amplitude
77	EYE	BLINKDUR[2]	Blink duration
79	EYE	CLOSINGVEL[2]	Eye closing velocity
86	EYE	OPENINGDUR[1]	Eye opening duration
87	EYE	OPENINGLVL[1,2]	Eye opening amplitude without blinks
80	EYE	EC	Energy of blinking
98	EYE	ECBL[1,2]	EC baselined
85	EYE	MICROSLEEP	Microsleep 0.5 s event rate
94	EYE	MICROSLEEP1S[1]	Microsleep 1.0 s event rate
81	EYE	EYEMEAS	Mean square eye closure
84	EYE	MEANCLOS	Mean eye closure
88	EYE	PERCLOS70	Percentage eyes >70% closed
89	EYE	PERCLOS80	Percentage eyes >80% closed
99	EYE	PERCLOS70BL[1,2]	PERCLOS70 baselined
100	EYE	PERCLOSEWBL[1,2]	PERCLOS80 EWMA baselined
90	EYE	HEADNOD	Head nodding
82	EYE	EYESOFF[1]	Eyes off road
83	EYE	EYETRANS[1]	Eyes transition rate

Table 3.8.: EYE features derived from DSS 3.0 eye-tracker eye-lid signals, sorted according to the underlying pattern. IDs are auto-incremented according to the implementation order.

Blink Duration (ID 77 and 95)

Different methods to estimate the blink duration `BLINKDUR` have been evaluated. Fig. 3.20 illustrates the derived parameters. The blink duration is defined as the time difference between the beginning and the end of a blink, each at the point where half of the amplitude is reached. A better definition is the sum of half the raise time and the fall time (Andreassi, 2000; Svensson, 2004; Thorslund, 2003). The raise duration is measured from half the raise amplitude to the maximum, then to half of the amplitude during the eye closure. Also the *plateau duration* (Fig. 3.20) of an eye blink was calculated. As reported by Hargutt (2001), the eye opening duration has been found to follow a Weibull-distribution. The parameters of the distribution was used for baselining.

Eye Closure (ID 79, 85 and 94)

One of the simplest measures for drowsiness is the `MICROSLEEP` event rate. Events are defined as eye closures longer than 0.5s (1s for `MICROSLEEP1S`). The opening duration is calculated in the same way as for `BLINKDUR`. `MICROSLEEP` events occur in a very advanced and dangerous phase of drowsiness (cf. 3.2). These features indicate fatigue much too late, but are very important when more sensitive methods fail. So a rate of long eye closure events was also worth to be analyzed.

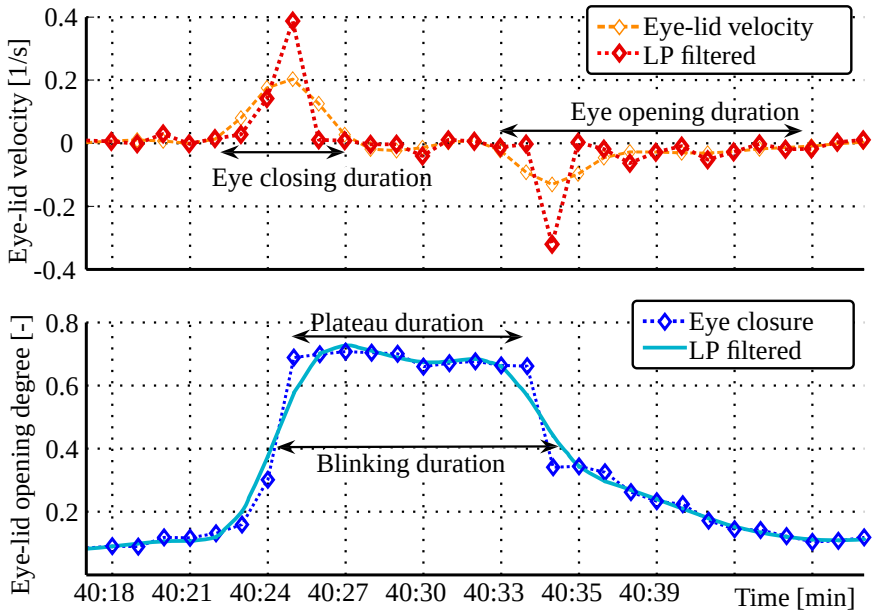

Figure 3.20.: Extraction of eye opening, plateau, blinking and closing duration and velocity from smoothed combined eye-lid signal e_c and its derivative.

PERCLOS, EYEMEAS and EC (ID 80, 88, 89, 98, 99, 100 and 81)

PERCLOS is the most common blinking based measure for drowsiness, first defined by Wierwille and Ellsworth (1994). It is the proportion of time during three minutes in which the eyes are at least 80% closed (cf. Fig. 3.21). Today, there are also other PERCLOS measures:

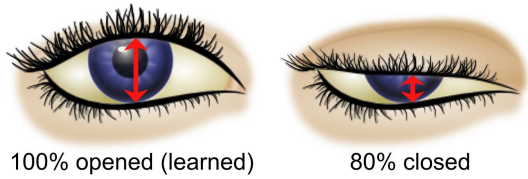

Figure 3.21.: Definition of PERCLOS as proportion of time when the eye is over 80% closed

PERCLOS70, which is the same, but with a threshold of 70% and EYEMEAS, which is the mean square percentage of the eyelid closure rating. EC is the averaged energy of blinks and is closely related to PERCLOS. PERCLOSEWBL is the same as PERCLOS80, but baselined and using an EWMA for averaging (cf. App. 4.1.2).

Fig. 3.22 shows PERCLOS for a night drive. The driver (ID=340) has entered the KSS more frequently and with more care than usual. Thus, it can be seen how well PERCLOS correlates with the KSS ($\rho_p = 0.74$) and EEG spindle rate ($\rho_p = 0.67$) measures. As the KSS entry is retrospectively hold and EEG spindle rate / PERCLOS are filtered with a three minute moving average, all signals are delayed. It is one of the major weaknesses that PERCLOS detects fatigue too late and fails to detect participants that are drowsy with eyes wide open.

Amplitude-Velocity Ratio (ID 74 and 75)

Hargutt and Krüger (2000) found that the ratio of amplitude and maximum blinking velocity APCV can be used well for drowsiness detection. AECS is the average eye closure veloc-

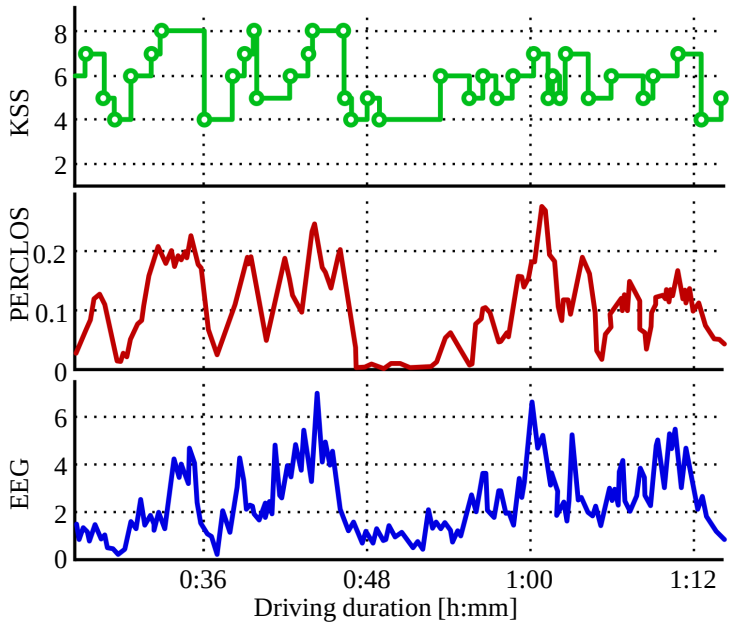

Figure 3.22.: Drive (ID=14 589) with PERCLOS and EEG and a more frequently entered KSS

ity (Batista, 2007; Picot, 2010) that is estimated by the maximum velocity during the eye closure, which is the amount of time needed to fully close the eyes and to fully open them. An individual eye closure speed is defined as the time period during which the eye opening degree $rate_{closure}$ is between $0.2 \leq rate_{closure} \leq 0.8$. The second variant is chosen as it is more practical.

Blinking Rate (ID 78)

`BLINKFREQ` is the blinking frequency. According to Andreassi (2000), a relaxed person blinks about 15-20 times per minute, which drops to 3 blinks per minute when performing cognitive tasks (Svensson, 2004). According to Hargutt and Krüger (2000), an increased blinking rate indicates reduced vigilance. As stated by Hargutt (2001), the blinking rate also increases with driving duration (time-on-task). During driving experiments, it was observed that `BLINKFREQ` varies severely between different drivers and is also related to the air humidity e.g. when using an air conditioner.

Remaining / Mean Eye Opening (ID 84)

`MEANCLOS` measures the mean eye opening between blinks. It was observed that drivers often do not completely open their eyes any more when they become sleepy. This has a lot of potential for the detection of fatigue before micro-sleeps occur.

Head Nodding Frequency (ID 90)

An often observed sign of drowsiness is head nodding `HEADNOD`. It is calculated from the head pitch angle φ with the EWVAR as described in Sec. 4.1.2. The estimation of φ was quite accurate. Drivers often start moving in the seat and move their head to fight sleep. A second reason for head nodding is related to micro-sleep events when a driver lets his/her head fall down and hastily pulls it up again, when he realizes his absence. The variance captures this pattern, but the detection of such patterns poses some potential for improvement.

3.6.8. Eye Feature Evaluation

The Pearson and Spearman correlation coefficients of the best 11 features against the linearly interpolated KSS are listed in Tab. 3.9. The *Bravais-Pearson* coefficient ρ_p is an indicator for linear and the *Spearman* coefficient ρ_s for monoton relationships between two measures (cf. Ch. 7.1.1).

ID	Feature Name	ρ_p	ρ_s
74	AECS	-0.43	-0.45
75	APCV	0.48	0.51
76	BLINKAMP	0.18	0.14
77	BLINKDUR	0.09	0.20
78	BLINKFREQ	0.11	0.04
80	EC	0.14	0.21
81	EYEMEAS	0.07	0.08
90	HEADNOD	-0.23	-0.21
84	MEANCLOS	0.09	0.07
94	MICROSLEEP1S	0.01	0.07
88	PERCLOS70	0.04	0.15

Table 3.9.: Pearson and Spearman correlation coefficients (ρ_p and ρ_s) of 11 EYE features against the linearly interpolated KSS.

In Fig. 3.23, the Spearman correlation coefficients between feature EC (feature-ID=80) and KSS of all drives are shown in a histogram. It can be seen that there is a tendency towards

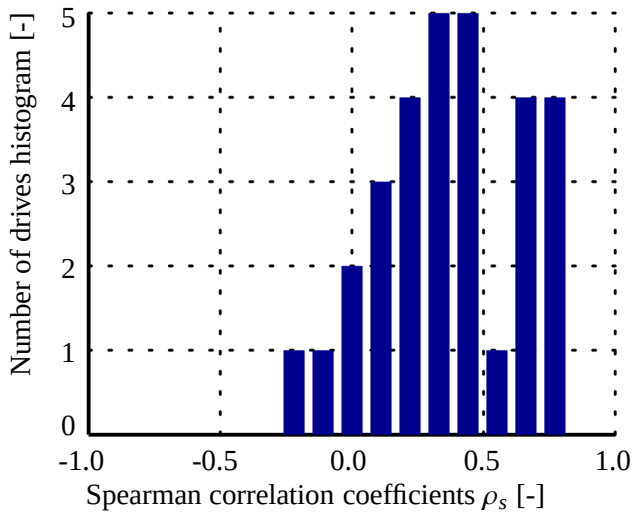

Figure 3.23.: Histogram of ρ_s coefficients between EC (feature-ID=80) and KSS for all drives

the right, which indicates that most drives are positively correlated with drowsiness. The feature's correlation coefficient over all drives is $\rho_s = 0.22$, which is relatively good for a causal feature (Friedrichs and Yang, 2010b). Scatter plots, class histograms and boxplots (Löfgren, 2007) are also used to get a visual impression of the features. The boxplots in Fig. 3.24 show the relationship between different features and the KSS. All plots show that the classes are

severely overlapping, which leads to a lot of difficulties for drowsiness classification. There are no drives with KSS below 3, so these were not included in the plot.

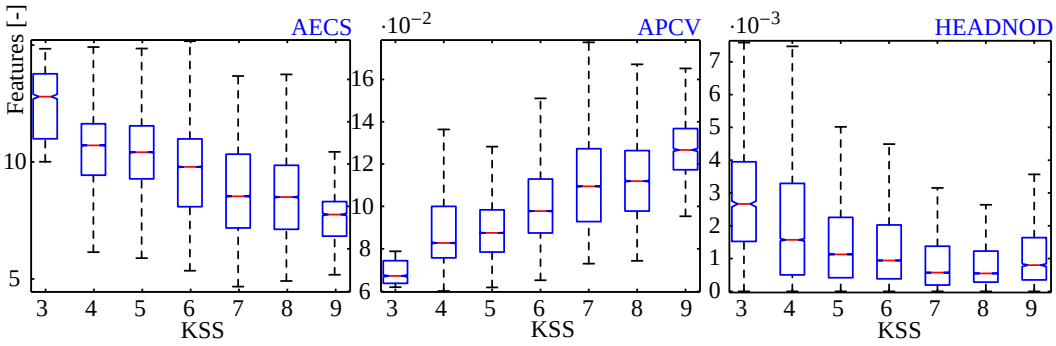

Figure 3.24.: Boxplot of features AECS, APCV and HEADNOD

3.6.9. Classification of Eye Features

The purpose of drowsiness classification is to combine these different features to a single continuous-valued drowsiness measure or the discrete classes *awake*, *acceptable* and *drowsy* (cf. class definition in Sec. 3.3.5).

All features were downsampled to a sampling frequency of 0.5 Hz, as it is assumed that the blinking behavior change is much slower than that. An *artificial neural network* (ANN) was used for classification (Duda et al., 2001).

Theoretically, the more features are incorporated, the more information can be exploited. However, when the number of features gets too high, the need for more training data cannot be fulfilled any more (*curse of dimensionality*). For this reason, dimension reduction techniques are applied. *Principal Component Analysis* (PCA) and *Fisher transform* (LDA) are methods to transform a given feature space to a lower dimensional one. However, the *sequential floating forward selection* (SFFS) algorithm, introduced in (Pudil et al., 1994a), was applied to select the most promising features for a classifier. The advantage of SFFS over feature transform techniques is its high transparency, as the selected features remain without any change. For practical applications that means that only the most relevant features need to be computed. In our study, PCA and LDA have shown poor results in comparison to SFFS. Hence only results achieved by SFFS are reported. Tab. 3.9 shows the most often selected features.

3.6.10. Classification Results for Eye Features

A feed-forward ANN with 25 neurons in one hidden layer was trained with the backpropagation algorithm. The confusion matrix of the ANN classification is given in Tab. 3.10. More classification results for Bayes, *k*-NN, GMM and LDA can be found in (Friedrichs and Yang, 2010a). The results are based on the best eleven features that have been selected by SFFS in combination with the Bayes classifier. The classification results have been obtained by leave-one-out cross-validation with a training to test set ratio of 80% to 20%. It is important to divide the data by entire drives so that the drives in the test set are completely unknown to the classifier. The results are averaged over several permutations of the training/test set to obtain a more stable result.

The total recognition rate with ANN is 83.4%, which is very good and reaches the accuracy of the KSS reference. It is expected that not all third variables related to the experiment drives could be eliminated completely and thus contribute to this good result by over-fitting. For instance, all drivers start awake and become tired after a similar distance where the traffic and environment become more monotonous. The head movements for instance decrease accordingly and the monotony may induce fatigue to the driver. This indicates that the classifier adapts to third variables in the training data that are not present in all real-world drives. This can only be solved by more heterogeneous training data.

True / Detected	**Awake**	**Acceptable**	**Drowsy**
Awake	39.6 %	60.4 %	0.0 %
Acceptable	2.2 %	90.5 %	7.3 %
Drowsy	0.0 %	42.2 %	57.8 %

Table 3.10.: Confusion Matrix for ANN (See Ch. 8.2.4 for definition of confusion matrix)

3.6.11. Discussion of Camera-Based Results

The camera-based results presented in this chapter are quite acceptable. Observations from the night experiments show that drowsiness detection works very well for some drivers, but is error-prone for others. Several of the analyzed features show good potential for fatigue detection. As reported in literature, PERCLOS and features related to the eye opening speed perform best. Thereof, the ratio of blinking amplitude to velocity is a good indicator. Using a higher sampling frequency than 60 Hz would be very valuable for a better estimation of the blinking velocity. For some drivers, also the eye blinking frequency increases with the driving duration and during early signs of fatigue. Another promising observation from driving experiments was that drowsy drivers do not completely open their eyes any more between blinks. It is difficult to find the maximum degree of eye opening since the driver may not fully open his eyes during the start of recording. More sophisticated expert knowledge in the image processing would be valuable here. Microsleep events are also very valuable cues for the detection of the latest phase of fatigue. At least, they are a valuable backup if the detection of the early phases fails.

A general problem of blinking based features is that they detect fatigue too late. Moreover, drivers who are sleepy can have micro sleep events with opened eyes that remain undetected. A major issue of this investigation is that only 1.6% of used data contain fatigue at KSS level 9, at which camera based approaches start to perform best. For safety reasons, it is not possible to allow these advanced fatigue levels on public roads. This is one of the factors, that spoke against using the driver camera as fatigue reference in this thesis. Another finding was that there are severe differences between drivers, especially in regards to their eye blinking frequency. Baselining as described in Sec. 5.4.1 was necessary to improve the results. There are drivers that generally blink rarely (i.e. only every one or two minutes), which makes it even more difficult to estimate a "frequency". As long as the blinking signals were correctly detected (high confidence), the drowsiness could be estimated well from the degrading of the blinking parameters for most drivers. Even after many improvements, the system availability is sometimes low due to various problems:

- Reflections on glasses lead to bad signal quality, see Fig. 3.25(a)

- Varying light conditions during daytime driving pose problems for the eye signal tracking, see Fig. 3.25(b)

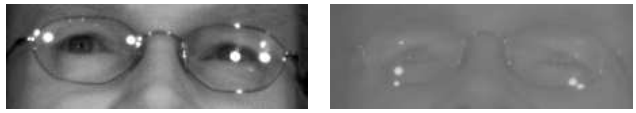

(a) Reflections on glasses (b) Bad light due to sun backlight

Figure 3.25.: Bad data quality

3.7. Comparison of Eye-Tracker and EOG

An alternative to using a camera to record the eye blinking is using Electrooculography (EOG). Similarly as for the recording of EEG, electrodes are attached to the head and recorded over a measurement amplifier (see (Brown et al., 2006)). The challenge of deriving eye blinks from EOG is that not the degree of eye lid opening is measured, but the eye ball movement over muscle contraction. The eye ball moves upwards every time the eye lid is closing. This movement is visible in the EOG signal, as illustrated in Fig. 3.26. Thus, the recorded signal makes only an indirect statement about the eye lid opening degree.

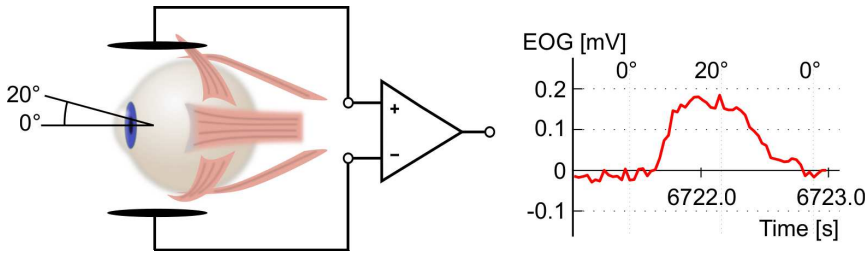

Figure 3.26.: Estimation of eye lid opening using eye ball movement by EOG

In order to estimate the eye lid movement from the eye ball movement, the camera and EOG signals are compared in Fig. 3.27. The similarity between both signal runs can be seen well. Also the scatter plot in Fig. 3.28 indicates a functional relationship that is roughly proportional. Thus, it is concluded that the eye closure can indeed be estimated by the eye lid movement in EOG.

EOG offers several advantage and disadvantages in comparison to camera-based approaches. A major disadvantage certainly are the wires connected to the electrodes that are attached to the head. Drivers of series vehicles would not accept this. EOG, however, ensures an uninterrupted recording, independent of light conditions and head rotations. Moreover, it works equivalently well for drivers with and without glasses.

Looks to the dashboard are paralleled by a light closure of the eye lid and, thus, cannot be distinguished from eye closure by a camera. In EOG, however, looks to the dashboard result in a light movement of the eye ball *downwards* and can, therefore, be distinguished from the upward eyeball movements of blinks. As it can be seen in Fig. 3.27, looks towards the dashboard (represented by black boxes) can be distinguished much better by EOG than using camera based detection.

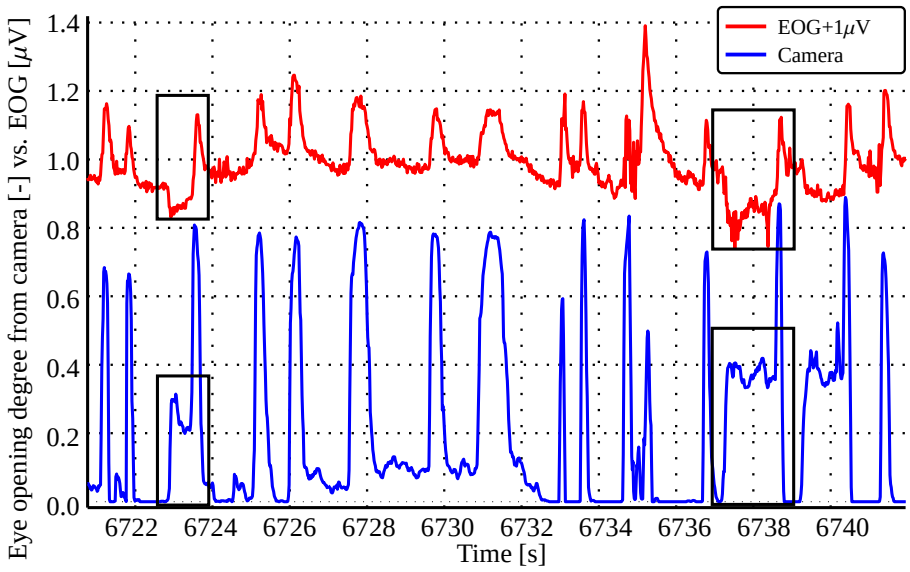

Figure 3.27.: Eye lid closure from camera based eye-tracking and EOG. Comparison of eye blinks derived from camera and EOG: Looks to the dashboard can be distinguished well using EOG, since the eye ball is turning downwards and not upwards as for eye blinks.

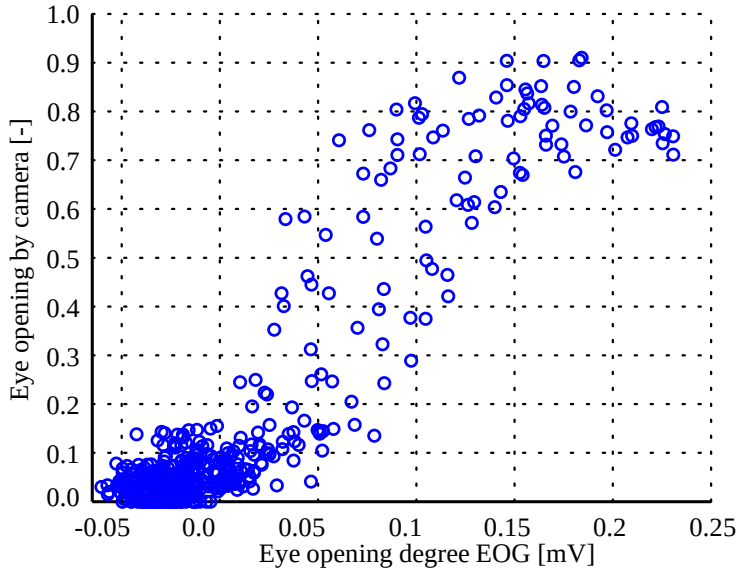

Figure 3.28.: Scatter plot shows a good monotonous relationship between EOG and camera signals

Fig. 3.29 shows the fatigue section of a measurement at KSS level nine. The long eye closure in the middle has a duration of one second and can, thus, be considered as microsleep. It can be seen that long eye lid closures are detected as well by EOG as well as by camera.

Based on the derived blinking signals, the same features (listed in Tab. 3.8) were calculated from EOG as from camera-based eye closure signals. Algorithms and parameters had to be

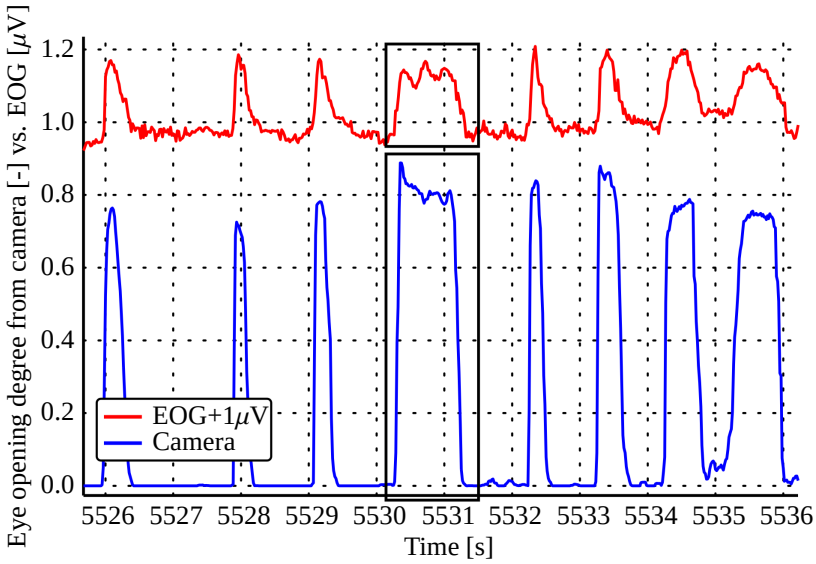

Figure 3.29.: Long microsleep blinkings at KSS 9 from camera and EOG

slightly adapted. Fig. 3.30 shows a histogram of Spearman correlation coefficients between PERCLOS and the KSS. Even if there is a tendency to the right, the drives with negative

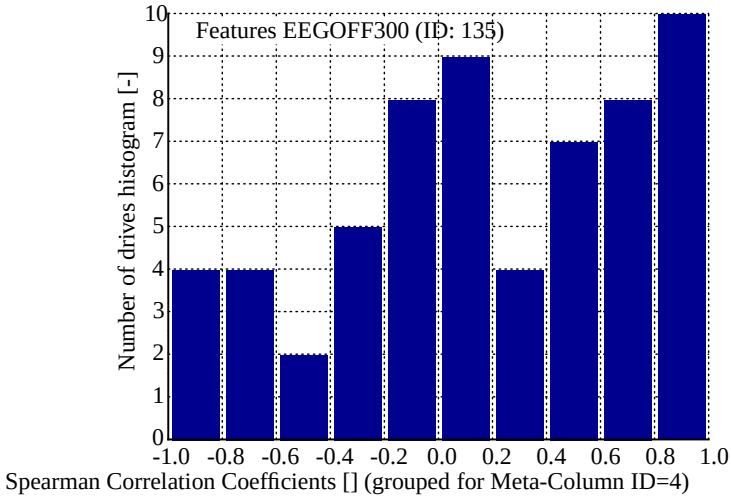

Figure 3.30.: Correlation histograms of KSS and PERCLOS calculated from EOG

coefficients indicate a result inferior to the camera pendant.

3.8. Discussion and Conclusions on Fatigue References

As mentioned before, there is no "ground truth" as fatigue reference which is one of the major challenges in online fatigue detection. The performance of the online algorithms can be at best as good as the fatigue reference, so the goal of this section was to evaluate different

approaches. The principal motivation is to investigate camera and EEG/ EOG based measures to overcome the main deficiencies of the subjective KSS self-rating, like its low temporal resolution and subjectiveness.

Nodine (2008) further investigated the reasons for the weak performances of universal fatigue detection methods and blames it on the large individual differences between drivers. She found that the steering range and variability have the strongest relationship with driver drowsiness, better than EEG or eye closure. She further claims that in-vehicle algorithms can outperform the reference, which however cannot be validated.

As discussed in this chapter, EEG has performed well for a few drivers, but was not suitable as a fatigue reference. This section has shown that the eye blinking signal can also be estimated from the EOG Signal. While EOG and camera-based features show potential for fatigue detection, it turned out at this point that they could not make the desired contribution for the following reasons:

- Recording EEG and blinking signals is laborious, which makes it unsuitable for the large number of free drives.
- The measurement equipment was not consistently available for most drives
- The camera device was not available for most drives and vehicles
- EEG and camera based features suffer from artifacts
- There is no confidence if the detection is reliable or not

EOG made a great contribution for the development of eye-tracking based algorithms.

The original goal to merge KSS, EEG and eye-tracking to a single reference (comparable to SLEEPER1/2/3 in (Wierwille and Ellsworth, 1994; Wierwille, 1996b) or (Hargutt, 2001)) failed because it was impossible to sufficiently validate the single and combined references. Knowing about the deficiencies of the KSS scale, the KSS and self-rated warning acceptance turned out to remain the best reference available and, thus, are used for several reasons:

- Warnings from the assistance system must be transparent and accepted by the *drivers'* opinion, which is most related to the KSS self-rating
- After verification, the KSS is much more robust compared to physiological measures
- The KSS is available for all drives
- The technical KSS recording is very reliable and relatively accurate, whereas EEG and eye-tracking does not work for everybody.

For these reasons, the KSS is used as the central criteria while EEG, EOG, eye-tracking, and distraction are only considered in certain aspects. Even if EEG and camera-based results cannot be used to augment or replace the KSS as a reference, they are still used to assess the vehicle data based features. Furthermore, camera-based features are high potential candidates for online in-vehicle fatigue detection.

The lack of a ground truth reference still poses one of the mission-critical hurdles in this research field.

Chapter 4.

Extraction of Driver State Features

This chapter presents the theoretical background about general signal processing methodologies to extract measures from sleepiness related driving patterns, so called "features". The main part of this chapter explains the pattern extraction of potential features from CAN-signals including their pre - and post-processing. The most essential signals originate from the lane keeping camera-tracker, the steering wheel angle sensor, inertial motion sensors, wheel rotation sensors, light sensors and GPS (as described in Sec. 2.3).

In conventional *machine learning*, feature extraction is a laborious manual process based on models and hypotheses. The most important features are then identified, selected and combined by classification. In *deep learning*, Artificial Neural Networks (ANN) with larger and more sophisticated structures can automatically learn features from raw data. This comes however at the cost of a vast demand of resources: a much larger amount of data and big data cluster and GPU computing are required (such as Hadoop/Spark technologies). Thus, neither the large amount of field data nor the computing resources were available off-board and on-board. For autonomous driving, the cost margin and thus the computation resources are much higher and purpose-designed ASICs and Systems-on-a-Chip (SOC) with a high degree of parallelization similar to GPUs can be designed. In contrast, driver monitoring systems are targeted to require no additional cost and must run on classical vehicle ECUs on top of the base software. For product liability reasons of safety systems in the automotive sector, a major design goal of ESP software are full transparency, model understanding and predictive behavior that is validated. Only few of the vehicle variants are available as prototypes prior to production, so adaption of parameters (so called "parameter application") to new vehicles must be possible without the need of recording training data. Classifiers can only learn patterns that are available in the training data and are generally not suitable for extrapolation. States and hyperparameters of ANNs do not provide the physical representation of parameters and decisions are not very transparent. Especially the extrapolation to operation points outside the range of training data (e.g. for different countries, driving cultures, road properties etc.) is a strength of models used in classical feature extraction. ANNs shall only be used if there is no alternative and if the results justify it. For these reasons, the major focus here was to investigate model based feature extraction in conjunction with machine learning.

Feature extraction is virtually the core of machine learning since it targets the separation of different independent patterns from the irrelevant clutter. The more precisely the features are extracted, the better the performance of classifiers combining these measures to a single continuous-valued drowsiness measure or the discrete classes *awake*, *acceptable* and *drowsy* (See Ch. 3.3.5). Drowsiness can result in different patterns for different drivers or situations. Classification can exploit the combined discriminatory properties of features if they are not redundant. A model based on expert knowledge that precisely understands the coherences is

generally superior to naive automated classification algorithms. This expert knowledge can be incorporated during the feature extraction.

In literature and according to own observations, there is a large number of patterns with drowsiness associative ability. Ideally, every feature is based on one pattern that can be, for instance, a quick steering correction, a lane exceeding, zick-zack lurching in the lane or a delayed reaction to a road unevenness.

Here, CAN-signals have a maximal sampling frequency of 50 Hz (100 Hz for FlexRay), which is necessary to properly detect fatigue related patterns like steering corrections. In comparison, drowsiness is a slowly deteriorating process and changes only within minutes. For instance, a shock induced by an adrenalin rush can wake up a driver within a second, but is not essential for detecting the onset of sleepiness. Hence, it is necessary to extract patterns with at least 50 Hz, whereas for performance reasons, it is not beneficial to aggregate the derived features with a sampling rate higher than 0.5 *Hz*.

Distraction leads to similar patterns as sleepiness and, thus, cannot always be distinguished. But the driver has more control and awareness over his distraction than over his drowsiness. On the other hand, the degree of distraction can change much faster than sleepiness. Since no reference for distraction was recorded, drivers are requested to avoid distraction in order to not affect the fatigue features.

Further, it is proposed to distinguish between *causal* and *a-priori* features. Causal features result from specific patterns that are caused by the driver *because* he is drowsy. A-priori features (e.g. `DAYTIME`) simply indicate that it is *probable* for the driver to become drowsy. Causal features are the most selective and thus most important ones. However, a-priori features are also important as they can make a significant contribution to the system performance. For instance, the (causal) features based on road exits are very probable to result from sleepiness when they occur in a monotonous driving situation (a-priori). A-priori features are discussed in Ch. 5.3 as they are considered in the context of external influences.

Another grouping of features can be made by classifying them into *event-based* and *continuous*. The latter can be calculated permanently, such as the lane deviation (`LANEDEV`), whereas zig-zag events, steering corrections or road exits occur relatively seldom. The fewer the number of events, the worse the temporal resolution of the signal is. A few events within one hour do not allow to make a qualified statement about the driver state. Hence, the goal is to focus on patterns that occur frequently and also catch small events by tuning parameters towards high sensitivity.

Another grouping of features is proposed: *base* features and *functionals* of base features. In the following section, the base features are described. In general, for event-based features, the presence of a single pattern does not directly indicate driver drowsyness. The rate and intensity of these events are relevant. For this reason, further processing steps are applied to the base features such as:

- Moving average, median or exponentially weighted moving average (EWMA)
- Standard deviation, interquartile-range or exponentially weighted moving variance (cf. 4.1.2)

4.1. Pre-Processing

A number of pre-processing steps were necessary before extracting the drowsiness-related features from the raw signals. The proposed methods have several advantages with regards to performance and computation time when compared to the common implementation in literature such as the mean or variance over a moving window.

Since the measurement of the steering wheel angle originates from four different vehicle categories with different properties, they needs to be calibrated. Further, a discrete derivative is necessary for many signals such as the *steering velocity*, the *longitudinal vehicle speed* and *acceleration* from the wheel rotation rate sensors and the *lateral acceleration* from the sensor and from the single track model. This section describes these pre-processing steps.

4.1.1. Digital Polynomial Smoothing- and Differentiation Filter

Many features require synchronized numerical smoothing and differentiation of some input signals. The calculation of the steering velocity $\dot{\delta}_S$, lateral or longitudinal velocity $\dot{y}_L, v_{veh}$ or acceleration $a_{x,whl}$ from the wheel rotation rate $WhlRPM_x$, are a few examples. The difference between two consecutive samples of a discrete-time signal $x[n]$ is given by

$$\dot{x}[n] = \frac{x[n] - x[n-1]}{T_s}, \tag{4.1}$$

with the *sampling interval* T_s in seconds can be described as a simple 1^{st} order FIR filter with the coefficients $b_0 = 1$, $b_1 = -1$ and one division by T_s. However, this difference calculation commonly used in literature (Pander et al., 2008; Bittner and Hana, 2000; Desai and Haque, 2006) increases high frequency components (noise) and, thus, requires low-pass filtering which again has the drawbacks of flattening peaks and shifting the phase.

A more appropriate method for digital smoothing and differentiation is to locally fit a polynomial, referred to as *Digital Smoothing Polynomial Filter* (DISPO). According to (Schafer, 2011), Savitzky and Golay's paper (Savitzky and Golay, 1964) introducing DISPO was rated in 2000 as one of the top 5 papers ever published in the journal *Analytical Chemistry*. Its major advantage is that the signal distribution, width and maximum height of impulses are maintained. The derivative is easily obtained by an analytical differentiation of the approximated polynomial. Savitzky and Golay (1964) have shown that a sliding polynomial-fit and evaluation of the polynomial at a single point is equivalent to discrete convolution with a fixed impulse response (i.e. a regular non-recursive FIR-filter), since the coefficients are constant for a given filter order P and window Size N. The polynomial smoothing and differentiation filter coefficients can be calculated by a least-squares fitting.

For a given input sequence $\mathbf{x}[n]$, $N = 2F + 1$ adjacent points $x[-F], \ldots, x[0], \ldots, x[+F]$ are considered to fit an (over-determined) polynomial

$$p(n) = \sum_{k=0}^{P} a_k n^k \tag{4.2}$$

of order P with $0 \leq P \leq 2F$ at the point of interest $n = 0$. An approximated solution for the coefficients $\mathbf{a} = [a_0, a_1, \ldots, a_P]^T$ can be found by minimizing the sum of squared errors

$$\epsilon_F(\mathbf{a}) = \sum_{n=-F}^{F} \Big(p(n) - x[n]\Big)^2 = \sum_{n=-F}^{F} \left(\sum_{k=0}^{P} a_k\, n^k - x[n]\right)^2 . \tag{4.3}$$

By introducing the notations

$$\mathbf{M} = \underbrace{\begin{pmatrix} 1 & -F & \cdots & (-F)^P \\ \vdots & \vdots & \ddots & \vdots \\ 1 & F-1 & \cdots & (F-1)^P \\ 1 & F & \cdots & F^P \end{pmatrix}}_{\textit{Vandermonde matrix } \mathbf{M}\in\mathbb{R}^{(2F+1)\times(P+1)}}, \quad \mathbf{a} = \underbrace{\begin{pmatrix} a_0 \\ \vdots \\ a_P \end{pmatrix}}_{\mathbf{a}\in\mathbb{R}^{(P+1)}}, \quad \mathbf{x} = \underbrace{\begin{pmatrix} x[-F] \\ \vdots \\ x[+F] \end{pmatrix}}_{\mathbf{x}\in\mathbb{R}^{2F+1}}, \tag{4.4}$$

the cost function from Eq. (4.3) can be written as

$$\epsilon_F(\mathbf{a}) = \|\,\mathbf{M}\,\mathbf{a} - \mathbf{x}\,\|^2. \tag{4.5}$$

The least squares solution $\mathbf{a}^*$ is obtained if the derivative of the error by all polynomial coefficients $\mathbf{a}$ is minimized:

$$\frac{\partial \epsilon_F(\mathbf{a})}{\partial(\mathbf{a})} \stackrel{!}{=} 0, \qquad \text{yields } \mathbf{a}^* = \underbrace{(\mathbf{M}^T\mathbf{M})^{-1}\mathbf{M}^T}_{\mathbf{M}^+}\mathbf{x} \tag{4.6}$$

where $\mathbf{M}^+$ is the *Moore-Penrose Pseudoinverse* of $\mathbf{M}$.

The smoothed output value is obtained by evaluating the polynomial at the central point $n = 0$, which is $y[0] = p(0) =$. The next output $y[1]$ is again obtained by shifting the analysis interval to the next sample to the right. As shown in (Savitzky and Golay, 1964; Schafer, 2011), this is equivalent to a convolution with a fixed set of weighting coefficients $\mathbf{h}(n)$. Since only the coefficient a_0 is needed, $\mathbf{h}^T$ is the 0th row of $\mathbf{M}^+(0,\ :)$ from Eq. (4.6). Since $\mathbf{M}^+$ is independent of the input samples it can be pre-computed for a given $2F+1$ impulse response length and polynomial order P. The smoothing is stronger, the more overdetermined the polynomial (i.e. the closer P to N) is. This applies for lower polynomial order P and is large window sizes N.

The first derivative of $p(n)$ from Eq. (4.2) can be calculated analytically by

$$\frac{\mathrm{d}p(n)}{\mathrm{d}n} = \sum_{k=0}^{P-1} (k+1)\, a_{k+1}\, n^k \,. \tag{4.7}$$

With the differentiation matrix $\mathbf{D}$

$$\mathbf{D} = \begin{pmatrix} 0 & 1 & 0 & 0 \\ 0 & 0 & \ddots & 0 \\ 0 & 0 & 0 & 1/P \\ 0 & 0 & 0 & 0 \end{pmatrix} \tag{4.8}$$

we obtain the differentiated sequence $\dot{\mathbf{y}}[n]$ by applying the differentiation matrix as derived in Orfanidis (1995, Ch. 8.3.5)

$$\dot{\mathbf{y}}[n] = \underbrace{\mathbf{M}\mathbf{D}\mathbf{M}^{+}}_{\mathbf{H}}\mathbf{x} \tag{4.9}$$

$$\dot{y}[n] = \mathbf{h}_d^T\mathbf{x} = \sum_{i=0}^{N-1} h_d[i]\,x[n-i] \tag{4.10}$$

with $N = 2F + 1$ and $\mathbf{h}_d^T = \mathbf{H}(1,:)$ as the 1st row of $\mathbf{H}$.

The phase delay of the FIR smoothing and differentiation filter is $\tau = (F+1)\cdot T_s$ and higher than for recursive filters, which is not problematic for this application. The signal needs to be synchronized with signals that are not filtered and for the correct amplitude the sampling frequency F_s must be multiplied. Fig. 4.1 shows for instance the steering wheel angle and its

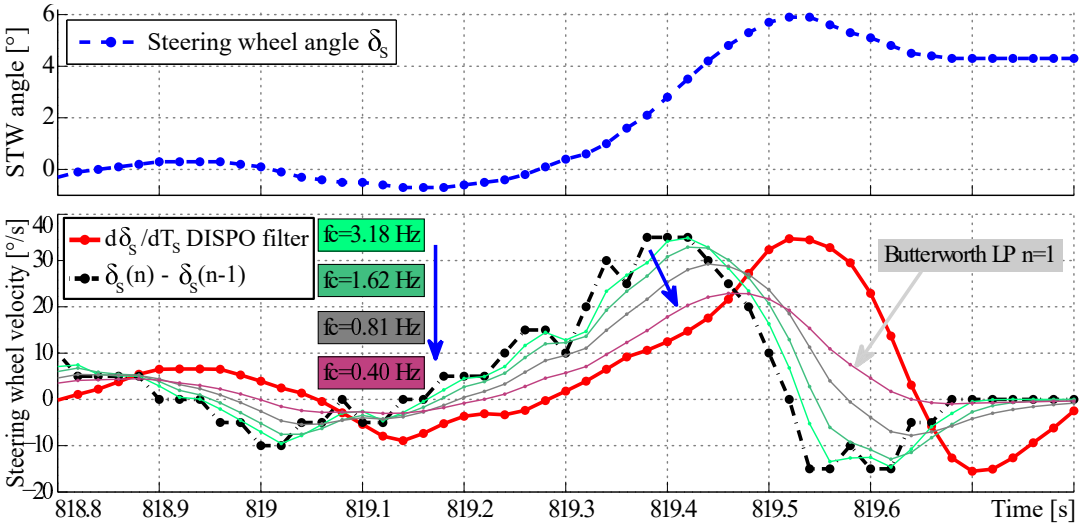

Figure 4.1.: Different methods to differentiate signals.

derivative obtained by the common and proposed method. Using a low-pass *Butterworth* IIR-filter with weak filtering i.e. a high cut-off frequency f_c (black dash-dotted line), preserves the peak height at the cost of a high noise. Stronger filtering, i.e. low cut-off frequency smoothes the signal but flattens the peak of the derivative. Since in the present application, the maximum steering velocity shall be determined with high robustness, the DISPO FIR filter properly preserves the impulse height while smoothing the signal (red solid line).

Application to CAN Signals

The steering wheel velocity in Fig. 4.1 is smoothed and derived by a DISPO filter of order $N = 13$ and polynomial order $P = 5$. These parameters are the best trade-off between preserving the peak height and avoiding toggling around zero for zero-crossing detection. Both yield a fix phase delay of $\frac{N+1}{2} = 7$ samples. The related smoothing and differentiation coefficients h and h_d are illustrated in Fig. 4.2.

The longitudinal acceleration $\mathbf{a}_{x,whl}$ is obtained by a DISPO differentiation filter with the same coefficients as in Fig. 4.2 on vehicle speed from the wheel rotation sensors in Ch. (2.2)

$$a_{x,whl}[n] = F_s \sum_{i=0}^{N-1} h_d[i]\, v_{veh}[n-i]\ . \tag{4.11}$$

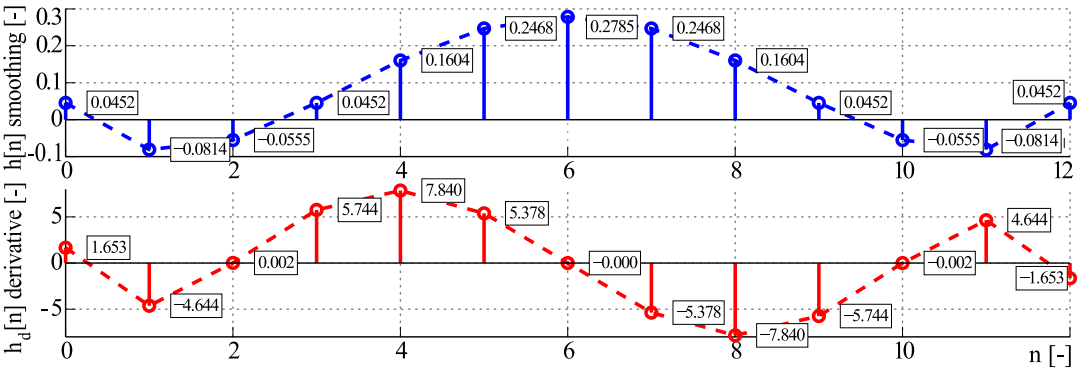

Figure 4.2.: Impulse response of smoothing and differentiation DISPO filter for $N = 13$, $P = 5$.

4.1.2. Exponentially Weighted Moving Average and Variance

Commonly, a regular moving average (MA) filter is used for signal smoothing or for calculating event rates (cf. Altmüller, 2007; Batavia, 1999; Schmidt, 2010; Bittner and Hana, 2000; Pander et al., 2008; Fairbanks et al., 1995; Desai and Haque, 2006; Löfgren, 2007, etc.). A simple, but very powerful improvement is the introduction of a recursive Exponentially Weighted Moving Average (EWMA) IIR-filter. In Sec. 4.1.1, the DISPO filter is primarily used for differentiation of continuous signals and smoothing of it's base signal with synchronous phase delay. However, this FIR-filter requires a high filter order and thus high computational cost. In comparison, EWMA severely reduces the phase delay and computational complexity since only one value must be stored instead of the entire window length. Secondly, this has the advantage of taking present values more into account than old values. EWMA is primarily used for the calculation of event rates.

Following the same principle, it is further proposed a way to approximate the sliding variance by an Exponentially Weighted Moving Variance (EWVAR) for a given *input signal* $x[n]$. The *forgetting factors* λ_μ and λ_{σ^2} are used from the adjusted window sizes N_μ and N_{σ^2}:

$$\lambda_\mu = \frac{N_\mu - 1}{N_\mu}, \qquad \lambda_{\sigma^2} = \frac{N_{\sigma^2} - 1}{N_{\sigma^2}}. \tag{4.12}$$

The EWMA $\mu[n]$ is calculated by weighting the previous average $\mu[n-1]$ and the current input sample $x[n]$ for the initial value $\mu[0] = x[0]$ by

$$\mu[n] = \lambda_\mu \cdot \mu[n-1] + (1 - \lambda_\mu) \cdot x[n]\ . \tag{4.13}$$

The EWVAR $\sigma^2[n]$ can be approximated using the EWMA $\mu[n]$ from Eq. (4.13) by

$$\sigma^2[n] = \lambda_{\sigma^2} \cdot \sigma^2[n-1] + (1 - \lambda_{\sigma^2}) \cdot (x[n] - \mu[n])^2 \tag{4.14}$$

with the initial value $\sigma^2[0] = 0$. For the EWVAR, the same window sizes have been used for both forgetting factors: $\lambda_\mu = \lambda_{\sigma^2}$.

Further, EwmaN and EWvarN were introduced as a special case of EWMA and EWVAR, where only the last N non-zero samples are taken into account. For samples that are zero, the update calculation is omitted and the memory value is kept. For instance, the maximum

steering velocity between inflection points is event-based and if the frequency of these events should not be considered, only the events must be considered.

EWIQR is introduced similarly to EWVAR , however with the Interquartile Range (IQR) instead of the variance. EWIQR is calculated by sorting the values in the preceding sliding window and calculating the range for 50% of the central values.

Fig. 4.3 illustrates the EWMA and EWVAR applied to the lateral acceleration $\mathbf{a}_{x,SC}$. It can be seen that the EWMA and EWVAR approximations (––) fit well their ordinary MA method (·–) for similar window sizes $N = 12s$. Especially the EWVAR is more responsive to changes in the signal variance and forgets them faster.

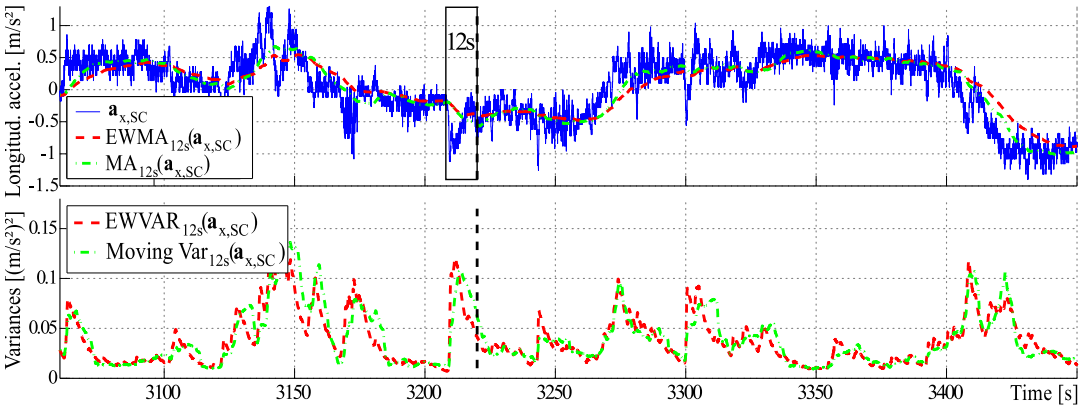

Figure 4.3.: Exponentially weighted moving average (EWMA) and variance (EWVAR)

Fig. 4.4 shows the advantage of the EWMA again, but for event rate calculation of road exit intensities. A road exit is an event that is detected if any part of the vehicle exceeds a solid lane marking. This can be used to measure the *temporal* density of events ("rate") including their intensity. It can be seen that the regular MA filter (·–) has stairs and drops every time an event leaves the sliding window while the EWMA smoothly forgets past events and never returns to zero (––).

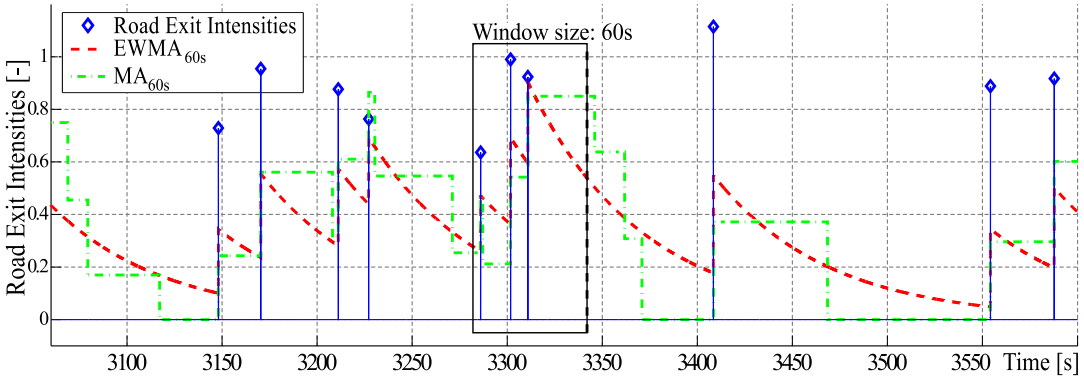

Figure 4.4.: Exponentially weighted moving average (EWMA) to calculate event rates

Computational Complexity: On a fixed-point processor, divisions and multiplications and especially memory for unit delays (each 32Bit) are very limited and expensive. In regards to computational complexity, Eq. (4.13) can be transformed to the more efficient Eq. (4.15) by replacing one multiplication by one subtraction. Compared to the moving average with one division, $N-1$ additions and $N-1$ unit delay elements, the EWMA now requires two additions and a multiplication:

$$\mu[n] = x[n] + \lambda_\mu \cdot (\mu[n-1] - x[n]) \; . \tag{4.15}$$

For EWVAR this works equivalently :

$$\sigma^2[n] = (x[n] - \mu[n])^2 + \lambda_{\sigma^2} \cdot \left(\sigma^2[n-1] - (x[n] - \mu[n])^2\right) \; . \tag{4.16}$$

Fixed-point Error: The weakness of this implementation in fixed-point arithmetics is that the error of the feedback is accumulated. For this reason, $\lambda + \frac{1}{N} \overset{!}{\equiv} 1$ must be fulfilled as precisely as possible. For Eq. (4.12), this is achieved by first pre-calculating the division and *then* the subtraction

$$\lambda = \frac{N-1}{N} \quad \longrightarrow \quad \lambda = 1 - \frac{1}{N} \tag{4.17}$$

since the subtraction in fixed-point is error free. Second, a 32Bit quantization (instead of 16Bit) is at least required for maintaining acceptable drift error of fixed-point towards floating-point after several hours. These countermeasures reduce the mean deviation of the fixed-point error by factor 16. Details about the results are presented in (Pape, 2008).

Adaptive Window Size: The adaption to strong signal changes and initialization of the EWMA and EWVAR can take very long for a large window size N_μ. Thus, further improvements are introduced:

- **Initial values:** The initial values $\mu[0]$ and $\sigma^2[0]$ are initialized to the average of the awake phase of each feature instead to 0 or $x[n]$.
- **Initialization:** Growing window size is an important improvement. For instance, starting with $N_\mu = 5$ increase N_μ by one for every sample or event up to the final window size.
- **Situation adaption:** The window size is reduced when the driving condition severely changes and a faster adaption is needed, e.g. for a changed vehicle speed in construction sites, i.e. $N_\mu(\mathbf{x}, \mathbf{v}_{veh})$.

4.1.3. System-Active Signals

For steering angle and lane based features, there are often driving situations (e.g. overtaking, curves, road condition etc.) that have a bad influence to the signals and features. As well, there are moments in which the signal quality is insufficient due to bad lane markings or bad weather. During the pre-processing, a Boolean *System Active Signal* for lane-based features SAS_{LANE} and a similar signal for steering and CAN based features SAS_{CAN} are calculated. They indicate when distortions requires to neglect a certain situation.

SAS_{LANE} is TRUE if *all* following conditions are fulfilled:

1. **Vehicle speed** is within the range: $P_{v,lower,LANE} \leq v_{veh} \leq P_{v,upper}$ with
   $P_{v,lower,LANE} = 70\,km/h$
   $P_{v,upper,LANE} = 200\,km/h$
2. No **lane change** takes place: the detection is described in Sec. 4.1.5 whereas $P_{laneChgPreSuppT} = 4s$ before and $P_{laneChgPostSuppT} = 6s$ after the lane change are also suppressed.
3. **Lane data quality** is sufficient: $LaneDataQual \geq P_{laneDataQual}$ with $P_{laneDataQual} = 80\%$
4. No **construction site**: the **lane width** is used for detection: $LaneWidth > P_{minLaneWidth}$ with $P_{minLaneWidth} = 3.05m$
5. No fast **velocity changes**: for instance, from 130 to 80 km/h in construction sites also cause artifacts in driving patterns and, thus, are suppressed for $P_{velChgPostSuppT} = 3s$: EWMA $_{3s}(|\dot{v}_{veh,LP}|) > 1.5\frac{km}{h \cdot T_s}$ with $v_{veh,LP}$ filtered by a Butterworth low-pass filter of 2^{nd} order and a cut-off frequency of 0.5Hz.
6. No **overtakings**: lane signals cannot be used during overtaking maneuvers. A change in the lane number $LaneNum$ accompanied by an acceleration pedal change of $\Delta AccelPdlPosn \geq 10\%$ is used for detection.
7. No **short active sections**: in order to avoid toggling, active sections with durations $P_{shortSectionsTh} \leq 3\,s$ are suppressed as well.

SAS_{CAN} is TRUE if the following conditions are fulfilled:

1. No **vehicle operation** from buttons and levers:
   turn indicator operation result in inactivity for $P_{tWghtLnCh} = 10s$,
   steering wheel buttons or clutch operation for $P_{tWghtOper} = 5s$ and
   operation of the heat-unit (COMAND) for $P_{tWghtDistr} = 10s$ are suppressed.
2. No **Curves**: lateral perceived acceleration $|\text{EWMA}_{s2}(a_{y,stw})| > 0.8\frac{m}{s^2}$ is suppressed for
   $P_{curveSuppT} = 0.4s$ using $a_{y,stw}$ from the single-track model (Sec. 6.3).
3. No **Road bumps**: longitudinal acceleration $a_{x,whl} \leq 4\frac{m}{s^2}$ is suppressed for
   $P_{RoadBumpSuppT} = 0.5s$ using $a_{x,whl}$ from wheel rotation sensors (cf. Sec. 4.1.1).
4. **Vehicle speed** must be within the range: $P_{v,lower,CAN} \leq v_{veh} \leq P_{v,upper,CAN}$ with
   $P_{v,lower,CAN} = 80\,km/h$ and $P_{v,upper,CAN} = 180\,km/h$.
5. **Steering wheel angle** must be within $|\delta_S| < P_{stwLevel}$ with $P_{stwLevel} \leq 40°$.
6. No **driving style suppression**: $w_{DynamicDrivingStyle}$ from Sec. 4.1.7 is suppressed.
7. No **Kick-down**: $AccelPdlPosn \geq 98\% \vee AccelPdlPosnRaw \geq 98\%$ are suppressed for $P_{tKickDownShort} = 0.1s$ if the pedal is pressed for shorter than $2s$ and
   $P_{tKickDownLong} = 20s$ otherwise.
8. No **safety assistance system is active**: Traction Control, Stability Control, Anti-lock Braking System or Hydraulic Brake Assist indicate very sportive driving: $ASR_{ctrl} \vee ESP_{ctrl} \vee ABS_{ctrl} \vee HBA_{ctrl}$. Events are suppressed for $0.1s$ for an intervention shorter than $2s$ and up to $20s$ otherwise.

9. No **Cross-wind**: the detection is described in Ch. 5.2.6 and suppressed for $P_{swPswgHoldT} = 3s$.

For most features, individual exceptions had to be made.

During feature extraction, the SAS signals are included to suppress the computation in these situations. However, this "blind" inactivity has a negative impact on the feature extraction. Depending on the feature, the following methods are used to fill these gaps:

1. *Event suppression:* for rate calculations (e.g. *EWMA* of steering corrections) the detected events are simply considered as zero. This conservative approach yields a drop of the event rate which appears right as the SAS inactivities are indebted by activating actions of the driver. If EwmaN is used instead EWMA, only the last N events are taken in which the SAS was active. Here, the event rate does not drop.

2. *Hold:* the last feature value is hold. This assumes that the fatigue level in such situations remains unchanged.

4.1.4. Driver Switch and Pause Detection

When a driver has a break or there is a change of the driver, the estimated fatigue level must be reset. Otherwise it often leads to false warnings. Technically, an engine restart resets the ESC controller and unless a non-volatile memory (EEPROM) is available, the algorithm restarts. However, many pauses or driver switches are performed with running engines and must be distinguished from stop-and-go traffic. Fig. 4.5 shows the state transition diagram of the detection conditions. In case the vehicle speed v_{veh} is below 5 km/h, a timer

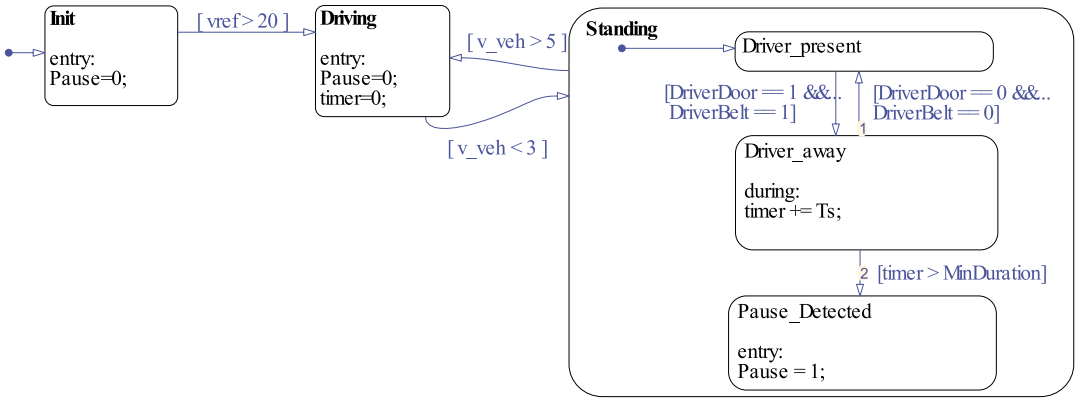

Figure 4.5.: Pause and driver switch detection to reset the features (cf. Patent (Friedrichs et al., 2012))

is started when door and buckle switch are opened. The utilized signals of the driver door state $DrRLtchFRStat$ and buckle switch $BcklSwD$ need to be debounced for $t = 0.3s$. The timer threshold $T_{gsP\_MinDuration} = 15s$ is set to the fastest realistic driver switch that we could perform. The timer is reset when the vehicle is driving over 5 km/h again.

4.1.5. Lane Change Detection

One benefit of the ALDW is that lane changes can be detected even if the driver does not use the turn indicator. According to (Batavia, 1999; Schmitz, 2004), the lateral distance und velocity are good indicators to detect lane changes. Detection of lane changes (cf. Fig. 4.6)

was performed by using the lange change status *LaneChangeStat* as well as detecting zero crossings in the lateral distance *laneLatDist* y_L: $laneChgDct = |\frac{dy_L}{dt}| > P_{LaneChgTh}$ and $LaneChg\_Stat \neq 0 \vee TurnIndLvrStat \neq 0 \vee laneChgDct$ with $P_{laneChgTh} = 1.8m$.

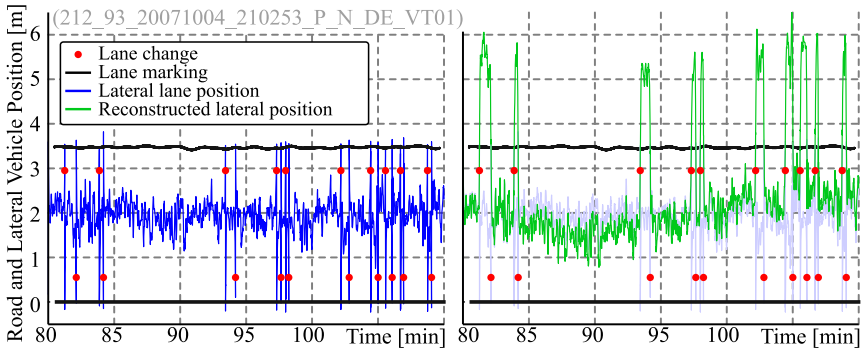

Figure 4.6.: Detection of lane changes and reconstruction of lateral lane distance

4.1.6. Subjectively Perceived Lateral Acceleration

It was observed that the *subjectively perceived* lateral acceleration is much higher for increasing vehicle speeds (cf. Patent (Katz et al., 2004)). At low speeds strong lateral accelerations occur without the driver noticing it. It was observed that this speed dependency needs to be compensated by a weighting according to the drivers perception.

The *subjective lateral acceleration* $\mathbf{a}_{y,stw,subj}$ in $[\frac{m}{s^2}]$ is calculated according to Eq. (4.18) from the *vehicle speed* $\mathbf{v}_{veh}$ in $[\frac{m}{s}]$ and the *lateral acceleration* $a_{y,stw}$ from the single-track model as described in Ch. 6.3. It is not distinguished between left and right curves.

$$\begin{aligned}\mathbf{a}_{y,stw,subj}(\mathbf{v}_{veh},\mathbf{a}_{y,stw}) = (\quad & \mathbf{v}_{veh}\cdot P_{aySubjAm} + \quad P_{aySubjAc}) \cdot |\mathbf{a}_{y,stw}| + \\ & \mathbf{v}_{veh}\cdot P_{aySubjBm} + \quad P_{aySubjBc}\end{aligned} \tag{4.18}$$

with the parameters obtained from parameter study

$$\begin{aligned} P_{aySubjAm} &= 0.036\tfrac{s}{m}, & P_{aySubjAc} &= 0.3985, \\ P_{aySubjBm} &= 0.01836\tfrac{s}{m}, & P_{aySubjBc} &= -0.8840. \end{aligned}$$

Fig. 4.7 illustrates the function $\mathbf{a}_{y,stw,subj}(\mathbf{v}_{veh},\mathbf{a}_{y,stw})$ from Eq. (4.18).

4.1.7. Driving Style Model

Sportive driving inhibits fatigue and thus needs to be distinguished. As illustrated in Fig. 4.8, inexperienced drivers tend to not mix longitudinal and lateral acceleration while experienced race drivers better exploit the physical limits of the tires. As mentioned in the patents of (Kuhn and Heidinger, 1997; Stolzmann et al., 2002), the right figure shows the thresholds for the detection of sportive, normal and calm driving style of drivers with average driving experience. The threshold curves were the result of a parameter study that optimized the classification results.

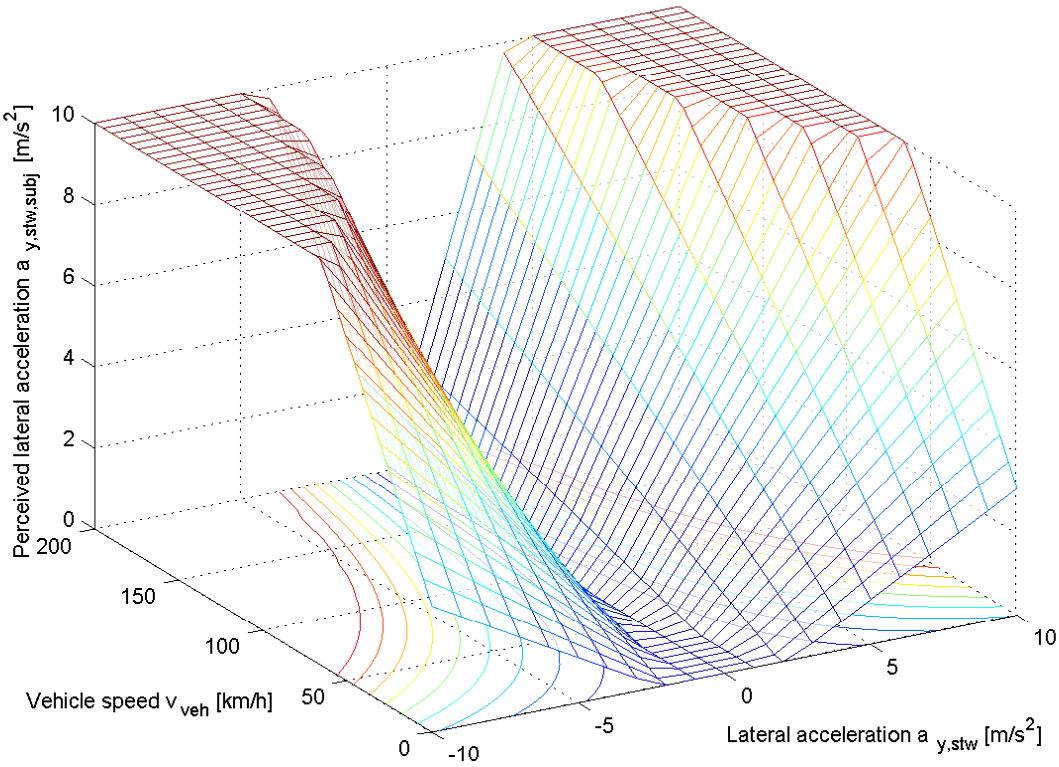

Figure 4.7.: Subjectively perceived lateral acceleration $\mathbf{a}_{y,stw,subj}$

Driving Style Suppression

Sportive driving was observed to alert a driver for a certain time. This hypothesis was indirectly confirmed by improved classification results. The decision how long sportive driving is suppressed is calculated based on the model from the previous Sec. 4.1.6. Using the threshold from Fig. 4.8, a counter C_{fd} is introduced that increments $P_{fdCntIncNear} = 0.08$ for every second while the acceleration magnitude $\mathbf{a}_{res}$ is inside the *normal* (orange) area and $P_{fdCntIncFar} = 0.12$ outside (red). The maximum for the counter is $P_{fdMax} = 2.4s$. $\mathbf{a}_{res}$ is calculated according to Eq. (4.19) as the magnitude of perceived lateral $a_{y,stw,subj}$ and longitudinal acceleration $a_{x,whl}$.

$$\mathbf{a}_{res} = \sqrt{\mathbf{a}^2_{y,stw,subj} + \mathbf{a}^2_{x,whl}} \tag{4.19}$$

The counter counts down as long as $\mathbf{a}_{res}$ is inside the *calm* (green) area and sets the *driving style weighting* $w_{DynamicDrivingStyle} = 1$. Parameters are a result of parameter optimization.

4.2. Overview of Features

In this section, an overview of features extracted in this thesis is given. In general, one extracts as many promising features as possible and selects those with the best performance by *feature selection* or *transformation* (Ch. 8). Inspired by own ideas and features in literature (App. A.9), this section discusses the most essential features.

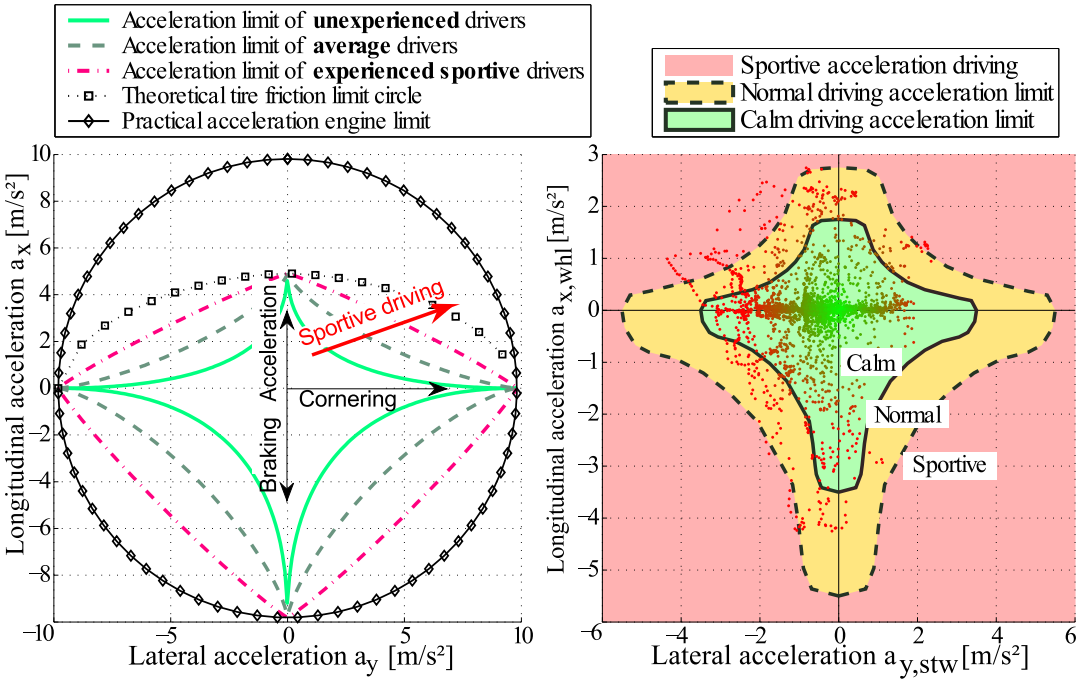

Figure 4.8.: Different driving styles are displayed in a so called "GG-diagram" of Longitudinal and (perceived) lateral acceleration. Left: Experienced drivers exploit physical tire limits better than inexperienced drivers. Right: thresholds from a parameter study for the detection of sportive, normal and calm driving styles for drivers with average driving experience.

4.2.1. Feature Matrix

All features are organized in a *feature matrix F* with a structure shown in Tab. 4.2. For each drive, the first three columns are the KSS reference with different interpolation methods. The next ten columns contain meta information about the drive, allowing fast access for the grouping, filtering and data analysis. The following columns contain the features with their *Feature-ID* in the head row. Each row contains one sample of all features with the features' sampling rate 0.5 *Hz*.

4.2.2. Feature Classes

Features that are based on similar patterns are structured into groups depending on the pattern or sensor type they are derived from. The class LANE describes whether they require camera-based lane information. AA contains measures from the ATTENTION ASSIST system, STW from the steering wheel angle, and CAN when they are based on other CAN-bus signals such as lateral or longitudinal acceleration, wheel rotation etc. The classes EYE and EEG are used for evaluation in Ch. 3 and otherwise as additional reference.

4.2.3. List of Features

Tab. 4.3 lists the 48 most important features out of all 144 features listed in App. A.9. Features with superscript [1] are better after baselining and superscript [2] are newly introduced.

	KSS Hold	KSS Linear	KSS Raw	Drive-ID	Driver-ID	Vehicle-ID	VehicleType-ID	VehicleNumber	Experiment-ID	Vehicle Width	VchU	Steering Ratio	Wheel Base	Feature-ID (f_1)	Feature-ID (f_2)	...	Feature-ID (f_N)
	a	b	c	d	e	f	g	h	i	j	k	l	m	1	2	...	N
Drive 1	5	5	5	19812	340	45	221	2844	31	2.0							
	5	5.33	0	19812	340	45	221	2844	31	2.0							
	5	5.67	0	19812	340	45	221	2844	31	2.0							
	6	6	6	19812	340	45	221	2844	31	2.0							
	6	6.5	0	19812	340	45	221	2844	31	2.0							
	7	7	7	19812	340	45	221	2844	31	2.0							
	⋮	⋮	⋮	⋮	⋮	⋮	⋮	⋮	⋮	⋮	⋮	⋮	⋮	⋮	⋮	⋮	⋮
Drive 2	5	5	5	19813	452	45	221	2844	31	2.0							
	5	5.33	0	19813	452	45	221	2844	31	2.0							
	⋮	⋮	⋮	⋮	⋮	⋮	⋮	⋮	⋮	⋮	⋮	⋮	⋮	⋮	⋮	⋮	⋮
N	⋮	⋮	⋮	⋮	⋮	⋮	⋮	⋮	⋮	⋮	⋮	⋮	⋮	⋮	⋮	⋮	⋮

Table 4.2.: Elements of the feature matrix F

ID	CLASS	Feature Name	Description
15	LANE	LANEDEV[1]	Lane deviation
17	LANE	ZIGZAGS[1]	Number of zig-zag events
19	LANE	LATMEAN[1]	Lateral mean
29	LANE	LNMNSQ[1]	Lane mean squared
32	LANE	LANEX[1]	Lane exceeding
33	LANE	LNERRSQ[1]	LANEX squared
34	LANE	ORA[1]	Overrun area
35	LANE	TLC1MIN[1]	Time-to-lane crossing
36	LANE	VIBPROP[1]	Lane departure warnings within 4 minutes
16	LANE	LATPOSZCR[1,2]	Lateral position ZCR
30	LANE	LNIQR[1,2]	IRQ of lateral position
31	LANE	LNCHGVEL[1,2]	Lane change velocity
37	LANE	DELTADUR[1,2]	Duration between inflection points
38	LANE	DELTALATPOS[1,2]	Lateral displacement
39	LANE	DELTALATVELMAX[1,2]	Maximum lateral velocity
14	LANE	LANEAPPROX[1,2]	Approximation to lane event rate
40	LANE	LANEAPPROXADP[1,2]	LANEAPPROX with adaptive threshold
42	STW	ELLIPSE[1]	Steering angle and velocity magnitude
50	STW	NMWRONG[1]	Number of times STW is suddenly corrected
69	STW	NMRHOLD[1]	Number of times STW is hold long
48	STW	AmpD2Theta[1]	Area between STW and its mean (Berglund, 2007)
72	STW	VHAL[1]	Ratio high vs. low STW velocities (King et al., 1999)
71	STW	MICROSTEERINGS[1]	Presence rate of micro-steering adjustments
18	STW	STWZCR[1,2]	Steering ZCR
25	STW	STWVELZCR[1,2]	Steering velocity ZCR
52	STW	STV25[1,2]	Steering velocity 1st Quartile
53	STW	STV50[1,2]	Steering velocity 2nd Quartile
54	STW	STV75[1,2]	Steering velocity 3rd Quartile
44	CAN	ACTIVE[2]	System active signal (SAS_{CAN})

24	CAN	LNACTIVE[2]	Lane signals active (SAS_{LANE})
41	CAN	VEHSPEED	Vehicle speed [km/h]
47	CAN	DAYTIME	Seconds since midnight
66	CAN	TOT	Time-on-task
22	CAN	DEGOINT[1]	Degree of vehicle-driver interaction (Kanstrup, 2006)
23	CAN	REACTIM[1]	Reaction time in STW to lateral acceleration
45	CAN	CIRCADIAN[1,2]	Circadian daytime weighting
51	CAN	STWEVNT[1,2]	Steering event rate as in ATTENTION ASSIST
55	CAN	CROSSWIND[1,2]	Cross-wind / road warping intensity
58	CAN	DYNDRIVINGSTYLE[1,2]	Dynamic driving style
59	CAN	MONOTONY[1,2]	Monotonous driving
61	CAN	OPERATION[2]	Vehicle lever and button operation
63	CAN	ROADBUMPS[2]	Road bump condition
67	CAN	TOTMONO[2]	Monotonous Time-on-Task (TOT)
68	CAN	TOTSPEED[2]	TOT around 130km/h
70	CAN	LIGHT[2]	Light intensity (day/night)
26	CAN	TRFCDENS[2]	Traffic density
27	CAN	TURNINDADVANCE[1,2]	Blinking time before lane change
28	CAN	TURNINDDUR[1,2]	Turn indicator operation duration
...	...	...	...
	EYE	...	EYE features are listed in Tab. 3.8

Table 4.3.: Selection of features

4.3. Lane-Data based Features

In comparison to the "microscopic" steering control, the lateral lane position is a rather "macroscopic" result of the smoothed reaction of the vehicle to the steering signal and road condition. The major additional information provided by lateral lane data is the knowledge of the *absolute* position in the lane. Another benefit is that lane changes can be detected even if the driver does not use the turn indicator.

According to Knipling and Wierwille (1994), "*drowsiness can be detected with reasonable accuracy using driving performance measures such as "drift-and-jerk" steering and fluctuations in vehicle lateral lane position*". Wierwille and Ellsworth (1994) concluded "*that lateral control measures are closely related to prolonged driving and might therefore be used to detect driver sleepiness*". Berglund (2007) summarized from Siegmund et al. (1996) "*that driver sleepiness is most likely indirectly measured either by the steering wheel control input or lane maintenance output, and that the lane maintenance is arguably the more complete parameter*".

A major problem during the offline development of features using measurement data is the gap of transparency. The majority of influences could either not be recorded or was difficult to access in the large number of signals. For this reason, a real-time online and offline vehicle "cockpit" was implemented (App. A.13.3) that brings both domains together: the visualization of driving signals and the features. Generally, it was observed that the features are sensitive to what they have been designed for. Yet, there were also other influences to which the features were sensitive. With this visualization, these influences could be identified and compensated.

4.3.1. Lateral Lane Position Features

Observations from many situations during night studies and free drives tell that some drivers tend to drive closer to the right lane border to clear space for overtaking vehicles or oncoming traffic. The same principle holds for the overtaking vehicles that tend driving to left side. The average lateral offset also depends on the driver's specific driving style. Further, it was observed that for very low traffic, there are drivers who neglect the lane markings and drive in between lanes, to increase the clearance space to the road boundaries for a sloppy lane keeping. LATMEAN is the average lateral lane position during system activity SAS_{LANE} within the last 1.4 *min*, calculated with the EWMA proposed in Sec. 4.1.2. LNMNSQ is the moving average (not EWMA) of the squared lane position while the zero position is defined as the position where the center of the front axle is located on the road center. LNMNSQ is used for comparison as reference for implementations in literature (Tijerina et al., 1998; Wierwille and Ellsworth, 1994; Kecklund and Åkerstedt, 1993).

Some other driver-specific features are TURNINDADVANCE, the duration between the utilization of the turn indicator prior to a lane change, LNCHGVEL, the average lateral velocity of lane changes and TURNINDDUR, the duration of turn indicator activation. For these features, only lane changes are suppressed instead of using SAS_{LANE}. These features are based on the observation that different drivers have different styles of lane changing and turn indicator usage according which they can be distinguished. Knowing about these driver-specific properties does not necessarily allow a causal conclusion about the driver type and state. This factor will be analyzed later in Ch. 5.4.

Some other base features are the average duration DELTADUR between lane center crossings, averaged over the last 15 events using EwmaN and the zero crossing rate LATPOSZCR. These two features correspond to the oscillation frequency around the individual lane center. Further features that describe the lane keeping performance are DELTALATPOS, the amplitude (cf. Fig. 4.9) and DELTAVELMAX, the maximum velocity between the inflection points of the lateral lane position (ZC). All these features are vehicle speed dependent and thus had to be normalized.

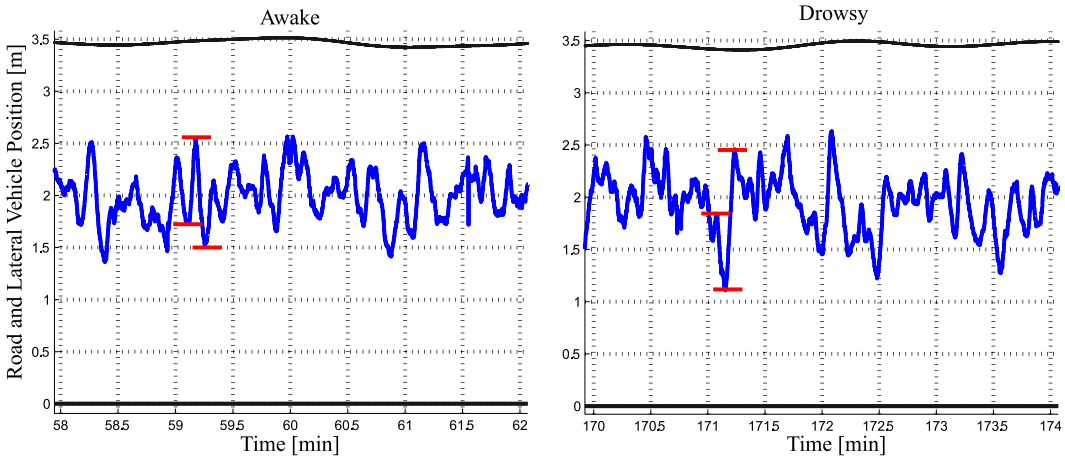

Figure 4.9.: Road markings and lane lateral offset to illustrate lane deviation LANEDEV and DELTALATPOS for *awake* and *drowsy* driving. The red bars illustrate examples of the largest lane deviations.

4.3.2. Lane Deviation (LANEDEV, LNIQR)

There is a large number of features associated with the vehicle's deviation in the lane, as it is assumed that the driver-specific lane keeping becomes more sloppy with increasing fatigue (Kircher et al., 2002; Pilutti and Ulsoy, 1999; Bittner and Hana, 2000) and (see Altmüller, 2007, Ch. 4.2.3). During the test drives, it was observed that some awake drivers can also have a bad lane keeping depending on their mood.

The most essential features are implemented. LANEDEV measures the lane keeping deviation using an EWVAR window of size 2 *min*, while the SAS_{LANE} is active. The often mentioned *SDLP* feature (Tietze and Hargutt, 2001; Hargutt, 2001; Kircher et al., 2002; Thiffault and Bergeron, 2003; Altmüller, 2007; Liu et al., 2009; Mets et al., 2011) is basically the same and, thus, not implemented. The lateral mean was observed to be driver-dependent and, thus, is subtracted before the variance is calculated. Simple variants of LANEDEV are used as *ground truth* for distraction in many studies with driving simulator data (Greschner, 2011). In fact, it is a simple measure for driving performance, but it cannot be completely transfered from simulator to real world driving. Fig. 4.9 depicts an example of how the variance increases with increasing fatigue. LANEDEVSQ and LANEDEV4 are obtained by taking the power of two and four respectively, as proposed by Wierwille and Ellsworth (1994); Kircher et al. (2002), to stronger weight large deviations from the driver's average. LANEDEVBL is simply the baselined version of LANEDEV, i.e. it is normalized by its *max* value between the 1^{st} and 20^{st} minute. LNIQR is the interquartile range (IQR) of the lateral position within the last two minutes. In comparison to the variance, the IQR does not take outliers into account and thus focuses more on the degradation of the small lane deviations. Again, the driver-dependent lateral offset had to be compensated. However, parameter optimization has shown that exponential weighting of the lateral position performed best. This allows the conclusion that large lane deviation events are more significant signs for fatigue than small deviations.

4.3.3. Over-Run Area (ORA)

The *Over Run Area* ORA is another deviation measure that senses the average overridden surface and is an alternative to LANEDEV. Details can be found in the thesis of (Olabe, 2008) and in literature (Löfgren, 2007; Wigh, 2007). Fig. 4.10 illustrates the ORA measure. For the

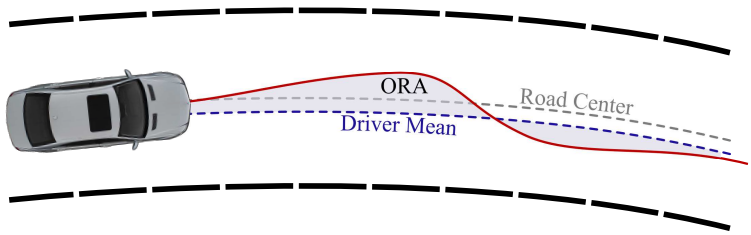

Figure 4.10.: Over Run Area (ORA) as measure for lane deviation

calculation, the lateral offset is subtracted and the absolute value is averaged over an EwmaN window of 3 *min*, while SAS_{LANE} is active.

4.3.4. Unintended Lane Approximation (LANEAPPROX, VEZ etc.)

LANEAPPROX is a feature that describes the number of times any part of the vehicle is entering a proximity-zone of the lane bounds. LANEAPPROXADAPT is basically the same, however using an adaptive, driver dependent zone.

Kozak and Pohl (2006) and Wigh (2007, 2.1) defined in their theses VEZ as a zone which focuses on a lane approaching pattern, illustrated in Fig. 4.11 and comparable to TLC1MIN. The latter uses a driver adaptive zone size, which can be interpreted as an 'almost' lane departure. The advantage is that these departures occur much more often than real lane departures and, thus, allow a higher temporal resolution. Unintended lane departures are suppressed if the driver steers towards the lane or acc-/decelerates (Schmitz, 2004). Different weightings for curves and lane types have shown to be practical. It was observed that some drivers almost never exit the lane boundaries, whereas others have over 50 lane exits per hour. Thus, it is proposed to adapt the ALDW warning sensibility to the driver state.

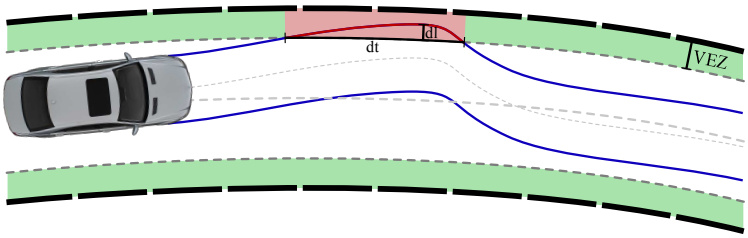

Figure 4.11.: Unintended lane approaches with intensity *dl* and duration *dt*

4.3.5. Unintended Lane Exceeding (LANEX, LNERRSQ)

The heuristic of distinguishing intended and unintended lane exceedances is discussed in (Schmidt, 2009) and also in the lane change detection (Sec. 4.1.5).

For some drivers, lane departure warnings LANEX and VIBPROP have been observed to be very helpful features during the onset of drowsiness. LANEX, LNERRSQ and VIBPROP are based on the intensity and frequency of lane departures and road exits (Wierwille, 1996b; Mattsson, 2007). Lane departures are defined as exceeding of a dashed road marking, while road exits describe the exceeding of solid road markings. LNERRSQ is the mean squared difference between the outer vehicle dimensions that exceed the lane marking. In contrast to VIBPROP, LANEX takes the intensity into account as shown in Fig. 4.12. The warnings are averaged by an EWMA filter with window size $P_{VibpropEwmaWinSize} = 4\,min$.

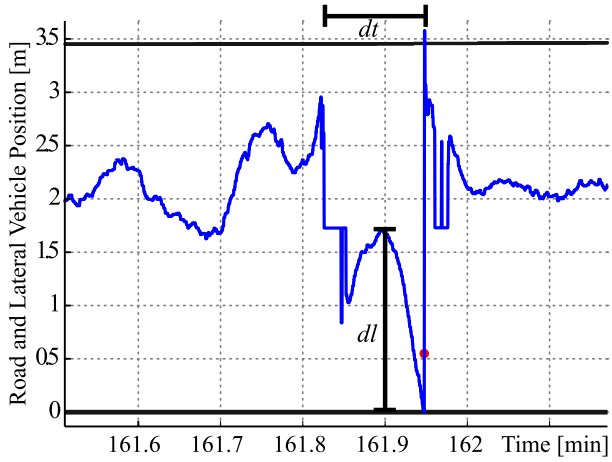

Figure 4.12.: Lane exceedances for intensity *dl* and duration *dt*

4.3.6. Zig-Zag Driving (ZIGZAGS)

ZIGZAGS are based on single lurching patterns as illustrated in Fig. 4.13. The maximum

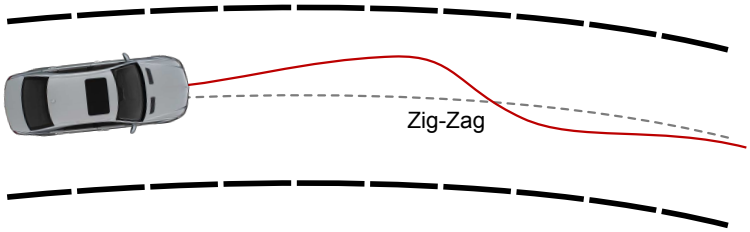

Figure 4.13.: Zig-Zag driving

lateral distance and velocity are calculated between all consecutive zero-crossings of the smoothed lateral distance. The lateral distance is filtered by a low-pass filter with cut-off frequency of 0.6 Hz. A 2^{nd} order Butterworth filter was used instead of EWMA, since stronger attenuation in the stop-band was desired for this cut-off frequency. The lateral velocity is obtained by differentiation with a DISPO filter (Sec. 4.1.1). Criteria for detecting ZIGZAGS events are at least two oscillations within the lane with an amplitude within 0.4 - 1.2 meters and a duration between 2.5 - 17.5 seconds. The resulting events are averaged with an EWMA window of $N = 4\,min$. Only events are taken into account when SAS_{LANE} is active. ZIGZAGBL is the baselined version, normalized by the saturated maximum of the ZIGZAGS value between the 1^{st} and 20^{st} minute. These parameters are obtained from parameter optimization.

4.3.7. Time-to-Lane-Crossing (TLC)

Time-to-Lane-Crossing (TLC) measures the estimated time remaining until any part of the vehicle exceeds the lane boundaries, if no other driving action is made (Glaser and Mammar, 2005; Mammarand et al., 2006). Fig 4.14 illustrates this principle. As described in

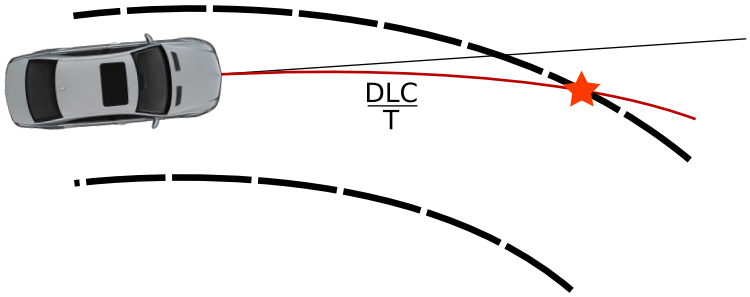

Figure 4.14.: Time-to-Lane-Crossing minima models

(Friedrichs and Yang, 2010b), there are again two models to calculate the TLC time, referred to as *TLC model 1* and *TLC model 2*. TLC model 1 is the simplest method calculated from the lateral position and velocity. The more accurate model 2a and 2b take the road curvature and vehicle track into account and therefore require additional signals. These, however, are not so robust as the road curvature signals are not reliable. The inclusion of the second clothoid parameter c_o has not shown any improvement, and, thus, is not considered. Details can be found in the thesis of Olabe (2008) or in literature (Batavia, 1999; Schmitz, 2004; Mammarand et al., 2006; Wigh, 2007).

TLC Model 1

The TLC duration can simply be calculated from the lateral distance to the left or right lane edge $y_{l,r}$ and lateral velocity $\dot{y}_L$ by

$$TLC1 = \frac{y_{l,r}}{\dot{y}_L} \,. \tag{4.20}$$

TLC Model 2

TLC Model 2 is the more detailed model that, however, requires more signals and, thus, is less robust. There are several variants to implement this model. However the definition described in the theses of Olabe (2008) and Wigh (2007) is used.

This definition is based on two models: the *vehicle path model* and the *road model*. The vehicle path model describes the future path of the vehicle if the motion parameters as the current yaw-angle would not change. The road model describes the road curvature ahead, based on the road characteristics obtained by the lane tracking camera. The intersection point of both trajectories describes the distance at which the vehicle will cross the lane boundaries.

Vehicle Path Model: There are two models described in (Wigh, 2007), whereof the second, more detailed model is used here. Taking the yaw angle $\Delta\psi$ between road and vehicle (*LaneYawAngl* from Tab. A.2) and the curvature of vehicle path $\kappa_c = \frac{1}{R}$ into account, yields Eq. (4.21) for the vehicle path model, where y_0 is the lateral distance, θ the angle against the lane marking and d is the distance in driving direction:

$$y_{veh}(d) \;=\; y_0 + \theta \cdot d + \frac{1}{2} \cdot \kappa_c \cdot d^2 \tag{4.21}$$

The radius R is obtained from Eq. (6.3) of the single track model described in Ch. 6.3.

Eq. (4.21) describes the center line of the future vehicle trajectory. Taking the vehicle width w_v into account, the left and right vehicle edges are obtained by:

$$\begin{aligned} y_{veh,l}(d) &= +\frac{w_v}{2} + y_0 + \theta \cdot d + \frac{1}{2} \cdot \kappa_c \cdot d^2 \\ y_{veh,r}(d) &= -\frac{w_v}{2} + y_0 + \theta \cdot d + \frac{1}{2} \cdot \kappa_c \cdot d^2 \,. \end{aligned} \tag{4.22}$$

Road Model: Road sections can be modeled by clothoids. Using the mathematical simplifications from Wigh (2007), the driven distance s and clothoid parameters c_0 and c_1 (*LaneClothoidPara* from Tab. A.2), the center line of the road can be formulated in x- and y-coordinates by:

$$\begin{aligned} x(d) &= x_0 + d \\ y(d) &= y_0 + \frac{1}{2} \cdot c_0 \cdot d^2 + \frac{1}{6} \cdot c_1 \cdot d^3 \end{aligned} \tag{4.23}$$

x_0 and y_0 are the starting positions of the vehicle and can be set to zero.

Analogous to the vehicle path model, the lane width w (*LaneWidth* from Tab. A.2) must be taken into account. Neglecting the small and noisy parameter c_1, yields the left and right road markings $y_{road,l}$ and $y_{road,r}$:

$$\begin{aligned} x(d) &= d \\ y_{road,l}(d) &= \frac{1}{2}(+w + c_0 \cdot d^2) \\ y_{road,r}(d) &= \frac{1}{2}(-w + c_0 \cdot d^2)\ . \end{aligned} \tag{4.24}$$

Intersection of both Models: The *Distance-To-Lane Crossing* (DLC) is calculated as the intersection of both models, $DLC = d$ subject to

$$\begin{aligned} y_{veh,l}(d) &= y_{road,l}(d) \\ y_{veh,r}(d) &= y_{road,r}(d)\ . \end{aligned} \tag{4.25}$$

Only the minimum of the positive solutions for DLC is relevant here:

$$DLC = d = \frac{\theta \pm \sqrt{\theta^2 - (c_0 - \kappa_c)(\pm w \pm w_v - 2y_0)}}{(c_0 - \kappa_c)} \tag{4.26}$$

In model 2, the TLC2 is obtained by using the vehicle speed v_{veh} from Ch. 2.3.1:

$$TLC2 = \frac{DLC}{v_{veh}}\ . \tag{4.27}$$

Comparison of Model 1 and 2

Using TLC minima as indicator for fatigue detection, it is not relevant to estimate the real TLC time, since drivers mostly take action prior to exceeding the lane. Small TLC values are already a good indicator of sloppy driving.

Due to calibration problems of the lane tracking camera, model 1 was used in this thesis, as it has shown more robust results. The `TLC1MIN` feature is finally obtained as the number of TLC minima below 10 seconds and averaged by an EwmaN filter of the last 15 values. Fig. 4.15 shows the lateral offset of the vehicle bounds (blue), the road markings (black) and the related TLC minima.

4.4. Steering Wheel Angle based Features

In contrast to the lateral lane position, the steering wheel angle is directly related to the driver's control action. The steering signal contains higher frequencies and a finer resolution of the *desired* vehicle track.

The idea of analyzing the velocity of the steering wheel angle goes back to the expired Ford Patent of Platt (1966) in 1962. Historically, older patterns like steering pauses and fast corrections have lead to a combination of steering corrections followed by slow steering. This again has lead to the detection of deadbands and the much more sophisticated definition of

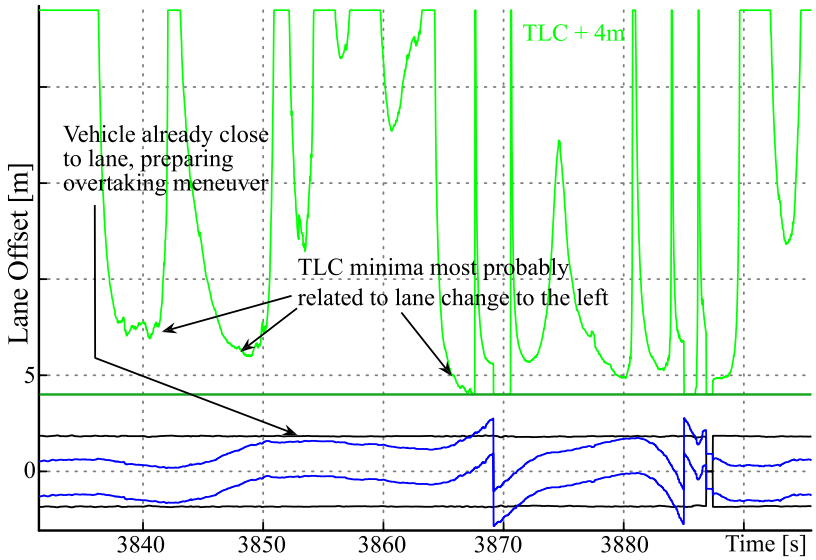

Figure 4.15.: `TLC1MIN` as TLC minima using the more robust model 1

steering events. Latest ideas focus on considering the driver and vehicle as a control system and evaluate the control parameters. So called "micro-corrections" and the "degree of interaction" are simpler measures for the driver control performance. Steering wheel angle and velocity frequency domain analysis focus on the frequency domain.

The combination of lane and steering based patterns on a feature level extends their discriminatory property. For instance, steering corrections towards the lane center are the most relevant for fatigue detection. The reaction time to Time-to-Lane Crossing Minima is another steering and lane mixed feature proposed in this thesis.

The steering wheel angle is measured with a 0.1 degree resolution and needs to be unwrapped and offset compensated for the lateral road trend[1]. In order not to flatten signal peaks, the steering velocity is calculated with the Digital Polynomial Smoothing- and Differentiation Filter (DISPO), described in Sec. 4.1.1.

4.4.1. Variance Criterion (VARCRIT)

According to the Daimler Patents of Stolzmann et al. (2002); Hentschel et al. (2005), the *variance criterion* describes the ratio of a long term and a short term sliding variance window. The goal is to measure the rate of detected patterns similar to "drift-and-jerk", where the driver is out-of-the-loop for a short period and then suddenly realizes the mistake by reacting with a quick steering correction. This is an improved detection method for the patterns in the expired Nissan Patents (Seko and et. al., 1986; Iizuka and Obara, 1986) for the detection of driver drowsiness by an abrupt steering change and no steering movement following.

Some changes were made to the feature `VARCRIT` such as using the DISPO filtered steering wheel angle velocity $\dot{\delta}_S$ from Sec. 4.1.1 and taking the variance ratio to the power of k:

$$\texttt{VARCRIT} = \text{EWMA}_N \left(\frac{EWVAR_{short}(\dot{\delta}_S[n])}{max(1, EWVAR_{long}(\dot{\delta}_S[n - P_{winSizeShort}]))} \right)^k \tag{4.28}$$

[1] Roads usually have a lateral gradient of up to 3% for rain water drain

with the sliding variance window sizes $P_{winSizeShort} = 0.5s$, $P_{winSizeLong} = 2.0s$ and exponent $k = 4$ to stress peaks. Fig. 4.16 illustrates the principle of the sliding short and long term variances. The longer steady phase represents the "out-of-the-loop" absent driver activity and

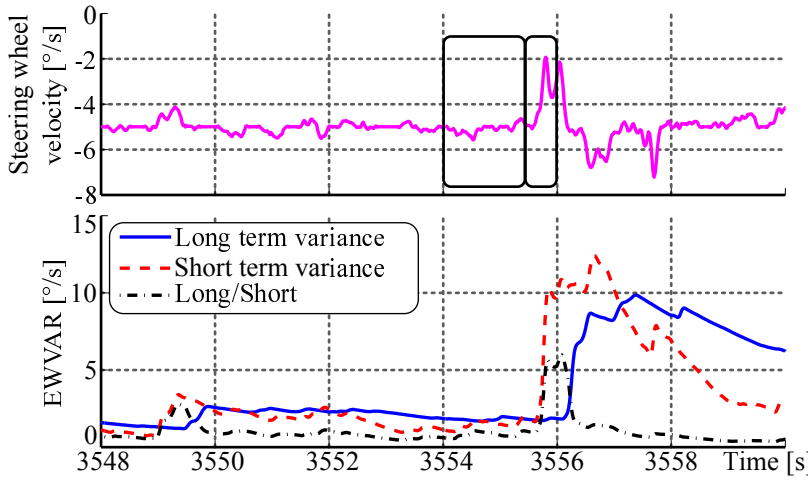

Figure 4.16.: Feature VARCRIT: Variance criterion - short over long term variance.

furthermore makes sure that sudden hectic steerings as in construction sites, traffic density or curvature changes do not lead to miss-detected peaks.

Similarly, a criterion IQRCRIT was investigated, where the variance is replaced by the interquartile range IQR[2] which neglects slow and fast outliers. However, the performance was inferior to the EWVAR because the peak height of steering corrections is neglected.

4.4.2. Local Driver Inactivity Event (DEADBAND)

The feature DEADBAND proposed by (Altmüller, 2007) describes very much the same pattern as (Seko and et. al., 1986; Iizuka and Obara, 1986) and the VARCRIT. Its name is motivated by events when all driver control signals are steady, i.e. steering wheel angle, gas pedal, lane drifting and all signals are "dead". This steady-only aspect of the DEADBAND idea (and the nature of its name) is further analyzed in relation to the feature NMRHOLD in Sec. 4.4.7. The name DEADBAND is slightly misleading because its proposed detection criteria require the followed steering correction as well. According to our findings, the correction is much more significant than the intensity and duration of the non-steering period. Furthermore, this feature is only based on the steering wheel signal and no other driver control signal. This "dead" pattern is strongly related to microsleeps and usually too late for an application in the vehicle, but still valuable if the early onset detection fails.

The Bosch Patent (Reichert, 2008) explains the same pattern and detection principle. However, it is based on the steering wheel *torque* as it is available for steer-by-wire. In [0021], the patent describes that the driver-related measure can, for instance, be the steering torque and the pattern detection in [0022] is described similarly.

[2]The moving IRQ had to be implemented in C++ (mex) as the involved sorting is computationally expensive with $O(n \log n)$. An efficient online estimation of IQR and quantiles is proposed in A.8.

Since the detection of the steering events STWEVNT was extensively investigated and focuses on the same pattern as DEADBAND, STWEVNT was used. Own findings show that some of the here presented additional criteria show more robustness for real-road drives.

4.4.3. Steering Events (STWEVENT)

As described in the Patent of Galley et al. (2006), the method to extract the feature STWEVNT focuses on a steering inactivity phase and a subsequent steering action. Therefore, the steering wheel velocity should not exceed a certain threshold for a minimum time and then exceed a second threshold. The thresholds are adaptive to driver and driving situations. Detected events are weighted by their intensity and by a factor that increases in monotonous situations and a factor that is speed dependent with its maximum at 80 km/h. The events are averaged using an EWMA filter. As explained in Sec. 4.1.3, various situations are detected to suppress steering corrections due to short-term distraction. External influences by cross-wind, road warping, road bumps and curves are suppressed as well as overtaking and sportive driving.

Driver-Adaptive Thresholds

STVmax ($\dot{\delta}_{S,max}$) is the maximum steering velocity between inflection points (i.e. zero crossings) of the steering wheel velocity $\dot{\delta}_S$ while SAS_{CAN} is active. Parameter study yielded that steering wheel angle δ_S of steering events has to exceed 0.898 to neglect noise and to make sure that the steering amplitude is relevant and observable by the driver. This is illustrated in Fig. 4.17 in which the inactive (–) and active $\dot{\delta}_{S,max}$ (–) are averaged using EwmaN, as described in Eq. 4.29 that is only updated on events and hold otherwise. The EwmaN is initialized by $\texttt{STV50}[0..4] = 10.5°/s$ with a window size of $N_{init} = 5$ that is increased by one up to $N = 110$ for every steering. Fig. 4.17 further illustrates the estimation of STV25

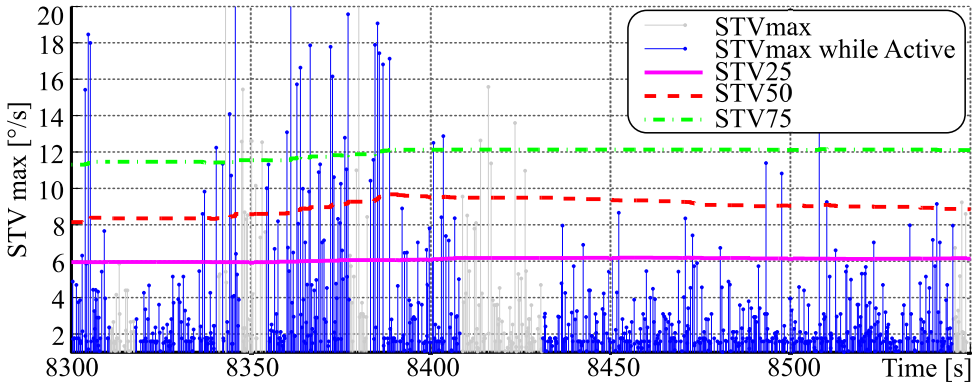

Figure 4.17.: Estimation of STV50 as the mean of $\dot{\delta}_{S,max}$ and STV25 and STV75 as the means of the corrections slower and faster than STV50.

and STV75 by *Mean Splitting* according to the calculation in Eq. 4.31 and Eq. 4.31 with $\texttt{STV75}[0..5] = 7°/s$ and $\texttt{STV75}[0..5] = 13°/s$. STV25 is the mean of the slow steering corrections and STV75 the mean for all fast steering corrections.

$$\texttt{STV50} = \text{EwmaN}_N(\dot{\delta}_{S,max}) \; . \tag{4.29}$$

The computation is only evaluated during steering wheel angle reversals.

$$\texttt{STV75} = \begin{cases} \text{EwmaN}_{\,N}(\dot{\delta}_{S,max}) & \dot{\delta}_{S,max} > \texttt{STV50} \\ hold & otherwise \end{cases} \tag{4.30}$$

$$\texttt{STV25} = \begin{cases} \text{EwmaN}_{\,N}(\dot{\delta}_{S,max}) & \dot{\delta}_{S,max} \leq \texttt{STV50} \\ hold & otherwise \end{cases} \tag{4.31}$$

This threshold estimation is motivated by the 1st and 3rd quartiles of the steering velocities that are, however, computationally too expensive. Using the STV50 for the decision whether the actual correction is faster or slower than the actual value, makes the estimation very sensitive to initialization and errors in STV50. Parameter optimization has shown that not exactly the 1st and 3rd quartiles are the best thresholds, but rather different percentiles. Further repeated mean splitting would be necessary, which would increase the sensitivity to errors even more. For this reason, two weighting factors w_{STV25} and w_{STV75} are introduced and multiplied to both thresholds

$$P_{steady} = \texttt{STV25} \cdot w_{STV25} \tag{4.32}$$
$$P_{event} = \texttt{STV75} \cdot w_{STV75}\,. \tag{4.33}$$

Fig. 4.18 shows the distribution of the $\dot{\delta}_{S,max}$. The three vertical lines represent an approximation of the 1st, 2nd and 3rd quartiles.

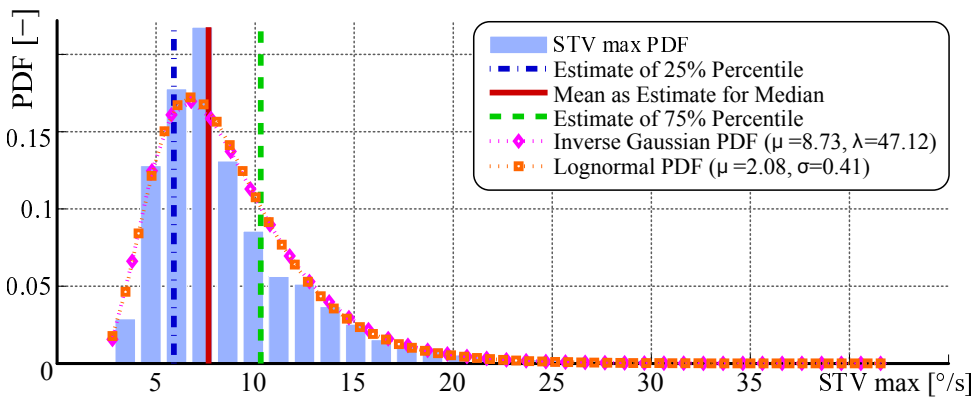

Figure 4.18.: Histogram over maximum steering velocities between inflection points.

The *Probability Density Function* (PDF) of $\dot{\delta}_{S,max}$ fits best the *Inverse Gaussian* PDF:

$$IG(x;\mu,\lambda) = \sqrt{\frac{\lambda}{2\pi x^3}} e^{\frac{-\lambda(x-\mu)^2}{2\mu^2 x}} \tag{4.34}$$

with $\mu = 2.075$ and shape $\lambda = 0.411$ for the selected drive. The parameters are estimated using the *Maximum Likelihood Estimate* (MLE). The asymmetric distribution explains why the STVxx measures increase much quicker for fast steering corrections that are far above the average than they decrease for slow steering velocities closely below the average. The rare occurrence of fast steering corrections also causes that the STV75 are rarely updated, especially if the STV50 is high.

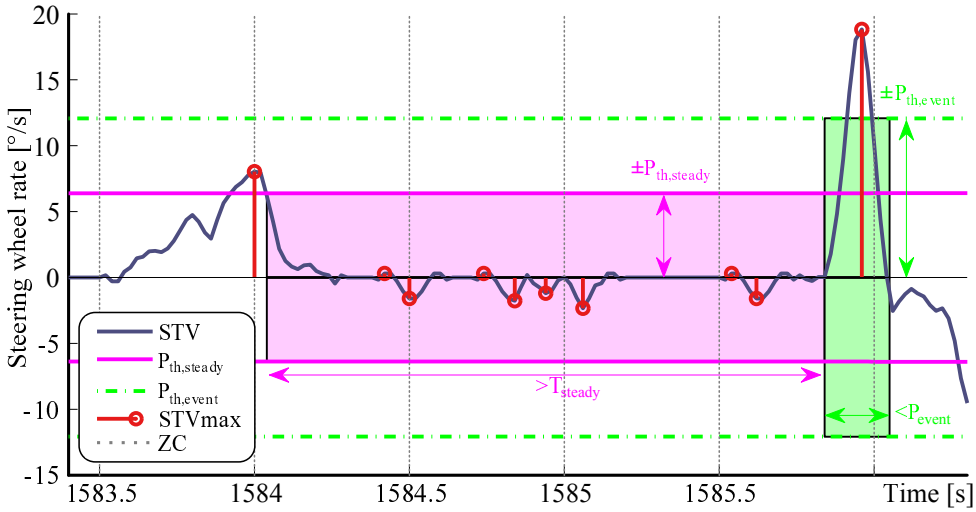

Figure 4.19.: Criteria to detect steering events as in (Galley et al., 2006; Iizuka and Obara, 1986).

Steering Event Detection Criteria

There are five criteria to detect the steering event pattern illustrated in Fig. 4.19. The criteria are implemented according to the Patent of Galley et al. (2006) and similarly to the expired Patent of Iizuka and Obara (1986). The thresholds are also comparable to the Patent of Reichert (2008) and the thesis of Altmüller (2007).

The five criteria are listed below. They are first combined logically (Galley et al., 2006, Claims 4,7,9) and finally improved by using fuzzy logic (Sec. 4.4.4):

1. a minimum steering wheel angle has to be fulfilled $\dot{\delta}_{S,max} > 1°/s$
2. inactive (steady) steering phase $\dot{\delta}_{S,max} < P_{th,steady}$ (**?**, Claim 15)
3. for at least the duration $T_{steady} > P_{steady,T}$ (**?**, Claims 6,14)
4. followed by the steering action of $\dot{\delta}_{S,max} > P_{th,event}$ (**?**, Claims 14,16)
5. for the maximum duration of $T_{event} < P_{event,T}$ (**?**, Claim 14).

Peaks are further scaled according to their magnitude, a factor of how monotonous the situation is, and the vehicle speed. Peaks are saturated to a minimum of 0.4 and a maximum of 3.0.

The feature STWEVENTBL is baselined using the maximum within the first $\tau = 14$ minutes active time:

$$\mathtt{STWEVENTBL} = \frac{\mathtt{STWEVENT}}{max(\mathtt{STWEVENT}_{\tau} \cdot SAS_{CAN})} . \tag{4.35}$$

4.4.4. Steering Event Detection using Fuzzy Logic

As presented in the thesis of Pape (2008), there are two reasons to use *Fuzzy Logic* to further improve the previous detection:

- increase the robustness of the detector if one out of the five criteria is slightly not fulfilled, but the remaining criteria are well satisfied.

- decrease the numerical error between *fixed-point* and *floating-point arithmetics* (App. A.13.1) if the event detection criteria from Sec. 4.4.3 are fulfilled in fixed-point, but not in floating-point and vice versa.

Fuzzy logic was a central goal of this thesis and the proposed improvements have increased the recognition rate by several percent so that this alteration was first introduced to the series ECU software of the 2009 E-Class. In practice, it means that also small peaks are detected, which improves the temporal resolution of the `STWEVENT` feature.

Theory of Fuzzy Logic

Fig. 4.20 shows different threshold functions. The step function (leftmost) is equivalent to the operator > in the classical logic which only has the output value 0 and 1.

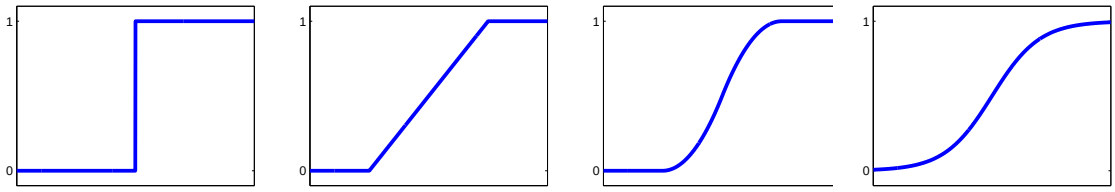

Step function | Linear threshold function | Sigmoid of polynomials | Sigmoid $\frac{1}{1+e^{-t}}$

Figure 4.20.: Different threshold functions.

Fig. 4.21 and Fig. 4.22 illustrate the threshold functions used in this thesis as they do not require a lookup table in fixed-point. Both threshold functions can be described by a center

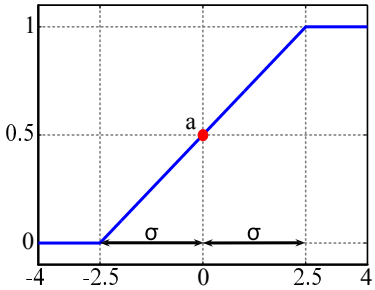

$$L(x,a,\sigma) = \begin{cases} 0 & x \leq a-\sigma \\ \frac{x-a+\sigma}{2\sigma} & a-\sigma < x \leq a+\sigma \\ 1 & x > a+\sigma \end{cases} \tag{4.36}$$

Figure 4.21.: Linear fuzzy logic threshold function ($a = 0, \sigma = 2.5$) (Pape (2008, page 10)).

point a and a width 2σ. Eq. (4.37) shows the polynomial threshold function from the class of the sigmoid functions characterized by their *s*-shape.

As in classical logic, conjunctions are also defined in Fuzzy Logic. A condition for the *negation* is, for instance, holding $\neg 1 = 0$ and $\neg 0 = 1$. The simplest variant to fulfill this condition in fuzzy logic is used here and defined by

$$\neg A = 1 - A\,. \tag{4.38}$$

The *conjunction* in fuzzy logic that fulfills the classical definition can be evaluated by

$$A \wedge B = \min(A,B) \quad or \qquad A \wedge B = A \cdot B \tag{4.39}$$

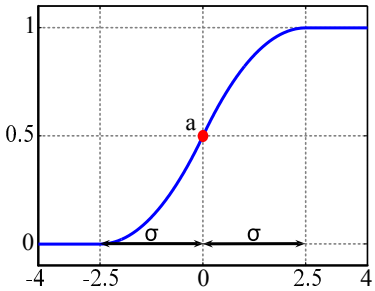

$$S(x,a,\sigma) = \begin{cases} 0 & x \le a-\sigma \\ 2\left(\frac{x-a+\sigma}{2\sigma}\right)^2 & a-\sigma < x \le a \\ 1-2\left(\frac{a-x+\sigma}{2\sigma}\right)^2 & a < x \le a+\sigma \\ 1 & x > a+\sigma \end{cases} \tag{4.37}$$

Figure 4.22.: Sigmoid polynomial fuzzy logic threshold function ($a = 0, \sigma = 2.5$) (Pape (2008, page 11)).

while the simplest and here used *disjunction* is

$$A \vee B = \max(A, B) \,. \tag{4.40}$$

Application to STWEVENT Decision Criteria for Tolerance Increase

Using Fuzzy Logic, the *logical connective* of the five criteria for the detection of steering events STWEVENT can be re-formulated from

$$\begin{aligned} \mathsf{PEAK}' = {} & (T_{steady} > P_{steady,T}) \wedge (\Delta\delta_{S,event} > P_{event,Stw}) \wedge \\ & (T_{event} < P_{event,T}) \wedge (\dot{\delta}_{S,event,max} > P_{event,Stv,max}) \end{aligned} \tag{4.41}$$

to

$$\begin{aligned} \mathsf{PEAK} = min(\quad & L(\, T_{steady}, \quad P_{steady,T}, \quad \sigma_{steady,T} \quad), \\ & L(\, \Delta\delta_{S,event}, \quad P_{event,Stw}, \quad \sigma_{event,Stw} \quad), \\ 1 - \quad & L(\, T_{event}, \quad P_{event,T}, \quad \sigma_{event,T} \quad), \\ & L(\, \dot{\delta}_{S,event,max}, \quad P_{event,Stv}, \quad \sigma_{event,Stv,max} \quad)) \,. \end{aligned} \tag{4.42}$$

The min()-function has shown the best results. Tab. 4.4 shows the thresholds from Eq. (4.41) and the related fuzzy thresholds for Eq. (4.42).

Table 4.4.: Essential fields of a CAN message

Criterion	Threshold / Center a	Fuzzy width σ
T_{steady}	2.2s	5.0
$\Delta\delta_{S,event}$	1.1°	0.4
T_{event}	0.5s	0.4
$\dot{\delta}_{S,event,max}$	P_{event}	0.01

Fuzzy Logic to Reduce Fixed-/Floating-point Errors

As illustrated in Fig. 4.23, all signals suffer from precision loss in fixed-point arithmetics. This is a major problem when applying parameters and predicting the detection rate in online fixed-point controller units. Controller in the vehicle run in fixed-point and need manual laborious scaling of every signal and operation, whereas development and simulation are easier in floating point. When decisions are made, for instance the five criteria to detect a steering events from the steering wheel angle and velocity, the differences of the signals lead

to missed detection of event in fixed point compared to the implementation in floating-point or vice versa. The idea was to use fuzzy logic to soften the decisions so that events are always detected, but with slightly different amplitudes and, thereby, to decrease errors.

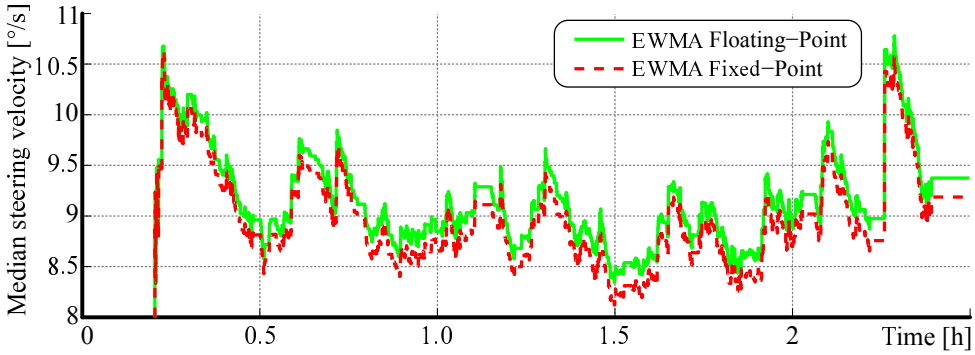

Figure 4.23.: Signal differences in median steering velocity from precision loss in fixed-point scaling arithmetics.

4.4.5. Steering Wheel Angle Area (Amp_D2_Theta)

`Amp_D2_Theta` ("the amplitude duration squared δ_S")[3], is a time-based feature with a weighting function to score variations. This feature is defined as the area of δ_S and its mean between *zero crossings* multiplied by the time for which the steering wheel angle is on the same side of its mean. This is another measure for the steering variance that performed well in (Berglund, 2007) for simulator drives. Eq. (4.43) shows the definition from (King et al., 1999) and Fig. 4.24 illustrates the areas A_j^δ and durations t_j^δ between zero crossings.

$$\texttt{Amp\_D2\_Theta} = \frac{100}{N} \sum_{j=1}^{J} \left(A_j^\delta t_j^\delta \right) \tag{4.43}$$

with

N ...number of samples in the window (scaling factor was neglected)
J ...number of area blocks in the sliding window (MA or EWMA)
A_j^δ ...area of the j-th block under $\delta_S - \mu(\delta_S)$
t_j^δ ...the duration of the j-th area block.

Optimization of the feature with the correlation coefficient yields a cut-off frequency $P_{fCut\_stwAngleOffset} = 2.75Hz$ for a 2nd order Butterworth low-pass filter for obtaining the mean δ_S. The moving average of the last $J = 90$ areas performs best for `Amp_D2_Theta` and $J = 45s$ for the EWMA of the event-rate feature `AmpD2ThetaEwma`.

4.4.6. Steering Wheel Angle and Velocity Phase (ELLIPSE)

According to (King et al., 1999), there are three different ways to evaluate steering wheel angle δ_S and velocity $\dot{\delta}_S$: time-based, frequency-based and *phase*-based, i.e. δ_S versus $\dot{\delta}_S$.

[3] In (King et al., 1999) Θ is the name of the steering wheel angle, which explains the name of the feature `Amp_D2_Theta`. However, we use δ_S, which is more common.

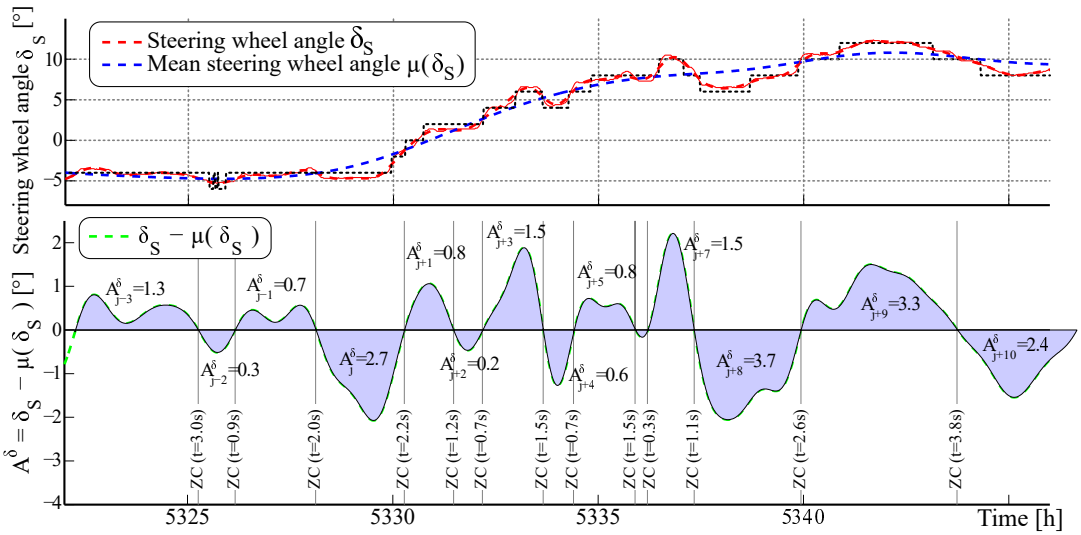

Figure 4.24.: Feature AmpD2Theta: Area between steering wheel angle and its mean multiplied by the duration for which the steering wheel angle is on the same side of the mean. Removing the steering offset (––) avoids the influence of curves and the vertical road inclination.

The ELLIPSE feature (King et al., 1999; Berglund, 2007) is calculated as the offset-compensated magnitude of steering wheel angle and velocity outside a threshold ellipse during a sliding window. Eq. (4.44) explains the calculation and is depicted in Fig. 4.25.

$$\texttt{ELLIPSE} = \text{EWMA}_N\left(\left(\sqrt{\left(\frac{\delta_S}{P_{\delta_S,radiusTh}}\right)^2 + \left(\frac{\dot{\delta}_S}{P_{\dot{\delta}_S,radiusTh}}\right)^2}\right) > 1\right) \tag{4.44}$$

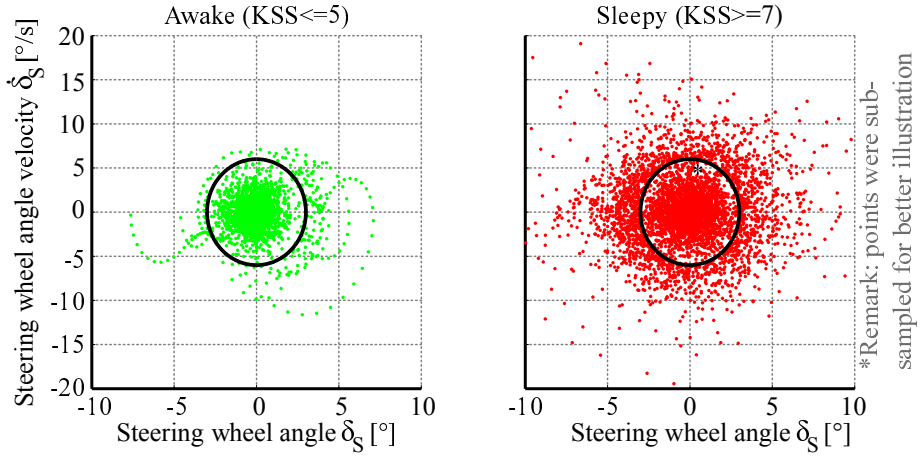

Figure 4.25.: Feature ELLIPSE: Steering wheel angle δ_S and velocity $\dot{\delta}_S$ versus their means outside a threshold ellipse. Removing the mean EWMA (δ_S) and EWMA $(\dot{\delta}_S)$ is necessary to compensate the influence of curves and the vertical road decay for the rainwater drain.

Optimization of this feature yields a cut-off frequency $P_{fCut\_stwAngleOffset} = 0.55Hz$ for a 2nd order Butterworth low-pass filter for obtaining the steering offset and $P_{fCut\_stvAngleOffset} =$

$0.125Hz$ for $\dot{\delta}_S$. The EWMA window size is $N = 60s$. The steering ratio, angle and velocity are different for every vehicle, thus the optimal weighting factors $P_{\delta_S,radiusTh} = 3°$ and $P_{\dot{\delta}_S,radiusTh} = 6°/s$ are different than in literature (King et al., 1999).

4.4.7. Steering Inactivity (NRMHOLD)

NMRHOLD was defined by (Wierwille and Ellsworth, 1994) as the number of times for which the steering wheel angle δ_S is hold for longer than the threshold value $P_{NMRHOLDT} = 400ms$. According to (Berglund, 2007), the maximum threshold for $|\delta_S|$ was set to $P_{maxLrw} = 0.5°$. An EWMA filter with $P_{EwmaWinSize} = 5\,min$ is applied after suppression of system inactivity SAS_{CAN}. Curves are removed similarly as for ELLIPSE. Further, a second variant of the feature, based on the SG-differentiator filtered steering velocity, is implemented NRMSTVHOLD with the threshold $P_{maxLrv} = 6°/s$ for $|\dot{\delta}_S|$.

4.4.8. Small Steering Adjustments (MICROCORRECTIONS)

The idea of MICROCORRECTIONS (discussed in Fagerberg, 2004) is that an alert driver permanently makes small steering corrections to compensate environmental factors such as road bumps and crosswinds. With increasing drowsiness, drivers become more sloppy and these micro-corrections diminish (Petit and Chaput, 1990; Hartley, 1995). According to Kircher et al. (2002), the after-market device "Steering Attention Monitor" (SAM) monitors the presence of micro-steerings.

Extending this concept, the presence of many small micro-corrections leads to low values of this feature, whereas rare and larger corrections yield high feature values. The feature extraction is updated for every steering wheel angle direction change interval by:

$$\text{MICROCORRECTIONS} = \begin{cases} \text{EWMA}\,(0) & P_{STW,Th,Min} \leq \Delta\delta_{S,event} \leq P_{STW,Th,Max} \\ \text{EWMA}\,(1) & SAS_{CAN} = 1 \\ \text{"hold"} & SAS_{CAN} = 0 \end{cases} . \tag{4.45}$$

For every interval, the magnitude between inflection points is calculated as $\Delta\delta_{S,event}$. Anytime the steering amplitude $\Delta\delta_{S,event}$ is between $P_{STW,Th,Min} = 0.8°$ and $P_{STW,Th,Max} = 2.5°$, a microsteering is detected and 0 is fed into the EWMA window with length $N = 0.7\,min$. Otherwise, if the system is active but no microsteering is detected, the feature increases by adding a 1 to the EWMA window. For an inactive system, the calculation is hold.

4.4.9. Fast Corrections (FASTCORRECT)

FASTCORRECT is a feature that is proposed here. It is focusing on a pattern that was often observed in night drives. The pattern is basically the same as in STWEVENT, however, focusing more on single events and the steering correction phase, especially taking into account its rate intensity. A single strong event can indicate an advanced fatigue level.

Maximum Likelihood Parameter Estimation (MLE) of Steering Velocity PDF

The adaptive threshold calculation for steering event detection in Sec. 4.4.3 suffers from the compound weakness that P_{steady} and P_{event} are raising within seconds for single fast events while taking up to an hour to settle for slow steering corrections. In this section, a superior, model-based approach is proposed. In Sec. 4.4.3 it was found that the STVmax distribution can be described best by the Inverse Gaussian PDF in Eq. (4.34), which is defined by two parameters μ and λ. Using the MLE in a floating window yields the estimated parameters $\hat{\mu}[n]$ and $\hat{\lambda}[n]$ of $\dot{\delta}_{S,max}$.

Evaluating the *Cumulative Distribution Function* (CDF) of the Inverse Gaussian $CDF(\dot{\delta}_{th}) = P_{th}$ at the given point P_{th} yields the new threshold for fast corrections $ICDFIG_{event}$ and the baseline $ICDFIG_{steady}$ (both in $[^\circ/s]$). The CDF of the Inverse Gaussian is defined by

$$CDF\left(IG(x;\mu,\lambda)\right) = \frac{1}{2}\,\mathrm{erf}\left(\frac{\sqrt{\frac{\lambda}{x}}(-x+\mu)}{\sqrt{2}\mu}\right) + \frac{1}{2}e^{\frac{2\lambda}{\mu}}\,\mathrm{erf}\left(\frac{\sqrt{\frac{\lambda}{x}}(x+\mu)}{\sqrt{2}\mu}\right), \quad x>0\,. \tag{4.46}$$

The *Inverse CDF* (ICDF) is then computed for instance by evaluating a look-up table:

$$ICDFIG_{steady} = ICDF\left(IG(P_{th,steady})\right) \tag{4.47}$$

$$ICDFIG_{event} = ICDF\left(IG(P_{th,event})\right)\,. \tag{4.48}$$

Fig. 4.26 shows a comparison between *Mean Splitting*, the here discussed *moving ML PDF fit* and *Moving Percentiles*, as proposed in A.8. It can be seen that the moving ML PDF fit and

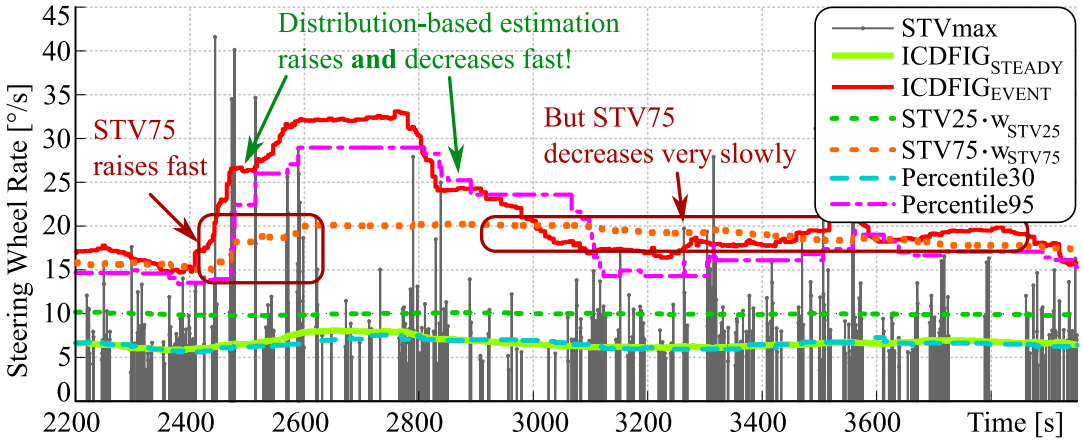

Figure 4.26.: Comparison between *mean splitting*, *moving ML PDF fitting* and *moving percentiles*.

Moving Percentiles adapt faster to changed situations and especially drop faster afterwards. According to the MLE for the Inverse Gaussian parameters, the following property holds: $\hat{\mu} \approx$ `STV50` and, thus, the parameter estimation of $\hat{\mu}$ can be refined by the EWMA again. Hence, this approach is also superior to the *Moving Percentiles* with regards to computational complexity. Further, this distribution model based approach takes every steering into account while the percentiles leave 50% of the steerings out. This property makes the adaption of moving ML PDF faster and much smoother. The PDF model approach is also more accurate as it accurately considers the driving style-related two parameters *mean* and *variance*, rather than just the *mean* in mean splitting.

Feature Calculation using Fitted Sliding Window PDF as Adaptive Thresholds

For peak detection, we use the moving thresholds $ICDFIG_{steady}$ and $ICDFIG_{event}$ obtained by a sliding window of duration $N = 2.4\,min$. The parameter for the steering correction threshold $ICDFIG_{event}$ is set to $P_{th,event} = 0.98$ to detect outliers of fast steering corrections that are above 98% of all regular steering reversals. The parameter of the baseline $ICDFIG_{steady}$ is found as $P_{th,event} = 0.30$ to represent the calm steering in the actual driving situation. The detected steering corrections are set in relation to the steering baseline $ICDFIG_{steady}$ in order to adapt to the current driving situation

$$\texttt{FASTCORRECT} = \begin{cases} EWMA_N\left(\left(\frac{\dot{\delta}_{S,max} \cdot SAS_{CAN}}{\text{sat}_4^{20}(ICDFIG_{steady})}\right)^{P_{w,exp}}\right) & \dot{\delta}_{S,max} > ICDFIG_{event} \\ hold & SAS_{CAN} = 0 \end{cases} . \quad (4.49)$$

The event rate including the peak intensity is averaged by a small EWMA window size of $N = 3\,min$. Weighting the peak by the exponent $P_{w,exp} = \frac{1}{2}$ allows to non-linearly adjust the influence of the peak intensity in comparison to its frequency.

4.4.10. Degree of Driver-Vehicle Interaction (DEGOINT)

DEGOINT is originally defined as the degree of interaction between driver and vehicle according to the 2005 Patent by Eriksson and Björkman and is explained in (Kanstrup, 2006). The idea behind this feature is that the vehicle motion trajectory can be considered as a system with low-pass characteristics which reacts to steering control by the driver and to lateral displacements by the road surface. Steering oscillations with high frequency cannot be seen in the vehicle trajectory. From steer-by-wire, it is known that the feedback from the road has to be provided to the driver via an actuator to enable a responsive steering control. High interaction means quick and precise control that indicates high driver vigilance and vice versa. DEGOINT is a simpler method to measure control parameters of a driver model discussed in Sec. 4.4.16. The original definition of (Kanstrup, 2006) is shown in Eq. (4.50)

$$\texttt{DEGOINT}' = \frac{1}{|\int f_a\,dt - \int f_b\,dt|}) \quad (4.50)$$

with f_a as the surface under the steering wheel torque and f_b under the lateral acceleration integrated over time. It has to be remarked that both areas have different units and are not motivated by an accurate physical model.

Since there was no steering *torque* sensor available in the series vehicles, a similar method is proposed to obtain DEGOINT based on the steering wheel *angle* instead. Therefore, the measured *lateral acceleration* a_y is compared to the *lateral acceleration* $\breve{a}_y$ calculated from the *steering wheel angle* δ_L using the single track model in Eq. (6.8) in Ch. 6.3. This way, the steering and vehicle trajectory interaction can be measured in a physically accurate model. The advantage of using the steering wheel torque, however, is that even when the steering wheel angle is not changing, it can be measured how strong the driver holds the steering wheel against the feedback from the road.

a_y and $\breve{a}_y$ are smoothed by a 2nd order Butterworth low-pass filter with corner frequencies 1 and 2 Hz to compensate different sensor properties, resulting in $a_{y,LP}$ and $\breve{a}_{y,LP}$. For synchronization, $\breve{a}_{y,LP}$ has to be delayed by $\tau = 280ms$. And in order to compensate the lateral road inclination offset, the difference of

$$\Delta_{ay} = a_{y,LP} - \breve{a}_{y,LP} \tag{4.51}$$

has to be highly low-pass filtered with a 2nd order Butterworth filter of $f_c = 0.03\,Hz$ and then subtracted from

$$\hat{a}_{y,LP} = \breve{a}_{y,LP} - \Delta_{ay,LP}\ . \tag{4.52}$$

After the system inactivity suppression, the feature is then obtained by

$$\texttt{DEGOINT} = EWMA_N\left(SAS_{CAN} \cdot (a_{y,LP} - \hat{a}_{y,LP})\right) \tag{4.53}$$

with a window size of $N = 50s$. Fig. 4.27 illustrates the feature principle by the marked area.

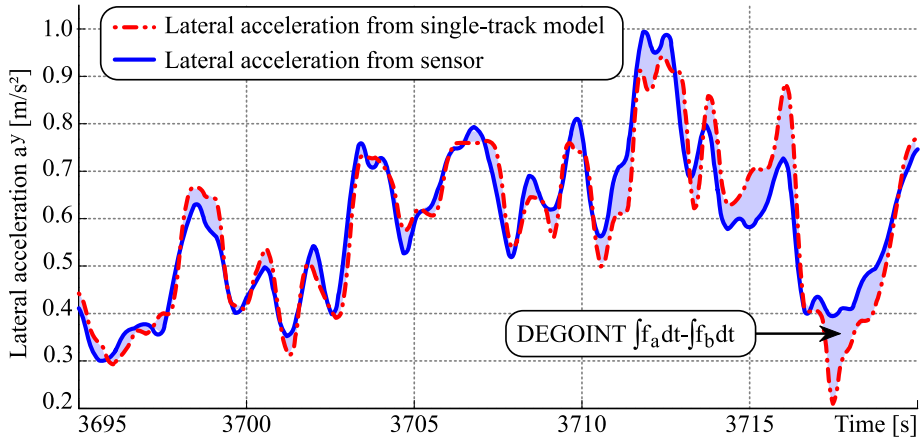

Figure 4.27.: Area representing the degree of interaction (DEGOINT) between driver and vehicle via lateral acceleration from sensor and steering wheel angle from single track model.

4.4.11. Reaction Time (REACTIM)

Reaction tests in various real-road and simulator studies have shown that the reaction time does not dramatically increase with fatigue, but the number of strongly delayed or even complete missed reactions. For this reason, one approach is to find a way to estimate the driver's reaction time. Equivalently, in a driving context, drivers constantly have to react to compensate small changes in road structure, gust of wind etc. The car follows the active steering of the driver after a short phase delay as reaction time. The driver reacts to lateral vehicle displacements in the same manner as the vehicle reacts to the driver control. The drivers' reaction patterns need to be analyzed and compared. The feature REACTIM is defined as the reaction time of the steering wheel angle to lateral acceleration peaks as discussed in (Kanstrup, 2006). Fig. 4.28 shows how the reaction to lateral displacement is detected.

4.4.12. Steering Reaction Time to TLC Minimum (TLCREACTIM)

The feature TLCREACTIM describes the reaction time to TLC minima. The essential advantage is that TLC minima occure more often than real lane exceedings. For implementation details, see the thesis of (Olabe, 2008).

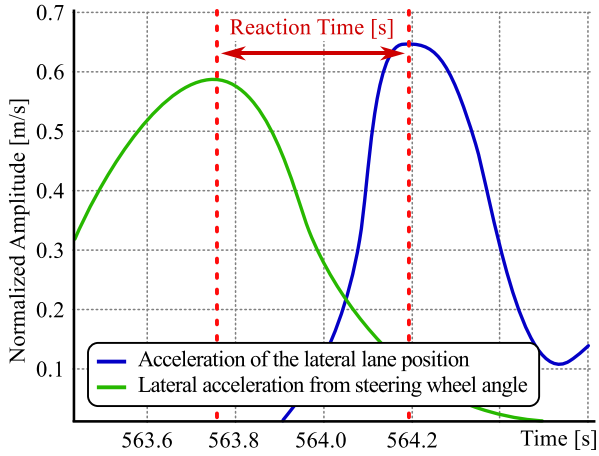

Figure 4.28.: Feature REACTIM: Steering reaction of driver to lateral displacements by environment.

4.4.13. High vs. Low Steering Velocities and Angles (WHAL, VHAL-Index)

According to Bittner and Hana (2000), the VHAL-Index is the ratio of high against low steering correction velocities and is assumed to diminish with reduced vigilance (Kircher et al., 2002). The feature is following the idea that fatigued drivers choose an easier driving strategy, i.e. only compensate large lane deviations. Eq. 4.54 explains the calculation

$$\texttt{VHAL} = \frac{EWMA_N\left(SAS_{CAN} \cdot FM\right)}{max(0.003, EWMA_N\left(SAS_{CAN} \cdot SM\right))} \tag{4.54}$$

with the EWMA window sizes $N = 2\,min$, FM as the number of fast movements and SM is the number of slow movements. The threshold ranges are $SH = 10(^\circ/s)^2 \leq \dot{\delta}_S^2 \leq 80(^\circ/s)^2$ and $MH = 80(^\circ/s)^2 \leq \dot{\delta}_S^2 \leq 2000(^\circ/s)^2$.

WHAL is an altered version of VHAL, based on the amplitude of the steering wheel *angle* between two zero crossings. EWMA with window size $N = 1\,min$ is used and only the velocity and steering wheel angle criterion of the SAS_{CAN} are used for suppression. The threshold to distinguish small from large amplitude deltas is $\Delta\delta_S > 2^\circ$.

4.4.14. Yaw-Rate Jerk (YAWJERK)

While Desai and Haque (2006) are focusing on the spikiness index[4] of the jerk profile, the idea of the proposed feature YAWJERK is to replace the extra-cost steering wheel sensor by the available and sensitive yaw rate sensor (Sec. 2.3.2). The extraction of the pattern is basically the same as for VARCRIT, but, with an exponent of jerk variance $P_{exp,short} = 1.3$.

Comparison between Yaw-rate and Steering Wheel Angle

The finer steering wheel angle has a resolution of 0.1°, while the yaw rate has $0.005^\circ/s$, which is 20 times lower. The signals can be compared since under ideal conditions, a constant yaw rate corresponds to a fixed steering wheel angle for a given velocity. Tab. 4.5 shows the standard deviation of the signal and noise for both signals during motorway drives. The standard deviation of the steering wheel angle is four times higher, which means that the quantization of the yaw rate signal is five times finer. However, since the standard deviation

[4] They defined the *spikiness index* as the local deviation of data from general trend, comparable to the EWVAR .

of the signal-to-noise ratio (SNR) is about eight times better for the sensor of the steering wheel angle, the latter is the slightly better signal.

Sensor	**Resolution**	σ_{signal}	σ_{noise}	$\sigma_{signal}/\sigma_{noise}$	$\mathbf{SNR}_{db}$
St.w. angle δ_S	0.1°	$\approx 3.00°$	$\approx 0.01°$	300	$117db$
Yaw rate $\dot{\psi}$	$0.005°/s$	$\approx 0.74°/s$	$\approx 0.02°/s$	37	$79db$
δ_S / $\dot{\psi}$:	20	4.05	0.5	8.1	$38db$

Table 4.5.: Signal qualities

Fig. 4.29 shows a comparison between the steering wheel angle vs. the raw and DISPO smoothed yaw rate. Fig. 4.30 shows the derivatives of both signals.

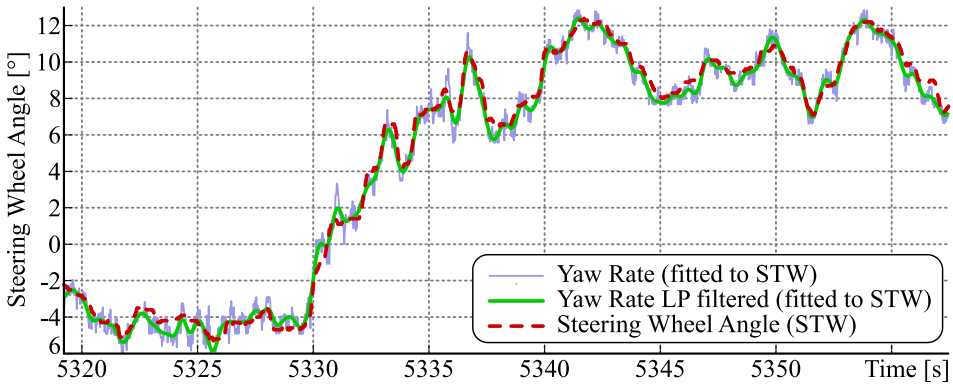

Figure 4.29.: Comparison between yaw rate and steering wheel angle. For this simple comparison, the yaw rate is fitted and shifted by $4.4s \cdot (\dot{\psi}[n - 1.06s] + 0.8\frac{°}{s})$ at 120 km/h.

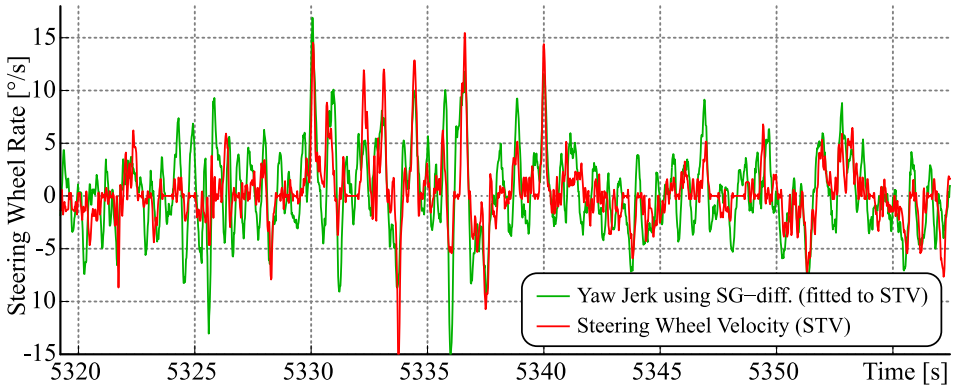

Figure 4.30.: Comparison of yaw *Jerk* vs. steering wheel rate. This confirms that both signals are roughly interchangeable when the speed is taken into account. The yaw jerk was fitted at 120 km/h by $4.4s^2 \cdot (\ddot{\psi}[n - 0.5s] + 0.1\frac{1}{s^2})$.

The yaw jerk $\ddot{\psi}_{SC}$ measured by the sensor is very noisy, but also very sensitive. Here, we can show only the signal $\ddot{\psi}$ from the DISPO differentiator using a polynomial order $P = 3$ and filter tap size $N = 19$. It can be seen that the signal remains noisier due to the fact that the yaw rate sensor is connected to the vehicle body and thus more sensitive to external influences and vehicle speed. Thus, especially bad road conditions have an impact on the yaw rate signal, while the steering signal is less affected due to the design of the steering unit.

When further investigating the signal, many steering corrections that are clearly present in the steering wheel rate, are not visible in the yaw jerk. At the other hand, some peaks in the yaw jerk signal are not present in the steering pendant and most probably caused by external influences. Thus, the signal of the steering wheel angle with a resolution of 0.1° is better.

4.4.15. Spectral Steering Wheel Angle Analysis (STWZCR)

The STWZCR and STWVELZCR simply measure the *zero-crossing-rate* (ZCR) of the steering wheel angle and velocity. It is a measure of how often a driver changes his steering direction. In a broader sense, the ZCR can also be related to the frequencies in the steering signal. It provides several advantages over the Fourier-transform as the frequencies are very low. A classification by different driving styles has also shown that the STWZCR is very characteristic for different drivers.

Looking at the frequencies of the signal of the steering wheel angle using a *Spectrogram* (*Short-time Fast-Fourier Transform* (FFT) and *Power-Spectrum-Density* (PSD), as also discussed by Altmüller (see 2007, Ch. 4.2.2), has not shown any useful results at all, which confirms the negative results from Kircher et al. (2002, Ch. 16) who used the Burg's and MUSIC eigenvector methods. Various different parameters are tried and a practicable result is obtained for the spectrogram at $F_s = 50\,Hz$ for a *Hamming Window* size of 64, small overlap 2 and a 128-point FFT. The ratio of the powers between different frequency ranges were made but no useful results can be achieved as it is shown in Fig. 4.31. The steering frequencies rather depend on the driving situation and individual driving styles. A time-based event detection appears more expedient since events vanish in the large sliding window.

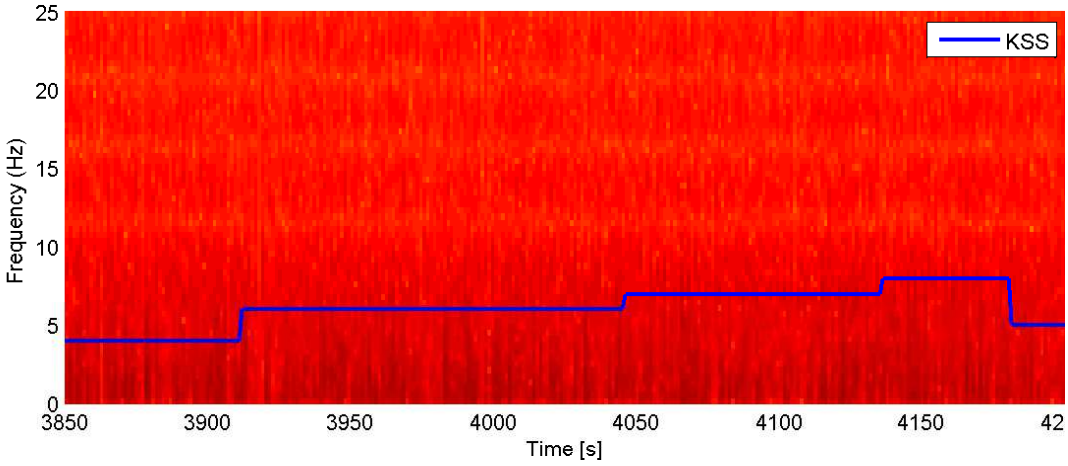

Figure 4.31.: Spectrogram of steering velocity

4.4.16. Driver Model Parameters

As discussed by Pilutti and Ulsoy (1995) and others (Altmüller, 2007; Pilutti and Ulsoy, 1999; Boyraz et al., 2007; Hermannstädter and Yang, 2013b,a), a promising approach is to reflect on how an ideal lateral control system would adjust the lateral lane position in comparison to a real awake or fatigued driver. Pilutti and Ulsoy (1995) use an auto-regressive model to learn the driver parameters and to infer from the changing parameters to fatigue.

4.5. Parameter Optimization

There are over 320 parameters involved in the extraction of the features in this chapter and 171 parameters in the ATTENTION ASSIST series code that are relevant for the system performance. The goal of *parameter optimization* is to find the parameter values for which the features contribute the maximum amount of information to identify the fatigue level of drivers. More generally spoken, optimization pursues the objective to find the best set of parameters for a system that minimize a given *cost function*. The definition of a cost function that represents the system performance is the most essential and difficult task in the present application. Physical parameters further have restricted *boundary conditions* that can be represented as *punishment terms* in the cost function.

It is distinguished between *local* or *global* optimization algorithms corresponding to their ability weather to overcome local minima and find the global optimum. Local algorithms have the advantage to execute much faster by exploiting the good-natured, "convex" property of a system with only one local optimum. Thus, the algorithm selection mainly depends on the cost function property of the system. Choosing good *initial parameters* can severely contribute to the performance and is either done empirically or part of the optimization.

This section will briefly summarize the application of parameter optimization to fatigue related feature extraction. For details refer to the thesis of Ibrahim (2009).

4.5.1. Optimization of Parameters

The general optimization principle is shown in Fig. 4.32. Choosing the new parameter set determines the heuristic of the algorithm.

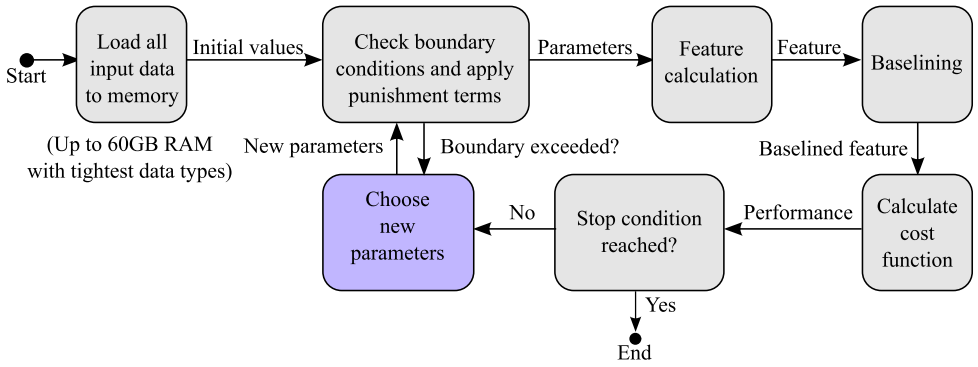

Figure 4.32.: General block diagram of parameter optimization.

Not only the parameters, but also some implementation details or the order of some signal processing steps can be optimized automatically. For instance, it can be examed if a *mean* or *median* yields better results. Tunable parameters and processing variants are for instance:

- Thresholds, weighting factors, exponents, window sizes
- Cut-off frequencies and tab-size of filters
- Suppression times before and after events (e.g. turn indicator lever)
- Baselining duration and method: max, mean and IQR
- Moving average vs. EWMA
- Moving variance vs. moving percentiles vs. EWVAR
- Low-pass and differentiation vs. DISPO differentiator, etc.

Run Level Charts: Due to limited resources, not all parameters could be optimized. Some parameters were identified to have no measurable influence on the result and thus could be excluded. In a first step, relevant parameters were identified using *run-level charts* as shown in Fig. 4.33. Exemplarily, the EWMA window size is varied for the feature LANEAPPROX for one single drive to identify its influence. EWMA parameters always have the effect to

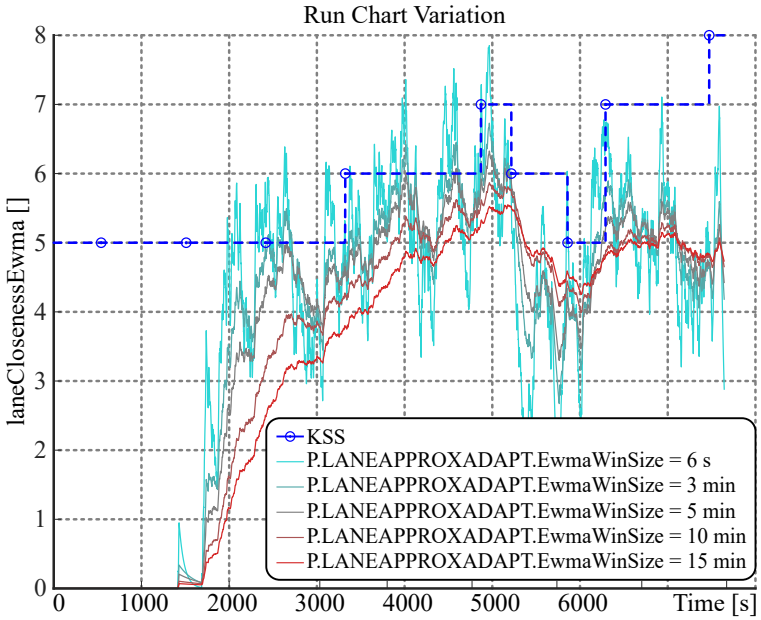

Figure 4.33.: Run-level chart that shows variation of one parameter for a LANEAPPROX to identify its influence

flatten peaks as shown in the figure. Due to the low temporal resolution of the KSS, the optimization favors larger window sizes. This, however, is questionable since sleepiness was observed to change faster than the KSS.

Initial Values: Initial parameters were chosen empirically by this method and were confirmed if they yielded good results for a few selected drives.

Cost Function: As cost function for the optimization of each feature, the inverse of the Spearman correlation coefficients (Sec. 7.1.1) and Fisher Linear Discriminant Metric MDA (Sec. 7.1.2) are used. The cost function is calculated as the difference between the feature and KSS fatigue reference (see Ch. 7 and 3).

Boundary Conditions: As boundary conditions, negative times and frequencies were for instance punished with high cost to prevent the optimization algorithm to chose such parameters. Furthermore, e.g. filter tab-sizes must be integer numbers and thus were rounded.

4.5.2. Computational Complexity Reduction

Most optimization algorithms require many iterations and a run-time of maximally minutes per iteration to converge within a practical time. Since the simulation of one ATTENTION ASSIST parameter set takes several hours for all valid drives, even efficient algorithms would take months to years. As the computation time was obviously the main limiting factor, several measures were taken to speed up the processing:

RAM instead of HDD: A major bottleneck is to load entire drives (including unnecessary signals) sequentially from the hard drive during every iteration. Read access from RAM is about 70 times faster[5]. Thus, only the needed signals for one feature are load and concatenated in RAM at once. 45GB to 80GB were necessary, depending on the features, varied parameters and dataset (ALDWvalidND or ALDWvalid).

Precision-lossy data type compression: As CAN-signals use 1 to 16 bit integers, using 64 bit double floating-point data types is another waste of resources. Thus, all signals are compressed to the tightest data type with a maximum precision loss of 1%.

Pre-computation and caching Resource consumption is often a trade-off between memory and computation. The open-loop pre-processing operations of CAN-signals could be computed in advance as they solely depend on the sensor signals. Depending on the varied parameter, further derived signals could be cached if parameters did not change or were calculated before: e.g. the system active signals, external factors and especially cross-wind detection. The reset of every drive (for baselining) could be triggered by a drive-ID change.

Causalization: Online algorithms perform all real-time processing steps sequentially. Model-based algorithms favor "causalized" software architectures (Simulink/TargetLink). Modern *arithmetic logic units* (ALU) (such as CPU, GPU and DSP) can process basic function much faster on vectors or matrices. However, this is only possible offline and if processing steps do not depend on the closed loop output of a previous time step.

Model-based porting to matrix operations: The complete ATTENTION ASSIST algorithm was ported bit-true from Simulink/TargetLink to MATLAB© where processor-optimized (MMX) matrix operation could be performed using LAPACK and BLAS. Recursive algorithms like EWMA, EwmaN, EWVAR , EWIQR etc. were implemented in MEX C++.

The total performance gain is on average factor 300-500 times faster in comparison to the Simulink model. This speed up allowed to simulate a smaller selection of drives in seconds. Optimization with up to six parameters became manageable this way.

Only the most promising features and parameters could have been optimized: `LANEDEV`, `VHAL`, `TLC1MIN`, `ZIGZAGSBL`, `LANEAPPROXADAPT`, `YAWJERK` and `STEVENT`. They all depend on the ATTENTION ASSIST pre-processing.

4.5.3. Application

The features described in this chapter were optimized in several stages:

Parameter Study: The ATTENTION ASSIST series algorithm was optimized independently from the features, with the cost function based on the detection and false alarm rate of fatigue warnings. The detection rate is quantized due to the discrete number of warnings, thus, automatic parameter optimization is not possible here. For obtaining the 171 parameters, the system understanding was part of the iteration loop, knowledge that optimization algorithms usually do not have. Iteratively, only five to ten parameters of one module were chosen in a predefined grid and combination, similar to *grid-* and *hierarchical search* while other parameters were kept at the best known point. Still, the simulation distributed to several workstations each with up to 16 cores required up to six weeks. The results were then analyzed and the understanding of parameters and effects lead to a refined selection of parameters.

[5] e.g. for DDR-3 1066 MHz, SATA 7.200 RPM, XEON server

Empirical Parameter Selection: Initial values were chosen empirically from physically plausible values based on graphical assessment for a small selection of drives (cf. Ch. 7.2).

Automatic Local Optimization: While the previously described method ensured that the algorithms perform as desired for every parameter set due to the understanding of the system, it is at the other hand very laborious and does not necessarily find the global optimum. With the fast implementation in Sec. 4.5.2, up to six parameters were varied. With this observation, the *Nelder-Mead simplex algorithm* as described in Lagarias and Reeds (1996) was applied and in fact further improved the feature performance.

Optimizing a combination of features: In a second step, the best features were combined by multiple regression resulting in a single fatigue measure. For this measure, the Spearman coefficients were again used as cost function.

Global Optimization: In the scope of the theses of Ibrahim (2009) and Olabe (2008), global optimization algorithms were implemented. The toolbox was covering the optimization algorithms: grid search, simplex, particle swarm, genetic and evolutionary algorithms, particle swarm and simulated annealing. Due to the computational complexity, only three features could be investigated. For convex problems, they did not show additional benefit.

4.6. Conclusion

Features from literature, improvements thereof and new features were discussed. Many more features (cf. App. A.9) have been studied, but did not show much potential. There are still more potential patterns that can be investigated. Different approaches to optimize the involved parameters and to overcome the computational complexity were presented. The parameters described together with the features are the result of one of the optimization steps.

One problem was that the optimization sometimes converged towards implausible values or very large window sized of over one hour. The later is most probably related to the fact that fatigue and especially the KSS entries are changing very slowly. Some parameters had to be set manually as the results of the optimization were implausible such as zero suppression times. This can be explained by the observation, that there were not enough occurrences of such events in the data to make a difference.

It would be better to optimize the combination of features, for instance, by using the classification error as cost function. However, this is not yet possible due to the computation time. Most of all, the major problem was that the optimization can only be as good as the cost function in respect to the reference.

Chapter 5.

External Factors and Driver Influences

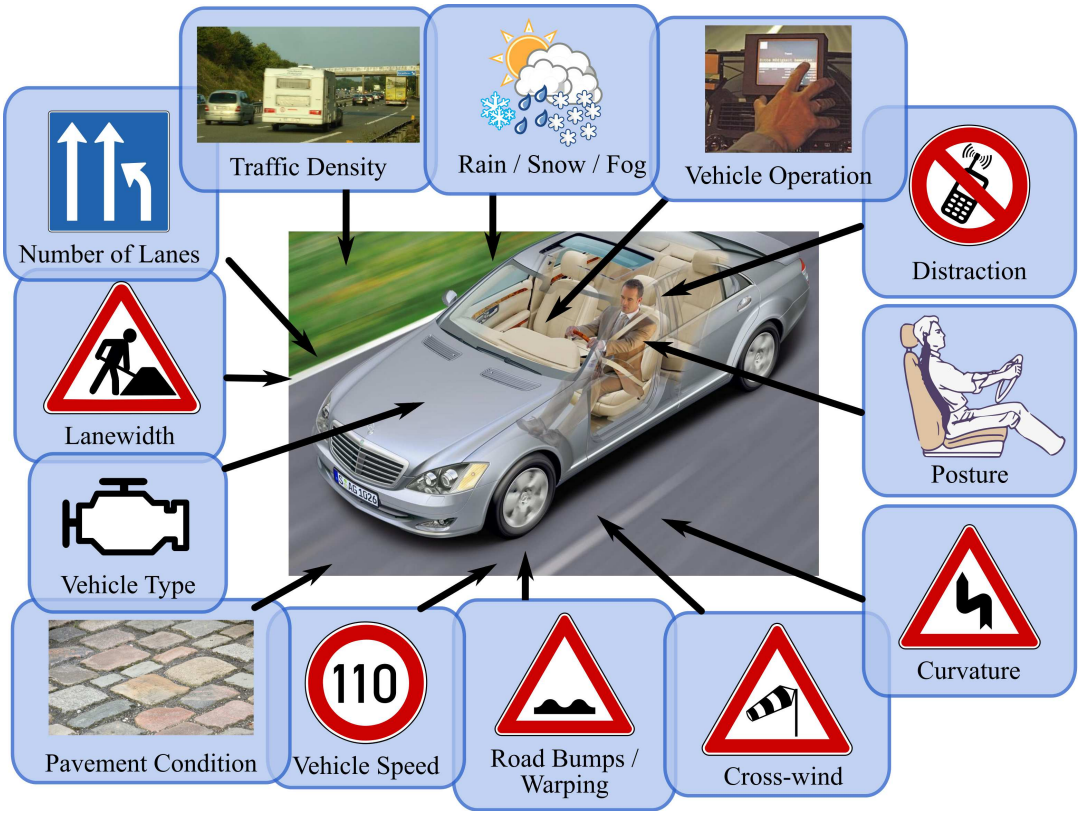

Figure 5.1.: External influences on the driving behavior that overlay sleepiness related patterns

The goal of feature extraction is to reduce the sensor information to only depend on fatigue and to be as independent as possible from other factors. In practice, driving performance features also depend on environmental influences, driver-individual and situation based factors. Fig. 5.1 illustrates the most important factors that affect the driving style in real-road driving situations (Friedrichs and Yang, 2011). The simplest approach to cope with this problem is to measure the influences and to provide the measures to a classifier that is sophisticated enough to automatically adapt to these conditions. This topic is not discussed in literature even though it is the key to transfer the results obtained under laboratory conditions to a real-road application. The present chapter investigates these influencing factors with the goal to derive features from them and, if possible, already consider them during the feature extraction.

5.1. Methodology to Quantify and Incorporate Non-Sleepiness-related Influences

In this thesis, new methods are presented to detect road bumps, traffic density and cross-wind. Specific test drives have been conducted at night to vary only one isolated factor, while keeping the others constant to identify the influence of a single factor. When, for instance, the factor vehicle speed was varied, it was assured that the other factors remained constant, for instance, the driver condition, traffic density, overtaking maneuvers, road curvature, road bumps, vehicle parameters, cross-wind as well as precipitation and light conditions. The detection methods have also been implemented in real-time to evaluate the performance while driving in different situations. In the offline analysis, the correlation between the varied factors and features, extracted for this road section, was evaluated. The driver's daily mood (e.g. economic or aggressive) is another factor, which is difficult to classify and discussed in Sec. 5.4. The way that drivers hold the steering wheel (e.g. with one or two hands) also has a significant influence on the steering behavior. However, additional sensors would be required for its detection and, therefore, this factor is not considered here. The results emphasize the importance of considering driving influences in driver monitoring.

The goal of this work is to find a measure for most of the thirteen factors from Fig. 5.1. The simplest factor is the vehicle velocity, which is already represented by its speedometer signal. However, measuring the curvature or road condition is not as simple. When we consider these thirteen dimensions, it is obvious that it's impossible to record drives for every combination of these factors. Thereby, we assume that superposition applies, i.e. factors overlay and the combination can be approximated as linear. Fortunately, the probability of multiple factors occuring at the same time is increasingly low. For instance, it is not very probable that a driver is driving on a construction-site that is curvy, during rain with cross-wind and road bumps at the same time etc. In this example, the SAS criteria for the system activity will set the system to inactive anyway.

After finding these measures, the next step is to analyze the relationship of these factors with the fatigue-related features. Usually and if possible, it is easier to compensate the raw input signals rather than every feature individually. Curvature can, for instance, be removed from the steering signal by a high-pass filter. The best but most difficult way, however, is to consider these influences during the extraction of every feature.

5.1.1. Evaluation of Geo-position mapped Events and Signals

Analysis of road bumps and the road surface would be a straightforward task, if there was a good reference to assess the quality of these signals. One approach to have a reference is mapping road bumps to real world position where they occur.

Fig. 5.2 shows a method of how events of one or several drives can be mapped to their geo-coordinates on a map. This way, clusters of steering corrections and road bumps were identified, that often occurred at the same place.

5.2. Influences from External Factors on the Driving Behavior

This section will explain the most relevant external factors. Details of the detection are provided and illustrations are given for important examples only.

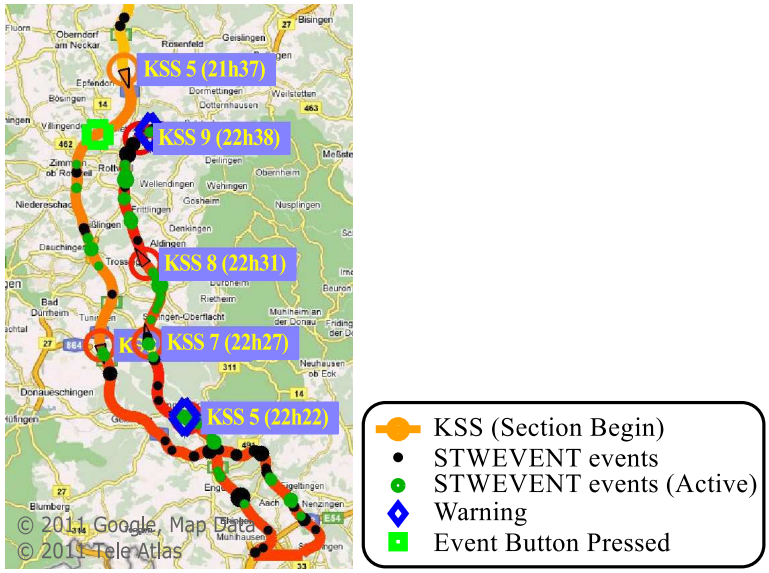

Figure 5.2.: Clustering of different events and assignment to geo-positions

5.2.1. Influence of Distraction and Vehicle Operation

Usually, drivers accept distraction in situations which they consider as safe enough to perform other tasks besides driving. Drivers can interrupt their side-activities when a traffic situation requires it. However, they cannot easily "switch off" their sleepiness. The major difference between fatigue and distraction is that fatigue is permanently impairing the driving style while distraction results in a strong and frequent alteration between being very present and accurately driving vs. being totally out of the loop for up to several seconds when the eyes are off the road. Thus, it is helpful to distinguish drowsiness from acceptable short term distraction (e.g. from vehicle operation) or long-term distraction such as phone calls or discussions with the co-driver.

Distraction can consist of several *channels*:

visual the driver's eyes are off the road, e.g. during looks to the head-unit or the outside
motoric the driver operates head-unit or adjusts the seat (not necessarily looking there)
audio discussing or listening, which can also increase the cognitive work-load
cognitive intensive thinking, e.g. calculation tasks increases the cognitive work-load

The *work-load* resulting from these channels is limited to a certain extend. This means that the driver can not look to two locations, listen to different sources or touch different objects at the same time. On the other hand, when a driver is busy by looking somewhere, he can additionally listen or talk at the same time, however with limitations.

Also the operation of the levers close to the steering wheel or the manual shifting can result in steering errors. Distraction from vehicle control can be detected by the vehicle signals of buttons and levers. Discussions on the phone can only be detected, if they are performed over the hands-free head-unit. A measure for this kind of distraction was already introduced using CAN-signals. Other distractions cannot be measured directly, yet. To simplify matters, steering operations or lane exceedances during intensive short-term distractions were suppressed from drowsiness detection.

Several levers, such as the limiter or high beam levers have multiple permanent states, but only the instant of operating is of interest for these. Therefore, only the raising and falling slopes of the signal have been considered.

5.2.2. Influences by Rain, Snow, Fog, Light Conditions and Tunnels

It was observed that the driving behavior changes severely during heavy rain or snow fall. Usually, the steering becomes more hectic and the driver has to concentrate more. This influence is refreshing at the beginning, but can become even more exhausting after a while. Rainfall and foggy weather usually require the driver to slow down. As illustrated in Fig. 5.3, rain can be detected well by the rain sensor and the lever position of the windshield wiper.

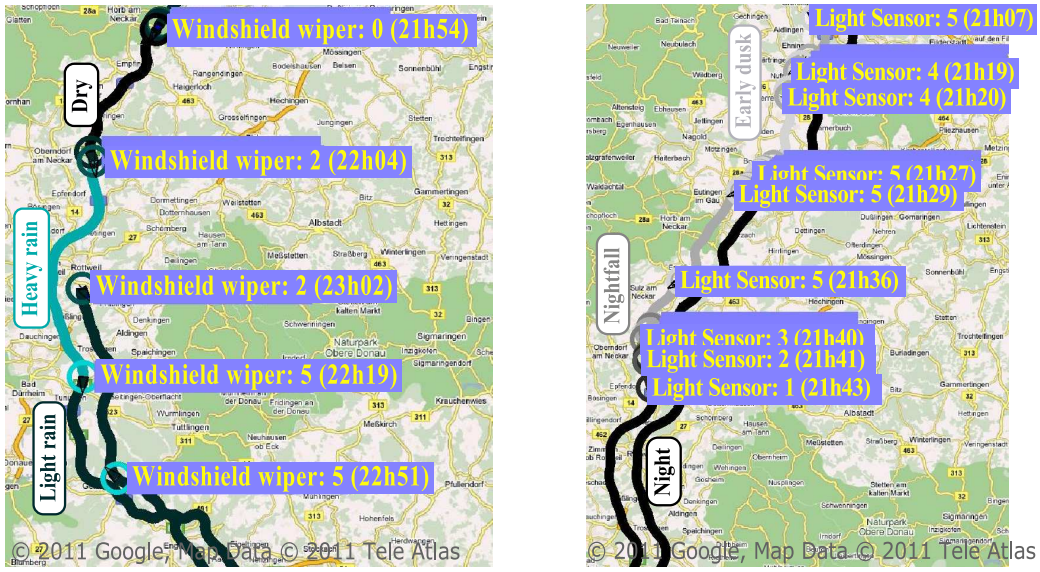

Figure 5.3.: Lever position of the windshield wiper, light sensor on the route for rain, snow and luminosity detection

It was observed that reduced vision due to dark light conditions also affects the steering and lane keeping performance for several persons even when they are awake.

These drivers need to concentrate more than during the day, which can be quite exhausting after a while. The light level can again be measured well by the light sensor and light switch (or automatic) as shown in Fig. 5.3. Illuminated tunnels or other road sections provide a certain degree of *novelty* to the driver and usually improve the level of attention for a short period. Tunnels can be detected well by looking for fast changes in the light sensor signal. To simplifiy matters, sections with intensive rain, fog or snow are suppressed here and treated as system inactivity.

5.2.3. Vehicle Speed Influence

The vehicle velocity has a big influence on the steering velocities and the necessary reaction times to vehicle displacements. The time remaining to react, when heading towards the lane markings at high speeds, is of course shorter than for lower speeds. Thus, the vehicle speed must be considered during the extraction of features. `VELOCITY` is simply the vehicle speed.

Experiment for Data Acquisition

In order to evaluate the speed dependency, a number of drives was recorded where all factors were held constant except for the vehicle speed. A 20 km section on a German autobahn was driven multiple times by the same driver with a Mercedes-Benz S-Class at different speeds. The speed was varied sequentially from 90, 110, 140 to 180km/h. The drives took place between 2 and 5 a.m. such that lane changes and interferences by traffic and trucks could be kept at a minimum. With the low traffic, the speed could be kept very constant without the use of ACC. The drivers rested well for two days before the experiment, so that they were driving fully awake (KSS ≤ 5) at this nocturnal time. Furthermore, a specially trained co-pilot supervised the drives. The acceleration pedal, the turn indicator lever signal and the steering wheel angle have been used to precisely detect the begin and end of the drive. Overtaking maneuvers were suppressed in the same way.

Results of Speed Dependency Analysis

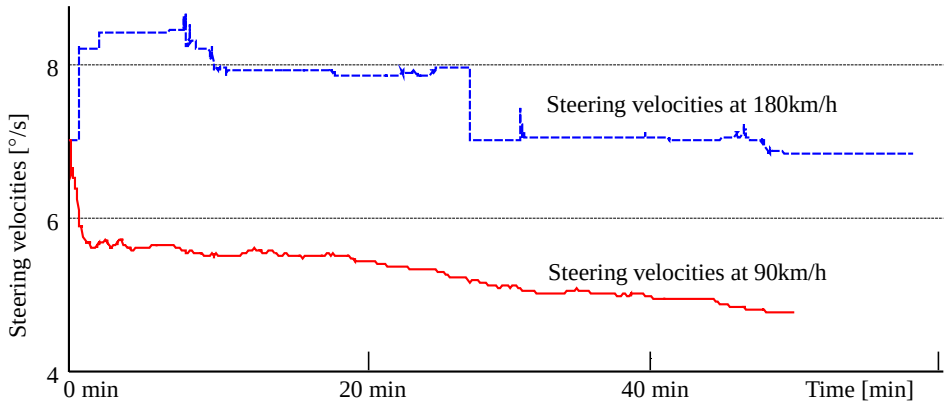

Figure 5.4.: Steering velocities STV50 for different vehicle speeds

After extracting the features for these drives as described in Ch. 4, some of the effects were very clear to see (Friedrichs and Yang, 2010b):

- The steering velocities increased almost proportionally to the vehicle speed. An example of the steering velocities at different vehicle speeds can be seen in Fig. 5.4.
- The steering amplitudes is also higher with increasing velocity.
- The number of overtaking meneuvers increased from $2/h$ at 90 km/h to over $84/h$ at 180 km/h, even with low traffic.
- The maximum lane deviation amplitude remained approximately the same, only the oscillation frequency increased.
- The variance of the accelerator pedal increased as more gas is required at higher speeds to obtain the same acceleration.
- When driving with different speeds on the same road section, the frequency of curvature increases with higher velocity.
- Likewise, on similar road sections, the lateral acceleration obviously increased with higher speeds.

Even when the amplitude of the lane deviation was quite constant, Fig. 5.5 depicts the increasing LANEDEV feature with increasing speed, which is caused by the increasing frequency and since the moving average is based on a fixed time-window.

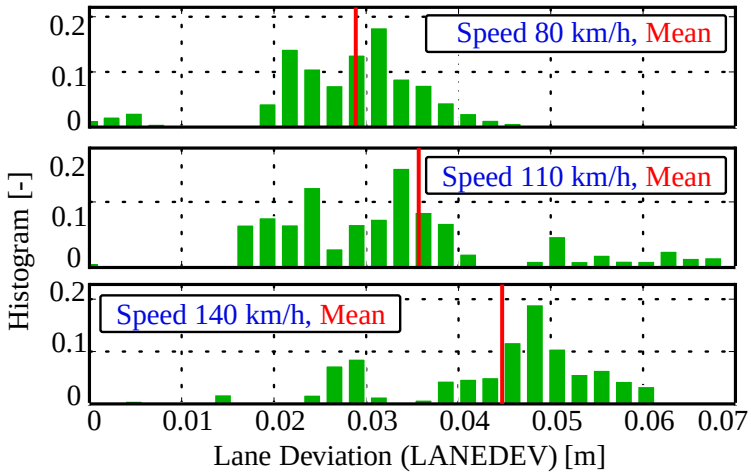

Figure 5.5.: Lane deviation LANEDEV for different vehicle speeds (80km/h, 110km/h and 140km/h)

Fig. 5.6 shows the steering event rate STWEVENT that is significantly larger for high speeds (red) than for low speeds (green). The simplest approach to compensate this influence is to normalize the feature by the vehicle speed as shown in the right.

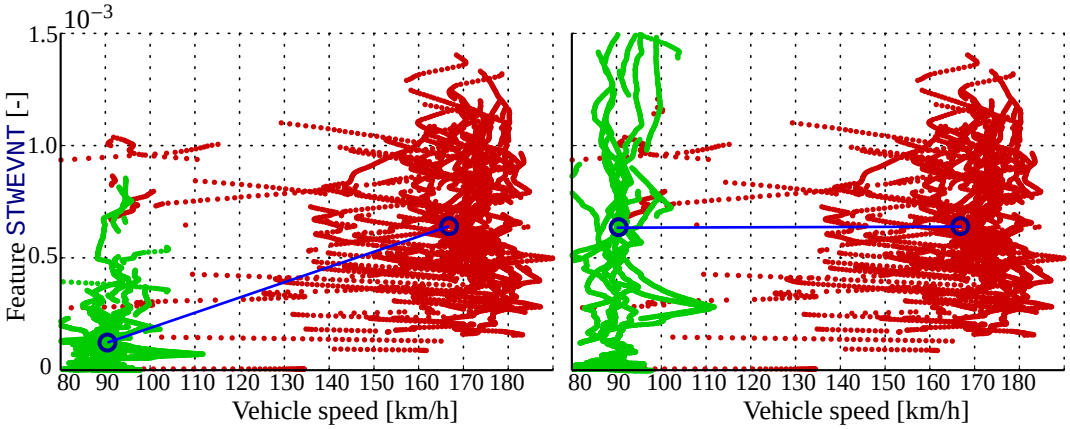

Figure 5.6.: Vehicle speed dependency of the steering event rate STWEVENT (left) and the feature normalized by the vehicle speed (right). The horizontal blue line indicates that the normalized feature is in average independent of the vehicle speed.

5.2.4. Influence by Construction Sites and Narrow Lanes

Road construction sites are usually characterized by more narrow lanes and, thus, accompanied by more hectic steering. Lane exceedances are often unavoidable. Even when the speed limit is reasonably low, people in many countries tend to drive faster than allowed. For this reason, the following combination of criteria was used to detect construction site passages:

- Narrow roads: lane width < threshold $P_{ConstSiteLnWth}$
- Vehicle speed < 85km/h
- Bad lane quality signal from the lane tracking unit
- Specific lane colors (In Germany, yellow lane markings indicate construction sites)

Construction sites were not implemented as an individual feature, but were part of the system active signal SAS_{CAN} and SAS_{LANE}, depending on the available signals. For the evaluation,

the same drives were used as for road bumps explained on page 117. The classification of road construction sites was performed for all available drives and then projected to the coordinates, where they occurred. The match of drives in several night experiments was, in average, very good (over ≈ 90%) and it could clearly be verified that one construction site was terminated from one day to the next. To simplify matters, construction sites were suppressed and treated as system inactivity.

5.2.5. Influence of Curvature

In order to evaluate the influence of the road curvature, drives from a straight (curvature radius $r = 4\,182m$), medium ($r = 2\,008m$) and strongly curved road ($r = 822m$) section were selected. 27 drives were taken from a night experiment with an average speed of 130 km/h. All drives were conducted at night with awake drivers (KSS ≤ 5). In general, it was observed that the transition from a straight road to a curve is often followed by steering adjustments that are more intensive than necessary. Fig. 5.7 shows how the lateral lane deviation increases for all drivers with increasing curvature. The correlation between the lateral lane deviation and the curvature appears stronger than the correlation between the lane deviation and drowsiness. This means that the external factors are stronger than the fatigue related patterns.

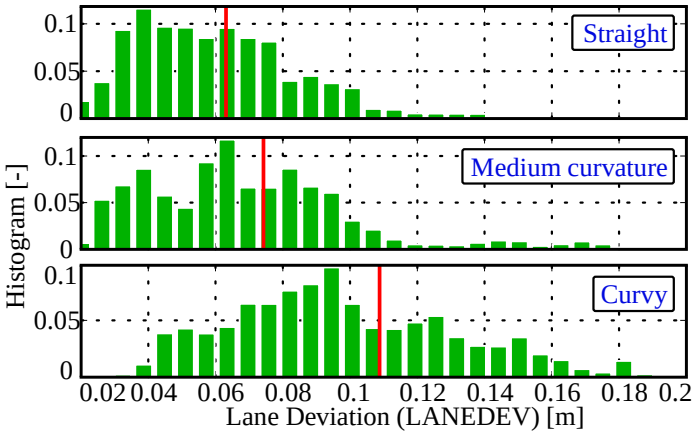

Figure 5.7.: Curvature dependency of the lane deviation LANEDEV

.

Fig. 5.8 shows how the fast steering velocities (significantly) increased with raising curvature. Since the steering velocities are very driver dependent, they were baselined by the mean of the steering velocities of straight road sections for each drive. The vertical line indicates the mean in each class. The measure for CURVATURE is calculated by

$$\text{CURVATURE} = EWMA_N(|\kappa_{LP}|) \tag{5.1}$$

with κ_{LP} as the low-pass filtered curvature from Eq. 6.1 in Ch. 6.3 and a EWMA window size of $N = 1\,min$.

5.2.6. Road Condition Influences

The road condition is another severe influence on the driving performance and comprises the three following aspects:

Pavement Condition irregularities of the road surface lead to permanent unevenness

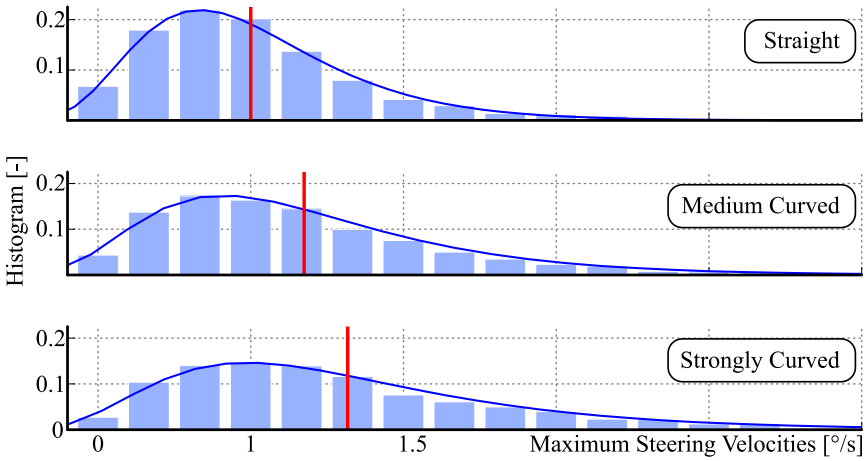

Figure 5.8.: Curvature dependency of the maximum steering velocity between inflection points. Especially the fast steering corrections increase.

Road Bumps short and stronger road bumps that usually affect both wheels

Road warping and Cross-Wind occur when the road changes its lateral inclination causing the vehicle to roll around the longitudinal axis. *Cross-wind* has the same effect as road warping. For the available sensors, it cannot be distinguished, whether the lateral displacement is caused by an uneven road surface or a wind gust.

Road Pavement Condition

Usually, the vehicle slides calmer on a new pavement than on an old, very damaged road surface. These irregularities are normally not immediately realized by the driver, but still result in small lateral displacements of the vehicle which the driver has to correct after a while. Estimating a measure for the road condition can be done by detecting a simultaneous vibration in different sensors. As the sensors are mechanically connected road unevenness and shocks can be observed by the following sensors:

- Wheel rotation sensor
- Longitudinal and lateral acceleration sensor
- Yaw rate sensor
- Vehicle level signals from every wheel[1]

A combination of all sensors would make the detection even more accurate, but is not necessary. The principle proposed here for the wheel rotation sensor can also be applied to other sensors, however with different parameters:

$$\texttt{PAVEMENT} = EWVAR_N(WhlRPM_{FL,HP}) \cdot EWVAR_N(WhlRPM_{FR,HP}) \qquad (5.2)$$

$WhlRPM_{FL,HP}$ and $WhlRPM_{FR,HP}$ are the high-pass filtered wheel rotation rate sensor signals with the cut-off frequency $f_c = 0.5\,Hz$ evaluated in an EWVAR window of length $N = 1\,min$. The variance of all sensors can then be combined by multiplication to favor a simultaneous vibration. After the EWVAR calculation, the signals do not necessarily need to be synchronous. This makes it less sensible to other variations such as the engine rotation.

[1] Vehicle level signals were available, if the vehicle was equipped with air suspension or active body control.

The vehicle speed should also have an influence on all sensors. However, it was not investigated due to the lack of suitable measurements. Imbalances of tires introduce a frequency of the wheel RPM and were filtered out by a notch filter with speed-adaptive frequency.

Fig. 5.9 shows an overlay of the road surface condition signals PAVEMENT for a selection of drives on the A81 motorway over the driven distance from a common starting point. It is very clear to see, that all vehicles detect the road condition in a similar way.

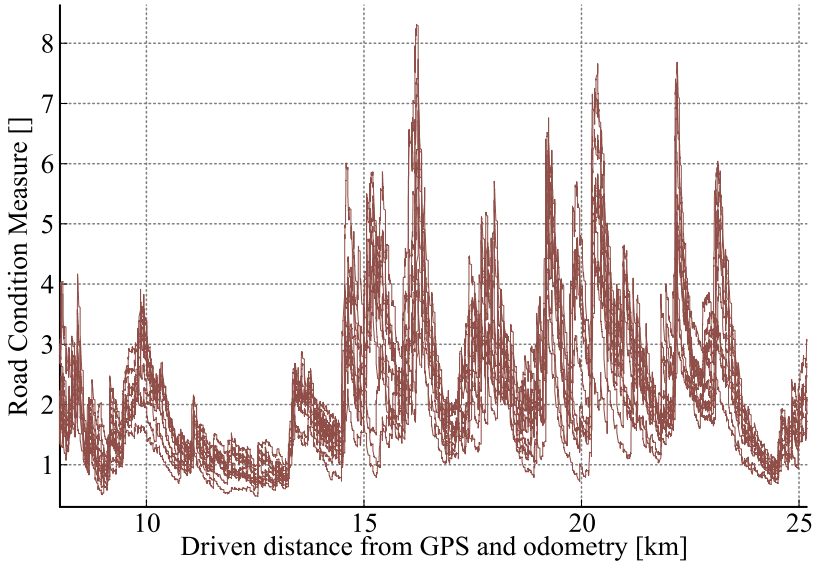

Figure 5.9.: Road surface condition measure PAVEMENT over driven distance from a common starting point for drives on the same motorway

Road Bumps

The signals used to detect road bumps are the same as for the road pavement detection. The wheel rotation sensors have again shown the most selective results, as they are closest to the road. Inertial sensors also work well, but are strongly separated from the road by the vehicle suspension that is designed to filter out road irregularities. Road bump detection from noisy signals becomes much more selective, when the front and the rear wheel sensor detect the road bump at the same location. Fig. 5.10 depicts how the motion of the vehicle can be used to assign the signals to the ground. The time difference between the front and rear wheel is determined by the wheelbase l and the vehicle speed $v[n]$:

$$\tau(n) = \frac{l}{v[n]} \tag{5.3}$$

For synchronization, a FIR filter is used that has an adaptive phase delay $\tau[n]$ depending on the current vehicle speed. Eq. 5.4 shows an FIR filter with adaptive coefficients $a_i[n]$ that depend on the wheelbase l and the vehicle speed $v[n]$ in $[\frac{m}{s}]$. $x[n]$ are the front wheel RPM signals $WhlRPM_{FL+R}$.

$$y[n] = a_0 x[n] + a_1 x[n-1] + \ldots + a_{\lceil \tau_{max} F_s \rceil} x[n - \lceil \tau_{max} F_s \rceil] \tag{5.4}$$

The filter has a higher delay for low vehicle speeds by setting all coefficients a_i to zero except the one corresponding to the vehicle speed. For $\tau[n]$ values that are between two

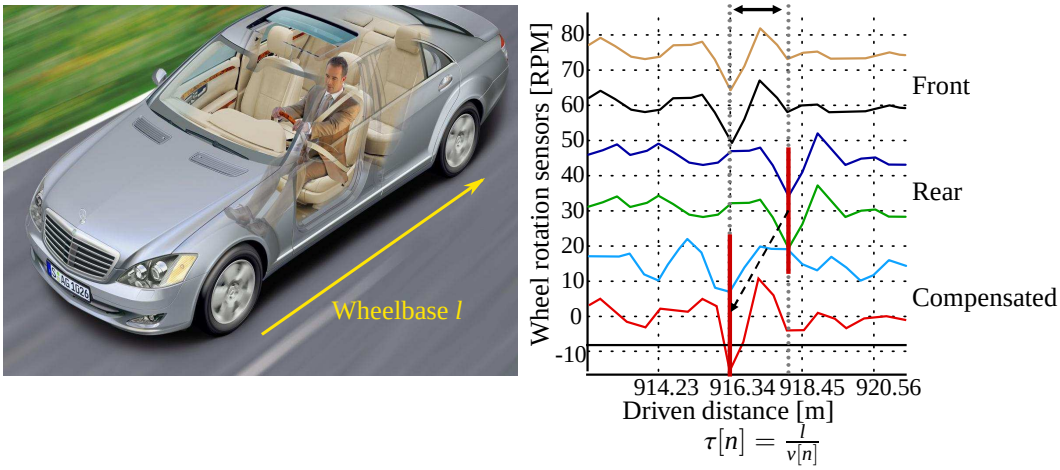

Figure 5.10.: Mapping the vehicle rotation signals to a position on the road. A road bump is detected if the duration between the observed peak in the front and the rear matches the vehicle speed and wheel base.

fixed delay elements, linear interpolation is performed by using modulo operation (Euclidean division):

$$a_i = \begin{cases} \mathrm{mod}(\tau,1), & \text{for } i = \lceil \tau F_s \rceil \\ 1 - \mathrm{mod}(\tau,1), & \text{for } i = \lfloor \tau F_s \rfloor \\ 0, & \text{otherwise} \end{cases} . \tag{5.5}$$

All a_i and unit delays $x[n-i]$ outside the speed interval 80-200 km/h can be removed, such that only $x[n - \frac{lF_s}{v_{max}}]$ to $x[n - \frac{lF_s}{v_{min}}]$ remain. In real-time implementation, it will save $\tau_{max} - 2$ unit delays, if only the detected peak value is hold in one unit delay and a counter for $t = \tau[v]$ assuming that only one peak is detected at a time. The feature ROADBUMPS2 is then calculated by

$$\begin{aligned} \texttt{ROADBUMPS2} = \Big(\mathrm{FIR}_{a_i[v]} \Big(& EWVAR_N(WhlRPM_{FL,HP}) \cdot EWVAR_N(WhlRPM_{FR,HP}) \Big) \\ & \cdot EWVAR_N(WhlRPM_{RL,HP}) \cdot EWVAR_N(WhlRPM_{RR,HP}) \Big) > P_{th} \, . \end{aligned} \tag{5.6}$$

All wheel rotation signals are pre-processed equally as for PAVEMENT, however with a much smaller EWMA window size of $N = 10\,samples$. Both front wheel rotation signals are delayed and multiplied with the variance of the rear sensors. A threshold $P_{th} = 8$ is used to detect a road bump.

Fig. 5.11 shows a histogram of the delay between steering corrections and all road bumps at $t = 0$. This proves that road bumps indeed have an influence on the driving behavior since the distribution in the surrounding of road bumps would be uniform otherwise. The time delay obtained from this histogram was used for the suppression of road bumps during extraction.

Road Warping and Cross-wind

The CROSSWIND feature detects cross-wind and road warping. It also measures the cross-wind and road-warping intensity from the measured and calculated lateral acceleration. Therefore, the measured lateral acceleration a_y is compared to the lateral acceleration $\breve{a}_y$ calculated

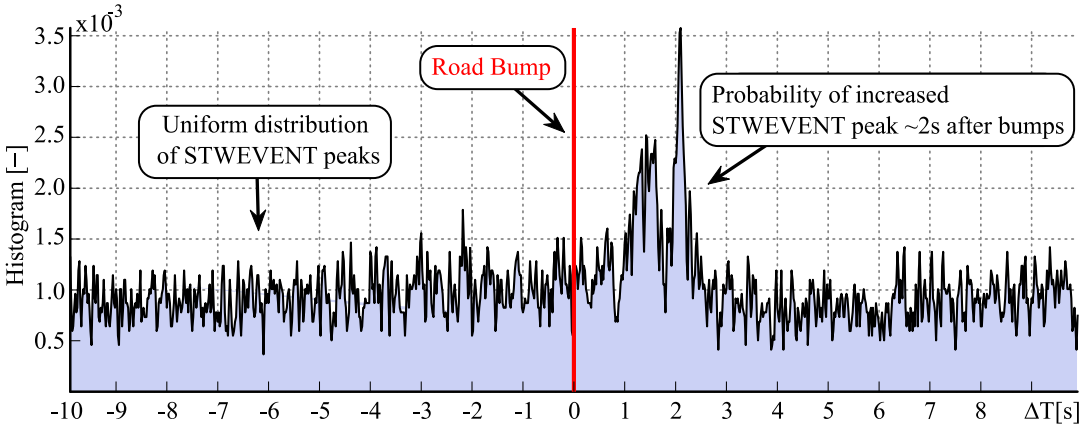

Figure 5.11.: Delay between steering corrections (STWEVENT) and road bumps (ROADBUMP2).

from the steering wheel angle using the single track model. The basic principle behind it is to detect whether the vehicle moves first laterally and then the driver corrects the displacement or whether the driver first steers and the vehicle follows.

The parameter calibration must be done for every vehicle individually by driving with steering steps on the driving dynamics surfaces of a proving ground (cf. Sec.2).

5.3. Influences from Drowsiness Supporting Situations

It is much better to detect fatigue from *causal* features that are directly related to the driver state than from a situation where the driver is probable to be drowsy. However, the best performance is achieved in practice, when all available *a-priori* information are taken into account. Known a-priori factors that increase the probability of reduced alertness are

- Driving time *"Time-on-Task"* (`TOT`),
- *Monotony* and *vehicle speed* (`MONOTONYSPD`),
- *Circadian rhythm* (`CIRCADIAN`),
- *Traffic density* (`TRFCDENS`) and
- *Light conditions* (`LIGHT`).

5.3.1. Driving Duration (Time-on-Task)

As already mentioned in Ch. 1.2.3 and shown in Fig. 1.5, the driving performance diminishes with increasing driving duration. Fig. 3.2 has already illustrated that fatigue increases by two KSS levels after 5 hours of driving. This is again confirmed in Fig. 5.12 that shows the KSS distribution over daytime and over driving duration for the DataSet ALDWvalid (App. A.2). The feature `TOT` simply contains the driving duration.

5.3.2. Monotony and Vehicle Speed

According to Thiffault and Bergeron (2003), sources of fatigue can be *endogenous* or *exogenous* factors depending on whether they belong to the initial driver condition or to driving characteristics. They have shown in a simulator study that monotonous situations are exogenous factors that can impair drivers in a way that they are more susceptible to passive fatigue symptoms. Oron-Gilad et al. (2007) state that drive characteristics like monotonous roads (inherent boredom) can be a cause of fatigue. Monotonous driving or "highway hypnosis" are situations with a lack of novelty and external stimuli that are often paired with constant

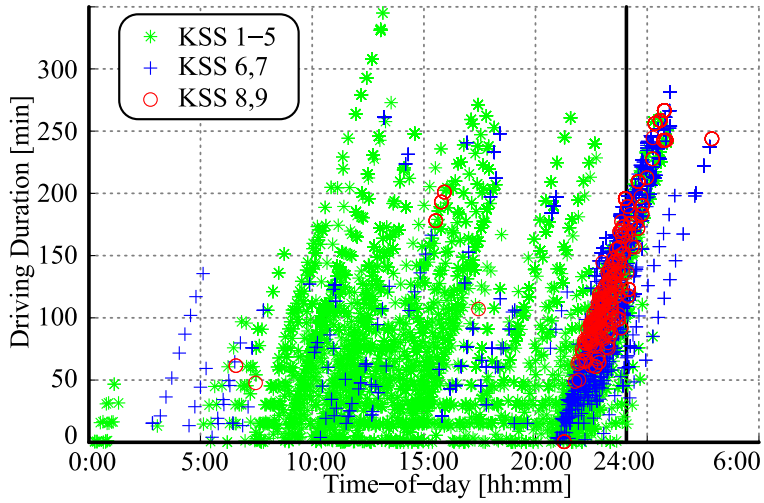

Figure 5.12.: Distribution of KSS over daytime and driving duration for all valid drives. The abscissa shows the starting point of the drive and are not wrapped in order to display entire drives without cut.

speed as well as empty and long, straight roads. Greschner (2011, 3.3) summarizes that also darkness, monotonous environments, constant noise levels and no or a sleeping co-passenger can make the driver more vulnerable to fatigue. From the experiments in Sec. 5.2.3, it can be concluded that low vehicle speeds also favor sleepiness as the accident risk is reduced, slower reaction is sufficient and the adrenalin level sinks.

The feature `MONOTONYSPD` increases for calm driving. It is weighted with a vehicle speed factor that is at maximum at 80 km/h.

5.3.3. Traffic Density

Traffic density is an exogenous factor that supports fatigue induced by monotony. It is another practical way to detect monotonous situations. It was observed that the lower the activation, the higher the probability of becoming sleepy. The presence of other vehicles in the proximity leads to more frequent acceleration, braking, steering and overtaking.

`TRFCDENS` measures the traffic density using the accelerometer, turn indicator and gas/braking pedal according to the following criteria within the last 5 minutes (EWMA):

- Rate of turn indicator lever use
- Magnitude of longitudinal acceleration $> 0.4\frac{m}{s^2}$
- Variance of the gas and brake pedal
- If available: lane changes from the lane tracker

Furthermore, the radar information could be taken into account. However, a radar sensor is not a standard equipment in today's vehicles and was thus not analyzed. In comparison, the driver activity `DRACTIVITY` measures how dynamic or sporty the drive is by using the lateral acceleration.

5.3.4. Circadian Rhythm and Light

According to numerous publications (Knipling and Wang, 1994; Horne and Reyner, 1995; Lenne et al., 1998; Mara, 1999), the crash probability is at maximum after midnight between 3 and 6 a.m., which is mostly caused by the endogenous *circadian rhythm* (lat.: *circa dies* =

about one day). The circadian rhythm also produces an alertness dip in the early afternoon around 2 and 4:00 pm, during which people are sleepier (Monk, 1991). This is supported by the crash statistic in Fig. 5.13 and 5.14.

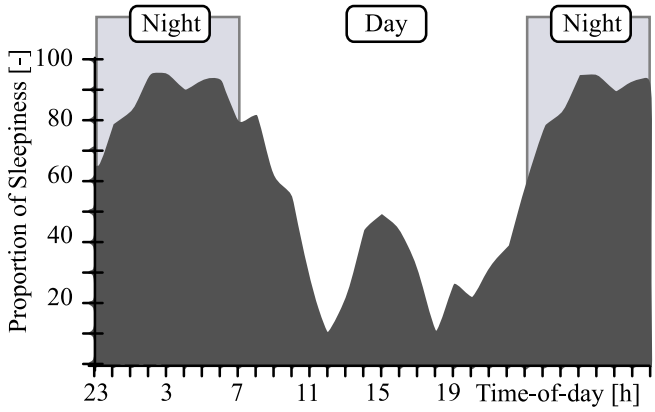

Figure 5.13.: Sleepiness tendency by daytime (Source: Zulley, 1995)

Daylight is the pacemaker of the internal biological clock synchronized to day and night (Zulley, 2006) through the production of the hormone *melatonin*. Light exposure to the retina in the eyes regulates the suppression of melatonin (Burgess et al., 2002; Greschner, 2011). After several days, the sleep-wake cycle is intrinsic and inevitable rather than voluntary (Mara, 1999).

Fig. 5.14 shows that young drivers, especially males (cf. Ch. 1.2.3), are particularly endangered at night, while the crash probability shifts to the afternoon with increasing age. Thus, age and gender could further be considered to improve the fatigue detection as soon as such driver details are available in vehicles.

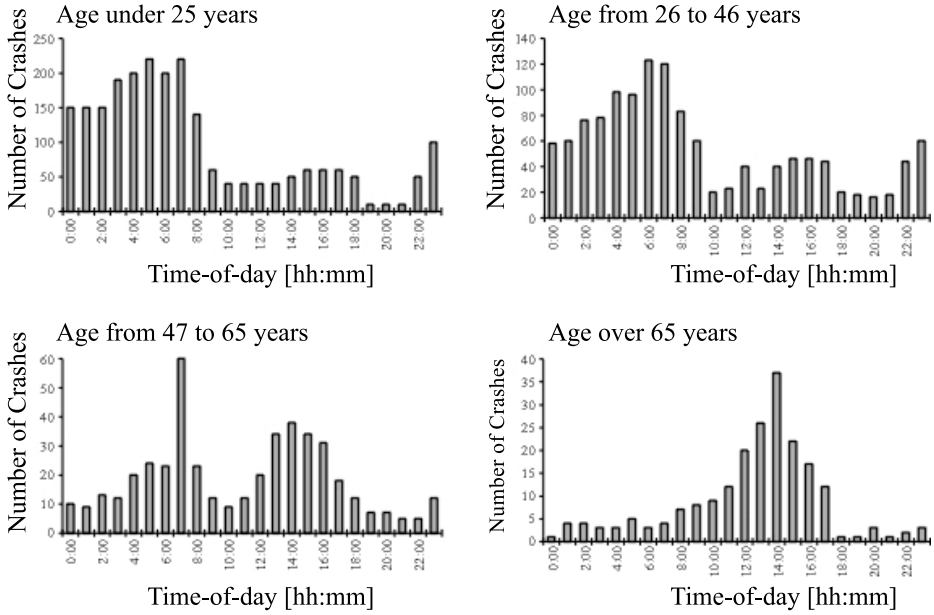

Figure 5.14.: Time of occurrence of crash for commercial drivers with different ages, published by the NHTSA for the years 1990 to 1992. (Source: Mara, 1999, Fig. 3)

Knipling and Wang (1994) found out that the driving duration (Time-on-task) and daytime correlate with fatigue and could be used for its detection. Motivated by these findings, the CIRCADIAN feature is defined as in Fig. 5.15.

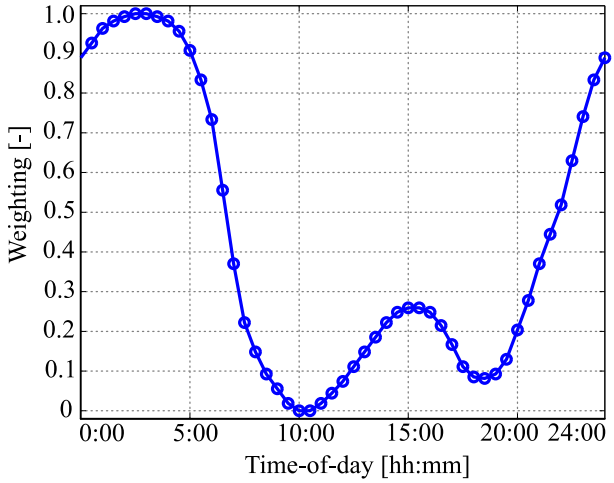

Figure 5.15.: CIRCADIAN weighting factor of daytime.

Fig. 5.12 shows the distribution of KSS entries for the DataSet *ALDWvalid*. This also confirms the a-priori daytime and driving duration influence in the recorded data.

Instead of using the circadian rhythm, the light sensor performs in a similar way in Fig. 5.16. It was clearly observed that the low or bad vision conditions are more straining and impair the driving style significantly. Drivers subjectively feel more awake while driving during daylight. The advantage of LIGHT is that it is more adaptive to the actual vision conditions whereas the Circadian does not change from day to day. The light sensor is used in the ESP to detect a wrong clock settings resulting in a false Circadian factor. Circadian is a rather endogenous factor while the light conditions are exogenous and thus more adaptive to the driving situation.

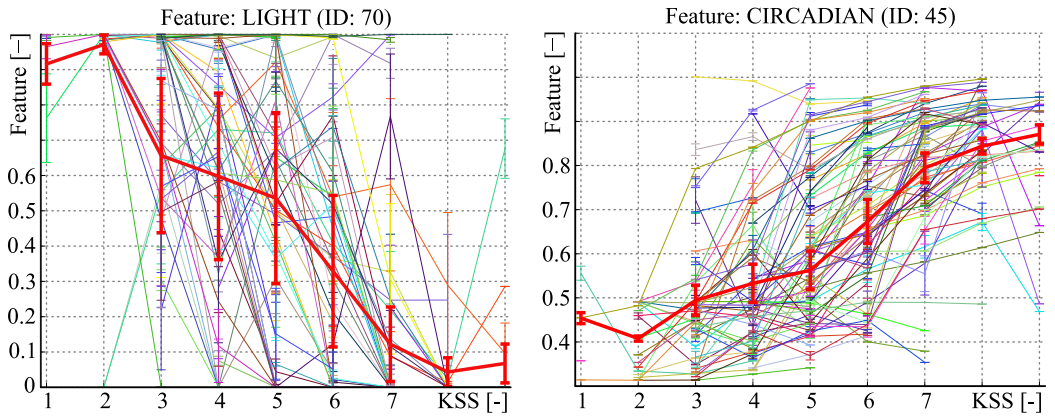

Figure 5.16.: LIGHT sensor to measure illumination as alternative for CIRCADIAN. The Errorbars (cf. Ch. 7.2.2) of all drivers individually (colored) and their combination (red) are shown.

Fig. 7.13 in Ch. 7.5 shows the strong influence of driving duration and circadian in a ROC-curve. These two a-priori features (as well as LIGHT) have the strongest contribution to

the classification result which is not desired as they are not sensitive to the individual driver state.

5.4. Influences from Inter-individual Driving Styles

The *inter-individual* driving style is another major topic with significant impact on the detection of fatigue-related patterns. Different drivers primarily differ in their steering and lane keeping behaviors, but also numerous other dimensions like clearance distance to surrounding vehicle, speed limit exceedances, blinkind behavior etc. Fig. 5.17 shows the large variety of the maximum steering velocities (STVmax) for the DataSet *ALDWvalid*. Both degrees of freedom of the *Inverse Gaussian* PDF (cf. Sec. 4.4.3) are necessary to adapt to the different drivers.

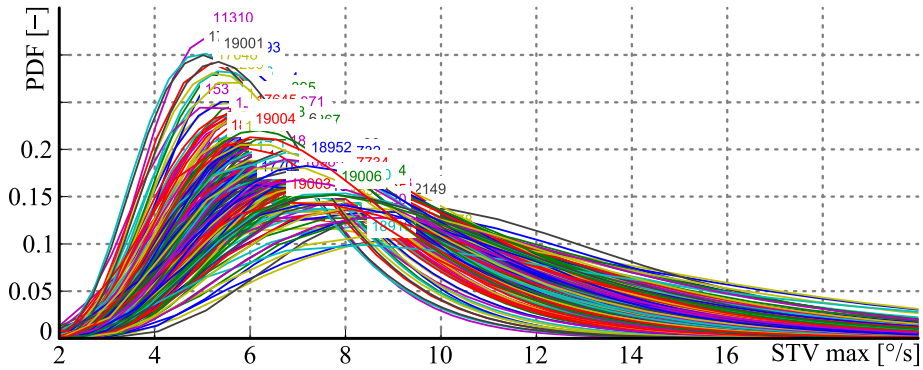

Figure 5.17.: PDF of STVmax while the system is active and drivers are awake over drives marked by driveID from DataSet *ALDWvalid*.

There are also *intra-individual* differences, i.e. a driver changes his driving style depending on time pressure, mood or with increasing driving experience. These effects mostly change slowly and since drivers cannot yet be identified after engine restarts, the driver has to be considered as unknown.

There are several approaches to overcome these variations. The most common approach is *baselining*, i.e. normalization to a period of normal driving at the beginning of a drive. A second way is the *adaption of thresholds* to the driver such that different patterns occur with the same frequency. In most cases, this is helpful but not sufficient to solve the problem.

A third, new approach proposed in the following section is based on the hypothesis that there are *driver groups* that can be adapted. For instance, it was observed that there are drivers who almost never make fast steering corrections. Fig. 5.18 compares the 2D histogram of the *efficient percentile calculation* of maximum steering velocities (cf. App. A.8) of a driver with virtually no high frequencies and of an average driver. This effect was observed to be reproducible over several hundred drives, over several years and without notable exception. At the other hand, the low level of steering control reciprocally reflected in sloppy lane keeping.

Another group of drivers had bad vision at night. They were observed to make more hectic steering corrections. While the eyesight can sometimes be improved by changing glasses, the vision at night can usually not be improved. This hypothesis is investigated in more details in the thesis of Gärtner (2009).

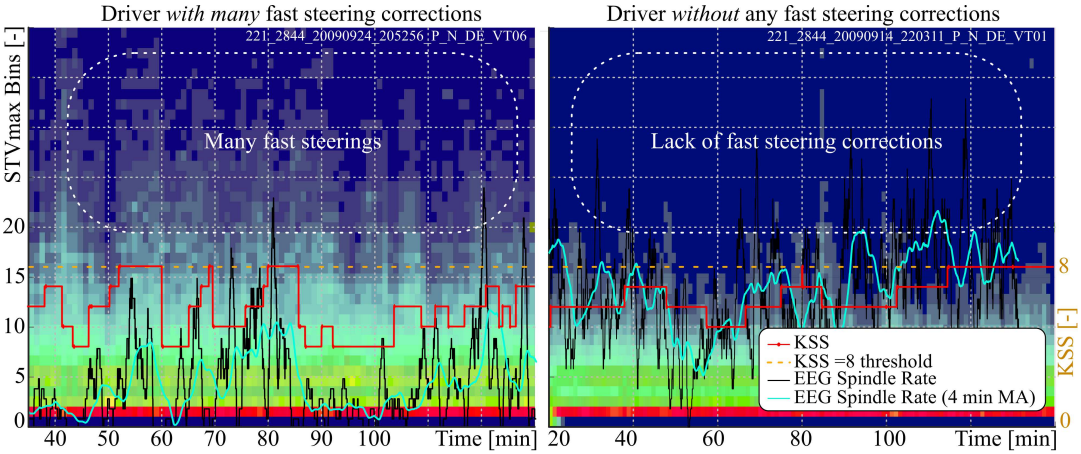

Figure 5.18.: 2D histogram (heatmap) of the efficient percentile calculation of maximum steering velocities for two mostly awake drivers. The left with many steering corrections, the right without any high frequency components.

The DataSet *validTopDrivers* designed for this study including only the top 15 drivers without fatigue was described in Ch. A.2.

In the first step, single drivers where classified. Then, different driving styles were grouped by unsupervised clustering with the *k-means* algorithm. In the last step, the driving style groups were classified in order to use different features to identify their fatigue level.

5.4.1. Normalization by Baselining

Baselining is a common, powerful method for the normalization and adaption of human processes. There are several possibilities for its implementation. A certain time frame at the beginning of a drive (e.g. the first 15 minutes) is considered when the system is active and the driving conditions are normal. Different statistical measures can then be calculated for this baseline period:

- Mean or median
- Maximum, 90% percentile or final value of the baseline period
- Variance or IQR

The *maximum* has shown the best performance, followed by the final value of the baseline period. The feature is then normalized by division through this baseline value. The *"'zero-mean unit-variance"' normalization* (also called *z-transform*) in this context was more suitable for some features and is most commonly used in psychology Sonnleitner (2012). It further takes the variance of the baseline period into account and is calculated for a feature $\mathcal{F}$ by:

$$\mathcal{F}_{BL} = \frac{\mathcal{F}_{raw} - \mu(\mathcal{F}_{15\,min})}{\sigma(\mathcal{F}_{15\,min})} \tag{5.7}$$

Since all features need some time to initialize, the first one to five minutes are omitted, depending on the features and especially their averaging window length.

Baselining also has two major drawbacks. First, it is based on the assumption that the driver is relatively alert at the beginning of a drive, which is not necessarily the case and second, the ability of the system to detect fatigue is delayed during this learning phase.

Every feature in Tab. 4.2 that is marked by [2] is baselined. Parameter-optimization has shown the best results when using the *maximum*. The optimization tends to favor window size of up to 40 minutes because the KSS reference also changes so slowly. Thus, not more than 20 minutes active time were used to preserve high feature dynamics and because the baseline period otherwise takes much too long for low system active levels SAS_x.

5.4.2. Driver-specific Features

While some of the features in Ch. 4 are suitable for driver group classification, also additional features were used that were not suitable for fatigue detection. The following features were investigated for the classification of driver groups:

- Ratio of lane changes with and without turn indicator use (`TURNINDMISS`: ratio averaged by the EwmaN of the last 10 lane changes)
- Lateral lane change velocity $\dot{y}_L$ (`LNCHGVEL`: EwmaN of the last 10 lane changes)
- Duration between turn indicator use and lane change (`TURNINDADVANCE`: duration differences between lever operation and lane change if below 10 seconds, averaged by the EwmaN of the last 10 lane changes)
- Duration of turn indicator use (`TURNINDDUR`: EwmaN of the last 10 lane changes)
- Lateral lane deviation and mean (`LANEDEV`: as described in Ch. 4.3.2, `LATMEAN` is the average lateral driver offset as described in Ch. 4.3.1)
- Maximum steering velocities (regular feature from Ch. 4 and Fig. 5.18)
- Maximum longitudinal and lateral acceleration at specific speeds and curvatures (`ACC75` regular features from Ch. 4)
- Rate of ALDW warnings (regular features from Ch. 4)

5.4.3. Driver Group Clustering and Classification

Fig. 5.19 shows the classification of twelve drivers by their driving style. Details can be found in the thesis of (Gärtner, 2009).

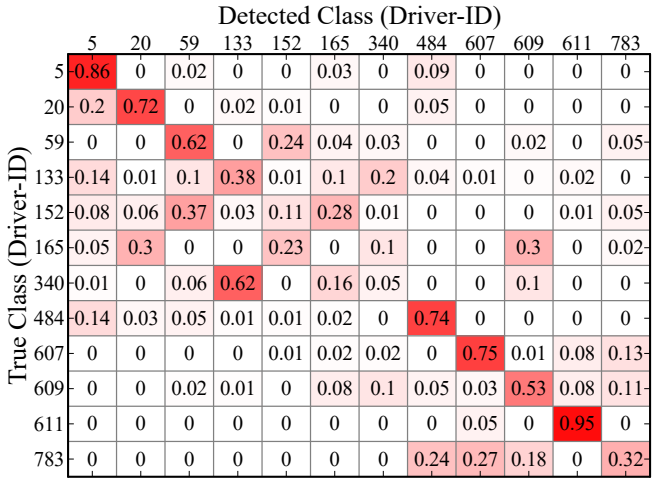

Figure 5.19.: Confusion matrix for drivers using GMM classifier (Courtesy of: Gärtner, 2009)

Drivers that were often mixed up during classification (as for instance driver-ID 133 and 340) could be combined to one group. Fig. 5.20 shows the classification result for the features `STV25`, `STV50`, `STV75`, `LATMEAN`, `LANEDEV`, `LNIQR` and `ACC75` and a reduced number of driving style groups:

- A: Very calm steering, sloppy lane keeping (Driver-IDs 5, 20, 484)
- B: Calm steering and lane keeping, sportive acceleration (ID 609, 783)
- C: Calm steering, lane keeping and acceleration (ID 59, 133, 152, 165, 340, 607)
- D: Hectic steering, precise lane keeping (ID 611)

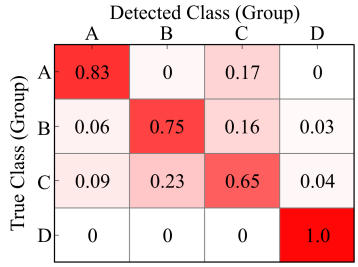

Figure 5.20.: Confusion matrix using Bayes classifier and four driving style groups (Courtesy of: Gärtner, 2009)

The results show that classification of at least two main groups of driving style is quite feasible. As the example in Fig. 5.18 shows, the fatigue level of hectic drivers can be detected better by their steering behavior, while the other group with a calm steering style has a more sloppy lane keeping. Thus, for the different groups, it is more appropriate to use different features for the classification of their fatigue level. In theory, the more appropriate methodology would be to train the classifier in a single step. However, this did not work due to the larger amount of involved features that require more training data than there were available here (see Ch. 8.4).

5.5. Conclusion

In this chapter, it was shown that there are at least the thirteen external factors from Fig. 5.1 that have a strong impact on the driving behavior. The factors are in many situations more dominant than the sleepiness patterns. Further, the a-priori factors daytime, driving duration, monotony, novelty and light have the largest effect. Most of them can easily be measured, however are not directly sensitive to the driver state. Driver monitoring does not work under real-road conditions without taking external factors into account.

For the most important factors, specific drives were recorded and evaluated, i.e. vehicle speed and curvature. For the factors road condition, light, rain and driving style, appropriate drives were filtered from the database. In order to consequently find all relevant parameters for their precise compensation, a matrix of hundreds of specific drives would be necessary for varying only one external factor at a time while keeping all other factors constant.

For most external factors, methods were proposed to incorporate them. Ideally, for important features, the normalization was already part of the the extraction. The system active signals suppress events resulting from external factors. Specific features were designed for the purpose of explicitly identifying external factors such as `PAVEMENT`, `CURVATURE`, `ROADBUMPS2`, `CROSSWIND` and the a-priori factors `TOT`, `CIRCADIAN`, `MONOTONYSPD`, `TRFCDENS` and `LIGHT`. For the fusion of features on the classifier level, these feature were provided for classification and feature selection in Ch. 8.

Baselining was presented as the predominant method to compensate individual driving styles during the extraction of features. A driving style classification has shown that different groups of drivers can be identified for a two-stage classification.

Chapter 6.

Approximation of Lane-based Features from Inertial Sensors

The major drawback of the utilization of lane data based features from Sec. 4.3 is that the ALDW camera is only available as special equipment and, thus, limited to the vehicles that have it installed. Furthermore, the lane data signals are often affected by missing road markings, bad sight etc. In comparison, inertial sensors are standard equipment and available for all vehicles.

Some lane-based features such as LANEDEV or ZIGZAGS do not require the *absolute* distance to the lane markings, but only depend on the lateral deviation within the lane. The idea of this chapter is to use odometric vehicle data only (yaw rate, steering wheel angle and vehicle speed) to approximate the classical lane-based features without the need of a lane-tracking camera.

The basic assumption behind this approach is that the curvature of the road can be estimated from the odometric data. As described in (Clayton, 2006), there is a minimum curvature radius for every speed limit. For instance, the minimum curvature radius at 120km/h is 750 meters. Thus, when speed limits are obeyed and if the vehicle would ideally follow the lane center, the road curvature never exceeds this low frequency limit. The vehicle trajectory is thus a combination of the road curvature and the lane keeping between lane markings. Thus, the deviation within the lane contains much higher frequencies than the road curvature and can be extracted by a high-pass filter. To estimate the vehicle trajectory, an extended Kalman filter and a vehicle motion model are applied to the available sensors.

Since fatigue changes slowly, its detection may be delayed by up to several minutes, so signals can be analyzed retrospectively. A second hypothesis is that the lateral mean of the lane keeping does not vary too much for one drive, so that the absolute lateral position can be assumed to be constant. In this case, also the time-to-lane-crossing and lane approximation features like TLC1MIN or LANEAPPROXADAPT can be approximated.

In addition to yaw rate and vehicle speed, the vehicle's GPS position is also included in an extended Kalman filter model in order to create a reference to evaluate the system performance.

Using odometric CAN data such as yaw rate, steering wheel angle, and wheel rotation highly improves the knowledge about the absolute position of the vehicle. Many other aspects in regards to drowsiness detection profit from this improved vehicle position. Short lane-tracking gaps can be filled and road-condition analysis benefits from this improved spatial resolution. The correlation between features based on lane data and odometric data as well as their relationship with sleepiness will be compared.

6.1. Literature review

There are many approaches for vehicle tracking with inertial vehicle data. Hasberg and Hensel (2009) uses splines and a Kalman filter for online estimation of train tracks. Buehren (2008) investigates the tracking of vehicle target lists by radar. Weiss (2011) uses a Kalman filter to match radar, lidar and map data for highly accurate ego-vehicle position estimation. Miksch (2010) and Guan (2008) use a vehicle motion model to estimate the ego-motion for motion compensation of camera data.

Forsman and Vilaa (2012) uses a transfer function of steering wheel angle motivated by cardiovascular regulation analysis in (Saul and Berger, 1991) to approximate the lateral lane position. They test their approach with a simulator study with twenty-nine subjects. Using a transfer function on the steering wheel angle is less accurate in comparison to additionally using inertial sensors and vehicle tracking with a Kalman filter. Lundquist and Schön (2010) uses the single-track model and a Kalman filter for road geometry and curvature estimation of the ego-vehicle. However, no literature was found that analyzes the estimation of lane-based features from inertial vehicle data.

6.2. Sensor Signals and Synchronization

The yaw rate sensor has a high resolution of $0.005\,^\circ/s$ and a sampling frequency of $F_s = 1/T \approx 50\,\text{Hz}$. The GPS signals are available with a sampling rate of $F_s \approx 1\,\text{Hz}$ and not always valid. Every second, when new GPS data is available, a Kalman iteration is called to update the position according to the GPS data. This way, the Kalman filter takes over the weighting between inertial data and GPS data.

Tab. 6.1 shows a matrix of the required lane signals for the different lane feature groups and the system active signal SAS_{LANE} to suppress special events. From this table, it can be derived, which features require the distance to the lane and which only focus on lurching within the lane and thus are suitable best for inertial features. For odometry-based features, the lane signal quality *LaneDataQual* is not needed since the signals are always valid. As well, lane changes (LaneChg_Stat) can be detected from the *LaneLtrlDist*. The odometry-based features are the ones (marked green) that have no other dependency than yaw rate or LaneLtrlDist, with the limitation that not the absolute offset is available.

6.3. Single-Track Vehicle Model

In order to estimate the ego-motion of a vehicle from inertial sensor data, different mathematical models are available. Zomotor and Klinkner (1987) consider inertia torques of the vehicle and tire models for the description of slip effects. Other approaches require additional sensors like vehicle mass sensors to determine the mass distribution in a vehicle (Weiss, 2011). Carlson and Gerdes (2002) propose a method for the determination and application of tire models, that, however, require vehicle specific parameters for the vehicle's inertia torque which again depends on the actual mass (occupied seats and baggage) distribution.

These specific sensors and parameters are not available here. For these reasons, several assumptions are made for simplification in practice (Mitschke and Wallentowitz, 2004, Ch. C.18). Under these assumptions, the *single-track model* (or *Bicycle Model*) can be used with

Features \ Signals	LaneDataQual	LaneChg_Stat	relative LaneLtrlDist	absolute LaneLtrlDist	LaneWidth	LaneYawAngl	LaneHrztCrv	LaneClothoidPara	LaneNum	NumLane
Lane change (SAS_{LANE})	×	×	(×)							
Overtakings (e.g. SAS_{LANE})									×	×
Lane deviation (e.g. `LANEDEV`, `ORA`)	×	(×)	×							
Lateral offset (e.g. `LATMEAN`)	×	(×)		×						
ZigZags (e.g. `ZIGZAGS`)	×	(×)	×							
Lane oscillation (e.g. `LATPOSZCR`)	×	(×)	×							
Yaw events (e.g. `YAWJERK`)						×				
Lane approx. (e.g. `LANEAPPROX`)	×	(×)		×	×					
TLC (e.g. `TLC1MIN`)	(×)	(×)	×	×	×	(×)	(×)	(×)		

Table 6.1.: Signals needed for lane-based feature types, where (×) indicates that these features are not absolutely necessary. Lane changes can also be detected by the blinking lever.

good approximation. It is the simplest mathematical model for the stationary and instationary lateral dynamic of a four-wheel vehicle (Riekert and Schunck, 1940, P. 210-224). Fig. 6.1 illustrates the model after a simplification by combining the two wheels of each axle.

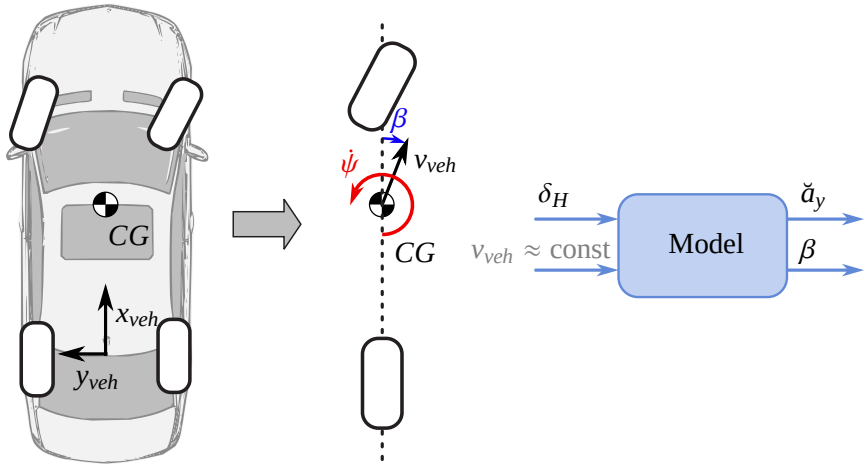

Figure 6.1.: *Left*: *Single-track model* simplification by combining the two wheels of one axis. *Right*: steering wheel angle δ_H and vehicle speed v_{veh} are the model input and lateral acceleration $\breve{a}_y$ and *sideslip angle* β the outputs. β is described in the following.

The vehicle dynamics model is mostly linear with good approximation on dry roads and for lateral accelerations under $4 m/s^2$. The appearing angles are then small and can be approximated by $\sin(\alpha) \approx \alpha$. According to (Schindler, 2007, Ch. 4) and (Schramm and Hiller, 2014, Ch. 10), further assumptions are made: the vehicle is assumed to be a rigid mass with *inertia torque* J_z and its *center of gravity* (CG) on the ground. Only the front axle is steerable and the vehicle speed v_{veh} is considered to be stationary, so that only two degrees of freedom remain: yaw rotation $\dot{\psi}$ and the *sideslip angle* β (also called *bodyslip angle*). β is illustrated in Fig. 6.2. It describes the angle between the longitudinal vehicle axis towards

the direction in which the vehicle is actually traveling, resulting from the direction in which the wheel is pointing. The lateral acceleration $\breve{a}_y$ in which we are interested is implied. This means that wheel load differences and related roll, pitch and vertical motion are neglected. The model is illustrated in Fig. 6.2 and introduces the notation for the following equations.

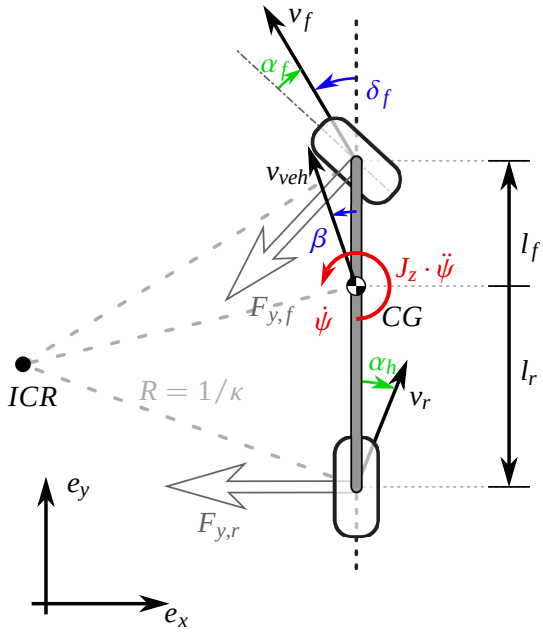

Figure 6.2.: Illustration of the single-track model

Instant Center of Rotation (ICR): As mentioned in App. A.4, every point of the rotating vehicle experiences a different velocity around an *Instant Center of Rotation* (ICR). The ICR is located at the point where all orthogonal lines to all velocities are crossing and describes the *curvature radius* R or *curvature* κ with

$$R = \frac{1}{\kappa} = \frac{v}{\dot{\psi}} \,. \tag{6.1}$$

Steering Ratio: The *Ackerman steering angle* δ_a of the wheel is obtained by the *steering transmission ratio* SR and the *steering wheel angle* δ_s measured in the steering column:

$$\delta_A = \delta_S \cdot SR. \tag{6.2}$$

Wheel and Sideslip Angles: Assuming that the *wheel slip angles* are zero and the wheels roll along their axis, the vehicle speed v and lateral acceleration a_y yield the driving radius:

$$R = \frac{v^2}{a_y} \,. \tag{6.3}$$

The *sideslip angle* β in Fig. 6.2 is defined as the angle between the vehicle motion of the CG and the longitudinal vehicle axis.

Self Steering Gradient: The *self-steering gradient* SG is defined in DIN 70000 as the difference between the steering angle gradient and the Ackerman angle over the lateral acceleration a_y:

$$SG = \frac{1}{SR}\frac{d\delta_S}{da_y} - \frac{d\delta_A}{da_y} \tag{6.4}$$

With the vehicle *characteristic lower velocity* v_{ch} and the *wheel base* l, it is obtained by:

$$SG = \pm\frac{l}{v_{ch}^2} \tag{6.5}$$

where v_{ch} and l are vehicle specific properties that are available for the vehicles.

Characteristic Velocity: It is the vehicle speed, at which under-steering vehicles ($SG > 0$) have the maximum of their yaw intensification

$$v_{ch} = \sqrt{\frac{l}{SG}}\,. \tag{6.6}$$

By Schramm and Hiller (2014), it is also described by "v_{ch} *is the velocity for which the vehicle reacts most sensitively to steering inputs. Typical values are between 65 and 100 km/h*".

An $SG > 0$ means that the vehicle is under-steering (front wheel slips), $SG = 0$ means neutral and $SG < 0$ means, that the vehicle is over-steering (rear wheel slips). For safety reasons, today's vehicles are designed to under-steer, which is easier to handle. This means that the vehicle tends to turn to the curve outside instead of observing additional rotation by the tail "drifting" out of the curve. All vehicles in this thesis are under-steering.

Yaw intensification: The *yaw intensification* is the ratio of stationary yaw rate and steering wheel angle for stationary steering wheel angles

$$\delta_H = SR \cdot \left(\frac{l}{R} + SG \cdot a_y\right) \tag{6.7}$$

Lateral Acceleration: The lateral acceleration obtained by the steering wheel angle describes the vehicle trajectory more precisely than the accelerometer value which is affected by the road inclination towards the road side (y-direction). For this reason, the *single-track model* is used. The *lateral acceleration* $\breve{a}_y$ is obtained by the *velocity* v, the *steering ratio* SR, the *steering angle* δ_a and the *self-steering gradient* SG:

$$\breve{a}_y = \frac{v^2 \cdot \delta_a}{l + SG \cdot v^2} \tag{6.8}$$

6.4. State Space Model

For the mapping of inertial sensor signals to real-world coordinates, a motion model is required that describes the trajectory in every calculation step. A description of the motion can be approximated either by the *line segment model* or the *arc segment model* (Guan, 2008, Ch. 3.2.2-3). He stated that in conjunction with the Kalman filter, the linear-segment model

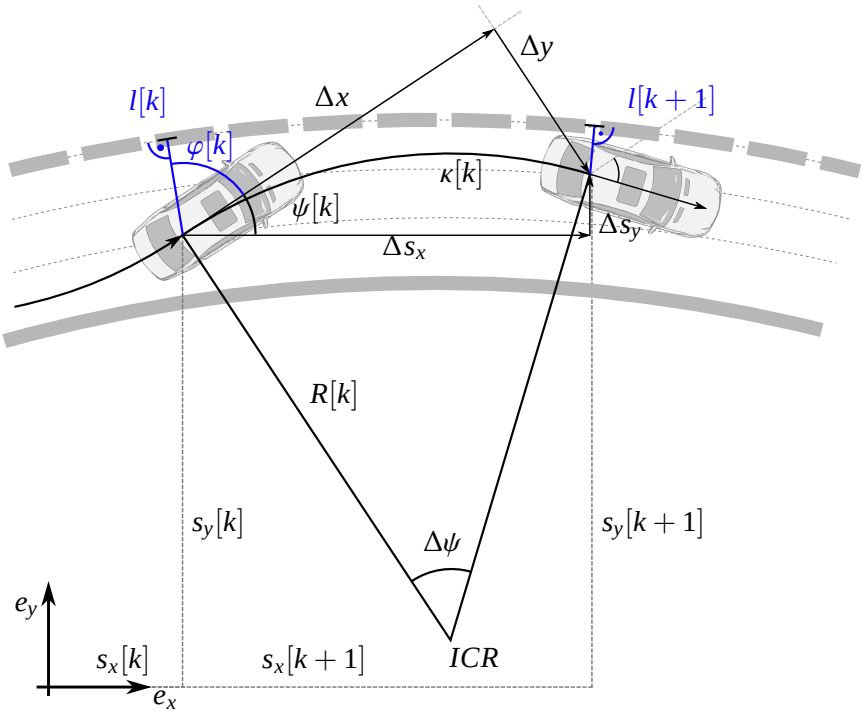

Figure 6.3.: Line segment motion model

performs far better than the arc-segment model. Fig. 6.3 illustrates the line segment model.

The vehicle motion is modeled in analogy to Buehren (2008); Miksch (2010) and Weiss (2011). The *state vector* $\mathbf{x}[k] \in \mathbb{R}^n$ describes the position and motion state at time instant k by:

$$\mathbf{x}[k] = \begin{pmatrix} s_x[k] \\ s_y[k] \\ \psi[k] \\ \dot{\psi}[k] \\ v[k] \\ a[k] \end{pmatrix} \begin{array}{ll} x\text{-position} & [m] \\ y\text{-position} & [m] \\ \text{yaw angle} & [^\circ] \\ \text{yaw rate} & [^\circ/s] \\ \text{longitudinal velocity} & [m/s] \\ \text{longitudinal acceleration} & [m/s^2] \end{array} \tag{6.9}$$

For linear systems, the system model with the *state transition matrix* $\mathbf{A}$ $(n \times n)$ describes the state change of $\mathbf{x}$ between two consecutive instants. Here, the system ist non-linear and the *state transition matrix* $\mathbf{A}$ is replaced by a *state transition function* $\mathbf{f}(\mathbf{x})$ (cf. Eq. (6.17)):

$$\mathbf{x}[k+1] = \mathbf{f}(\mathbf{x}[k]). \tag{6.10}$$

The second part of the system model is the measurement equation that maps the system state to the *measurement vector* $\mathbf{z}[k] \in \mathbb{R}^m$ using the *measurement matrix* $\mathbf{H} = \begin{pmatrix} \mathbf{0} & \mathbf{I} \end{pmatrix}$ $(m \times n)$:

$$\mathbf{z}[k+1] = \mathbf{H}\,\mathbf{x}[k+1]\,, \quad \mathbf{z}[k] = \begin{pmatrix} \dot{\psi}[k] \\ v[k] \\ a[k] \end{pmatrix} \tag{6.11}$$

According Fig. 6.3, the non-linear movement of the vehicle is given by

$$\begin{pmatrix} s_x[k+1] \\ s_y[k+1] \end{pmatrix} = \begin{pmatrix} s_x[k] \\ s_y[k] \end{pmatrix} + v^+[k] T_s \begin{pmatrix} \cos\left(\psi^+\right) \\ \sin\left(\psi^+\right) \end{pmatrix}. \tag{6.12}$$

with $v^+ = v[k] + a[k]\frac{T_s}{2}$, $\psi^+ = \psi + \dot{\psi}\frac{T_s}{2}$ and the *cycle time* T_s.

6.5. Kalman Filter

The Kalman filter is an optimal state estimation algorithm for linear systems to estimate the system state vector $\mathbf{x}[k]$. For optimality, it requires that the measurement and process noise have zero mean, white, uncorrelated and normally distributed additive noise (Welch and Bishop, 2006). After initialization, the iterative algorithm consists of a *prediction* and an *innovation* (or *correction*) step for each iteration k. The prediction step derives from the previous iteration $k-1$ updated state variables and uncertainties under the consideration of the motion model. The current measurement is included under consideration of its uncertainties form the innovation step. The Kalman Gain is a feedback that weights the influence of the model or measurement based on their covariances.

6.5.1. Optimal State Estimation using the Kalman filter

The state transition and measurement equation in Eq. (6.10) and Eq. (6.11) are expanded by the *model noise* $\mathbf{w}[k]$ and the *measurement noise* $\mathbf{v}[k]$ (with *process* and *measurement noise covariance matrices* $\mathbf{Q}$ and $\mathbf{R}$):

$$\mathbf{x}[k+1] = \mathbf{A}\mathbf{x}[k] + \mathbf{B}\mathbf{u}[k] + \mathbf{w}[k], \tag{6.13}$$
$$\mathbf{z}[k+1] = \mathbf{H}\mathbf{x}[k+1] + \mathbf{v}[k+1] \tag{6.14}$$

The influence of l *input parameters* $\mathbf{u}$ can be included by the $(n \times l)$ *input matrix* $\mathbf{B}$, which is not relevant here. $\mathbf{w}[k]$ and $\mathbf{v}[k]$ were found to be additive normally distributed white noise with zero mean:

$$\begin{aligned} \mathrm{E}[\mathbf{w}[n]\mathbf{w}^T[k]] &= \mathbf{W}\delta_{nk} \\ \mathrm{E}[\mathbf{v}[n]\mathbf{v}^T[k]] &= \mathbf{V}\,\delta_{nk} \\ p(\mathbf{w}) \propto \mathcal{N}(0,\mathbf{Q}),\quad p(\mathbf{v}) &\propto \mathcal{N}(0,\mathbf{R}) \\ \mathrm{E}[\mathbf{w}[k]] = \mathrm{E}[\mathbf{v}[k]] &= \mathbf{0}. \end{aligned}$$

Model noise, measurement noise and initial states are uncorrelated:

$$\mathrm{E}[\mathbf{w}[k]\mathbf{v}^T[k]] = \mathrm{E}[\mathbf{w}[k]\mathbf{x}^T[0]] = \mathrm{E}[\mathbf{v}[k]\mathbf{x}^T[0]] = \mathbf{0}.$$

Details for the Kalman filter and the validity of its requirements for the yaw rate, vehicle speed and acceleration sensors can be read in (Welch and Bishop, 2006; Buehren, 2008; Weiss, 2011). The *prediction* and *correction* steps of the linear Kalman filter state estimation are illustrated in the following:

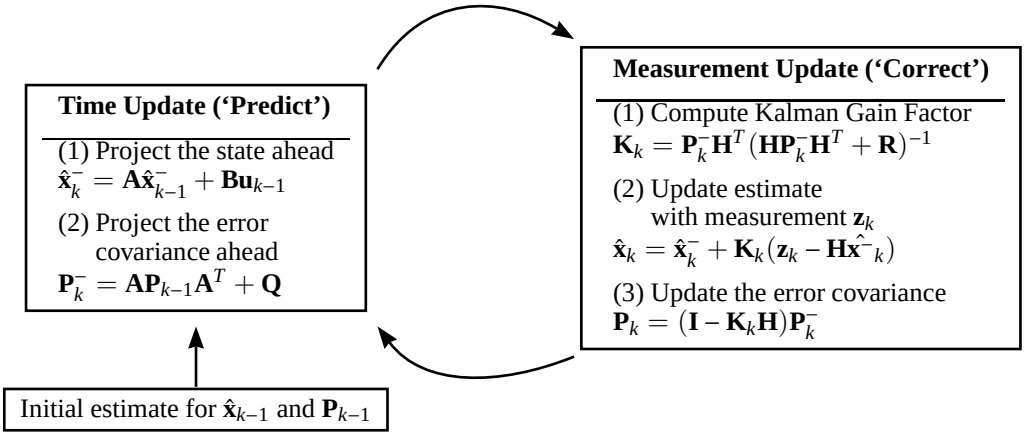

6.5.2. The Extended Kalman Filter

The Extended Kalman filter (EKF) is necessary, if the state transition is non-linear, as in our case. Now the system is described by the non-linear, differentiable functions **f** and **h**:

$$\mathbf{x}[k+1] = \mathbf{f}\Big(\mathbf{x}[k], \mathbf{u}[k], \mathbf{w}[k]\Big) \tag{6.15}$$

$$\mathbf{z}[k+1] = \mathbf{h}\Big(\mathbf{x}[k+1], \mathbf{v}[k+1]\Big) \tag{6.16}$$

In our case, the measurement equation stays as in (6.14). The Extended Kalman filter state estimation is again computed in two steps: *prediction* and *correction*, but now with the linearized function.

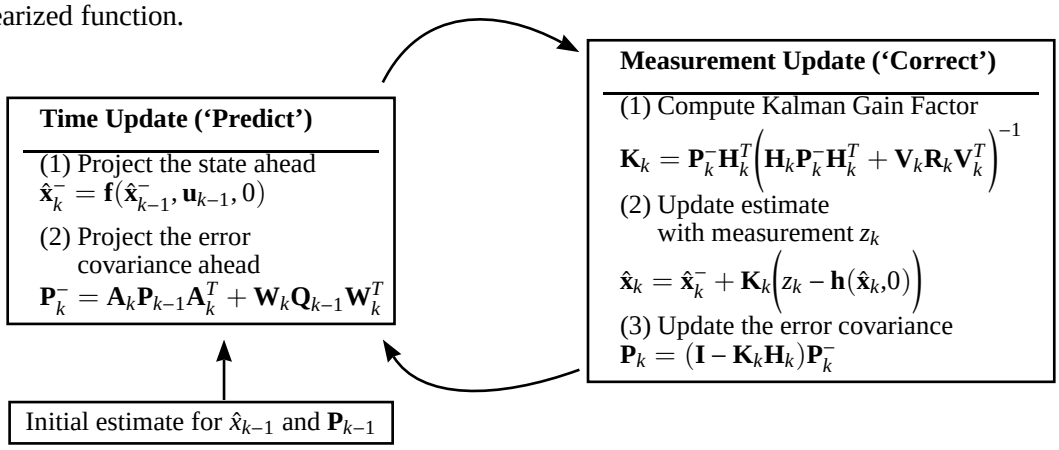

As the yaw rate in Eq. (6.12) changes very slowly within the cycle time $T_s = 20ms$, we use the first order *Taylor series approximation*, $sin(\alpha) \approx \alpha$ and $cos(\alpha) \approx 1$ for $\alpha \ll \pi/2$, we can linearize the trigeonometric functions to the dimensions in Eq. 6.9 as follows:

$$\mathbf{f}(\mathbf{x}, \mathbf{q}) = \begin{pmatrix} s_x[k] + \cdot v^+[k]T_s\cos\left(\psi^+\right) \\ s_y[k] + \cdot v^+[k]T_s\sin\left(\psi^+\right) \\ \psi[k] + \dot{\psi}T_s \\ \dot{\psi}[k] \\ v[k] + a[k]T_s \\ a[k] \end{pmatrix}. \tag{6.17}$$

The system is still non-linear so that the EKF is required. Thus, we need to linearize the non-linear, differentiable function $\mathbf{f}$ in each working point, which is the current system state $\mathbf{x}[k]$. For linearization, the *Jacobi-Matrix* of the differentiable function $\mathbf{f}\colon \mathbb{R}^n \rightarrow \mathbb{R}^m$ is needed. Finally, we obtain for $\frac{\partial \mathbf{f}(\mathbf{x},\mathbf{q})}{\partial \mathbf{x}} =$

$$\begin{pmatrix} 1 & 0 & -\sin(\psi^+)v^+T_s & -\sin(\psi^+)v^+\frac{T_s^2}{2} & \cos(\psi^+)T_s & \cos(\psi^+)\frac{T_s^2}{2} \\ 0 & 1 & \cos(\psi^+)v^+T_s & \cos(\psi^+)v^+\frac{T_s^2}{2} & \sin(\psi^+)T_s & \sin(\psi^+)\frac{T_s^2}{2} \\ 0 & 0 & 1 & T_s & 0 & 0 \\ 0 & 0 & 0 & 1 & 0 & 0 \\ 0 & 0 & 0 & 0 & 0 & 0 \\ 0 & 0 & 0 & 0 & 1 & T_s \\ 0 & 0 & 0 & 0 & 0 & 1 \end{pmatrix}.$$

Then, the measurement matrix $\mathbf{H}$ is $\begin{pmatrix} \mathbf{0} & \mathbf{I} \end{pmatrix}$.

When a new GPS sample is available, the measurement matrix H and vector $\mathbf{z}[k]$ are extended:

$$H = \begin{pmatrix} 1 & 0 & & \\ 0 & 1 & & \vdots \\ & & \mathbf{0} & \\ & \cdots & & \mathbf{I} \end{pmatrix}, \quad \mathbf{z}[k] = \begin{pmatrix} U_e[k+1] \\ U_n[k+1] \\ \dot{\psi}[k+1] \\ v[k+1] \\ a[k+1] \end{pmatrix}$$

where U_e and U_n are the *easting* and *northing* positions where the vehicle is located in UTM coordinates (cf. Ch. 6.6). The process and measurement noise covariance matrices $\mathbf{Q}$ and $\mathbf{R}$ of the EKF algorithm are chosen by using the measurements.

6.5.3. Estimation of the Lateral Distance

As illustrated in Fig. 6.3, the yaw angle $\varphi[k]$ between the vehicle and the lane must be known in order to calculate the lateral distance $l[k]$. The lane is estimated by the low-pass filtered vehicle trajectory using a 2$^{\text{nd}}$-order Butterworth filter with cut-off frequency 0.05 Hz. The relative lateral displacement Δl related to the lane mean is calculated for every sampling period T_s. The lateral distance is then obtained by updating the estimated lateral position in each sampling period:

$$l[k+1] = l[k] + \Delta l \tag{6.18}$$

with the initial condition $l(0) = 0$. The lateral distance signal obtained from the vehicle model is again high-pass filtered to remove accumulating bias errors. Furthermore, it was low-pass filtered to remove noise and road influences with a 2$^{\text{nd}}$-order Butterworth filter with the cut-off frequency 0.1 Hz.

6.6. GPS Data in UTM Coordinates

A standard GPS sensor was used for all recorded drives, since the recorded CAN-signal from the head unit was map-matched and thus disturbed by discontinuous gaps. Its temporal sensor resolution with 1Hz is not very high. Also the absolute position is not very accurate. There

are often invalid sections from tunnels, synchronization problems, insufficient signal quality or too few satellites. Furthermore, there are severe outliers in the signal. All these influences had to be suppressed by post-processing described in Czupalla (2007).

The UTM representation (cf. Hasberg and Hensel, 2009; LVGB, 2009) of GPS has the advantage that the units use a metric world-coordinate system similar to the information obtained by the vehicle data. Maps from OpenStreetMaps.org (2020) were used for visualization.

In order to convert global GPS longitude and latitude coordinates to x, y positions in meters, the following equations can be used:

$$d = \underbrace{60 \cdot 1.852 \cdot \frac{180}{\pi}}_{Earth\ radius} \cdot \arccos\Big(\sin(\varphi_1) \cdot \sin(\varphi_2) + \cos(\varphi_1) \cdot \cos(\varphi_2) \cdot \cos(\lambda_2 - \lambda_1)\Big) \quad (6.19)$$

with d being the distance between two GPS positions (latitudes φ_i, longitudes λ_i).

The *Universal Transverse Mercator* (UTM) system splits the world in tiles of six degree in vertical direction (from 80° south to 84° north) (Weiss, 2011). The transversal Mercator projection flattens the zone and defines a Cartesian coordinate system for every tile. Germany is zone U 32 for instance. App. A.10 shows an illustration of this principle. The converted GPS coordinates to meters in relation to the zone coordinate system allows the calculation with metric scales.

6.7. Inertial Feature Extraction

An overview of analyzed lane data based features and the methods to extract them, are described in (Friedrichs and Yang, 2010a). This section explains the features that are selected and for which the odometric data are sufficient.

6.7.1. Inertial Features

Tab. 6.2 lists the selected features which have been investigated here. Lane data based and odometric features are calculated with the same algorithms, but different input data.

ID	Feature Name	Description
15	LANEDEV	Lane deviation
17	ZIGZAGS	Number of zig-zag events
29	LNMNSQ	Lane mean squared
34	ORA	Overrun area
16	LATPOSZCR	Lateral position ZCR
30	LNIQR	IRQ of lateral position
37	DELTADUR	Duration between inflection points
38	DELTALATPOS	Mean lateral amplitude
39	DELTALATVELMAX	Max lateral velocity

Table 6.2.: Selection of lane-based features

6.7.2. System Active Signal

As the lane changes are not detected by the camera anymore, the turn indicator lever signal was used to suppress lane changes. Three seconds before and ten seconds after lever operation have been suppressed. Yaw rates $\dot{\psi} > 3°/s$ have been neglected as well. Furthermore, the system was defined to be active only at velocities over 80 km/h.

6.8. Results

This section describes the comparison between lane data and inertial-data based signals. The correlation of lane-based and odometric features is shown, as well as the correlation between odometric features and the KSS drowsiness reference using the Spearman correlation coefficient.

6.8.1. Comparison of Lane Data and Inertial Data

Fig. 6.4 shows the lateral deviation ("distance") signal obtained after removing the offset. However, the mean deviation between the two signals is 38cm, which indicates that there are

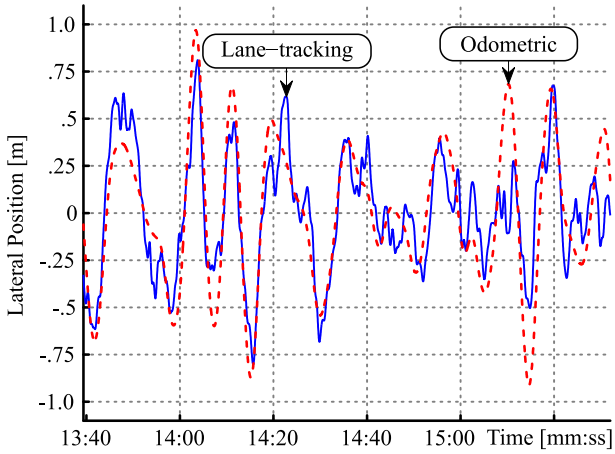

Figure 6.4.: Lateral position from lane-based (blue, solid) and odometric sensors (red, dotted)

certain different influences in the signal. The Pearson and Spearman correlation coefficients between the features derived from the yaw rate and the original lane-based features are shown in Tab. 6.3.

ID	Feature Name	ρ_p	ρ_s
15	LANEDEV	0.241	0.367
17	ZIGZAGS	0.512	0.634
29	LNMNSQ	0.051	0.394
34	ORA	0.338	0.414
16	LATPOSZCR	0.908	0.350
30	LNIQR	0.286	0.505
37	DELTADUR	0.768	0.540
38	DELTALATPOS	0.239	0.467
39	DELTALATVELMAX	0.634	0.633

Table 6.3.: Correlation coefficients between lane-data and odometric features

6.8.2. Feature Evaluation

Features were assessed and optimized in multiple ways. The Spearman correlation coefficient between the KSS and the features derived from yaw rate and the original lane-based features are compared in Tab. 6.4.

Feature Name	ρ_S Lane vs. KSS	ρ_S Odom. vs. KSS
LANEDEV	0.240	0.064
ZIGZAGS	0.318	0.103
LNMNSQ	0.268	0.080
ORA	0.325	0.105
LATPOSZCR	0.223	0.328
LNIQR	0.187	0.105
DELTADUR	0.281	0.117
DELTALATPOS	0.295	0.079
DELTALATVELMAX	0.266	0.106

Table 6.4.: Spearman Correlation coefficients between lane data and inertial features vs. KSS

Even if some features (ZIGZAGS and LATPOSZCR, zero-crossing rate) correlate very well with the lane-based pendant, they do not perform as good in regards to drowsiness detection. Only the feature LATPOSZCR performs better.

6.9. Conclusions

The basic motivation of the presented work is to estimate the classical lane-based features solely from inertial sensors instead from camera-based lane data. In this thesis, we present a comparison of these two methods. This has the benefit that odometric data is available in almost every vehicle nowadays. In contrast, lane tracking cameras are special equipment and, thus, still rarely available in today's fleets. Another major advantage of inertial data is its independence from weather, camera calibration and lane-marking quality. This property highly increases the operability of the system. A motion model for inertial sensor signals using the EKF was presented to derive the lateral lane deviation from odometric data. For a comparison and visualization of lane data and data derived from inertial sensors, GPS was additionally used. As the GPS signal is only available every second, whereas the CAN data has a cycle time of 20 ms, a method to include the GPS measurements into the motion model was proposed. Inertial and GPS data have been converted to the UTM coordinate system to have the same metric representation. This study shows that the features extracted from odometric data correlate well with the lane-based features. A large set of data was compared. However, there are relevant differences in the signal which make the exact estimation of the lane deviation impossible. The major problem remains the separation between road curvature and vehicle lurching between the lane markings. The nine "lane-based" features estimated by inertial data have been analyzed for their performance to detect impaired driving. The correlation of the features with the KSS reference is comparable but inferior to the performance of real lane data based features. Generally speaking, some lane-based features can be approximated very well by odometric data whereas others cannot. Only LATPOSZCR performs better, because of the continuous system availability of the inertial sensors.

Chapter 7.

Assessment of Features

After the features have been extracted (Ch. 4) under the consideration of external and driver influences (Ch. 5) and with a new alternative approach to estimate lane features from inertial sensors (Ch. 6), they are assessed in this chapter. The features are assessed and optimized in multiple ways. The focus is to assess the performance of single features but also their combinations according to different references in Ch. 3.

In the first step, quantitative metrics for the correlation analysis and their results are presented. The metrics were used in Ch. 4.5 as cost function for parameter optimization. Visual evaluations like boxplots, class histograms, correlation coefficient histograms or scatter plots lead to a higher transparency of features to identify their characteristics. The metrics from the first part of the chapter are the basis for these visual methods. The correlations and visualizations suffer from the discrete interval scale of the KSS. Thus, the KSS values were interpolated and smoothed as described in Ch. 3.3.6. Linear and multiple regression is used to assess the correlations by fitting linear functions by least mean squares. Statistical tests like t-test, F-test or MANOVA are powerful methods to identify whether differences are significant. Finally, a visual user-interface (GUI) combines all the methods at once and allows filtering of the data and reference. The results motivate several improvements in the feature extraction. Subjective, rather qualitative and empirical observations from night drives are also summarized. A proposal for potential features is given that comprises the various assessment aspects and knowledge of the nature and potential of features. Features that are highly correlated and based on the same patterns are reduced to the best of them.

7.1. Feature Assessment by Metrics

The goal of this section is to evaluate different measures that describe the relation between two signals best. There are various potential metrics such as correlation coefficients or the Fisher metric to assess the correlation and variance between features and reference. The covariance, correlation and scatter matrices describe the relation between features. The Spearman correlation coefficient, for instance, has also been used for parameter optimization.

7.1.1. Correlation Coefficients

The correlation describes the linear (or monoton) relationship between two measures $\mathbf{X} \in \mathcal{F}$ and $\mathbf{Y} \in \{\mathcal{F}, \mathrm{KSS}, \mathrm{EEG}, \mathrm{EYE}\}$. The metric is desired to be high when high and low sample values of the one measure $\mathbf{X}$ occur at the same time as for the other measure $\mathbf{Y}$. This can be illustrated by the scatter plot (cf. Sec. 7.2.1) of the two measured $\mathbf{X}$ and $\mathbf{Y}$ in Fig. 7.1.

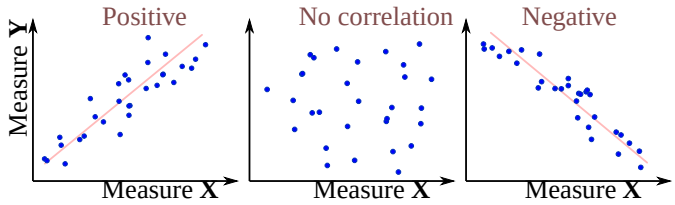

Figure 7.1.: Scatter plot to illustrate correlation: positive, no and negative correlation.

This relationship can be quantitatively captured by the *correlation coefficients* after *Bravais-Pearson* ρ_p for linear and *Spearman* ρ_s for monoton relationship. The range of values of both coefficients lies in $-1 \leq \rho_p \leq 1$. In case $\rho > 0$, the measures are positively correlated and vice versa. The *p*-value of correlation indicates the probability with which the same result could be achieved randomly. With other words, it indicates the reliability of the result and is relevant only for fewer test samples.

Pearson Correlation Coefficient

The empiric *(Bravais-)Pearson Correlation Coefficient* (Fahrmeir et al., 2003) measures the *linear* relationship between two measures $\mathbf{X} = [x_1, .., x_N]^T$ and $\mathbf{Y} = [y_1, .., y_N]^T$ (with $\bar{\cdot}$ as the average):

$$\rho_p(\mathbf{X}, \mathbf{Y}) = \frac{\sum_{i=1}^{N} (x_i - \bar{x})(y_i - \bar{y})}{\sqrt{\sum_{i=1}^{N} (x_i - \bar{x})^2 \sum_{i=1}^{N} (y_i - \bar{y})^2}} = \frac{\mathrm{Cov}(\mathbf{X}, \mathbf{Y})}{\sqrt{\mathrm{Var}(\mathbf{X}) \cdot \mathrm{Var}(\mathbf{Y})}} \,. \tag{7.1}$$

Spearman Correlation Coefficient

The *Spearman correlation coefficient* ρ_s describes how well the relationship between two measures can be described by a *monotonic* function. It is calculated in the same way as the Pearson coefficient, only that a *rank function* $rg(\cdot)$ converts the values $\mathbf{X}$ and $\mathbf{Y}$ to a sorted rank order. For instance, the highest value is mapped to 1, the second highest value becomes 2 and so on. If samples occur multiple times, they will be assigned to mean rank values. The calculation is defined (see Fahrmeir et al., 2003) by:

$$\rho_s(\mathbf{X}, \mathbf{Y}) = \frac{\sum_{i=1}^{N} (rg(x_i) - \overline{rg}(\mathbf{X}))(rg(y_i) - \overline{rg}(\mathbf{Y}))}{\sqrt{\sum_{i=1}^{N} (rg(x_i) - \overline{rg}(\mathbf{X}))^2 \sum_{i=1}^{n} (rg(y_i) - \overline{rg}(\mathbf{Y})^2}} = \frac{\mathrm{Cov}(rg(\mathbf{X}), rg(\mathbf{Y}))}{\sqrt{\mathrm{Var}(rg(\mathbf{X})) \cdot \mathrm{Var}(rg(\mathbf{Y}))}} \,, \tag{7.2}$$

with the rank means $\overline{rg}(\mathbf{X})$ (and $\overline{rg}(\mathbf{Y})$) given by

$$\overline{rg}(\mathbf{X}) = \frac{1}{N} \sum_{i=1}^{N} rg(x_i) = \frac{N+1}{2} \,. \tag{7.3}$$

Even though the KSS scale is defined to be linear from a psychological perspective, it is known that the scale is not interpreted and used linearly. This is one reason why the Spearman correlation coefficient has shown to be more meaningful in this application.

7.1.2. Fisher Linear Discriminant Metric

The *Fisher Linear Discriminant Metric* is motivated by the fitness function of the Fisher LDA (Welling, 2005) and closely related to regression analysis. It sets the scatter between classes in relation to the scatters within each class.

Multi-dimensional case: The *Multiple Discriminant Analysis* (MDA) is defined as explained in (Yang, 2018; Uhlich, 2006; Duda et al., 2001) by the quotient of the matrix determinants:

$$\text{MDA}(\mathbf{X}) \quad = \quad \frac{|\mathbf{S}_B|}{|\mathbf{S}_W|} \tag{7.4}$$

where S_B is the scatter matrix *between* the c classes

$$\mathbf{S}_B \quad = \quad \sum_{i=1}^{c} n_i(\bar{\mathbf{m}}_i - \bar{\mathbf{m}})(\bar{\mathbf{m}}_i - \bar{\mathbf{m}})^T \tag{7.5}$$

where n_i is the number of patterns in class i. $\bar{\mathbf{m}}$ is the average over all classes and $\bar{\mathbf{m}}_i$ are the averages of each class i. $\mathbf{S}_W$ is the scatter *within* classes:

$$\mathbf{S}_W = \sum_{i=1}^{c} \mathbf{S}_i \;\text{ with }\; \mathbf{S}_i = \sum_{x \in \mathbf{X}_i} (x - \bar{\mathbf{m}}_i)(x - \bar{\mathbf{m}}_i)^T \,, \tag{7.6}$$

the scatter matrix $\mathbf{S}_i$ of the patterns $\mathbf{X}_i$ in class i. The advantage of MDA is that multiple features can be assessed by one scalar measure. This measure is invariant to a linear transformation, i.e. no normalization is required in advance.

Fig. 7.2 illustrates the strengths and weaknesses of the MDA by four examples with three bivariate Gaussian distributed clusters and serves as validation of the implementation. Another weakness of the measure is that when one cluster is rotated, the center of all classes and, thus, the metric is not changed much, even when the two classes overlap more.

In the two-dimensional case and especially for more than two classes, the correlation coefficients are more meaningful since they describe the ordinal linearity. Further, it has to be noted that the KSS cannot be used for the MDA, since it is only defined for classes.

7.1.3. Results

Tab. 7.1 lists all metrics from this section, the correlation coefficients, the one-dimensional MDA metric for 9 classes and the AUC (Ch. 7.5). The ending 'BL' indicates that a feature is baselined. Only the best out of all redundant features are used for the comparison with the KSS. External influences are only relevant after the fusion of features. It can be seen that most a-priori features perform best, but on the same level as the major ATTENTION ASSIST feature `GGGLWF`. Further, the TLC-based and lane approximation features show the best results underneath the causal features.

ID	Feature Name	ρ_p	ρ_s	MDA (9 classes)	AUC
45	`CIRCADIAN`	0.4911	0.4880	84.824554	0.80057
68	`TOTSPEED`	0.3825	0.4088	12.859585	0.52957
122	`GGGLWF`	0.3644	0.3541	11.141940	0.74449
66	`TOT`	0.2579	0.2656	10.385206	0.67326
156	`DISTRACTION`	0.2266	0.2590	22.924826	
160	`NMRSTVHOLD`	0.2501	0.2415	10.857038	

ID	Feature Name	ρ_p	ρ_s	MDA (9 classes)	AUC
175	TURNINDMISS	0.1866	0.2295	6.906748	
59	MONOTONY	0.2190	0.2202	2.173279	0.54915
121	STWEVENTBL	0.1695	0.1910	3.540389	0.64316
155	TLC1MINBL	0.1795	0.1838	13.077203	0.63736
159	AmpD2ThetaEwma	0.1555	0.1620	5.025147	
161	TLCREACTIM	0.1392	0.1485	14.907812	
14	LANEAPPROX	0.1391	0.1464	9.264948	
151	LANEAPPROXBL	0.1400	0.1420	8.597869	0.50169
171	MONOTONYSPD	0.1353	0.1344	3.060937	
67	TOTMONO	0.1353	0.1344	3.060937	0.52957
69	NMRHOLD	0.1473	0.1313	2.796519	0.60884
167	NMRHOLDBL	0.1472	0.1313	2.792206	0.61344
38	DELTALATPOS	0.1414	0.1299	4.858002	0.56556
158	AmpD2ThetaBL	0.0576	0.1197	6.671112	
51	STWEVENT	0.0988	0.1138	3.120092	
32	LANEX	0.0917	0.1103	5.736944	
39	DELTALATVELMAX	0.1148	0.1101	5.302499	
65	DRACTIVITY	0.0438	0.1067	0.419859	
48	AmpD2Theta	0.1126	0.1045	4.915033	
17	ZIGZAGS	0.1158	0.1024	6.153849	
139	ZIGZAGSBL	0.1158	0.1024	6.153849	
33	LNERRSQ	0.0504	0.1014	57.698357	
168	MICROCORRECTIONS2	0.0339	0.1007	0.479821	
15	LANEDEV	0.0938	0.0965	2.961627	
137	LANEDEVBL	0.0938	0.0965	2.961627	
146	LANEDEVSQ	0.0699	0.0946	1.821851	
30	LNIQR	0.0903	0.0885	1.995599	
36	VIBPROP	0.0777	0.0845	4.479706	
34	ORA	0.0917	0.0806	2.368282	
72	VHAL	0.0799	0.0800	1.389162	
27	TURNINDADVANCE	0.0573	0.0528	2.102021	
145	LANEDEV4	0.0444	0.0504	10.567072	
71	MICROCORRECTIONS	0.0337	0.0430	5.809846	
22	DEGOINT	0.0698	0.0375	1.024265	
147	MICROCORRECTIONSW	0.0168	0.0346	5.174747	
152	LRVFAST	-0.0021	0.0248	1.019020	
29	LNMNSQ	0.0290	0.0108	0.439556	
170	FASTCORRECT	-0.0545	0.0104	0.892245	
40	LANEAPPROXADAPT	0.0248	0.0070	2.263082	
18	STWZCR	0.0028	-0.0124	2.697696	
154	LRVVERYFAST	-0.0379	-0.0128	1.250960	
37	DELTADUR	-0.0352	-0.0311	1.197629	
25	STWVELZCR	-0.0430	-0.0319	3.105123	
150	LANEAPPROXAD	-0.0267	-0.0333	0.286441	
16	LATPOSZCR	-0.0216	-0.0437	0.342992	
169	YAWJERK	-0.0703	-0.0719	1.805102	
28	TURNINDDUR	-0.0647	-0.0744	2.632143	
42	ELLIPSE	-0.0524	-0.0757	7.906066	
19	LATMEAN	-0.0534	-0.0771	1.344164	
142	VARCRIT	-0.0179	-0.0936	8.110901	
153	LRVPERCHIGH	-0.1894	-0.1933	4.820714	
31	LNCHGVEL	-0.1238	-0.1998	2.224121	
165	STV50	-0.2646	-0.2697	10.243395	
26	TRFCDENS	-0.2535	-0.2913	23.574284	
164	STV25	-0.2966	-0.2990	15.787481	
166	STV75	-0.3149	-0.3255	18.138641	
70	LIGHT	-0.4353	-0.4354	116.210213	

Table 7.1.: Correlation coefficients and MDA measure for selected features sorted by ρ_s. That all values are significant is indicated by the $p < 0.001$ due to the high number of samples.

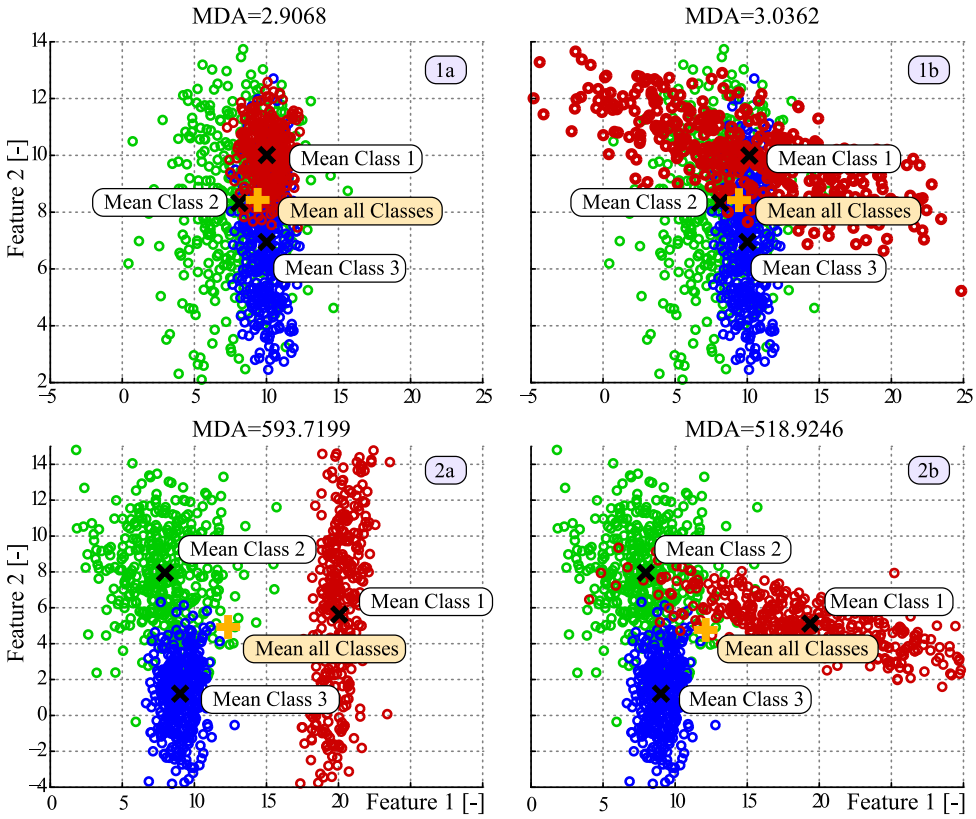

Figure 7.2.: Fisher MDA to measure the scatter between classes in relation to the scatter within classes. The left and right means are similar. Class 1 in *1b* has a larger spread than in *1a* which allows better discrimination, decently reflected by the MDA. Class 1 in *2b* is rotated and overlaps which causes worse discrimination, which is reflected by the slightly lower MDA.

7.2. Visual Feature Assessment

Visual assessment of features gives much more transparency than a quantitative measure. This section shows the most practical visualizations in a few selected examples.

7.2.1. Scatter Plots

The most transparent method to compare the combined correlation between two or three features is the *scatter plot*. A scatter plot for three features with marked classes is shown in Fig. 7.3.

7.2.2. Boxplots and Error Bars

Boxplots (or *Box-Whisker-Plots*) serve to visually illustrate the median, scatter, range and outliers of class distributions. For every class, the median, IQR and the *Whiskers* are marked, as illustrated in Fig. 7.4. The latter are defined as $Whisker = 1.5 \cdot IQR$ and define the limit for outliers. The *Notches* display the variability of the median between the classes (MathWorks, 2007). The notches of classes, that do not overlap, have different medians at the 5% significance level assuming the samples to be normally distributed, which, is, however, also reasonably robust for other distributions. This method can be compared to a visual

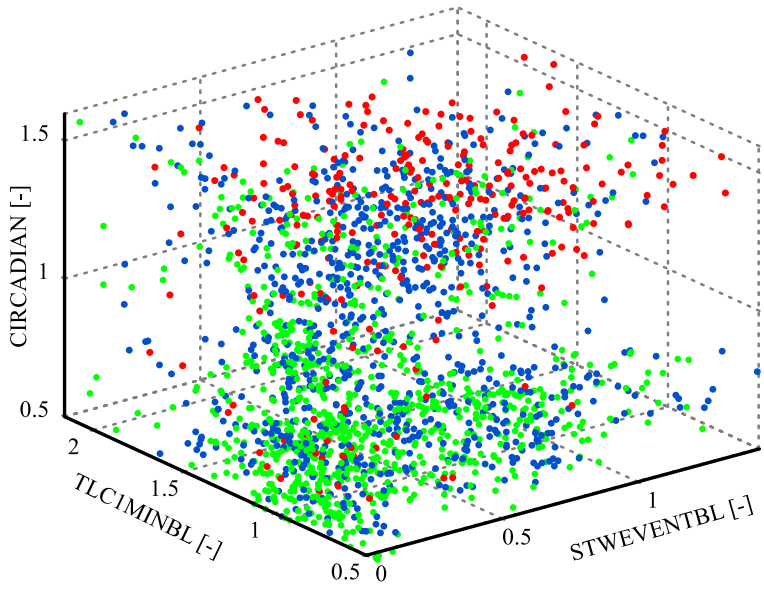

Figure 7.3.: Scatterplot for selected features CIRCADIAN, TLC1MINBL and STWEVENTBL for the three classes *awake* (●), *acceptable* (●) and *drowsy* (●).

hypothesis test analogous to the t-test for means. Thus, in this example, it can be seen that the feature NMRSTVHOLD increases with increasing KSS with significant differences between classes.

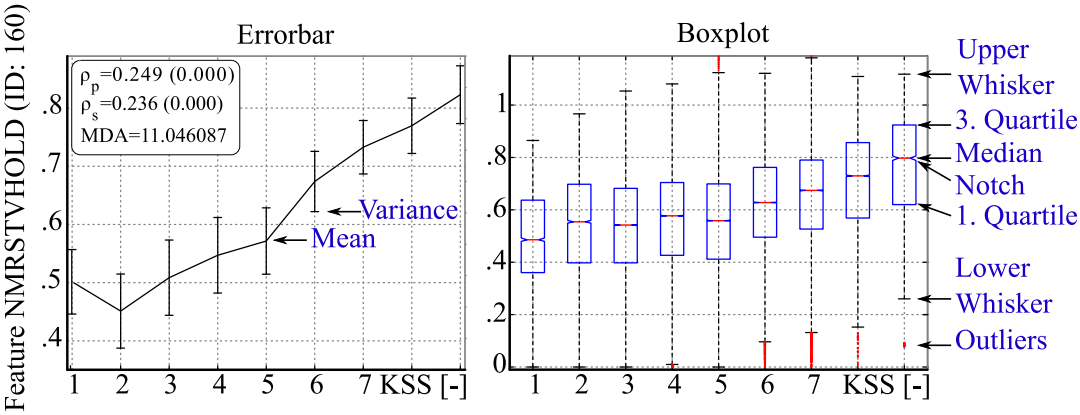

Figure 7.4.: Illustration of Boxplot for feature NMRSTVHOLD.

The Boxplots in Fig. 7.5 show the relationship between different other features and the KSS. All plots show that the median of the classes significantly differ, but are still overlapping which pose difficulties for the drowsiness classification. There are very few drives with KSS below 2, so these levels should be neglected.

Error bars show the confidence level of data or the deviation along a curve (MathWorks, 2007). In our case, the variance is used as displayed in Fig. 7.4. In this example, the difference between mean/median and variance/IQR can be seen due to the influence of outliers that can be essential for some features.

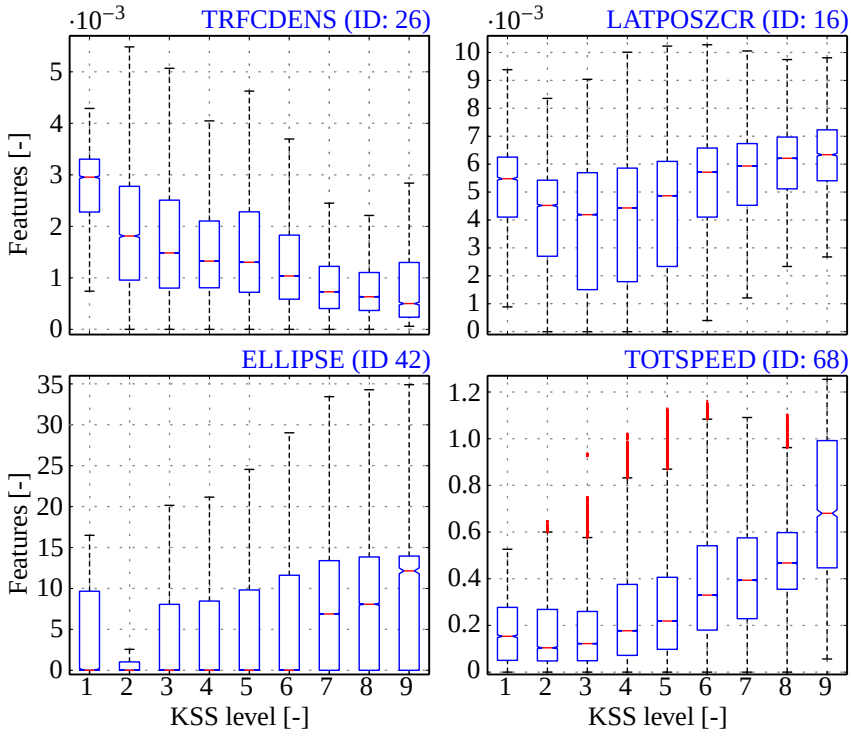

Figure 7.5.: Boxplot of selected features

7.2.3. Class Histograms

Class histograms were also used to get a visual impression of the features. The STV50 class histogram can be found in Fig. 7.6 as an example. It can be seen that the steering velocities decrease with increasing vigilance.

7.2.4. Histogram of Correlation Coefficients

Another method of correlation analysis proposed by Simon (2012) is to cluster the features by drives (or drivers) and calculate the Spearman (or Pearson) correlation coefficients between features and KSS reference. A histogram of the coefficients then indicates, for how many drives this feature correlates well with fatigue. If one portion of the drives correlates negatively and the other portion positively, it is a contradicting statement and does not speak for an useful feature. It has to be considered that a long drive contributes as much as a short drive. However, in App. A.11 the limits of this metric are discussed. Even if all correlation coefficients are one, the overall correlation can be very bad. With other words, this metric would work sufficiently, if the online-adaption of every drive by baselining was optimal.

Fig. 7.7 shows other examples of the causal features LANEX, ORA and NMRHOLD. It can be seen that there is a tendency towards the right, that indicates, that most drives are positively correlated with drowsiness. Further, it can be seen, that the last feature, with the best overall Spearman coefficient, performs worst from the histogram's perspective. We can conclude, from these three examples, that LANEX profits most from driver (drive) adaption, i.e. baselining.

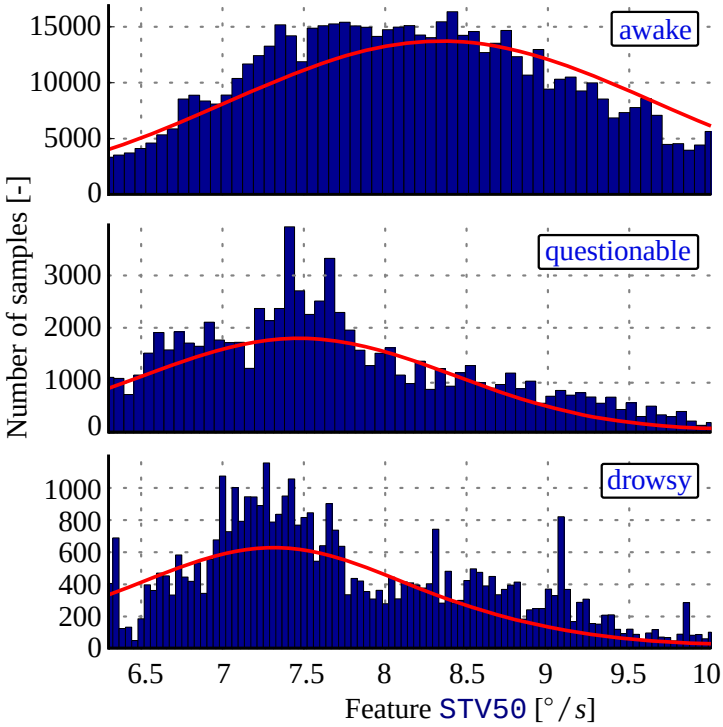

Figure 7.6.: The class histogram of feature STV50 split up by classes *awake*, *questionable* and *drowsy* (ID: 53; $\rho_p = -0.30; \rho_s = -0.33$ ($bothp = 0.0$); MDA = 16.9)

7.3. Assessment of Correlation between Features

If two features correlate well with fatigue, this does not mean that their combination performs better. Generally, features based on different patterns and sensors have the tendency to be less correlated. The correlation *between* features is subject of this section.

7.3.1. Scatter Plot Matrix

Fig. 7.8 shows the scatter plot matrix that give transparency of how correlated features are. It is a matrix of scatter plots between all features. Ideally, both features are uncorrelated, but correlate with the reference, so that the values are scattered and the classes can be distinguished well. It shows that lane based and steering based features are more uncorrelated, such as LANEDEV and YAWJERK. No correlation between features is desired (except with KSS).

7.3.2. Correlation Matrix

Correlation Matrix consists of the pairwise correlation coefficients between the measures $\mathcal{F}_i \in \mathcal{M}^n$ in their column and row. It indicates how strong the features are correlated with each other:

$$\mathrm{C}(\mathcal{F}) \begin{pmatrix} \rho(\mathcal{F}_1,\mathcal{F}_1) & \cdots & \rho(\mathcal{F}_1,\mathcal{F}_n) \\ \vdots & \ddots & \vdots \\ \rho(\mathcal{F}_n,\mathcal{F}_1) & \cdots & \rho(\mathcal{F}_n,\mathcal{F}_n) \end{pmatrix} \tag{7.7}$$

where ρ can be calculated after Pearson ρ_p and Spearman ρ_s respectively.

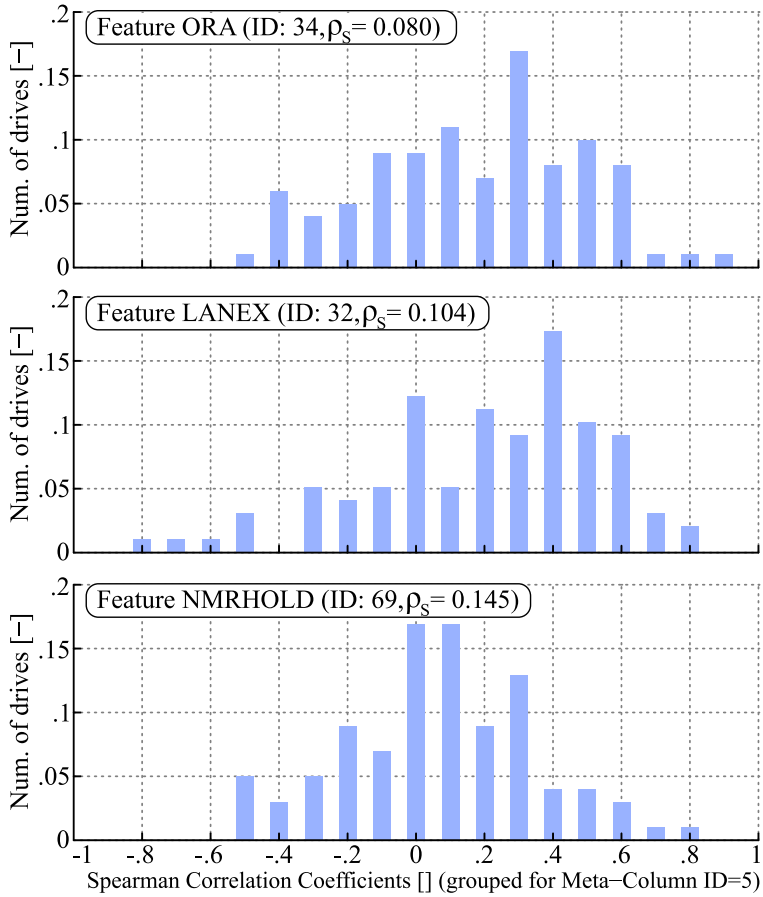

Figure 7.7.: Histogram of ρ_S coefficient of KSS and features LANEX, ORA and NMRHOLD grouped by drives

Fig. 7.9 shows an example of the matrix. Baselined features are often correlated. The road condition features and all LANEDEV derivates are correlated, but also with ORA, LANEIQR and TLC1MIN. CIRCADIAN are negatively correlated with LIGHT.

7.4. Linear and Multiple Regression Analysis

Regression Analysis is a method of statistical analysis that pursues the goal to quantitatively determine the relationship between a dependent variable (*regressand*) and one or several independent variables (*regressor(s)*). In our case, the KSS reference is the regressand and the regressor(s) is (are) the feature(s). Regression analysis for driver state detection was already used by Knipling and Wang (1994); Wierwille and Ellsworth (1994); Wierwille (1996b); Belz (2000) and (Mattsson, 2007; Berglund, 2007, Both Sec. 2.5) for identifying the most potential features. When features are normalized, the coefficients indicate, which contribution a feature makes for the final result and which features are redundant. *Linear* and *Multiple Regression* are closely related to LDA and classification. Hence, the other application of this method is prediction or classification, discussed in Ch. 8.

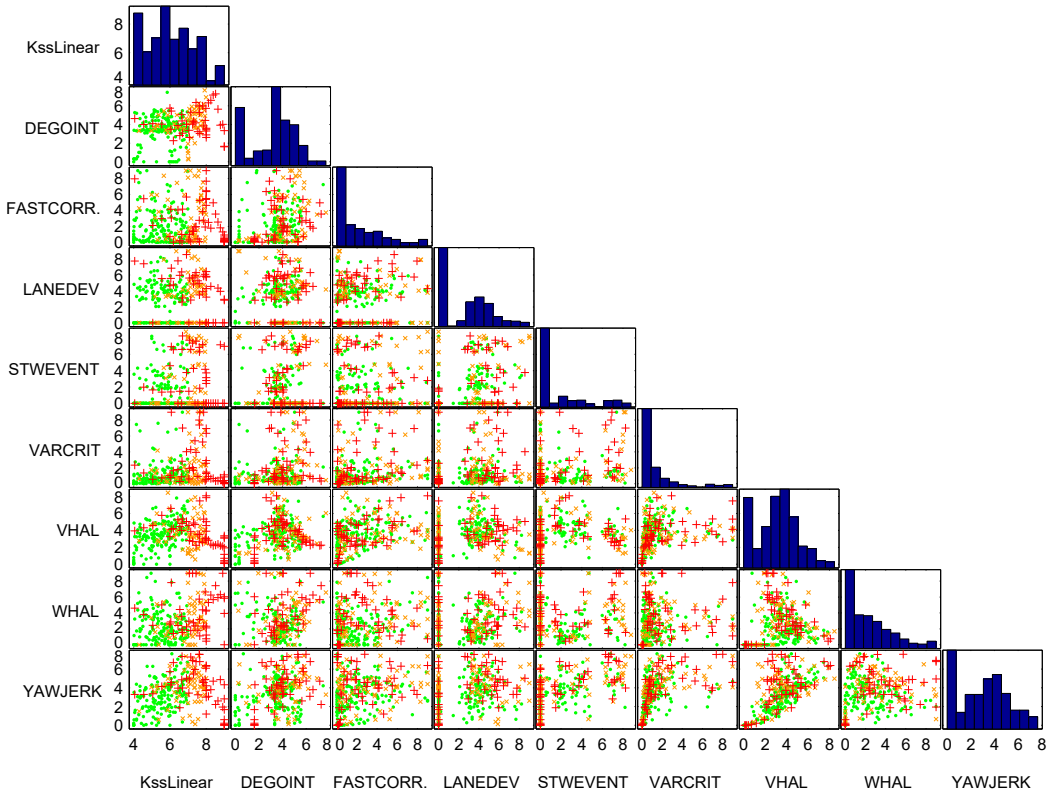

Figure 7.8.: Scatter plot matrices for some selected features to show the correlation between features. Their combined discriminative performance can be seen, since classes are marked individually: • for awake, × for questionable and + for drowsy. The diagonal shows the distribution of the features.

7.4.1. Multiple Regression Analysis

In multiple regression analysis, every feature is combined linearly (or by any other function) to obtain a combined measure. The regression equation can be formulated mathematically, in our case, for the one dimensional version as follows:

$$\mathrm{KSS} = f(\mathcal{F}_0) + \varepsilon \tag{7.8}$$

and for the N-dimensional case:

$$\mathrm{KSS} = f(\mathcal{F}_0, \mathcal{F}_1, \ldots, \mathcal{F}_{N-1}) + \varepsilon \tag{7.9}$$

with the features from the feature matrix $\mathcal{F}_i \in \mathbf{F}$ and ε as the *residual* error that is to be minimized. The residual also indicates, how strong the correlation is. In the next step, $f(\cdot)$ can be expanded by using the *regression coefficients* $\boldsymbol{\beta}$:

$$\mathrm{KSS} \quad = \quad \beta_0 \cdot \mathcal{F}_0 + \beta_1 \cdot \mathcal{F}_1 + \ldots + \beta_N \cdot \mathbf{1} + \varepsilon \tag{7.10}$$

The last coefficient β_N allows the adaption of an offset through the vector $\mathbf{1}$. For instance, in our application, this yields:

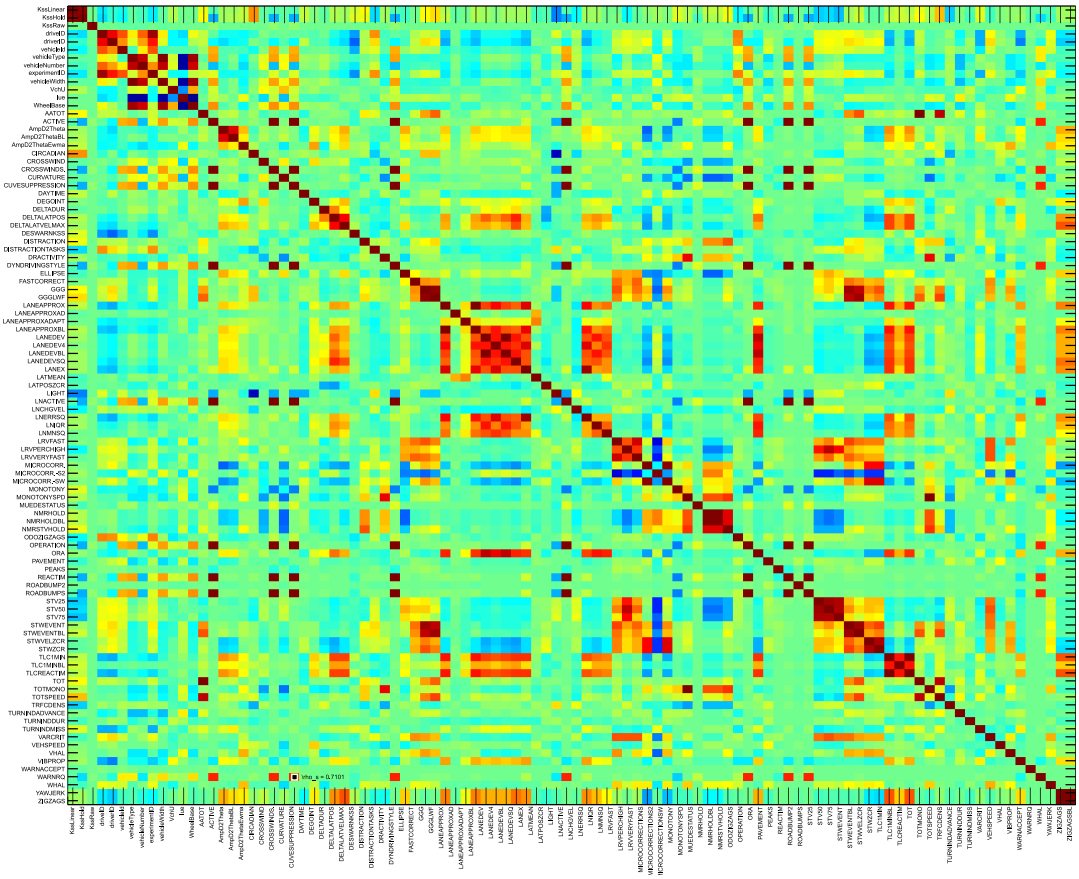

Figure 7.9.: Correlation matrix of selected features (Correlation: negative (blue), no (green), positive (red))

$$\mathrm{KSS} = \boldsymbol{\beta} \cdot F = \begin{pmatrix} \texttt{ZIGZAGSBL} \\ \texttt{NMWRONG} \\ \texttt{NMWRONGBL} \\ \texttt{LANEDEV} \\ \texttt{LANEAPPROX} \\ \texttt{LIGHT} \\ \cdots \\ \texttt{GG} \\ \texttt{ELLIPSE} \\ \texttt{DEGOINT} \\ \texttt{LANEAPPROXADAPT} \\ \texttt{AATOT} \\ \texttt{CIRCADIAN} \\ \mathbf{1} \end{pmatrix} \cdot \begin{pmatrix} 95.2, \\ 6.9, \\ 0.0, \\ 1.8, \\ 234.5, \\ -0.074, \\ \cdots \\ 0.081, \\ -0.034, \\ 1.18, \\ -411.2, \\ 0.000061, \\ 1.5, \\ 2.9 \end{pmatrix}^T \tag{7.11}$$

The regression coefficients $\boldsymbol{\beta}$ are obtained by minimizing the MSE of the residuum:

$$\in \quad = \sum_{patterns} [\mathrm{KSS} - \boldsymbol{\beta} \cdot \mathcal{F}]^2. \tag{7.12}$$

The solution of this least-squares minimization problem is well known. Fig. 7.10 shows the KSS reference and the resulting signal $f(\mathcal{F}_0, \mathcal{F}_1, \ldots, \mathcal{F}_{N-1})$. The trend is correct, but not

very precise, probably due to fact that the KSS is not a simple linear scale.

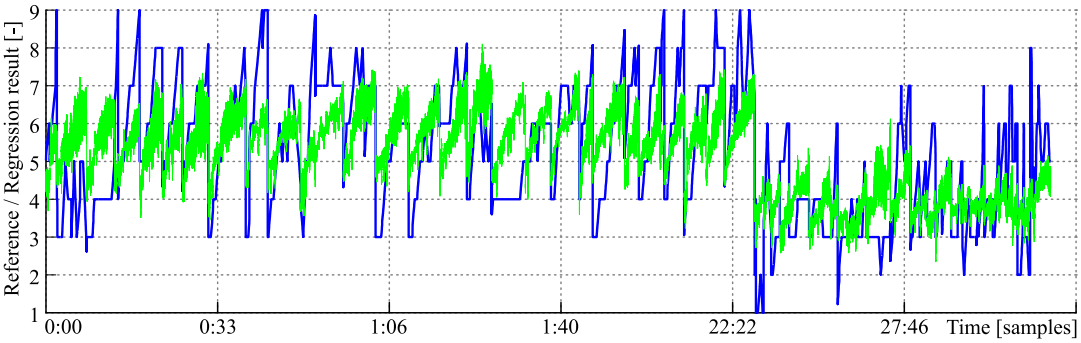

Figure 7.10.: KSS reference and the resulting linear combination signal from the multiple regression for concatenated drives.

Fig. 7.11 shows the resulting scatter plot of $f(\cdot)$ with the improved total correlation $\rho_s = 0.68$ and $\rho_p = 0.66$. Still, the detection of the fatigued instances is not optimal.

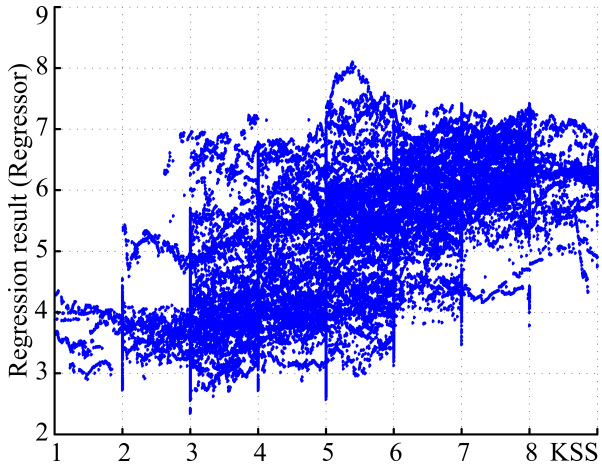

Figure 7.11.: Scatter plot of the multiple regression result

7.5. Receiver-Operating-Characteristics (ROC)-Analysis and Area Under Curve (AUC)

The performance of a feature or a binary classifier can be tested in a graphical illustration, the *Receiver-Operating-Characteristics* (ROC) (cf. Fawcett, 2004). It allows choosing a working point as a trade-off between sensitivity (detection rate) and specificity (false alarms). Therefore, the classifier needs to allow that this trade-off is tunable by either weighting the cost function or in the simplest case by variation of a threshold from the feature range minimum to the maximum. For the Bayes classifier, the a-priory distribution of classes can also be varied in order to obtain the ROC. However, this would be related to a loss of performance, due to the neglection of valuable training data.

In case that both PDF's are known (sensitivity and specificity), the ROC curve is obtained by plotting the CDF of the detection probability in the ordinate vs. the CDF of the false alarm probability in the abscissa.

Fig. 7.12 depicts an example ROC curve for the feature GGGLWF based on a two-class classification. The *sensitivity* (True-Positive-Rate) is displayed on the ordinate and $1 - specificity$ (False-Positive-Rate) as abscissa. The target area is marked as well as the region in which the classification result should be.

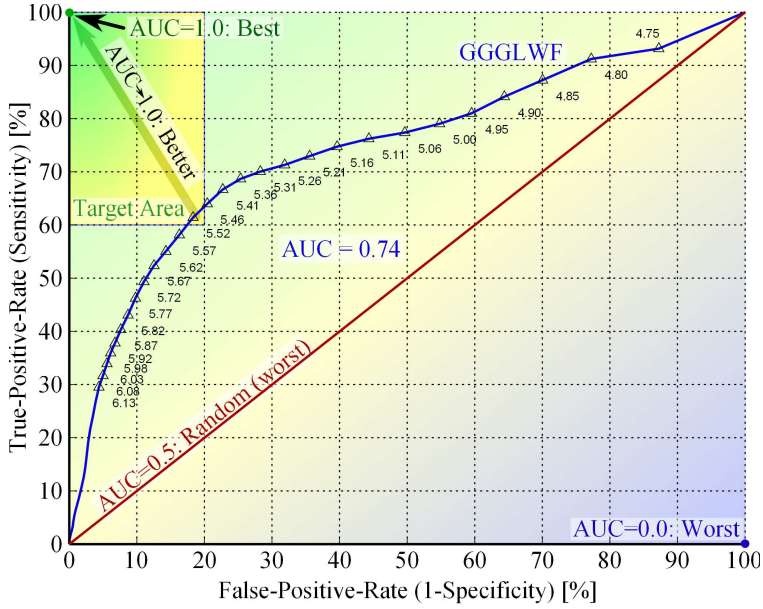

Figure 7.12.: ROC explanation exemplarily on GGGLWF based on a two-class classification

The *Area Under Curve* (AUC) measures the area under the curve, which is a measure for the general classification performance, but makes no statement about the shape on which end it performs better. Values near 1.0 indicate an ideal classification result, while 0.5 means the worst possible random result. A tendency towards 0.0 expresses a miss-interpretation of the classes.

Tab. 7.1 shows the AUC for some selected features. Fig. 8.5 in Ch. 8 shows some ROC curves of the classification results of different classifiers. Fig. 7.13 shows the strong influence of driving duration and circadian as explained in Ch. 5.3.4.

7.6. Conclusion

This section has shown useful methods to assess features by metrics and visually in regards to different perspectives. Primarily, in addition to the straight forward metrics, visual methods pursue the goal to provide more transparency over the characteristics of features. For reasons of space, only a selection of the results could have been shown exemplarily. The focus of this chapter was to assess and optimize the amount of sleepiness associative information of features. However, the scope here was limited to single feature ranking rather than their combination. With correlation coefficients, only linear and monotonous functional relationships between single features and reference could be assessed. This was motivated by the

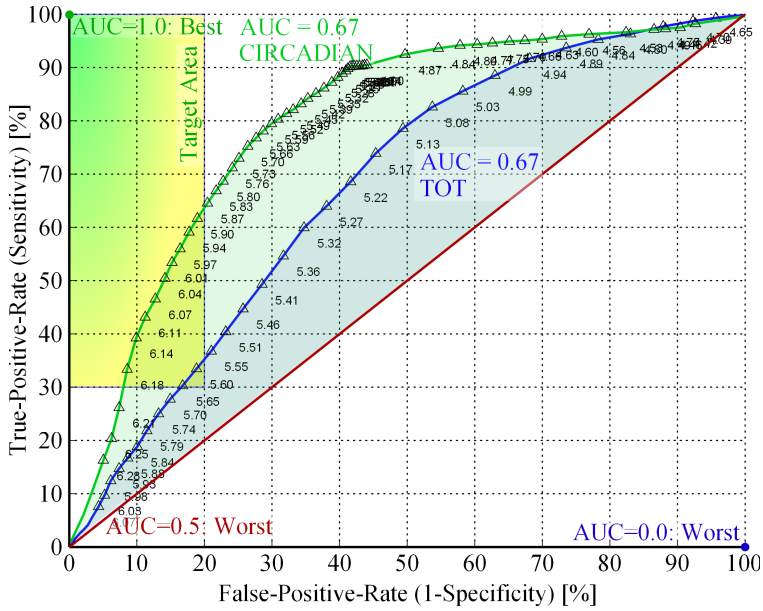

Figure 7.13.: ROC curve for Time-on-Task `TOT` and `CIRCADIAN`

fact that sleepiness is an ordinal scale rather than a multi-modal phenomenon. In contrast to Pearson correlation coefficients, the Spearman coefficients are more suitable to describe the single feature correlation for the development of a bargraph. To determine and optimize the discriminative property of classes, the other measures are also valuable for transparency. While the correlation is of central interest, also the redundancy in between features was investigated. The nonlinear combination of this information by *Classification* is subject to the next chapter.

The presented methods show that there are good features in every group. It is obvious that the a-priori features perform best, as they detect the time instant in driving studies, when subjects become tired. Sleepiness occurs much more often during night experiments compared to real field drives. Thus, this systematic factor is considered separately and taken into account for the final classifier based on a dataset that has an a-priori distribution that is representative for the real field scenario (DataSet *FreeDrives*). The system performance profits most from these features, even when they are not causal, i.e. sensitive to the driver.

The most potential pattern appears to be the steering corrections, especially followed by a steering pause. This pattern is highly analyzed and is further improved in various ways in this thesis.

The lane features based on lane approximation and exceeding performed best among the lane features. For a few drivers, the ALDW warning worked really well and prevented them from drifting out of the lanes. Zig-zag events and its odometry based variant also appear to have high potential, especially in regards to robustness when the vision conditions are impaired. Features that are based on the same pattern as lane deviation for instance are highly correlated and only one of them could be used.

Chapter 8.

Classification of Features

As already stated by Knipling and Wang (1994, P. 9), no *single* feature is capable to detect fatigue. Thus, multiple features must be used in a combined manner. The purpose of classification is to *fuse* multiple features to a single measure (e.g. the KSS scale) or to assign patterns to classes (e.g. whether to issue a warning to the driver or not). In theory, the decision in a higher dimensional features space is always better than for one single feature, presuming that each feature contains information that is not completely redundant and that enough training data are available. In Sec. 7.3, the correlations between features were analyzed. This chapter will discuss the reduction of feature dimensions and classification of fatigue and show results.

8.1. Fusion of Features

The combination of different features can be done on several *fusion levels*:

- **On Decision Level**: A decision can be made for every feature and then be combined by a majority voting. There is always a majority for odd numbers of decisions. This is motivated by the fact that different features work for different drivers and situations. The fusion on decision level is the simplest, however, with a loss of accuracy, since it is not considered that one very certain decision could overrule several other uncertain decisions. For instance, if a threshold is applied, the information is lost in how far the threshold is exceeded.
- **On Classification Level**: The combination of features can be completely done by a classification algorithm. In comparison to the decision level fusion, the certainties of decisions are taken into account. Classification is most expedient when little is known about the problem or when it is too complex to manually understand and model it. The feature extraction is also a lossy compression of information. Even if the classifier finds the optimal solution for a given set of features, the drawback will be that its underlaying model is not further adapted to the problem and the feature extraction algorithms remain untouched.
- **On Feature Level**: Similar to feature extraction, classification is also an information reduction process to get rid of the entire clutter that is irrelevant for the decision. This has the drawback that also valuable information is omitted. Hence, the most difficult method for the fusion of patterns is to understand the underlying processes and to model the fusion directly during feature extraction. For instance, if one feature extracts the number of steady-state steering events and another feature denotes the number of corrections per minute, and if the essential crux is that the steady event must occur directly before the correction, this can only be detected during the feature extraction,

since no conclusion about the temporal relation of the two events would be possible after the sliding averaging. Completely understanding the problem is often very difficult and laborious in practice, but this is sometimes the only way when the patterns are weak and difficult to separate from noise.

Deep Learning is an "end-to-end learning"-approach that comprises all stages at once through very sophisticated network structures. This alternative topic will be discussed in Ch. 8.6.

In the present application, fatigue-related patterns rarely occur. They are relatively vague and vanish in other influences. For this reason, it is necessary to conduct the fusion on an early feature level. Classification is, however, useful to identify potential patterns, combinations and to better understand the underlying mechanisms.

8.2. Pattern Recognition System Design

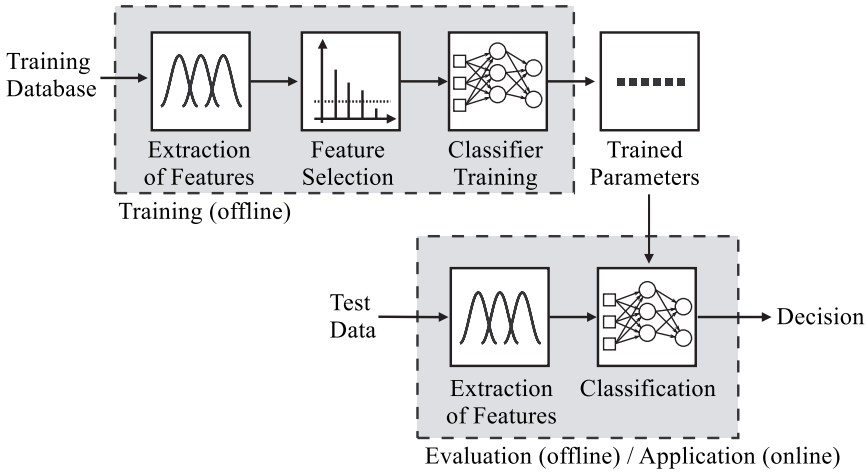

Figure 8.1.: Block diagram of classifier training, evaluation and application (Friedrichs, 2006)

The development of a pattern recognition system commonly follows the steps illustrated in the block diagram in Fig. 8.1. The following steps are always involved:

1. **Features Acquisition** Even the best classifiers will fail, if the underlaying features do not contain enough information about the desired class labels. The feature extraction is the core of any pattern recognition system and comprises implementation and verification of hypotheses about fatigue-related patterns, efficient extraction algorithms that are capable of real-time online processing, normalization of other influencing factors and optimization of parameters. Chapters 4, 5 and 6 describe these main issues in detail. It is usually necessary to evaluate features individually and optimize the involved parameters before proceeding with the next pattern recognition step. The goal is to extract as many ideas for features as possible and then to analyze, which correlate best with the desired classes. This was described in Ch. 7.

2. **Feature Dimension Reduction** Due to the *curse-of-dimensionality* (Sec. 8.4), it is important to reduce the high number of features gathered in the precedent step to the *best combination* of features that are provided to the classifier. Selecting the top features that perform best individually does not mean that also their combination leads to the best performance, because other combinations may better complement each other.

The ideal number of features depends on the amount of available training data and is limited by processing resources. There are two dimension reduction techniques to tackle this problem: selection of the most significant features and feature transformation. Both are discussed and applied in Sec. 8.4.

3. **Classifier Comparison and Selection** In literature, there is a large number of classification algorithms of different types: *statistical* and *non-statistical* as well as *parametric* and *non-parametric*. This topic will be intensified in Sec. 8.2.1 and 8.5.

4. **Classifier Training** Most classifiers involve parameters that need to be trained. While it is distinguished between *unsupervised* and *supervised learning*, the latter is the most prevalent in our application, since offline training data with labeled class references are available. The training topic is subject to Sec. 8.2.2.

5. **Validation** To make a reliable statement about the performance and generalization potential of a trained classifier, it is essential to permute training and test data appropriately. Repeated k-fold cross-validation yields an average training error and the variance of the iterations allows a meaningful statement about the generalization performance. If the trained classifier performs bad with test data or in the field despite a low training error, it is *overfitted* and the previous steps have to be repeated until the desired result is obtained.

6. **Classifier Deployment** The trained classifier parameters obtained from the training can then be used for a real-time implementation. The feature extraction and classifier evaluation must be implemented, so that it fulfills the real-time condition.

8.2.1. Classifier Comparison and Selection

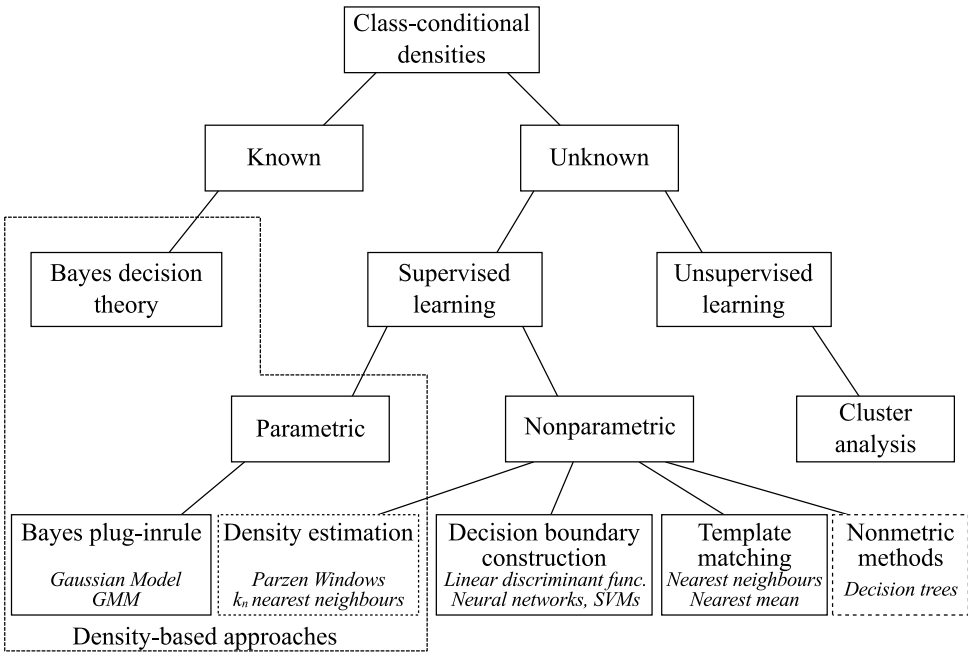

Figure 8.2.: Overview over classification algorithms (Source: Yang and Uhlich (2013); Uhlich (2006))

A large number of classifiers are known in literature and the most important can be found in (Duda et al., 2001). The different approaches for pattern recognition can be structured as shown in Fig. 8.2.

Unsupervised algorithms, for which no class labels are available, are *Independent Component Analysis* (ICA) (Sec. 3.5.1), *Principal Components Analysis* (PCA) or clustering algorithms like the K-Means algorithm (Duda et al., 2001). The K-Means algorithm is used here to identify clusters of driver types.

Supervised classification algorithms to predict categorical labels can be grouped in *parametric* or *non-parametric* methods. Parametric methods make assumptions about known feature distribution shape for each class, such as the Gaussian shape. *Linear* and *quadratic discriminant analysis* are examples for parametric methods. Non-parametric algorithms make no assumption about the features' distribution shapes per class and estimate the distribution from the features. *Decision trees*, *k-Nearest-Neighbor* (*k*-NN), the *Naive Bayes classifier*, *Neural Networks* (multi-layer perceptrons) (ANN) and *Support Vector Machines* (SVM) are a few examples.

The available classification algorithms have different strengths, pitfalls and properties. The selection of the method is determined by feature properties and conditions like computation resources. Then it has to be evaluated by trial-and-error comparison of the different classifiers, which one performs best after adequate adjustment of parameters. The *k-Nearest Neigbour* (*k*-NN), *Linear Discriminant Analysis* (LDA), Bayes classifier, *Gaussian Mixture Models* (GMM), and *Artificial Neural Networks* (ANN) are evaluated for this application. Practical considerations like normalization, parameter tuning and classification results can be found in Sec. 8.5.

Hidden Markov Models (HMM) is a general parametric algorithm for predicting arbitrarily-structured labels of categorical sequences, such as a sequence of *phonemes* in speech (i.e. vowels, consonants and sibilants). HMMs can be trained supervised or unsupervised. The hypothesis that fatigue might be characterized by a temporal sequence of different patterns and states, further motivates the evaluation of HMM in the thesis of Fuersich (2009). The evaluation of *Bayesian Networks* (BN) in the scope of this thesis is also motivated by the idea to use and model expert knowledge and temporal aspects in the design of the network.

Support Vector Machines (SVM), *Boosting*, *Bootstrap aggregating* ("Bagging") and *Parzen Window estimation* are evaluated for the application of fatigue detection in the thesis of de Mattos Pimenta (2011, Ch. 2.2.1).

Categorical Classification vs. Ordinal Regression

Two goals are pursued in this application: to issue a warning to the driver and to show a bar-graph of the driver's fatigue level. As soon as more than two classes are involved, their *ordinal rank* plays a role. This means that mis-decisions of KSS levels are worse the further they differ. *Categorical* (or *nominal*) classifiers suffer from the problem to sometimes vote for instance for a high probability of *awake* and *drowsy* and a low probability of *acceptable*, which is contradicting for the ordinal classes. Especially in this application, is not acceptable or transparent to show a jumping bargraph or toggle warning states from one instant to the other. Thus, smooth transitions are highly desired. Gutierrez (2016) has shown that it is generally better to take this ordering information into account.

Most of the previously mentioned classifiers perform categorical decisions by default. For a categorical ANN classifier, the last layer has one neuron for each class. The KSS represents a discrete quantization of a continuous-valued quantity. As described in Ch. 3.3.6, the KSS entries can be considered as sample points and missing values in between were interpolated. This represents an *ordinal regression* problem that can be performed by a single neuron in the last layer of an ANN, that retains the ordinality and punishes large deviations (cf. (Costa, 2005; Gutierrez, 2016)). The single neuron represents a linear combination of all weighted inputs (and the bias that is present in every layer). Finally the sub-intervals are mapped to three classes or the bar-graph levels. In the present application, this speaks for classifiers that take rank information into account.

8.2.2. Classifier Training

After selection of the potential classifiers their unknown parameters must be trained by validated features. The heuristic of the classification algorithm consists of estimating good or optimal parameters that minimize the training error. The training of most classifiers is computationally intensive while the classification in online-application is generally much faster. One distinguishes between three kinds of training:

- **Supervised learning** means that the data used for training contain reference labels that define the class membership of a set of feature values. In our application, the class membership of features is defined by the ATTENTION LEVEL, that is represented by the KSS interval scale or the reduced classes *awake*, *acceptable* or *drowsy*.
- **Unsupervised learning** means that no labels are available for the training and the features have to be clustered into natural groups according to some similarity measures. In this thesis, unsupervised learning was only used to identify driver classes in Sec. 5.4 by a clustering analysis (Duda et al., 2001).
- **Reinforcement learning** means that training parameters are updated online in the vehicle based on feedback about the correctness of decisions. This is difficult in this application since there is no reliable way to confirm if a decision was correct and a much higher demand of resources is needed. An conceivable option would be to adjust the sensitivity of hyperparameters of a classifier on-board as false warning if drivers continue to drive after they received a warning. Drivers that make a brake after a long drive without warning and without refueling/recharging could indicate a missing warning. Often, only few different drivers share the same car and, since it was shown in Sec. 5.4 that a small group of drivers can be identified well by their driving style, the reinforced training parameters could be loaded when a driver was identified after some time of driving.

In the training, a trade-off between training error reduction and remaining *generalization* capabilities must be found. *Over-fitting* of the data leads to low training errors, whereas the generalization capability suffers.

8.2.3. Unbalanced A-priori Class Distribution

A-priori information also covers the proportion of time the driver is drowsy and the time drivers are awake. When a classifier is trained, the distribution of the classes is considered. Knowledge of the a-priori ratio is, thus, advantageous. Due to the extensive night studies, the proportion of drives that contain fatigue is much higher in this database than it is expected

in the field. The proportion of time with KSS $\geq$ 8 in the dataset *ALDWvalidND* is 5% and, thus, not very representative. It has to be noted that drowsy driving is usually quite rare, but still much more frequent than crashes occur. The dataset *FieldDrives* (Sec. A.2) based on "free drives" and "Customer Near Driving" (KNFE) in Europe, USA, South Africa and Japan contains regular all-day drives. This dataset can be considered as representative for real traffic in every-day life and here, the proportion of fatigue is only 1.9%. The a-priori distribution of the dataset *FreeDrives* is taken into account by weighting the number of class samples during the creation of the series code.

Vehicle speed, daytime and driving duration are not included in the classifier training as these features suffer from over-fitting of the data, i.e. the night drives are all conducted at about the same time and at a mean speed of 130km/h.

8.2.4. Metrics for Assessment of Classification Results

The assessment of a trained classifier is essential to make meaningful statements about its *generalization* capabilities to classify unknown data or on-board in the vehicle. The classifier-independent assessment of results also allows the comparison of different classifiers.

If the same data were used for the training as for assessment, the training error would be reduced to its minimum, but strong adaption to the training data would lead to *over-fitting*, which does not allow a realistic assessment. To avoid this, the available samples are partitioned into disjunct subsets, the *training*, *validation* and *testing set*. The classifier model is selected and trained by using the training and validation sets and the generalization is tested by the testing set. The estimation error of the validation set is biased since it is used for the model selection while the test set is more representative for the true estimation accuracy as it is not taken into account for the model tuning (e.g. number of hidden layers). Ratios of 80% for training, 10% for validation of the hyper-parameters and 10% for testing of the generalization are used. The more data are used for training, the better the classifier, but the more inaccurate the prediction of the real generalization error becomes.

In the present application, it is of utter importance that *drives* and especially *drivers* of the testing set are unknown during the training set to obtain reliable results. If parts of a drive and especially random samples from the test data are used for training, it will be much easier for the classifier than it will be in practice. Hence, testing data are always selected by *entire drives* and *unknown drivers*.

A proven method for the splitting of data is *cross-validation*. The classification results can then be assessed by a *confusion matrix* and derived measures like *sensitivity*, *specificity*, *recall*, *precision*, *accuracy*, and F_β*-Score*. All principles are used in the following sections.

K-fold and Leave-One-Out Cross-validation

Cross-Validation is a validation technique to assess how the training of a classifier will be generalizable to unknown samples. The data are partitioned into complementary, permuted sets and the training error is averaged over multiple rounds of classification to reduce variability. It is distinguished between the *K-fold* and the *Leave-One-Out Cross-Validation*.

In **K-fold Cross-Validation**, the originally available N samples are randomly segmented into $k \leq N$ preferably equally sized subsets $\mathcal{T}_1, ..., \mathcal{T}_k$. Over $i = 1 \ldots k$ rounds, the subset $\mathcal{T}_i$ is used for testing and the $k-1$ subsets $\{\mathcal{T}_1, ..., \mathcal{T}_k\} \backslash \{\mathcal{T}_i\}$ for training. The total training error is averaged over the k rounds and its variance indicates the stability of the result. The advantage

is that each of the k subsets is used exactly once for validation and $k-1$ times for training purposes. $k = 10$ repetitions are often used in literature. In *stratified* k-fold cross-validation, the folds are selected such that the k subsets have about the same a-priori distributions of class labels to reduce the variance between the different rounds.

The **Leave-One-Out Cross-Validation** is a special case of the K-fold cross-validation with $k = N$. Since stratification is not possible here, the results may be wrong under certain circumstances. Another drawback is the augmented processing time.

In our application, subsets are randomly selected according to the desired a-priori class distribution ratio.

For series-deployment of the algorithm, we suggest to train the clasifier with and without the test set and compare the classifier parameters. If the parameters are not severely different, it can be assumed that the generalization potential is better when all available samples are used for training. The test set contains also valuable information to improve the model. Under most circumstances, using all available data for training will perform better in the field with the drawback that the actual generalization performance is not known exactly.

Confusion Matrix

The *Confusion Matrix* represents the result of a classification, as shown in Tab. 8.1. The columns describe the true reference and the rows show the classification result. The results are converted in % by normalization of all samples in one class. In our application, the distribution of the classes *awake* and *drowsy* can vary, so the assessment of the classification should be made together with the measures like *sensitivity* and *specificity*.

True / Detected	**Alert (N)**	**Drowsy (P)**	**Accuracy**
Alert detected (N)	True Negative (TN)	False Negative (FN)	Negative Predictive Value $NPV = TN/(FN+TN)$
Drowsy detected (P)	False Positive (FP)	True Positive (TP)	Positive Predictive Value $PPV = TP/(TP+FP)$
Total	Specificity $\frac{TN}{TN+FP}$	Sensitivity $\frac{TP}{TP+FN}$	Accuracy $\frac{TP+TN}{TP+TN+FP+FN}$

Table 8.1.: Confusion matrix or contingency table

The *Confusion Matrix* represents the result of a multidimensional classification process as shown, for instance, in Fig. 5.19.

Sensitivity/Recall: or a *True Positive Rate* (TPR) means that all fatigue drivers are warned correctly or get the right ATTENTION LEVEL shown. We can also refer to it as "detection rate" of fatigue drivers. In drowsiness detection, it is important to achieve a high sensitivity value, since it was found out that drivers do accept false warnings, but not missing warnings. It is defined as the probability that a driver was detected to be *awake* under the condition that he was *awake*:

$$\text{Sensitivity} = \text{Recall} = P(Drowsy|Drowsy) \quad or \quad \frac{TP}{TP+FN} \quad [\%]. \tag{8.1}$$

Specificity: or a *True Negative Rate* (TNR) of 100% means that not one awake driver got a wrong warning or, with other words, this is the false alarm rate.

$$\text{Specificity} = P(Awake|Awake) \quad or \quad \frac{TN}{TN+FP} \quad [\%] \tag{8.2}$$

The *False Positive Rate* (FPR) or false alarm rate is defined as:

$$1 - \text{Specificity} = P(Drowsy|Awake) \quad or \quad \frac{FP}{TN+FP} \quad [\%] \tag{8.3}$$

Precision: is also referred to as *positive predictive value* (PPV). On the other hand, precision or positive predictive value is defined as the proportion of true positives against all positive results (both true positives and false positives)

$$\text{Precision} = \frac{TP}{TP+FP} \quad [\%] \tag{8.4}$$

Accuracy: (ACC) is the proportion of true results (both true positives and true negatives) in the entire population. An accuracy of 100% means that all classified values are exactly the same as the reference classes.

$$\text{Accuracy} = \frac{TP+TN}{TP+TN+FP+FN} \quad [\%] \tag{8.5}$$

8.2.5. The F_β Score

F_β-score is a measure for the overall performance of a classifier with a single indicator and defined by

$$F_\beta = (1+\beta^2)(precision \cdot recall)/(\beta^2 \cdot precision + recall), \tag{8.6}$$

where β is a parameter to differently punish precision vs. recall. The F_1-score is a special case:

$$F_1 = 2(precision \cdot recall)/(precision + recall)\ . \tag{8.7}$$

β is adapted according to the desired design goals as illustrated in Fig. 8.5 and $\beta = 1.2$ is used in this context. It is used as a combined measure.

8.3. Warning Strategy Assessment

8.3.1. Conversion of Classification Results into Warning

The characteristic of a warning strategy and concept in the ATTENTION ASSIST is to issue a warning at the onset of fatigue. The driver can acknowledge the warning by pressing the OK steering wheel button. If the drive is continued, the warning will repeatedly be issued again after 15 minutes of driving in a state classified as *drowsy* in order to remind him having a pause. If the warning is not confirmed, it will be assumed that the driver has not seen the warning and will be issued again after 5 minutes. The warning can only be triggered by a corrective event that the driver notices.

Now, for the offline evaluation, we assume that the driver always confirms the warning. To convert the classification result into a warning, the first sample for which the class *drowsy* is classified is set as the first warning. Then, the next warning is issued after at least 15 min, as soon as drowsy is classified again.

8.3.2. Warning Assessment with Temporal Tolerance

Warnings can be assessed for an entire drive or by segmenting drives into time slots of 15 minutes. In the scope of the ATTENTION ASSIST series introduction, the system warnings were assessed according to the definition below. A temporal tolerance was introduced for the assessment of warnings as drivers accept warnings during the phase of their fatigue onset.

An **entire drive** can be evaluated in relation to the *desired warning level* (cf. Ch. 3.3.3) by the following tolerance criteria:

TN	*No warning necessary*	No warning was issued and the maximum KSS < DWL
FN	*Missing warning*	No warning received, but maximum KSS ≥ DWL
TP	*Correctly warned*	Warning received and KSS ≥ DWL-1 during first warning or within 5 min afterwards. (The first correct warning is essential as the driver is supposed to stop the drive then).
TPE	*Warned too early*	Warning received within 5-15 min before KSS ≥ DWL-1
TPL	*Warned too late*	Warning received over 15 min after necessary KSS ≥ DWL
FP	*False alarm*	(otherwise) Warning received while KSS < DWL-1 and at least 15 min before KSS ≥ DWL-1

These modified classification results can be combined as described below. The number of warnings in relation to drowsy intervals or first warnings:

$$\text{TPR} = \frac{\text{TP+TPE}}{\text{TP + TPE + TPL + FN}} \tag{8.8}$$

Everyone, who did not get a warning in time vs. everyone, who needed a warning:

$$\text{Missing Warning Rate} = \frac{\text{FN+TPL}}{\text{TP + TPE + TPL + FN}} \tag{8.9}$$

Everyone who got a warning much too early or if no warning was necessary in relation to everyone who was awake

$$\text{False Alarm Rate} = \frac{\text{FP}}{\text{FP + TN}} \,. \tag{8.10}$$

The correct decisions in total vs. all outcomes is then:

$$\text{Correct Total} = \frac{\text{TP + TPE + TN}}{\text{TP + TPE + TPL + FP + FN + TN}} \tag{8.11}$$

15 min time slots: This principle can now be evaluated for all 15 minute time slots. In this concept, we will categorize a warning again as wrong, if it is issued in a period, in which the driver is awake for at least 15 minutes before and after, even if fatigue has been involved during the beginning of the drive. Tab. 8.2 shows this criteria for a selection of features. At first, only one feature is used for classification as this is the main evaluation method used to develop the ATTENTION ASSIST. The improved ATTENTION ASSIST feature performs better for this criteria, however, it was not allowed to be published.

	1st warning					15 min interval				
Feature	**TPR**	**PPV**	**FPR**	**ACC**	F_β	**TPR**	**PPV**	**FPR**	**ACC**	F_β
STWZCR	95%	28%	83%	36%	48%	45%	43%	16%	76%	44%
LRVFAST	70%	37%	56%	52%	51%	22%	42%	7%	81%	28%
STWVELZCR	77%	31%	63%	47%	48%	30%	40%	10%	79%	34%
LRVVERYFAST	79%	33%	70%	44%	51%	26%	39%	9%	80%	30%
LNCHGVEL	96%	26%	88%	33%	46%	42%	41%	17%	75%	42%
MICROCORRECTIONSW	81%	33%	59%	51%	50%	29%	42%	9%	80%	34%
STWEVENT	67%	45%	38%	64%	56%	25%	49%	6%	83%	31%
TURNINDDUR	96%	27%	85%	34%	46%	41%	42%	14%	77%	41%
DEGOINT	93%	29%	83%	38%	49%	35%	40%	13%	78%	37%
DYNDRIVINGSTYLE	97%	25%	88%	32%	45%	47%	42%	18%	74%	45%
REACTIM	91%	28%	85%	35%	47%	34%	38%	13%	77%	36%
LRVPERCHIGH	94%	27%	85%	35%	47%	42%	40%	16%	75%	41%
LATPOSZCR	79%	34%	62%	50%	52%	21%	40%	7%	81%	26%
DELTALATVELMAX	89%	33%	78%	42%	52%	32%	42%	10%	79%	35%
ZIGZAGS	86%	36%	70%	47%	55%	30%	44%	9%	80%	35%
ELLIPSE	94%	27%	85%	34%	46%	46%	43%	17%	75%	45%
DELTADUR	97%	25%	88%	32%	45%	47%	42%	18%	74%	45%
VIBPROP	68%	35%	58%	50%	49%	23%	43%	7%	81%	29%
LNERRSQ	99%	29%	87%	36%	50%	47%	44%	16%	76%	46%
TURNINDADVANCE	97%	25%	89%	31%	45%	47%	43%	18%	75%	45%
LNMNSQ	96%	27%	87%	34%	47%	41%	42%	15%	77%	41%
LANEX	99%	29%	87%	36%	50%	47%	44%	16%	76%	46%
LATMEAN	92%	30%	82%	39%	50%	41%	46%	13%	78%	43%
LANEAPPROX	79%	32%	70%	44%	50%	29%	43%	9%	80%	34%
LANEAPPROXAD	83%	39%	62%	52%	57%	25%	46%	7%	81%	31%
LANEAPPROXADAPT	83%	34%	65%	49%	52%	26%	41%	8%	80%	30%
DELTALATPOS	81%	34%	70%	46%	52%	31%	46%	8%	81%	36%
LANEDEVSQ	66%	36%	58%	50%	49%	19%	44%	5%	82%	25%
NMRHOLD	73%	37%	50%	57%	52%	29%	51%	6%	82%	35%
LANEDEV	85%	32%	76%	42%	51%	35%	45%	10%	79%	39%
ORA	96%	28%	87%	34%	48%	45%	44%	16%	76%	45%
LNIQR	93%	31%	80%	40%	51%	36%	44%	11%	79%	39%

Table 8.2.: Warning assessment of single feature classification results (without a-priori features), for which F_β is maximal for $\beta = 1.2$. All features are baselined by *max* of the first active 1 to 20 min.

8.3.3. False Alarms by Driving Duration

Up to this point, we have not considered that the warning acceptance is much higher at night, in monotonous situations and after several hours of driving. Our studies show that drivers accept false warnings, but not missing warnings. However, a major concern is that drivers get "spammed" by too many false alarms. Our study shows also that drivers accept wrong warnings after longer driving duration more than warnings at the beginning of a drive. For this reason, Fig. 8.3 shows the false alarm rate by driving duration. Within 2h of driving, there are still under 1.4% false alarms.

8.4. Feature Dimension Reduction

Theoretically, the more uncorrelated the features are to fatigue, the better the classification. But if the number of features gets too high, the need of more training data cannot be fulfilled any more due to the *Curse-of-Dimensionality* problem. For instance, if 10^2 samples are enough to accurately describe the distribution of an one-dimensional random number, 10^{20} observations will be needed to obtain the same accuracy level in 10-dimensional space.

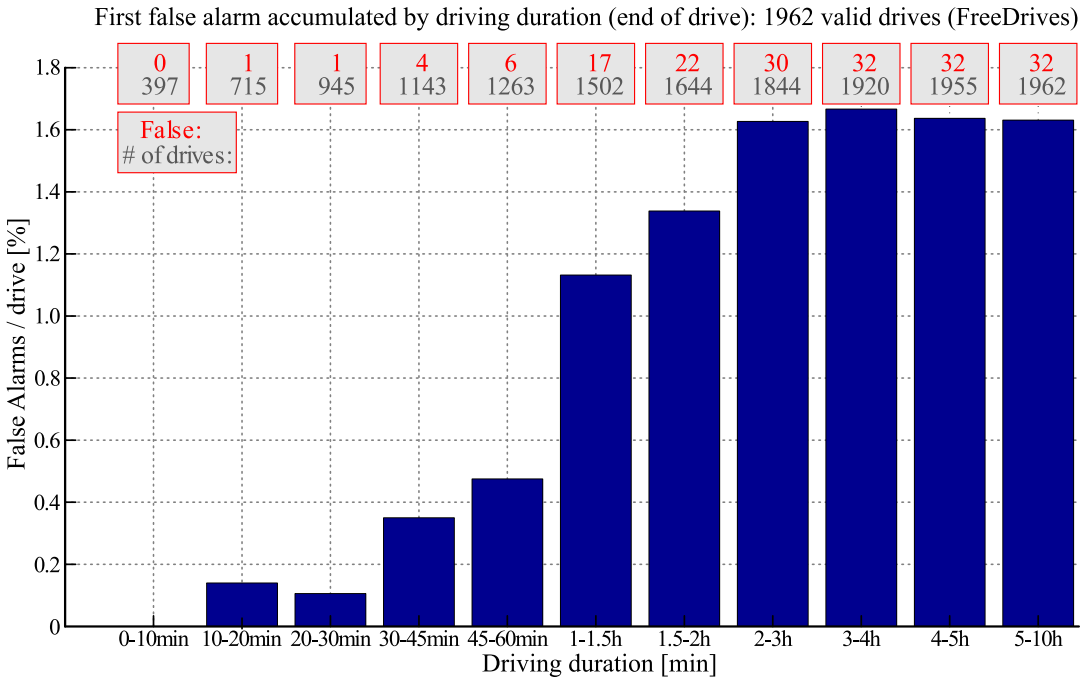

Figure 8.3.: False-alarms accumulated by driving duration.

The curse of dimensionality can be tackled by the reduction of feature dimension or selection techniques that focus on the most relevant features. For this reason, dimension reduction techniques are applied. *Principal Component Analysis* (PCA) and *Fisher transform* (LDA) are methods to transform a given feature space to a lower dimensional one (Duda et al., 2001).

The *Sequential Floating Forward Selection* (SFFS) algorithm was first introduced by Pudil et al. (1994a,b). In the forward step, SFFS sequentially adds the most significant new feature to the set until a given number of features is reached. In order to avoid going straight to a local optimum, conditional exclusion steps (backward steps) are repeated until an improvement of the performance is achieved or the performance starts to decrease. It is assumed that a new added feature can contain redundant information that is already inside the selected subset. This way, redundancy can be reduced while not loosing too much discrimination performance.

PCA does not yield any useful results, since the precondition that the variance of the signal is larger than of noise, is not fulfilled. Also LDA has shown poor results compared to the SFFS. The advantage of SFFS is its high transparency as the selected features remain unchanged and only these features need to be extracted. SFFS is applied here to select the most promising features for a classifier.

Tab. 3.9 shows the frequently selected EYE features from the SFFS selection of the features listed in Tab. 4.2.

A statistic is made of how often features are selected after repeated runs of the non-deterministic SFFS. It was often observed that related features were selected during different iterations (e.g. LANEAPPROX and LANEAPPROXADAPT). Thus, we can assume that such features can be used interchangeably and all features of a family would not provide any performance gain.

For this reason, only the best feature out of its family is used, the one that was selected most often. Tab. 8.3 lists a statistic of the most frequently selected features after 30 SFFS repetitions in combination with the Bayes classifier. It can be seen that correlation coefficients of individual features are not necessarily related to the performance of the features in combination.

ID	Feature Name	Selections	ρ_p	ρ_s
45	CIRCADIAN	30	0.49	0.51
43	TOT	30	0.26	0.27
22	DEGOINT	30	-0.19	-0.22
29	LNMNSQ	30	-0.03	0.01
51	STWEVNT	29	0.16	0.17
52	STV25	29	-0.30	-0.34
54	STV75	29	-0.32	-0.36
38	DELTALATPOS	19	0.14	0.13
39	DELTALATVELMAX	18	0.11	0.11
17	ZIGZAGS	17	0.12	0.10
34	ORA	14	0.09	0.08
40	LANEAPPROXADP	14	0.02	0.01
53	STV50	14	-0.27	-0.32
33	LNERRSQ	13	0.05	0.10
35	TLC1MIN	11	0.18	0.18
30	LNIQR	9	0.09	0.09
14	LANEAPPROX	6	0.14	0.15
19	LATMEAN	5	-0.10	-0.11
36	VIBPROP	5	0.08	0.08
26	TRFCDENS	4	-0.33	-0.40
31	LNCHGVEL	3	-0.12	-0.20

Table 8.3.: Correlation coefficients of frequently selected features

8.5. Classification Results

For classification, features in the matrix **F** from Sec. 4.2.1 are cleared for NaN and ∞ values and filtered for time instants, for which SAS_{CAN} and SAS_{LANE} are active. F is downsampled to $F_s = 0.5\,Hz$ to speed up processing time, based on the assumptions from Ch. 4 that fatigue changes slowly. All features are used with baselining from Sec. 5.4.1.

Different classifiers, such as k-nearest neighbor, linear discriminant analysis (LDA), Bayes classifier, Gaussian mixture models (GMM), support vector machines (SVM) and artificial neural networks (ANN). Results are obtained by cross-validation with a training, valdation and test set ratio of 80:10:10 percent for ANN and 80 to 20 percent for all others. The results were averaged over ten permutations of the training/testing set to obtain a more stable result.

Since the classification does not take into account the signal history (except HMM), the classification result is smoothed based on a majority decision towards adjacent classification results. A majority weighting is applied by a median filter using the $N = 7$ adjacent values to obtain a more stable result. Details can be found in the thesis of de Mattos Pimenta (2011).

A comparison of test errors for different classifiers is given in Tab. 8.4. The best results are achieved with the best 11 features that have been selected by SFFS in combination with the Bayes classifier.

Classifier	**Test Error [%]**	AUC
***k*-NN (*k*=5)**	44.0	
GMM (3. Modes)	43.3	
Linear discriminant	32.4	
Bayes classifier + SFFS	36.6	
SVM ($C = 2^{-2}, \gamma = 2^{-7}$, RBF kernel)	27.9	0.76539
ANN	16.6	

Table 8.4.: Test error for three fatigue classes with a training/testing ratio 80:20 (80:10:10 for ANN) and 10-fold cross-validation

Tab. 8.5 presents the confusion matrix for Bayes with a full covariance matrix and GMM with two Gaussian mixture modes. GMM performs better in predicting fatigue, however, with more false alarms.

		Correct		
		Awake	Acceptable	Drowsy
Estimated Bayes	Awake	63.2 %	25.9 %	3.7%
	Acceptable	32.1%	62.8 %	62.1 % %
	Drowsy	4.7 %	11.3 %	34.2 %
Estimated GMM	Awake	64.4 %	34.5 %	6.1 %
	Acceptable	27.8 %	47.8 %	51.6 % %
	Drowsy	7.8 %	17.7 %	42.3 %

Table 8.5.: Confusion matrix for Bayes with full covariance matrix and GMM with three modes

8.5.1. Neural Network Classification Results

The best results are obtained by a neural network with the interpolated KSS, as it allows the modeling of more complex structures. The detailed confusion matrix in Tab. 8.6 stems from a feed-forward neural network with three hidden layers, each with 30 neurons trained by backpropagation.

		Correct KSS								
		1	2	3	4	5	6	7	8	9
Estimated KSS	1	0.0	0.0	0.0	0.0	0.0	0.0	0.0	0.0	0.0
	2	100.0	61.3	0.1	0.0	0.0	0.0	0.0	0.0	0.0
	3	0.0	38.7	75.6	2.1	0.0	0.0	0.0	0.0	0.0
	4	0.0	0.0	20.2	90.6	5.4	0.1	0.0	0.0	0.0
	5	0.0	0.0	3.7	7.3	90.8	5.6	0.6	0.6	0.6
	6	0.0	0.0	0.4	0.0	3.8	91.4	6.8	2.4	0.6
	7	0.0	0.0	0.0	0.0	0.0	2.8	91.3	28.5	7.2
	8	0.0	0.0	0.0	0.0	0.0	0.0	1.4	68.4	46.1
	9	0.0	0.0	0.0	0.0	0.0	0.0	0.0	0.0	45.6

Table 8.6.: Confusion matrix for ANN classification results in percent

Application of the ANN with the same parameters to the classes *awake* and *drowsy* (including *acceptable*) yields:

	Awake	Drowsy
Awake	96.4 %	10.7 %
Drowsy	3.6 %	89.3 %

Fig. 8.4 shows a scatter plot with regression line of the classification result compared to the true KSS. The classification result for every KSS level has a scatter of ±1 level. It can be seen that the KSS level 9 is sometimes mixed up with more awake classes. It is interesting to see that at KSS level three, almost every KSS level is estimated by the ANN. A plausible reason for this is, that drives with missing KSS entries are filled with the default KSS level three during the plausibility check without really knowing the real driver state. It shows that the ANN is able to interpolate missing KSS values better than using default values.

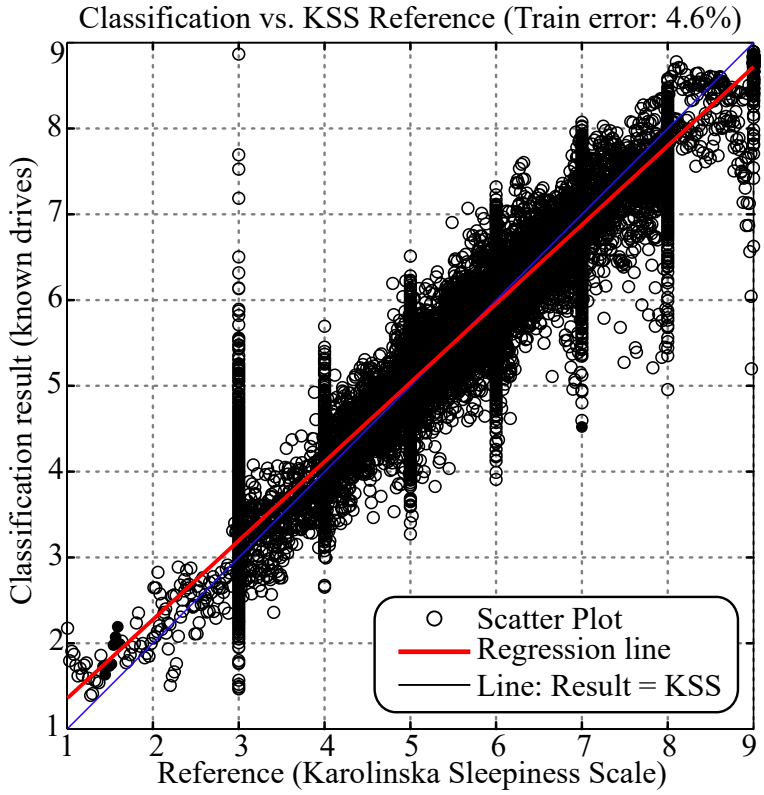

Figure 8.4.: Scatter plot and regression line of ANN classification results plotted against and trained by the nine interpolated KSS levels

Fig. 8.5 shows the ROC curves of different feature groups and classifier combinations. The selection of the best lane and steering features (blue) classified by the Bayes classifier perform better than the single feature `STVEVENT` from the (black). The baselined ATTENTION ASSIST series feature `GGGLWF` (black) that includes the time-on-task `TOT` and `CIRCADIAN` just reaches the target area specified by the project. The causal (blue) features set in combination with `TOT` and `CIRCADIAN` perform about 6% better in the target area and much better for high detection rates at the cost of unacceptable false alarms. The combination of causal features (blue) and the improved steering event rate `STVEVENT` yield the best results. For

the ANN result, only the point with the minimum test error was available and was included for comparison. It shows by far the best results inside the specified project target, however at a much lower false alarm rate.

It can be seen, that the ANN lies much better in the target area than the other methods.

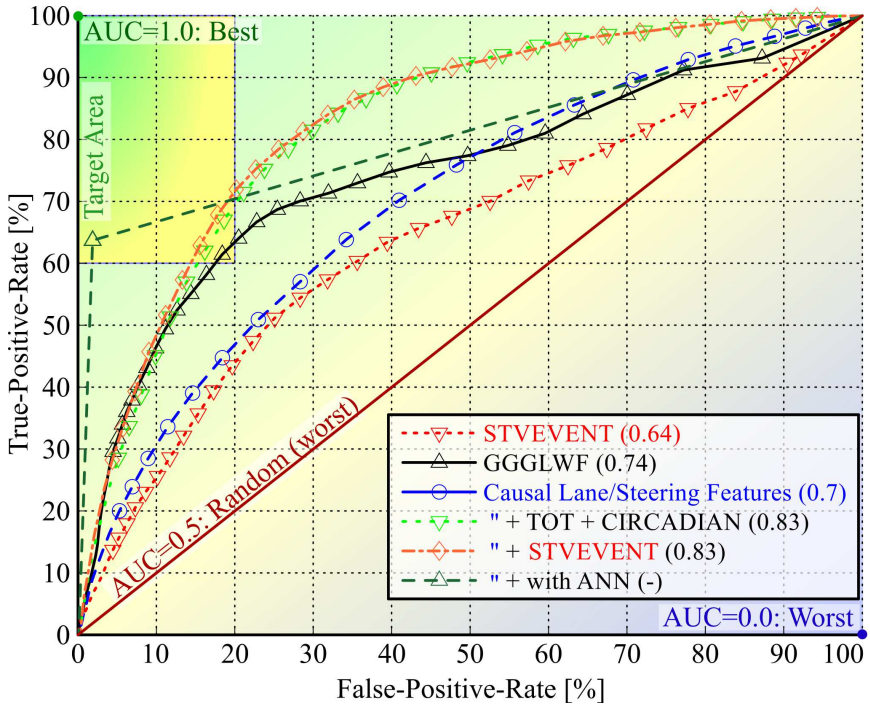

Figure 8.5.: Comparison of ROC curves of different feature groups

8.6. Deep Learning

Deep Learning (DL) is a subset of *Machine Learning* (ML) that has grown exponentially within the last decade (Goodfellow et al., 2017). For instance, *Convolutional Neural Networks* (CNN) (Patterson and Gibson, 2017) reached a brakethrough in image segmentation (Krizhevsky et al., 2012). Natural language processing (NLP) or hand writing recognition often times surpass the level of human accuracy with *Recurrent Neural Networks* (RNN) or more specifically *Long Short-Term Memory* (LSTM) networks. In contrast to traditional machine learning, *Deep Neural Networks* (DNN) can learn from raw signals and laborious manual feature engineering is not required, however traded in by higher computational demands. Tab. 8.7 shows a comparison between conventional ML and DL.

Conventional *Machine Learning* (ML)	***Deep Learning* (DL)**
+ Fast training of models	− Expensive training
+ Good performance with small amount of data	− Vast amount of data required
− Manual feature engineering	+ Learns features and network parameters automatically

Table 8.7.: Comparison between traditional Machine Learning (ML) and Deep Learning (DL)

In CNNs, feature extraction can be represented through convolution with trained kernels moving with a given step size (stride) over the raw input signals. The convolution takes place in the neurons of convolutional layers that can represent any type of spatial or temporal filter to smooth, differentiate, integrate or match patterns. The network structures can consist of a few or up to over hundred cascaded layers (e.g. VGG, ResNet). As *activation functions* of neurons, sigmoidal functions can limit large values. The *ReLU* function (simplified diode equation) became very popular, since it significantly speeds up the learning rate (gradient descent) and non-linearity is introduced. One or several convolutional layers are generally followed by *pooling* to condense information to save computational cost and reduce overfitting. *Average* or *max pooling* are commonly used, since the largest value represents the highest activation. The last layers generally consist of classical neurons (often dense, i.e. fully connected) that represent the classification and use the output of convolutional neurons as features. In case of a classification problem, the final *softmax* normalization converts the outputs to probabilities in order to make a decision.

For time-series applications, RNNs are frequently used, where neurons additionally have a feedback memory that can learn sequential information (Patterson and Gibson, 2017). However, RNNs particularly suffer from numerical problems during training ("vanishing/exploding gradient problem"). LSTM networks (introduced by Hochreiter (1991) respectively Hochreiter and Schmidhuber (1997)) do not suffer from this problem and appeared most appropriate in the present application in conjunction with convolutional elements.

For some applications (e.g. WaveNet (Oord et al., 2016)), a CNN with a large enough receptive field (i.e. the kernel size) can successfully be used instead of an RNN, with other words: a purely feed-forward filter (FIR) instead of a recursive filter (IIR).

For training of DNNs, the *back propagation* algorithm is used in analogy to traditional ANNs. In order to reduce the computational complexity for large networks and amounts of data, the processing of *batches* allows to use only representative subsets of the data for training.

8.6.1. Application of Deep Learning to CAN-Signals

Firstly, the simplest approach to use DL to solve the present problem is to use DNNs on the manually designed features. Using improved algorithms allows to use more features concurrently and suffers less from the curse-of-dimensionality problem. This is an alternative for dimension reduction with SFFS or PCA. Recursive (such as RNN and LSTM) or convolutional network structure in conjunction with pooling aggregation, dropout and processing of batches allow to train with a sequence of features. A DNN can be used for *ordinal regression* (cf. Ch. 8.2.1) and exploits the rank information of interpolated KSS levels (cf. Ch. 3.3.6), which generally improves the performance (Costa, 2005; Gutierrez, 2016). However, information that is lost during the feature extraction cannot be recovered and poses limitations to the achievable accuracy.

Concepts for Automatic Feature Extraction: As mentioned in Sec. 8.1, an *end-to-end* DNN can automatically learn features from raw data. Principally, a DNN is able to model all signal processing steps of traditional feature engineering such as smoothing, differentiation, pattern matching etc. Structures and parameters are learned automatically at the cost of computational complexity. Reducing the computational inference cost (i.e. the network complexity) is still a manual process. No literature on using DL on CAN-signals was found that would have been useful for this application.

CNNs have shown their strength in detecting patterns in 2D images, but lately also in 1D time-series applications (e.g. ConvLSTM, ALSTM-FCN, cf. (Cui, 2016; Gehring, 2017; Karim et al., 2018; Janos, 2018)). LSTMs have shown their strength in long time-span sequence applications, especially for high sampling rates where temporal CNNs would require to store a huge amount of the input data.

In the previous chapters, we found that the causal information about fatigue is expected to be in events and sliding windows in the steering and lane signals mostly. For instance, in order to detect steering patterns that usually take up to five seconds, a temporal convolution can be performed on the steering velocity. For the inference of a CNN, this requires to store 250 samples of the input sequence. However, the event itself does not yet correlate with fatigue and their *frequency* over a time-span over at least 20 min is required. The same temporal convolution would be able to find lane-based patterns such as zig-zag events, lane deviation or approximations. For lane data, the time-spans are even higher and last up to one hour (180k samples per signal). The detection of single events is possible with a CNN, but especially for the inference, the memory demand for a large perceptive field to retain event rate information cannot be met. For such long time-spans, LSTM structures are much more promising.

Recent publications (Shi, 2015; Cui, 2016; Wang et al., 2016; Karim et al., 2018) show, that a combination of convolutional and recurrent/LSTM networks can outperform solitary structures. Thus, the most promising approach would be a combination of CNN layers, followed by LSTM layers for the stage of feature extraction.

As input, the steering wheel angle velocity, absolute lateral lane position and width, vertical and lateral acceleration, accelerator pedal position and wheel rotation speed are suggested to be used. To remove useless noise, it is proposed to use the DISPO filter for smoothing and differentiation, suggested in Ch. 4.1.1. Inputs shall be standardized to zero-mean and unit-variance.

Patterns that are induced by external events, such as lane-camera inactivity, lane changes, overtaking, cross-wind, road warping, curves, construction sites etc. are not related to fatigue. These useless patterns that stem from such situations can be muted by removing samples when the *system-active-signal* is passive (cf. Ch. 4.1.3).

Dense layers take over the classification of these features and the last neuron of the DNN shall be an ordinal regression neuron. As target reference, the interpolated nine level KSS entries are most suitable for the regression. The predicted classes finally have to be mapped to the bar-graph levels or the warning strategy. Finally, tuning the network structure and hyper-parameters is one of the most challenging tasks. *AutoML* approaches gained high popularity and can perform *Neural Architecture Search (NAS)* (Hutter et al., 2019) where the structure of the network and involved parameters can be searched according to predefined strategies and restrictions, however at the cost of additional complexity.

Challenges: As already argued in Ch. 4, due to on-board inference cost and intransparency, DNNs are not the first choice for deployment on automotive ECUs. For off-board training, processing of big data and GPU in liaison with cluster/cloud computing would be necessary and were not available for this thesis.

A-priori factors such as *daytime*, *time-on-task*, *vehicle speed*, *curvature monotony* and *light* shall also be included. These signals need no pre-processing to directly correlate with fatigue. As a consequence of the very unbalanced class distribution, classifiers strongly tend to detect night experiment situations in which fatigue is much more prevalent than in real road

drives. These driving situations are not causal indicators for fatigue. Based on the a-priori distribution of free drives, random oversampling the minority (sleepy) or undersampling the majority (awake) is a common approach (e.g. *Synthetic minority Over-sampling TEchnique* (SMOTE) using *k*-NN). This would either loose information or blow up the amount of training data by magnitudes. At the other hand, continuous-valued external factors such as speed, traffic density, curvature and road condition have a strong influence on features as shown in Ch. 5.2. Features need to be independent of these factors. It appears challenging to design a DNN that is able to distinguish between normalization and taking the a-priori distribution of free drives into account. When removing samples to mute events, the timing and event rate information is lost and cannot be learned by the classifier any more. The reaction time to external events, such as the steering correction after road bumps is also no longer contained in the inputs. Adaption to new vehicles types and different countries is a major issue and only works if all dozens relevant vehicle variants were available prior to production to record training data, e.g. for transfer learning.

Another challenge is certainly the adaption to the driver in analogy to baselining. In order to adapt to individual driving styles, the result of the feature extraction layers from the beginning of the drive would have to be stored, aggregated by max pooling (in analogy to max baselining) and later fed into the decision stage of the network.

Due to the large spectrum of external factors and driver types that overlay the weak fatigue patterns, a lot more data and situations would be required to train a DNN. This could only be achieved by the oncoming over-the-air (OTA) infrastructure where sensor signals are permanently preprocessed on-board and transferred to the back-end. For supervised learning, a ground truth reference is mandatory. Using real field data may fill the lack of data and solve the unknown a-priori distribution problems, however will raise an even bigger problem: customers will not estimate their fatigue level every few minutes nor will they wear EEG/EOG electrodes. Transfer of driver-camera video data for offline labeling would require a driver camera and is not possible over 4G (LTE+) or even 5G since the produced traffic would be way too expensive. Centrally storing driver videos would also be very critical for data protection and crash liability reasons. If a camera would be available, it would make more sense to investigate eye-tracking based approaches.

Reinforced learning would require to interpret the reaction to warnings as reference, as described in *reinforcement learning* in Ch. 8.2.2. However, this is even much less reliable than the KSS and lacks temporal resolution and fatigue levels. An option would be to incentivize customers to rate their warnings and thereby "entertain" them with an experiencable car that is self-learning.

8.6.2. Application of Deep Learning to Driver Camera

Especially eye-tracking camera-based driver state classification can potentially profit from DL. Parkhi et al. (2015); Mukherjee and Robertson (2015) and Han et al. (2018) have confirmed, that classification with multiple stages work best for eye-blinking detection. At first, the face is detected in consecutive driver-video images by a CNN. After initialization, the search region-of-interest (ROI) can be reduced by tracking. As face model reference, existing databases can be used or manually labeled for this stage. Face models of known drivers can be stored to accelerate initialization.

In the second stage, the eyes, pupils and eye-blinks can be detected in the again narrowed down, but higher-resolutional ROI. The EOG signals from Ch. 3.4 can be used as reference for eye-blinks in this stage.

In the last fatigue classification stage, an RNN or LSTM can be used for deriving the sleepiness level from the eye-blinks. As shown in Ch. 3.6.11, a video frame rate of at least 100 fps is required to reliably detect eye-opening and -closure speed. As reference, the KSS entered by the driver can again be used. Video recordings even allow a majority voting of experts, which is actually considered to be the most accurate method (cf. Ch. 3.3.1). By training these stages independently, the eye-blink signal is free from influences in the video image that could lead to over-fitting to the training data. For instance, a full end-to-end approach that works on the raw data could exploit that fatigue is more prevalent during night experiments, i.e. low light conditions. Fatigue also occurs most often during low traffic, which results in fewer shoulder checks, i.e. horizontal head rotations. However, these relationships are only valid for the training data with artificial night experiments and no causal indicators for fatigue during real road drives. It is desired to be independent of such situation based a-priori factors, since the amount of fatigue during night and day or traffic density is unknown. Training an end-to-end CNN for facial expressions (e.g. yawning or head-nodding) is an additional option.

8.6.3. Conclusion on Deep Learning for Fatigue Detection

Even if DL is superior in many applications, the fatigue patterns are quite weak and obscured by other factors in the CAN data. In summary, straightforward deployment of a DNN will be inferior to the ML approach in which expert knowledge is explicitly modeled during feature engineering.

In comparison, DL approaches based on driver-camera are expected to be most feasible and promising. The gained features are causal and can be mostly independent from the a-priori distribution or external influences. The missing ground truth problem also remains here. However, for this thesis, the amount of representative state-of-the-art camera-data with high frame-rate and with KSS reference were not available. The focus was explicitly on using CAN-signals, since there was no camera on the market that was ready for production.

Chapter 9.

Conclusion

9.1. Summary

Fig. 9.1 shows a "graphical abstract" of the entire system and development process.

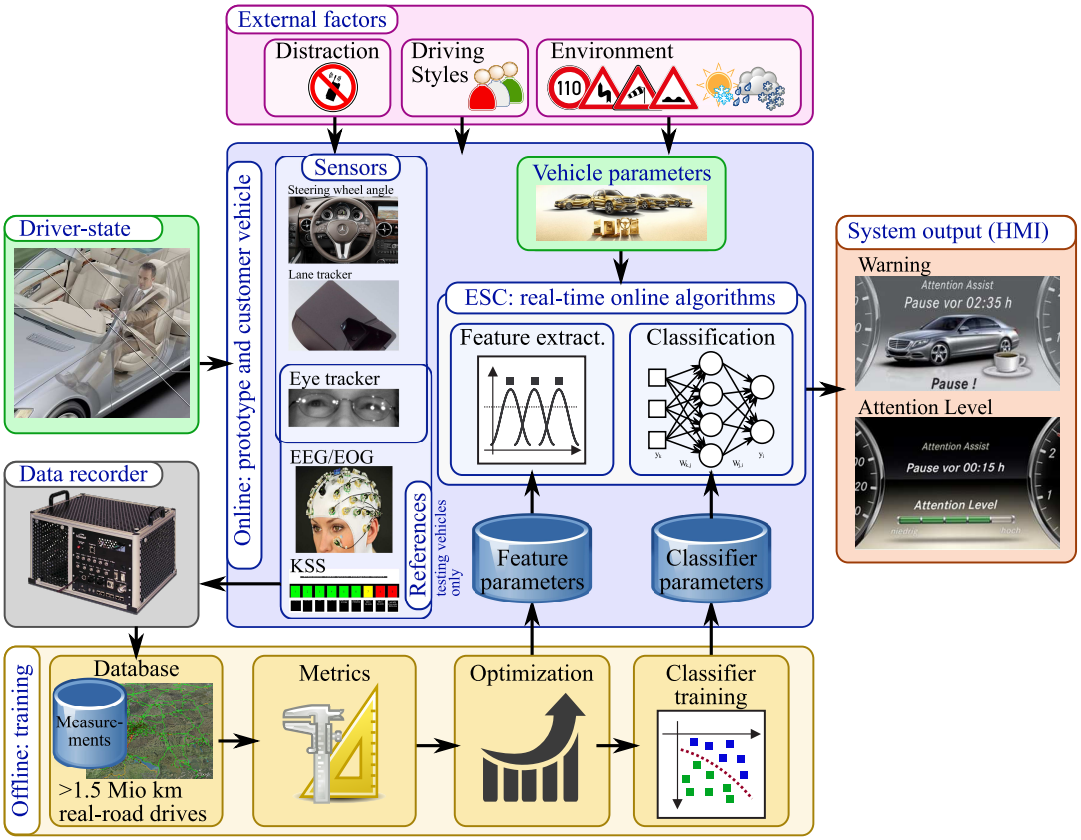

Figure 9.1.: Visual abstract: overview of the entire system

Pursuing the goal of developing an assistance system, to detect the driver sleepiness state, many steps were necessary that have been refined over many iterations.

Starting with only one feature that detects steering corrections by a driver adaptive threshold, it soon became clear that more effort is needed to reliably detect driver fatigue.

A major restriction during the optimization of the system was the lack of a reliable "ground-truth" reference. For this reason, EEG, EOG and camera-based features were evaluated. Although the results in literature are often reported to be very good, the use of real-road drives did not show satisfying results. Direct camera-based blinking features have shown the most promising results. However, a camera system was not yet available at that time that was robust enough to cope with realistic driving conditions. Further, a large amount of data were only recorded by using the KSS reference. For this reason, the KSS was found to be the most practical reference. Numerous features were analyzed regarding their correlation with the KSS drowsiness reference. Many of them correlated relatively well, especially a-priori features, such as time of day, time-on-task, monotony and traffic density. However, a-priori features need to be treated carefully as they are not sensitive to the real driver condition.

For the series introduction of the ATTENTION ASSIST 2.0 with the ATTENTION LEVEL, a bar graph was implemented based on several features with continuous output. An extensive night study with a real-time implementation of the ATTENTION LEVEL was conducted to verify its acceptance. Plausible levels were shown most of the time, but it was observed that a system active / passive detection was introduced which indicates to the driver, whether the system is passive and unable to detect the ATTENTION LEVEL.

The lane based features have shown results comparable to the steering based features. An important requirement of our application, however, is to use sensors from series equipment instead of using a special equipment lane-tracking camera, that is not available for the majority of vehicles in the field. For this reason, the idea was to estimate the same lane-based features from inertial sensors and vehicle tracking. Not with the same, but still good accuracy, some lane-based patterns could be used in this way.

In the last iteration, another major impact on features was addressed, the influence of undesired factors like external influences and inter-individual driving styles. Especially under real world conditions, the suppression of external influences and adaption to the driver is very important. It was observed that there are different types of drivers, those who accurately keep the lane by lots of steering corrections and those who do not hastily correct the lateral position and have a rather loose lane keeping. Specific measurements have been recorded to quantify and compensate for their effects as good as possible.

Based on the extracted features and a feature selection step, different classifiers have been compared. In general, lane based features were often selected in combination with steering based features, as they provided complementary information. Neural networks, LDA and the Bayes classifier, in combination with SFFS feature selection, performed best for the difficult features. Especially neural networks have shown to enhance the system performance. But even with a large set of new and improved steering and lane based features, the classification performance was not as good as the results reported in literature, using a smaller amount of data from a simulator or using drives under testing conditions.

9.2. Future Work and Outlook

An optimally operating fatigue detection system can only be developed by jointly taking all the factors mentioned in this thesis into account. Investigation on the following approaches could further improve the results:

- Installation of a steering wheel *torque* sensor in order to measure reaction times, as described in Ch. 4.4.12

- Merging EEG, eye-signals (e.g PERCLOS (Batista, 2007)) and a distraction measure in addition to the KSS for a better temporal resolution of the reference
- Further analyze multi-level classification to use driving style specific features
- Further investigate Hidden Markov-Models and Bayes networks to model temporal aspects and expert knowledge
- Derive driver-model control system parameters, as described in Ch. 4.4.16
- Using unsupervised learning to incorporate the driver reaction, whether he is following the proposed warning or not, to update classification sensitivity
- Applying more extensive parameter optimization, not only of single features but with the classification performance of selected features as cost function
- Investigate Deep Learning methods and its ability to learn features automatically from source signals. Convolutional and recurrent/LSTM neural network structures appeared to be most appropriate.
- Using existing over-the-air and cloud infrastructure for reinforcement off-board learning and adaption to known drivers, environments and vehicle properties.

Driving in a driving simulator and under supervised conditions has a big influence on the driver's behavior. It was observed that many awake drivers will also drive sloppy, if the motorway is empty or if they are distracted by talking or other actions. The driving behavior in these situations is the same as for drowsiness and, thus, cannot be distinguished. For this reason, a good strategy would be to provide feedback to the driver about his/her objective driving performance over the ATTENTION LEVEL bargraph. In the actual system, only one feature is used instead of the ANN result in Ch. 8.5.1. Usually, drivers tend to drive more aware, if they get a feedback on their driving performance.

The temporal unavailability of the lane-tracking has already been considered during the feature extraction. The block diagram in Ch. **??** shows how to cope with the case that lane data are temporarily unavailable due to bad vision, mis-calibration, missing lane markings or in case the ALDW is not installed or damaged. If the *LaneDataQual* indicate unavailability, the training parameters and classification input features should be switched.

In the big picture, after decades of research, one has to accept that the driving parameters contain only a limited information about the driver state and by magnitudes lower than other external influences. Indirect fatigue monitoring through driving parameters will still be relevant for at least two decades as manual driving will still play a role until 2040 even in level 5 driverless vehicles and vehicles in lower segments.

In any case, **camera-based** eye blinking detection was shown in this thesis to be most suitable as a reference and for on-board implementation in series application. Especially under the viewpoint of a future autonomous driving, a driver camera allows not only direct driver state estimation by eye-tracking, but also a broad variety of other applications such as driver distraction detection ("'eyes-on-road"'), driver identification, driver vitality (heart rate), gesture, emotion and facial expression detection. This direct method also works for automated driving and is less affected by external influences and driving styles. For partial automated driving it must be assured that drivers remain alert to hand the operation over to the driver in situations the car can't handle. The driver camera has further benefits such as drivers can also be identified to continuously learn their driving style. The latest over-the-air and cloud computing infrastructure are enablers with the highest potential for improved performance. ADAS warning thresholds can be lowered if the driver's eyes do not point towards a braking vehicle.

Appendix A.

Appendix:

A.1. Proving ground Papenburg and Idiada

Fig. A.1 shows a map of the commonly used proving grounds Papenburg and Idiada. The longest oval course has a length of 12 km.

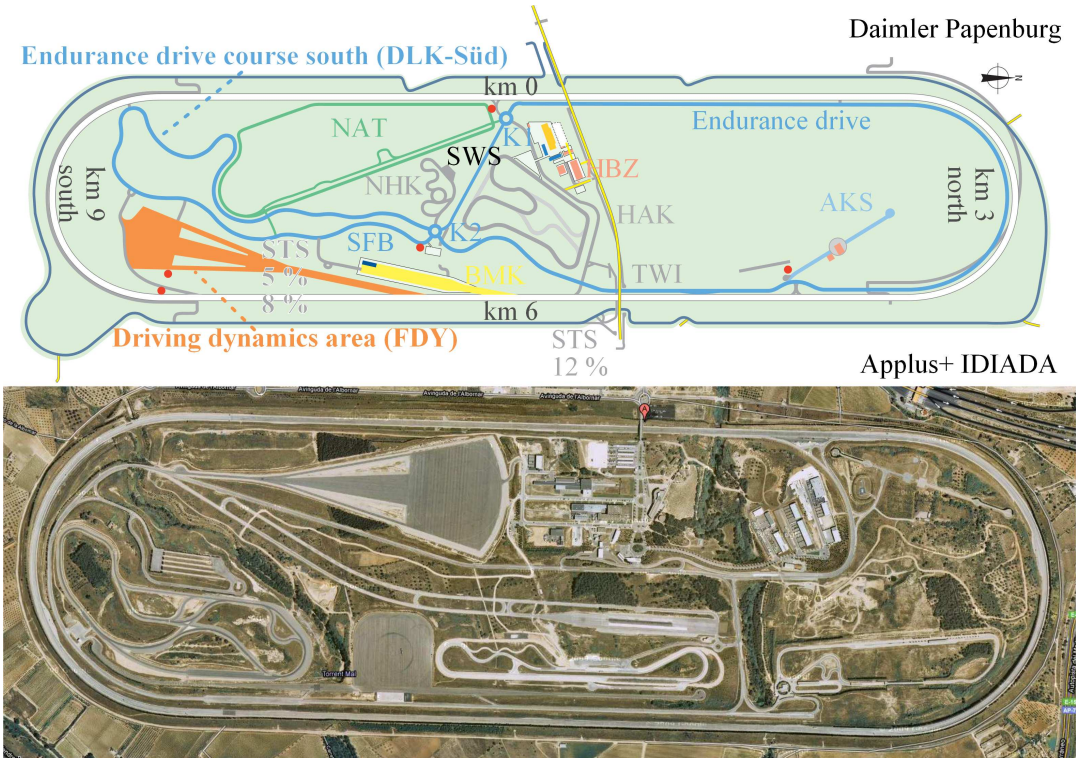

Figure A.1.: Proving ground Papenburg (above) and Idiada (below). (Sources: (ATP Papenburg, 2012) and (Idiada, 2012))

A.2. Datasets

Different *datasets* were defined that were dedicated to specific evaluations. These datasets are criteria to select drives with certain patterns implemented as SQL queries. The resulting fixed set of drives serves to compare the results. Using a smaller data set speeds up the

simulations. The results can then be refined and validated on a larger or full dataset. The most important datasets used in this thesis are described in the following section.

For faster processing, the dataset *ALDWvalidND* was a smaller set of drives that contained a large portion of fatigue. It excluded all free and KNFE drives in which fatigue was rare and the driving situations varied too much. After filtering the full database, 82 269km of real drives with 781 hours remained:

- 323 drives (141 night drives; 124 free drives; the rest were excursions)
- 10 vehicles (Six E- and four S-Class)
- 103 drivers (26% by women)

The criteria for drives in this data set were:

- Drives were *valid* according to the validation criteria in Sec. A.7.3
- KSS self-rating was valid and plausible
- At least one KSS entry was made
- The driven distance was at least 30 km
- Lane-tracking data had to be valid and without measurement errors
- No driver switch (otherwise the drive would have to be cut up every time)
- Only E- and S-class vehicles (excluding vehicleID=69 due to its miscalibrated camera)
- Availability of plausible and valid ALDW data for over 50% of the time

ALDWvalid was defined equally to ALDWvalid*ND*, just that additional drives from all experiments with ALDW were included (32 of 91 experiments). Especially Customer Near Driving (KNFE) and free drives were added. The quality of these drives is lower, especially with regards to the KSS self-estimation. From 25 vehicles, 1.642 drives with over 2.722 hours of driving, and 265.469 km remained. Here, the percentage of women was only 14.3%. The lane data quality and active time of drives in Sweden and Italy were sometimes very bad due to bad road conditions.

FieldDrives was a good representation of customer drives in the field and therefore covered only free drives and customer near driving (KNFE). The 2.133 drives from 425 drivers covered 299.170 km of driven distance during 3.174 hours, but only 12.5% women.

validTopDrivers For the classification of drivers and clustering of driving styles in Ch. 5.4, the DataSet *validTopDrivers* had to be defined. The filter criteria were the same as for *ALDWvalid*, except with the additional filter criteria:

- Only the top 15 drivers with the highest number of drives were selected: $driverID \in 20, 152, 609, 607, 133, 59, 5, 340, 753, 165, 483, 485, 484, 19, 482$.
- Only drives with $\max(KSS) \leq 7$ were selected.
- Only excursion experiments and free drives, no night studies

233 drives with 542 hours and 57.835 km of driven distance remained and 27% of them were made by women.

A.3. CAN Signals

Tab. A.1 lists the names and abbreviations of the essential CAN signals used in this thesis. The signals are grouped by the sensors they originate from, i.e. the steering wheel angle sensor (STW), accelerometer (ACCEL), Yaw rate sensor (YAW), accelerator pedal (ACCPDL), switches and buttons (SW), levers (LEVER), rain and light sensor (LIGHT), clock (CLK), wheel rotation rate sensors (WHLRPM), control system ECU active (CTRLECU), global positioning system (GPS) and lane tracking camera (ALDW).

Tab. A.2 lists the available signals for the system from *Robert Bosch GmbH*.

A.3.1. Synchronization of CAN-Bus Signals

In this thesis, a novel interface for communication with the vehicle CAN-bus was implemented for real-time visualization, measurement and data conversion. The Controller Area Network (CAN)-bus is an asynchronous, serial message-based bus protocol designed for automotive application.

Every CAN message ID originates from one dedicated device, to which multiple bus members can listen. Message IDs must be unique on a single CAN bus. The message ID is used as a priority to achieve a bus load of up to 80%. The lower the ID, the more important the message. The 11-Bit ID Base frame format in CAN 2.0A allows up to 2048 different message IDs while the Extended frame format in CAN 2.0B allows 2^{29} IDs. Carrier Sense Multiple Access / Collision Resolution (CSMA/CR) is used for arbitration to avoid collisions. Every bus member is listening bitwise and submitting its ID. If multiple units try to submit at the same time, the dominant bit of the member with the lowest ID is overwriting the recessive bits of the other units which, then, stop submitting. For this reason and with the present high bus load, the transmission time instant cannot be assured.

A CAN frame is composed as described in Tab. A.3. In addition, the measurement hardware stores the message counter and the timestamp of the message reception.

Messages can be transmitted with different rates, depending on the sampling frequency of the contained signals. Mostly, high-speed CAN with bitrates of up to 1 Mbit/s are used at network lengths below 40 meters. There are also low-speed CAN with a maximum bitrate of 125 kbit/s.

Every CAN signal is defined according to the structural properties listed in Tab. A.4. The payload of a CAN-signal cannot be interpreted without this decoding information. These definitions of all signals of a CAN bus is stored in a DBC-file (along with signal descriptions). Depending on this definition, every payload of one CAN message is composed of one or several signals. Signals with more than 32 Bit have to be distributed on multiple CAN messages. The interpretation of the data bits is only possible with this definition (DBC file), as it defines every signal.

Tab. A.4 shows the header and payload definition bits of a CAN-message as defined in DBC-files.

Signal Synchronization

Another challenge is the synchronization of different CAN-signals and sensors that work with different asynchronous sampling times. The CAN-bus is not deterministic. Hence, a message can arrive delayed and lead to gaps and jitter in the signals. Fig. A.2 illustrates

ID	Abbreviation	Description	Class
1	δ_S	Steering wheel angle sensor with high-precision	STW
2	$\delta_{S,ESC}$	Steering wheel angle sensor from ESC	STW
3	$\delta_{S,offset}$	Steering wheel angle sensor offset	STW
4	$\hat{a}_x$	Longitudinal acceleration from accelerometer	ACCEL
5	$\hat{a}_{x,offset}$	Est. a_x offset (correct mounting tolerance, cf. Sec. 2.3.2)	ACCEL
6	$\hat{a}_y$	Lateral acceleration from accelerometer	ACCEL
7	$\hat{a}_{y,offset}$	Est. a_y offset (mounting, road inclination, cf. Sec. 2.3.2)	ACCEL
8	$\dot{\psi}$	Yaw rate	YAW
9	$\ddot{\psi}$	Yaw acceleration from sensor	YAW
10	*AccelPdlPosn*	Accelerator pedal	ACCPDL
11	*AccelPdlPosnRaw*	Accelerator pedal before manipulation by ACC/limiter	ACCPDL
12	*TurnIndLvrStat*	Turn indicator	SW
13	*TlmSwPsd*	Telemetry switch pressed	SW
14	*StWSwPsd*	Steering wheel switches 0 to 15 pressed	SW
15	*HrnSwPsd*	Horn pressed	SW
16	*DTRDistRq*	Distronic distance state	SW
17	*Phcall_Act*	Phonecall active	SW
18	*AirConSw*	Air conditioner switches	SW
19	*SeatAdjSw*	Seat adjustment switches	SW
20	*MirrorSw*	Mirror adjustment switches	SW
21	*CLUTCH*	Clutch	SW
22	*DrRLtchFRStat*	Driver door state	SW
23	*BcklSwD*	Driver sear buckled up	SW
24	*SpdCtrlLvrStat*	Speed control lever state	LEVER
25	*HiBmLvrStat*	High beam light lever state	LEVER
26	*WprWashRSwPosn*	Windshield wiper position	LEVER
27	*LgtSens*	Light and rain sensor	LIGHT
28	$TIME_{HR}$	Time of day in hours	CLK
29	$TIME_{MN}$	Time of day in minutes	CLK
30	$WhlRPM_{FL}$	Wheel rotation rate front left	WHLRPM
31	$WhlRPM_{FR}$	Wheel rotation rate front right	WHLRPM
32	$WhlRPM_{RL}$	Wheel rotation rate rear left	WHLRPM
33	$WhlRPM_{RR}$	Wheel rotation rate rear right	WHLRPM
34	ASR_{ctrl}	Traction Control System active	CTRLECU
35	ESP_{ctrl}	Electronic Stability Control active	CTRLECU
36	ABS_{ctrl}	Anti-lock Braking System active	CTRLECU
37	HBA_{ctrl}	Hydraulic Brake Assist active (e.g. BAS, BAS+)	CTRLECU
38	GPS_{lon}	GPS longitude	GPS
39	GPS_{lat}	GPS latitude	GPS
40	GPS_{head}	GPS heading	GPS
41	GPS_{speed}	GPS speed over ground	GPS
42	GPS_{alt}	GPS altitude	GPS
43	GPS_{valid}	GPS valid	GPS
44	MM_{lat}	map matched latitude from head-unit	GPS
45	MM_{lon}	map matched longitude from head-unit	GPS

Table A.1.: The simplified list of major CAN sensor signals

how the timing is disturbed by the CAN-bus transmission and must be recovered to the fixed sampling rate. It is important to map the samples not to the receive-time but according to their order. In the real-time ECU system, this works only with a delay that is larger than the longest delay. This delay can be compensated to zero for offline computation. Samples that have not arrived within the timeout, must be filled by holding the sample. Where needed (e.g. for cross-wind detection), different signals have to be synchronized with individual delays that are practically measured for every vehicle "electric/electronic" (EE) environment. Therefore,

ID	Abbreviation	Description	Class
39	*LaneClothoidPara*	lane clothoid parameter	ALDW
40	*LaneHrztCrv*	lane horizontal curvature at vehicle position	ALDW
41	*LaneMark_Lt_Stat*	lane marking left state	ALDW
42	*LaneMark_Rt_Stat*	lane marking right state	ALDW
43	*LaneMarkCol_Lt*	lane marking color left	ALDW
44	*LaneMarkCol_Rt*	lane marking color right	ALDW
45	*LaneMarkType_Lt*	lane marking type left	ALDW
46	*LaneMarkType_Rt*	lane marking type right	ALDW
47	*LaneSiteDtct_Stat*	lane site detection state	ALDW
48	*VehPitchAngl*	vehicle pitch angle	ALDW
49	*LaneChg_Stat*	lane change state	ALDW
50	*LaneDataQual*	lane data quality	ALDW
51	$LaneLtrlDisty_L$	lateral lane position, lane center to vehicle middle	ALDW
52	*LaneNum*	lane number	ALDW
53	*LaneTrckTm*	lane tracking time	ALDW
54	*LaneWidth*	lane width (typically 3.2 meters)	ALDW
55	*LaneYawAngl*	yaw angle of longitudinal axis to tangential lane	ALDW
56	*NumLane*	number of lanes	ALDW
57	*RoadExit_Stat*	road exit state	ALDW
58	*RoadType*	road type	ALDW
59	*IndLmp_On_Rq*	indication lamp on request	ALDW
60	*LaneMarkWidth_Lt*	lane marking width left	ALDW
61	*LaneMarkWidth_Rt*	lane marking width right	ALDW
62	*Menu_Enbl_Rq*	menu enable request	ALDW
63	*MsgDisp_Rq*	message display request	ALDW
64	*OnCal_Stat*	online calibration state	ALDW
65	*OnCalExecDist*	online calibration execution distance	ALDW
66	*VibInsty_Rq*	vibration intensity request	ALDW
67	*Warn_Rq*	warning request	ALDW

Table A.2.: List of measured and used lane departure input signals (Bosch)

a special driving maneuver was performed in this thesis for every car on the driving dynamics ground. In order to synchronize the lateral acceleration, the driving maneuver represents a step function of the steering wheel angle from 0° to 10° and back at different speeds between 60 and 180 km/h.

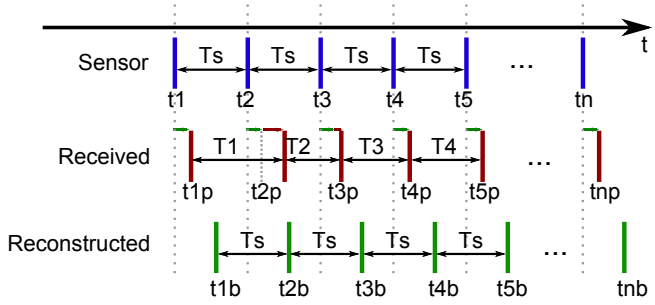

Figure A.2.: Recovering sampling rate after CAN-bus transmission

A.4. Accelerometer Mounting Transform to Center of Gravity

Fig. A.3 illustrates the yaw rotation and acceleration dimensions over ground measured at 90° to each other directly onboard in the ESC.

Field	Length [Bits]	Description
Identifier field	11	ID that describes the message (0...2047)
Identifier extension bit	1	Bit that indicates whether the message type is extended
Extended identifier field	18	The longer ID for more than 2048 messages
Data Length Code (DLC)	4	Lenght of the payload
Data	0...64	Payload
CRC checksum	15	Cyclic Redundancy Checksum

Table A.3.: Essential fields of a CAN message

Property	Description
start-bit	Index of the startbit (0...63)
signal length	Length of signal in bits
offset	Offset of the signal
quantization	Size of smallest (least significant) bit (LSB)
sign	Signed or unsigned
byte-order	Wheter first startbit is LSB or MSB
signal type	*motorola* or *intel* byte order

Table A.4.: CAN signal definition (DBC)

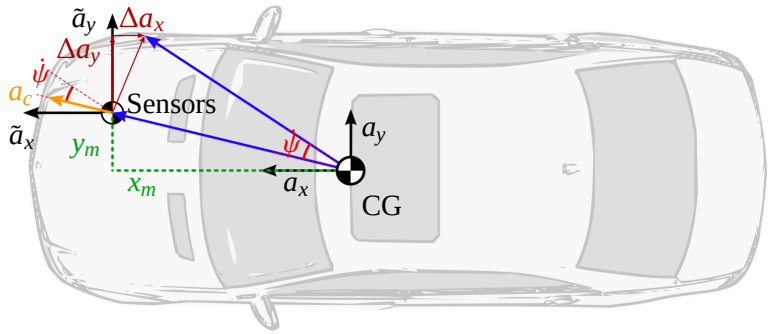

Figure A.3.: Dimensions measured by gyroscope and accelerometers transformed to the vehicle's *center of gravity CG*. Correction transform of accelerometer values to vehicle center of gravity *CG*.

As mentioned in Ch. 2.3.2 and (Schindler, 2007, Ch. 3.2.2), the yaw rate $\dot{\psi}$ sensor position is invariant to the mounting position whereas the vehicle speed v is different in every position of the vehicle if rotation is involved. Thus, also the measured acceleration $\tilde{a}_x$ and $\tilde{a}_y$ are different and need to be transformed to the vehicle's center of gravity *CG*. With other words, if a steady object rotates around it's *CG* with $\dot{\psi} \neq 0°/s$ or experiences a torque with $\ddot{\psi} \neq 0°/s^2$, no force can be measured in the *CG* point. At any other point $\neq CG$, a *centrifugal acceleration* a_c can be measured for $\dot{\psi} \neq 0°/s$. In addition, as illustrated in Fig. A.3, if the object experiences a torque ($\ddot{\psi} \neq 0°/s^2$), a force component in x or y direction can be observed at every point $\neq CG$.

With the known sensor mounting position x_m and y_m and the rotation radius R, the centrifugal acceleration $a_c = v^2/R = \dot{\psi}^2 R$ is obtained according to Eqn. (A.1). Its decomposition in $x-$ and $y-$components is then given by Eqn. (A.2) and (A.3).

$$a_c = \dot{\psi}^2 \cdot \sqrt{x_m^2 + y_m^2} \tag{A.1}$$

$$a_{c,x} = \dot{\psi}^2 \cdot \sqrt{x_m^2 + y_m^2} \cdot \cos(\arctan \frac{y_m}{x_m}) \tag{A.2}$$

$$a_{c,y} = \dot{\psi}^2 \cdot \sqrt{x_m^2 + y_m^2} \cdot \sin(\arctan \frac{y_m}{x_m}) \tag{A.3}$$

For an applied torque with $\ddot{\psi} \neq 0°/s^2$, the undesired $x-$ and $y-$components of the measured acceleration are calculated by Eqn. (A.4) and (A.5).

$$\Delta a_x = \frac{1}{T_s^2} \cos(\frac{\ddot{\psi}}{2} + \arctan \frac{y_m}{x_m}) \cdot 2 \cdot \sqrt{x_m^2 + y_m^2} \cos \frac{\ddot{\psi}}{2} \tag{A.4}$$

$$\Delta a_y = \frac{1}{T_s^2} \sin(\frac{\ddot{\psi}}{2} + \arctan \frac{y_m}{x_m}) \cdot 2 \cdot \sqrt{x_m^2 + y_m^2} \cos \frac{\ddot{\psi}}{2} \tag{A.5}$$

With Eqn. (A.2) to (A.5), the compensated signals of interest a_x and a_y in the vehicle's *CG* from the measured $\tilde{a}_x$ and $\tilde{a}_y$ is then given by Eqn. (A.6) and (A.7).

$$\hat{a}_x = \tilde{a}_x - \Delta a_x - a_{c,x} \tag{A.6}$$

$$\hat{a}_y = \tilde{a}_y - \Delta a_y - a_{c,y} \tag{A.7}$$

According to (Schindler, 2007, Eqn. 3.5), this can be simplified to

$$\hat{a}_x = \tilde{a}_x - y_m \ddot{\psi} - x_m \dot{\psi}^2 \tag{A.8}$$

$$\hat{a}_y = \tilde{a}_y + y_x \ddot{\psi} - y_m \dot{\psi}^2 \tag{A.9}$$

To cope with mounting tolerances and road inclination, the sensor offsets $\hat{a}_{x,offset}$ and $\hat{a}_{y,offset}$ with the range $\pm 2.56 \frac{m}{s^2}$ are estimated online by assuming that the vehicle is on average driving straight ahead without road inclination and elevation. These four CAN signals are transferred as unsigned values and the offsets are subtracted according to Eq. (A.10) and (A.11).

$$a_x = \hat{a}_x - \hat{a}_{x,offset} - 2.56 \frac{m}{s^2} - 10.24 \frac{m}{s^2} \tag{A.10}$$

$$a_y = \hat{a}_y - \hat{a}_{y,offset} - 2.56 \frac{m}{s^2} - \begin{cases} 10.24 \frac{m}{s^2} & \text{for Robert Bosch ESC} \\ 12.5568 \frac{m}{s^2} & \text{for Continental ESC} \end{cases} \tag{A.11}$$

A.5. Steering Wheel Angle Sensor Principles and Unwrapping

Optical sensors have two code-slotted discs that are scanned by photo interrupters. One disc is for the absolute angle and an auxiliary disc is connected over a gearing to turn faster and obtain the high resolution. The sensor from Kostal provide non-contact, absolute measurement ranging from -420 to +420° (cf. (Kostal, 2012)).

Magnetical principles always rely on hall sensors. As described in the Patent (Delphi, 2006), Delphi introduced an auxiliary plate connected by a gear bearing to achieve the 0.1° precision. Beyond the *Permanentmagnetic Linear Contactless Displacement* (PLCD) technology,

the Tyco Electronics (Tyco, 2010b) sensor uses a 3D-Hall sensors array triggered by a 360-degree moving magnet. Fig. A.4 shows this slim sensor package and illustrates the operating principle. This sensor works in an ambient temperature from -40C° to +85C° and has a microprocessor for signal evaluation, linearization, and integrated failure diagnostics. However, the Tyco sensor does not provide an absolute angle and has different resolutions in different angular sections. A proposed algorithm to unwrap the signal is explained in App. A.5.

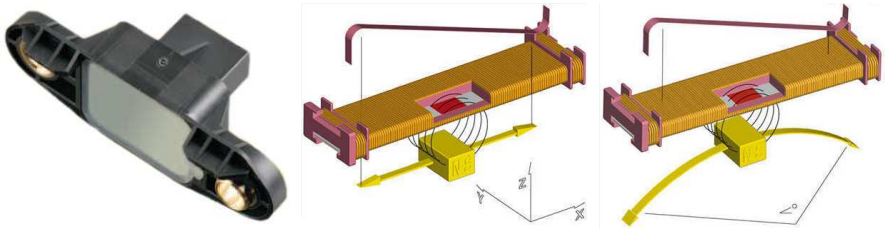

Figure A.4.: Tyco 3D-Hall sensors array (Source: Tyco, 2010a) and operating principle of way and angle registration (Source: Munzig, 2008)

Micro-Electro-Mechanical Systems (MEMS) The high resolution gyroscope and accelerometer are so called *Micro-Electro-Mechanical Systems* (MEMS) as discussed in (Liu, 2005). Conceptually, an accelerometer behaves as a damped proof mass attached to springs (Liu, 2005; Dietmayer, 2008). Depending on the sensor manufacturer, the spring deflection can be measured by capacitive, piezoelectric or piezoresistive (silicon semiconductors) principles. For instance, a movable plate is mounted with springs between two fixed plates (Liu, 2005; Schnabel, 2012). Applied forces result in displacement of the inert plate which can be measured as a capacity change. Ubiquitously, modern MEMS accelerometers consist of a cantilever beam with a proof mass (so called "seismic mass") that oscillates in resonance. An applied force to the cantilever shifts the resonance frequency that can precisely be measured using heterodyne techniques. MEMS gyroscopes work according to the same measurement principles, but use a Foucault pendulum as vibrating element.

Steering Wheel Signal Unwrapping

Due to technical reasons, the magnetically coded disc has different encoding resolution quantizations for different angle ranges (lower quantization outside ±35°). The absolute angle is not known and thus the current section must be unwrapped. The code disc is also accompanied by non-linearities.

The sensor for 216 and 221 vehicles has a sensor from Tyco that has a *modulo "overflow"-behavior*. Furthermore, different quantizations resolutions are used for different areas. This makes the absolute steering wheel angle position ambiguous. Furthermore, a mounting offset of several degrees has to be considered.

For certain recorded data, there are intermediate values between the modulo "overflow"-jumps. This behavior can be seen in Fig. A.5.

Fig. A.6 shows the histogram of the recovered sensor signal. It can be seen that the quantization changes from linear to logarithmic in different sections. Fig. A.7 shows the intermediate values that appear for a measurements recorded in 2008. The discrete histogram calculation has proven to be valuable the analysis of such fixed-point signals. The wrapped and

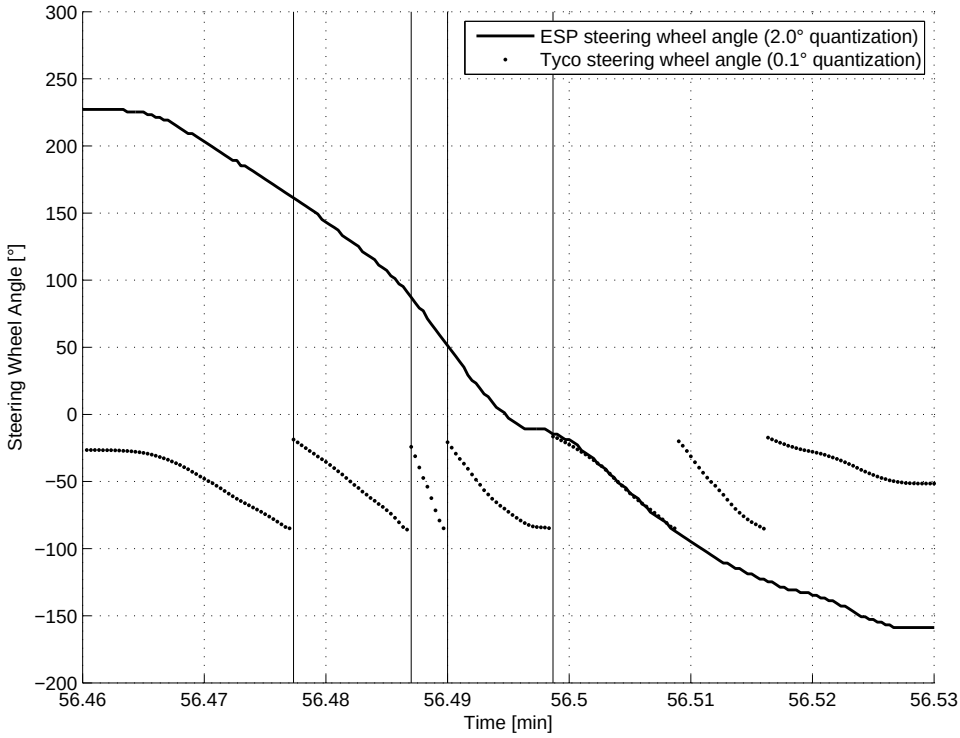

Figure A.5.: Tyco steering wheel angle sensor ambiguities

unwrapped signals are shown in Fig. A.8. Fig. A.9 shows that also the yaw rate sensor has blind spots.

A.6. Measurement Equipment

Over 1.000 selected CAN signals were recorded for every drive. All data communications in the vehicle work over CAN, LIN, FLEXRAY or *Automotive Ethernet* buses. Two automotive computers are used in every vehicle, one with linux for real-time measurement and one with Miscrosoft Windows for configuration and operation. CANape from VECTOR (Vector, 2012) is running on the windows operation computer. The measurement computer features three high- and one low-speed CAN. The *CAN Calibration Protocol* (CCP) is supported to read ECU internal signals over a *measurement technique adapter* (MTA). Custom device drivers were written to measure touchscreen inputs and a supplementary USB GPS device. Measurements are stored on an internal hard drive and have to be copied by a Samba share to an external USB drive.

A.7. Data Conversion

The data conversion is the most complex process step in the entire tool chain. Reasons for that are discussed in Sec. A.7.2. The quality of the database is one of the most important basis of this thesis and also for series-production readiness. Thus, over half a year of development, over 16.000 lines of MATLAB code and one internship were inevitable to create a solid basis for credible results. There are several tasks for the conversion:

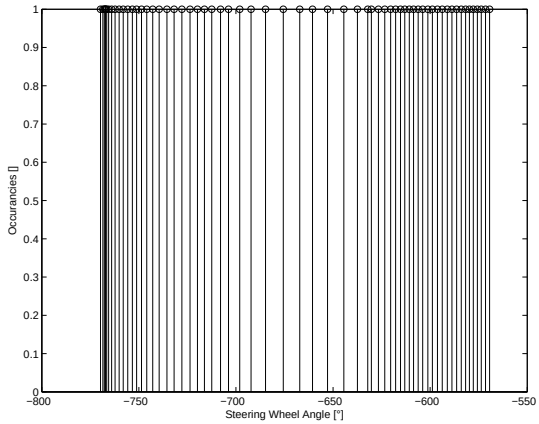

Figure A.6.: Different Tyco steering wheel angle quantization sections

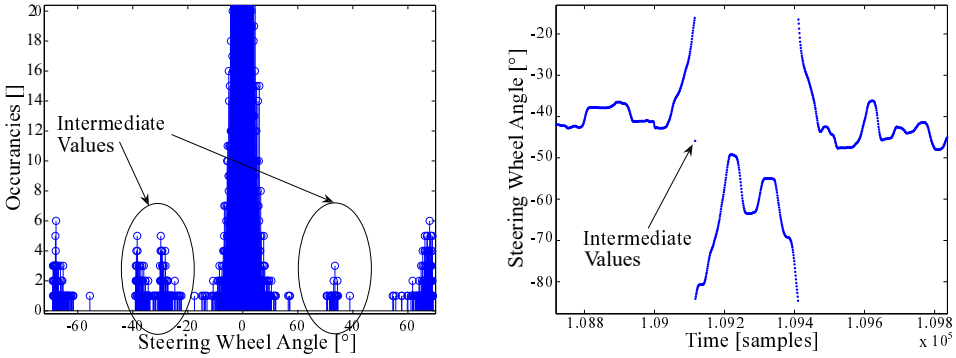

Figure A.7.: Intermediate values between modulo overflow steps for Tyco steering wheel angle sensor.

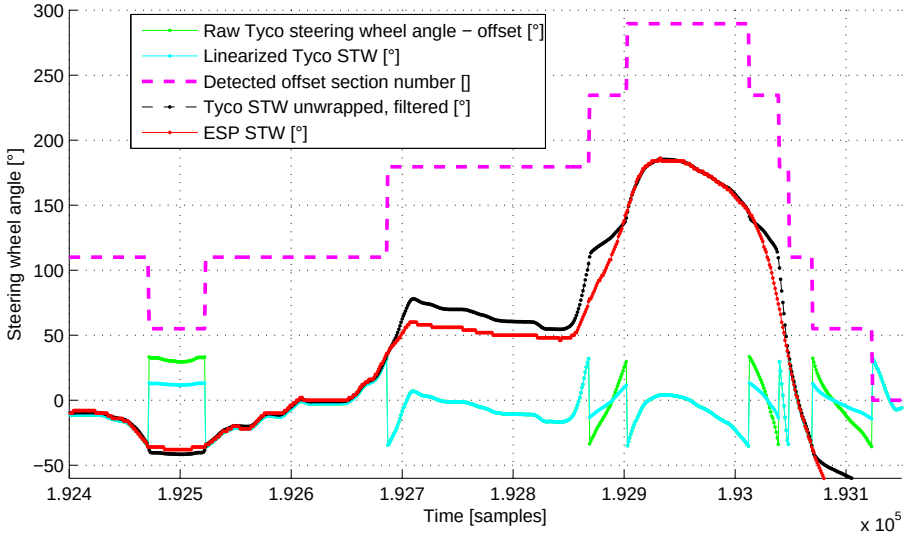

Figure A.8.: Wrapped and unwrapped Tyco steering wheel angle signal

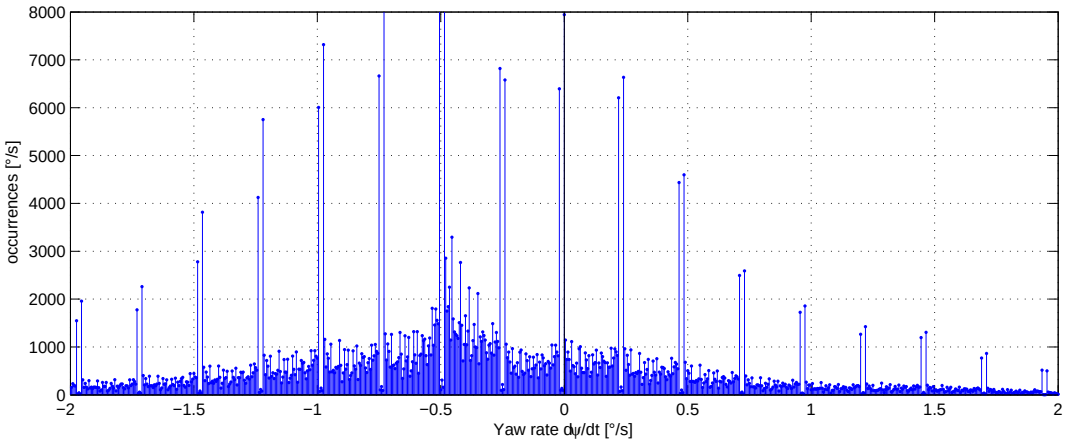

Figure A.9.: Also the yaw rate sensor has blind spots

- convert the wireshark data stream to MATLAB
- read the driver profile and store the questionnaire answers to the database
- check whether the driver names are spelled correctly and consistently use the fuzzy *levenshtein* string distance
- make various plausibility checks on missing signals, wrong measurement configurations, and wrong touch screen entries
- manipulate or fix wrong signals
- store event markings when the driver has pressed *event*
- map varying CAN signal names to a unique name
- synchronize input data with individual sampling rates to equi-distant timestamps using *linear interpolation* for "physical" signals and *nearest neighbor* for discrete signals
- store all relevant information and metrics (such as driven distance, number of warnings, etc.) to the SQL database

A.7.1. SQL Database and Entity Relationship-Diagram

Introducing a SQL database (SQLite) with MATLAB interface allowed to access drives and features according to application specific filter and grouping criteria. Basically, the database is structured using the tables *drives*, *drivers*, *vehicles*, *experiment*, *measurement* and *questionnaire*.

A.7.2. Plausibility Check

Every step in the tool chain, from the sensors, over the measurement, conversion, validation, to the classification results, can contain errors. The entire system highly depends on the quality and correctness of the input data. Impaired data integrity can, for instance, be indebted by the malfunction of sensor prototypes, communication hardware, or measurement equipment due to vibrations, dirt, humidity, and temperature variations. The ongoing development of the numerous prototype vehicles and software release updates are also causes of problems as well as improvements and changes of interfaces and measurement configuration.

Similarly to sensor errors in Sec. 2.3.3, systematic errors in the input data can drastically corrupt simulation results. For this reason, the converted and validated input data were automatically checked after the conversion using physical redundancy and knowledge about signal properties. All important input signals were checked by their valid range, distribution,

magnitude etc. Only samples at a vehicle speed over 10 km/h and steering wheel angles below $\pm 10^{\circ}$ were taken into account. In order to verify the correctness of the sign and magnitude of the most important signals, a physical model was used to match the signals within a confidence tolerance. In our case, it was sufficient to use the *single track model* (see Sec. 6.3) to compare yaw-rate $\dot{\psi}$, wheel rotation $WhlRPM_{FL/FR/RL/RR}$, accelerations $a_{x/y}$, and steering wheel angles δ_a. The *mean squared error (MSE)* and *cross-correlation* function were used as metrics. The conversion process must be reliable enough to meet quality requirements of the series production. Further on, error memory records, such as ESC errors or sensor errors were considered. Vehicle parameters and discrete encoded bit-signals were tested by the validity of values. Pressing a button too long has been detected and suppressed.

Verification of input data does not yet cover mistakes in the simulation or evaluation environment. For instance, a mistake in the evaluation can completely falsify the results. This could only be resolved by systematic software reviews and plausibility checks of results and calculations. The simulation result plots and evaluation metrics of each drive also helped to unveil implausibilities. The visual plots have the advantage that they reveal much more errors than automatic testing for a limited number of predefined errors. A lot of test drives for development purposes could be removed as the driving behavior was abnormal. The combination of all methods has shown to be very effective. This way, all input data could have been verified, corrected, or set to *not valid*.

A.7.3. Data Validation

The data conversion process is followed by a manual validation procedure. Data that contain mistakes could not be used for classification training, so a set of hard and soft criteria were defined:

- KSS entries and other user inputs must be valid and plausible
- A desired warning level of less than KSS 6 is an indicator of careless entries
- The highest reached KSS is consistent with the number of desired warnings
- The number of desired warnings is implausible
- The received number of warnings does not match the obtained number of warnings
- Automatic check for signal errors, measurement gaps, or byte-shifts successful
- Check of the signal runs and other abnormalities successful
- Drives shorter than 30 km for experiments and 10 km for free drives were set to invalid
- Drives inside the plant, on testing tracks, and test drives are generally invalid

In most cases, the decision was very clear as the hard criteria applied. In the few difficult cases, several experts had to agree to avoid systematic influences. During the validation process, all new drives of one driver were grouped by this driver to quickly point out unreliable drivers. An automatic rating was given for each driver on how reliably he entered his KSS level and questionnaire to easier sort out drivers that were unreliable. Moreover, an indicator for inconsistency is, when the driver indicates a different desired warning level for each drive. For instance, some drivers rated their fatigue level to KSS 6 even when they already had lane exceedances. Other drivers, in comparison, rated them as KSS 9 without any signs of fatigue. These drives have been neglected. If not a single KSS entry was made, a separate field in the database *noKSS* was set for a drive and the drive was set to "not valid". Depending on the error, different consequences had to be drawn:

- Drives without KSS entry can not be used for simulation
- Drives without driver profile can be simulated anyway

- The algorithm must be tolerant to minor measurement gaps or mistakes
- Drives with severe errors cannot be used for simulation

For the verification step, a separate MATLAB GUI was implemented that automatically detects specific implausibilities and highlights them red.

A.8. Efficient Online-Histogram and Percentile Approximation using EWMAs

Histogram or online quartile calculation is extremely expensive in regards to computational complexity as the entire window length must be sored and values be sorted. The sorting result can be stored and every new sample sorted into this list, which still requires a lot of memory, especially for large window sizes N. For this reason, we propose an approximation using l EWMA filters where l is the number of required delay elements which only depends on the desired quartile, independent of the window size N. l bins are defined for the $x_{min} = \min(\mathbf{x}[n])$ and $x_{max} = \max(\mathbf{x}[n])\ \forall n$. For $k(i,n) = i(x_{max} - x_{min})/l \leq x[n] < i(x_{max} - x_{min})/l\ \forall i = 1 \dots l$, the EWMA for this bin is updated:

$$\mu_i[n] = \mu_i[n-1] + \lambda_\mu \left(\delta(k(i,n)) - \mu[n-1]\right) . \tag{A.12}$$

The $i/l \cdot 100\%$ percentile is then the value of $\mu_i[n]$. Values in between can also be interpolated to save memory.

A.9. List of all Features

Tab. A.5 list all 144 features implemented in this thesis.

Num.	ID	CLASS	Feature Name	Description
1	43	AA	AATOT	Time-on-task
2	44	AA	ACTIVE	System Active
3	45	AA	CIRCADIAN	Circadian rhythm
4	55	AA	CROSSWIND	Road warping and cross-wind intensity
5	56	AA	CROSSWINDSUPPRESSION	Cross-wind suppression
6	57	AA	CUVESUPPRESSION	Curve suppression
7	58	AA	DYNDRIVINGSTYLE	Driving style suppression
8	120	AA	GGG	AA fatigue measure including all weightings (GGG)
9	122	AA	GGGLWF	GGG baselined (division by baseline)
10	59	AA	MONOTONY	Monotonous driving style
11	60	AA	MUEDESTATUS	AA drowsy (warning threshold exceeded)
12	61	AA	OPERATION	Vehicle operation
13	62	AA	PEAKS	Steering correction event (unweighted)
14	63	AA	ROADBUMPS	Road bumps
15	164	AA	STV25	Mean of slow steering wheel rates [1]
16	165	AA	STV50	Mean steering wheel rates [1]
17	166	AA	STV75	Mean of fast steering wheel rates [1]
18	51	AA	STWEVENT	AA weighted fatigue measure from steering corrections (GGG)
19	121	AA	STWEVENTBL	GG baselined (division by baseline)
20	64	AA	WARNRQ	AA warnings
21	22	ACC	DEGOINT	Degree of interaction from steering wheel angle and velocity
22	171	ACC	MONOTONYSPD	A-priori factor increasing for monotonoous situations and at speeds around 130 km/h [1]
23	23	ACC	REACTIM	Reaction time of steering corrections to lateral displacements
24	169	ACC	YAWJERK	Yaw rate jerks used to identify drift-and-jerk patterns [1]

Num.	ID	CLASS	Feature Name	Description
25	156	CAN	DISTRACTION	Distraction based on CAN signals (vehicle operation) [1]
26	65	CAN	DRACTIVITY	Driving style (monotonous or dynamic)
27	70	CAN	LIGHT	Environment luminosity
28	149	CAN	ODOZIGZAGS	ZIGZAG feature but based on odometry from inertial sensors
29	66	CAN	TOT	Time-on-task
30	67	CAN	TOTMONO	Time-on-task of monotonous driving
31	68	CAN	TOTSPEED	Time-on-task weighted with vehicle speed (max. at 100km/h)
32	26	CAN	TRFCDENS	Traffic density
33	27	CAN	TURNINDADVANCE	Duration between turn indicator and lane change
34	28	CAN	TURNINDDUR	Duration of turn indicator activation (driver dependent)
35	116	EEG	EEG300	EEG alpha-spindle rate with 300 second MA
36	117	EEG	EEG300BL	EEG300 baselined
37	118	EEG	EEG60	EEG alpha-spindle rate with 60 second MA
38	123	EEG	EEGOFF300	
39	124	EEG	EEGOFF300BL	
40	143	EEG	EEGOFF300Z	EOG off with 5 min MA using z-transformation
41	101	EOG	EOGAECS	AECS but using EOG (Average eye closure speed)
42	113	EOG	EOGAECSBL	EOGAECS baselined
43	102	EOG	EOGAPCV	APCV but using EOG (Eye-lid amplitude/velocity ratio)
44	103	EOG	EOGBLINKAMP	BLINKAMP but using EOG (Eye-lid blink amplitude)
45	104	EOG	EOGBLINKDUR	BLINKDUR but using EOG (Eye-lid blink duration)
46	114	EOG	EOGBLINKDURBL	EOGBLINKDUR baselined
47	105	EOG	EOGBLINKFREQ	BLINKFREQ but using EOG (Eye-lid blink frequency)
48	115	EOG	EOGBLINKFREQBL	EOGBLINKFREQ baselined
49	106	EOG	EOGENERGY	EC but using EOG (Energy of eye-blinks)
50	107	EOG	EOGEYEMEAS	EYEMEAS but using EOG (Mean square eye closure)
51	112	EOG	EOGEYEMEASBL	EOGEYEMEAS baselined
52	108	EOG	EOGMICROSLEEP	Microsleep events rate with eye-lid closed > 0.5 s but based on EOG
53	125	EOG	EOGOFFAECS	
54	126	EOG	EOGOFFAECSBL	
55	127	EOG	EOGOFFAPCV	
56	128	EOG	EOGOFFBLINKAMP	
57	129	EOG	EOGOFFBLINKDUR	
58	130	EOG	EOGOFFBLINKDURBL	
59	131	EOG	EOGOFFBLINKFREQ	
60	132	EOG	EOGOFFBLINKFREQBL	
61	133	EOG	EOGOFFENERGY	
62	134	EOG	EOGOFFMICROSLEEP	
63	135	EOG	EOGOFFPERCLOS80	
64	136	EOG	EOGOFFPERCLOS80BL	
65	109	EOG	EOGPERCLOS80	Proportion of time eye-lid is >80% closed but based on EOG
66	111	EOG	EOGPERCLOS80BL	EOGPERCCLOS80 baselined
67	74	EYE	AECS	Average eye closure speed
68	75	EYE	APCV	Eye-lid amplitude/velocity ratio
69	92	EYE	APCVBL	APCV baselined
70	76	EYE	BLINKAMP	Eye-lid blink amplitude
71	77	EYE	BLINKDUR	Eye-lid blink duration
72	95	EYE	BLINKDURBL	BLINKDUR baselined
73	78	EYE	BLINKFREQ	Eye-lid blink frequency
74	79	EYE	CLOSINGVEL	Eye-lid closing velocity
75	80	EYE	EC	Energy of eye-blinks
76	98	EYE	ECBL	EC baselined
77	91	EYE	EYEACTIVE	Eye-tracking system active
78	81	EYE	EYEMEAS	Mean square eye closure
79	82	EYE	EYESOFF	Inattention, proportion of time the drivers eyes off the road (3 min interval) (Belz, 2000)
80	83	EYE	EYETRANS	Inattention, number of eye transitions made by the driver (3 min interval) (Belz, 2000)
81	90	EYE	HEADNOD	Head nodding
82	84	EYE	MEANCLOS	Mean eye closure amplitude (Wierwille, 1996b)
83	85	EYE	MICROSLEEP	Microsleep events rate with eye-lid closed > 0.5 s
84	94	EYE	MICROSLEEP1S	Microsleep events rate with eye-lid closed > 1.0 s
85	86	EYE	OPENINGDUR	Eye opening duration
86	87	EYE	OPENINGLVL	Eye-lid amplitude level when opened between blinks
87	88	EYE	PERCLOS70	Proportion of time eye-lid is >70% closed
88	99	EYE	PERCLOS70BL	PERCLOS70 baselined
89	89	EYE	PERCLOS80	Proportion of time eye-lid is >80% closed

Num.	ID	CLASS	Feature Name	Description
90	93	EYE	PERCLOS80EWMA	PERCLOS80 however with EWMA instead MA
91	100	EYE	PERCLOS80EWMABL	PERCLOS80EWMA baselined
92	37	LANE	DELTADUR	Duration between lateral inflection points
93	38	LANE	DELTALATPOS	Delta between lateral displacement
94	39	LANE	DELTALATVELMAX	Delta maximum lateral velocity
95	14	LANE	LANEAPPROX	Approximation to Lane proximity
96	150	LANE	LANEAPPROXAD	Road marking approximation with driver-adaptive threshold
97	40	LANE	LANEAPPROXADAPT	Approximation to driver adaptive warning range
98	151	LANE	LANEAPPROXBL	LANEAPPROX baselined
99	15	LANE	LANEDEV	Deviation in the Lane
100	145	LANE	LANEDEV4	LANEDEV but to the power of 4, stronger punishing of large deviations
101	137	LANE	LANEDEVBL	LANEDEV baselined
102	146	LANE	LANEDEVSQ	LANEDEV but squared, stronger punishing of large deviations
103	32	LANE	LANEX	Lane exceeding
104	19	LANE	LATMEAN	Mean lateral position
105	16	LANE	LATPOSZCR	Zero-crossing rate lateral position
106	24	LANE	LNACTIVE	Lane active signal
107	31	LANE	LNCHGVEL	Lane change velocity
108	33	LANE	LNERRSQ	Lane error squared
109	30	LANE	LNIQR	IQR of lateral position
110	29	LANE	LNMNSQ	Mean squared lane deviation
111	34	LANE	ORA	Over run area
112	35	LANE	TLC1MIN	Time-to-Lane Crossing
113	155	LANE	TLC1MINBL	TLC using model 1 baselined
114	161	LANE	TLCREACTIM	Reaction time of steering corrections to TLC 1 minima
115	36	LANE	VIBPROP	Warning rate of lane exceedings
116	17	LANE	ZIGZAGS	Zig-Zag Event
117	139	LANE	ZIGZAGSBL	ZIGZAG baselined
118	47	META	DAYTIME	Time of day
119	119	META	DESWARNKSS	Desired warning level (DWL)
120	144	META	DISTRACTIONTASKS	Distraction task reference
121	140	META	LAT	GPS latitude
122	141	META	LON	GPS longitude
123	41	META	VEHSPEED	Vehicle speed
124	148	META	WARNACCEPT	Warning acceptance question
125	48	STW	AmpD2Theta	Lane amplitude duration squared Theta
126	158	STW	AmpD2ThetaBL	AmpD2Theta baselined by max between 3 and 10 minutes active time, saturated by 0.5 and 2.0
127	159	STW	AmpD2ThetaEwma	AmpD2Theta using EWMA rate (time-based) instead MA
128	42	STW	ELLIPSE	Magnitude of steering wheel angle and velocity (ellipse)
129	170	STW	FASTCORRECT	Focusing on few fast steering corrections in calm situations using moving fitted Inverse Gaussian PDF model for threshold determination [1]
130	163	STW	IQRCRIT	Like VARCRIT however using IQR insted variance [1]
131	152	STW	LRVFAST	Fast streering wheel velocity corrections
132	153	STW	LRVPERCHIGH	Upper percentile of streering wheel velocities
133	154	STW	LRVVERYFAST	Very fast steering wheel velocity corrections
134	71	STW	MICROCORRECTIONS	Small steering corrections
135	168	STW	MICROCORRECTIONS2	Absense of small micro-steering corrections indicate fatigue, using own improved implementation (Petit and Chaput, 1990)
136	147	STW	MICROCORRECTIONSW	Rate of small steering wheel angle corrections
137	69	STW	NMRHOLD	Steady steering event rate below 0.5 degree
138	167	STW	NMRHOLDBL	NMRHOLD baselined
139	160	STW	NMRSTVHOLD	Number of steering wheel velocities below threshold [1]
140	25	STW	STWVELZCR	Steering wheel angle velocity zero corssing rate
141	18	STW	STWZCR	Steering wheel angle zero corssing rate
142	142	STW	VARCRIT	Variance criterion
143	72	STW	VHAL	Ratio of fast over slow steering velocities (Kircher et al., 2002; Bittner and Hana, 2000)
144	162	STW	WHAL	Large steering wheel angle amplitudes vs. small amplitudes [1]

Table A.5.: List of all potential features, including the sources if they are based on features in literature. Features marked with [1]are own proposals.

A.10. UTM Zones

In order to match intertial data with GPS data, the longitude and latitude were mapped to real-wold positions in the UTM system such that they also have the unit meters. Fig. A.10 shows the UTM zones and illustrates the principle used in this thesis.

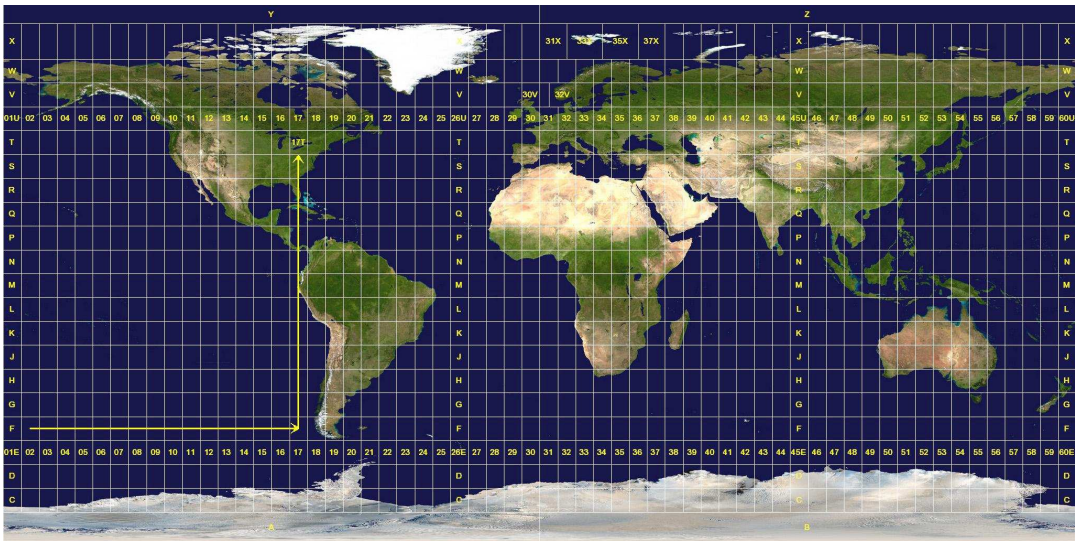

Figure A.10.: UTM Zones

A.11. Histogram of Correlation Coefficients for Single Drives

In order to further illustrate the Metric *Histogram of Correlation Coefficients* in Ch. 7.2.4, Fig. A.11 shows an artificial KSS reference signal for 20 consecutively concatenated drives. Further, an artificial feature with some random noise is shown, that is comparable to the Time-on-Task TOT, but for each drive with different inclination. This inclination describes the different sensitivity of features for different drivers or drives respectively. The temporal order of the samples is irrelevant for the correlation.

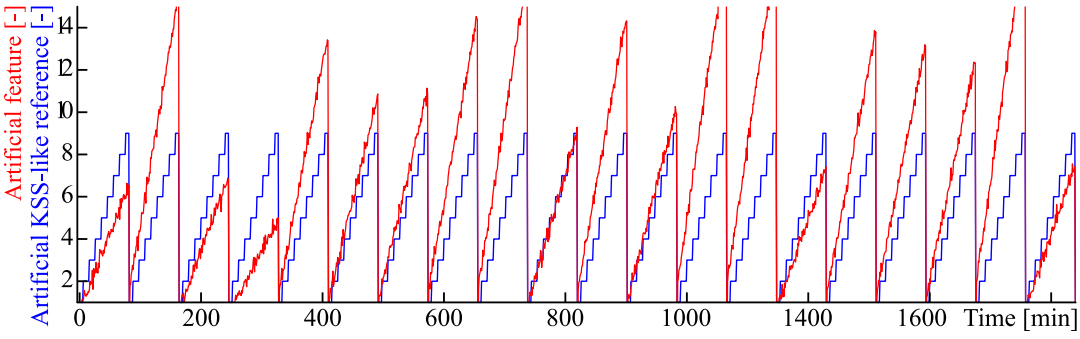

Figure A.11.: Artificial reference (comparable to KSS) from level 1 to 9 and noisy feature with varying inclination to illustrate Spearman histogram. The total correlation of all drives is not as good as for every drive separately. This represents the performance of a feature for which baselining would be ideal.

Fig. A.12 shows at the left a scatter plot and correlation coefficient calculated for all drives at once. The Spearman correlation coefficient of all drives at once is only $\rho_S = 0.811$ while almost all coefficients in the Spearman histogram, grouped by drives, are $\rho'_S \approx 1$.

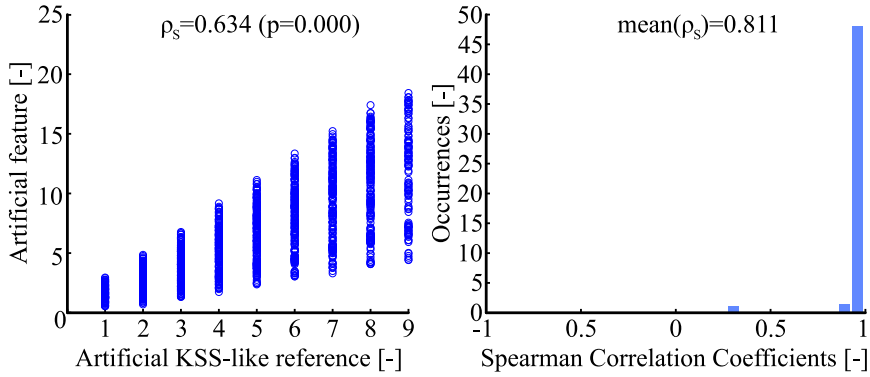

Figure A.12.: Scatter plot over all drives and Spearman histogram of coefficients grouped by drives

As a conclusion, we can see that this method of correlation analysis method serves to evaluate a feature independently from the drive or driver-specific baseline or sensitivity. With other words, the same result would be achieved, if the online-baselining would be ideal. We have to consider that this can unfortunately not be achieved in practice.

Another aspect is, that the KSS should be most accurate at the moment when it is entered. For this reason, alternatively only the instants of the KSS entries are used for evaluation and the feature was used at this time instant or aggregated from its adjacent values.

A.12. Feature Analysis and Evaluation GUI

Fig. A.13 shows an evaluation GUI to analyze single features. All displayed information is contained in the feature matrix $\mathcal{F}$. This makes it possible to select different features and filters for references, vehicles, experiments, drivers and drives. Scatter plots, error bar plots, and correlation measures are updated according to the selection. This allows a combination of qualitative and quantitative assessment of features. This figure provides a good impression, that the feature `PERCLOS80` performs very well for this driver. The signal plot shows that the feature matches better the hold KSS (green) than the linear interpolated signal due to the delay of the smoothing.

A.13. Real-time System

The majority of the transparency about driving situations cannot be captured by the measurements. For this reason, it is very valuable to test the implemented features online in the vehicle to relate signals and events to situations and tune parameters. The ATTENTION ASSIST algorithm was developed and tested in Fixed-point TargetLink directly running on a programmable developer ESP. This is much to laborious and limited in resources to implement sophisticated algorithms. In comparison to the Micro-Autobox MAB II from DSPACE or Vector CANoe CAPL, an alternative, own implementation in MATLAB, Mex C++ and C# was chosen for several reasons. A Vector CAN Card and CAN cases were available, but

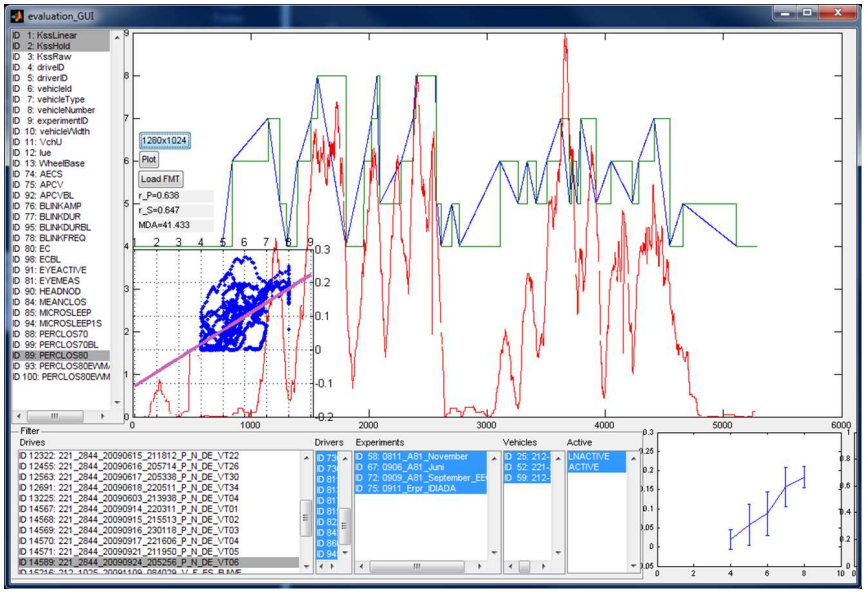

Figure A.13.: Evaluation GUI to analyze correlation of features

no own expensive Vector or DSPACE hardware were available. The own cost-free CAN interface MEX C++ implementation allowed much more flexibility, allowed using the same MATLAB GUI (MathWorks, 2007) for offline and online evaluation of features that were already implemented in MATLAB. The Vector or DSPACE solutions would have required to port everything in SIMULINK and eventually TargetLink.

This section will explain some basics about the CAN bus, the MATLAB GUI, the CAN-Interface, the DBC can signal database parser and the conversion of raw CAN messages.

A.13.1. Fixed-Point Arithmetic

In digital signal processing, there are different ways to represent real numbers. Due to memory and word-size limitations on processor units, numbers are limited to a fixed with. In **floating-point arithmetics**, a number is defined by the *signed*, fixed-length *significand s* (or *coefficient* or *Mantissa*) for a given *base b* (or radix) and the *exponent e* that modifies the magnitude of the number. The length of the significand defines the precision while the radix point is usually defined to be directly after the most significant (leftmost) digit. For instance $1.2345 \cdot 10^{-5}$ is represented in

$$x \approx s \times b^e \tag{A.13}$$

by the significand $s = 1.2345$, the base-10 $b = 10$ and exponent $e = -5$.

In **fixed-point arithmetics**, however, only integer numbers are used where the position of the point is fixed by the *Least-Significant Bit* (LSB). Optionally, an *offset o* and a *signed u* property can be used to better exploit the value range used in the application. In this representation

$$x \approx u \cdot n \cdot LSB + o \tag{A.14}$$

the precision of x when processing only the *integer number n* is then defined by the word length, i.e. the number of Bits. For instance, a signed 8 Bit number can represent the values

-128 to 127 where one Bit for the sign. If it is scaled by a LSB=2^{-4} and an offset $o = 10.0$, the precision (or resolution) is 0.0625 and the fixed-point representation allows to cover the range $[2 \ldots 17.9375]$ ($-128 \cdot LSB + o$ to $127 \cdot LSB - o$).

The computation in fixed-point is many times faster since the position of the radix point does not need to be considered. As is can be seen in Fig. A.14 using an offset increases precision but slows down the computation time. Also, an arbitrary LSB is more precise but less performant than using a dual based LSB. Divisions or multiplications with a dual factor 2^k with $k \in \mathbb{N}$ can be computed very fast by logical shift of the binary number to the right or to the left.

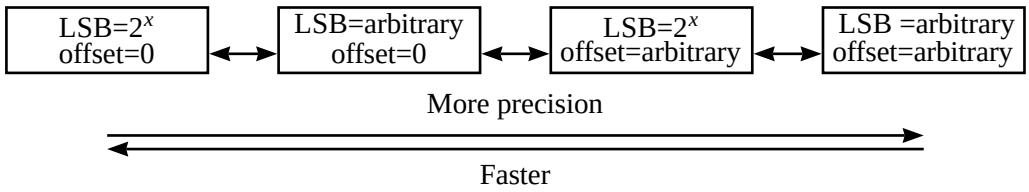

Figure A.14.: Scaling performance vs. accuracy

Representation of a floating point number in fixed-point always leads to a loss of precision and thus an error on a 16 bit architecture. A multiplication of two 16 bit numbers requires a 32 Bit intermediate result, even if the final result is rescaled to 16 bit again. Such operations can be performed with two 16 bit numbers that require however more resources and are thus not expedient. Depending on the signal processing operations, systematic errors lead to accumulated errors in integrators for instance. An error is thus more severe the earlier it occurs in the signal processing chain.

For this reason, especially the filters of the input signals had to be scaled manually and as good as possible. This is exemplarily shown in Ch. A.15. The ATTENTION ASSIST ist running on the controller unis of the ESP.

A.13.2. Fixed-point Low-pass Filter

Especially the Butterworth filter of 2^{nd} order of the lateral acceleration a_y has been identified as a major cause for fixed- / floating-point errors that are accumulated in the feature extraction. App. A.13.1 explains this problem in more detail. For this reson, the filter has to be optimally scaled as shown in Fig. A.15.

A.13.3. Offline and Online Real-Time Attention Assist Vehicle Track Viewer

Fig. A.16 shows the GUI of the offline- and real-time online *Attention Assist Plus* System (AAP). It allows online visualization of vehicles signals and features as well as offline playback of measurements.

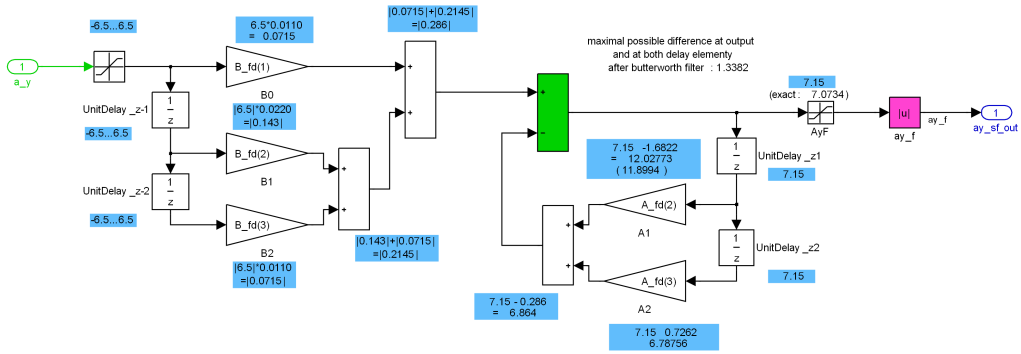

Figure A.15.: Fixed-point scaling of IIR-filter (see Yang, 2011, DSP lecture) of 2^{nd} order on input signal $a_{y,SC}$ to obtain $a_{y,SC,LP}$ to minimize propagated and accumulated error.

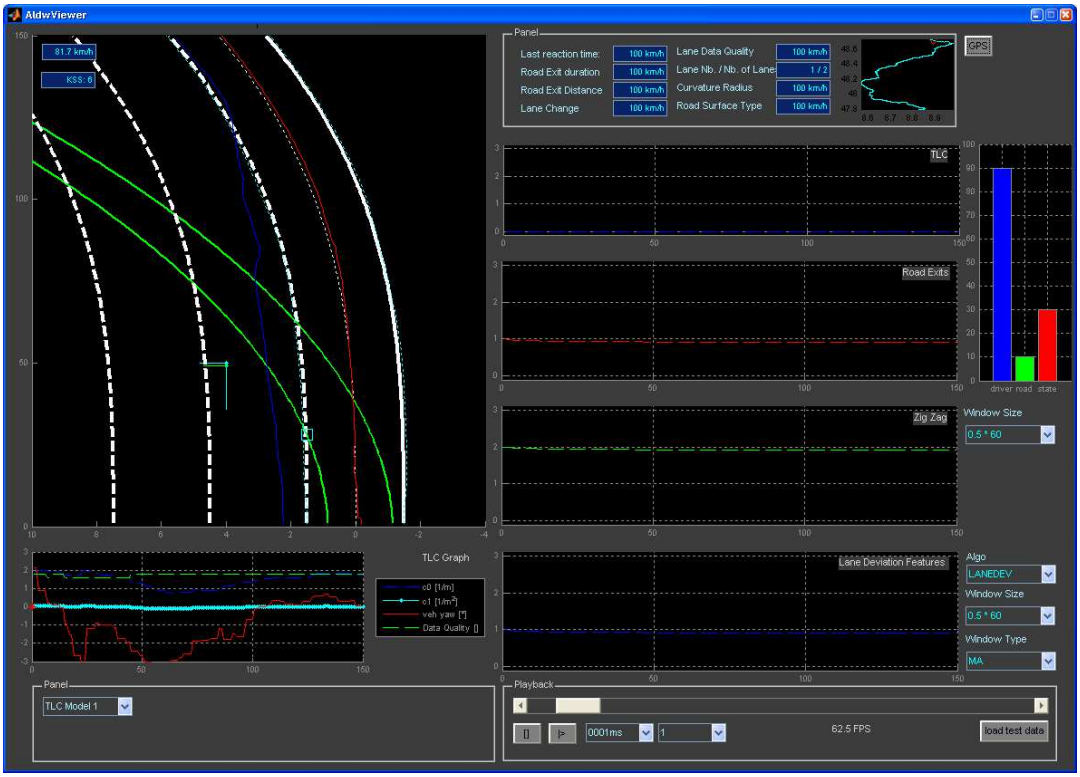

Figure A.16.: Offline- and real-time online ATTENTION ASSIST vehicle track viewer

Bibliography

AAA, 2013: Foundation for Traffic Safety AAA 2013 *How to Avoid Drowsy Driving,* https://exchange.aaa.com/safety/driving-advice/drowsy-driving/ (last visited: May 11, 2020).

Akerstedt, 1980: T. Åkerstedt and M. Gillberg 1980 *Subjective and objective sleepiness in the active individual,* International Journal of Neuroscience, Volume: 52: pp. 29–37.

Akin, 2007: Özgür Akin 2007 *Müdigkeitserkennung mit dem Driver State Sensor (DSS) in Kraftfahrzeugen,* Master's thesis, Fachhochschule Giessen-Friedberg.

Altmueller, 2007: Tobias Altmüller 2007 *Driver Monitoring and Drowsiness Detection by Steering Signal Analysis,* PhD thesis Universitaet der Bundeswehr München.

Andreassi, 2000: J. Andreassi 2000 *Psychophysiology: Human behavior and physiological response,* Londin: Lawrence Erlbaum Associates.

Angermann, 2011: Roman Matthias Angermann 2011 *Die Entwicklung der Aktiven Sicherheit von ihren Anfängen bis zum Jahr 2000 - Unter besonderer Berücksichtigung der Daimler-Benz AG,* Number 978-3-8348-1543-9 Vieweg & Teubner https://www.buchhandel.de/buch/Die-Entwicklung-der-Aktiven-Sicherheit-v-9783834815439 (last visited: May 11, 2020).

Anund et al., 2008: Anna Anund, Göran Kecklund, Björn Peters and Torbjörn Åkerstedt 2008 *Driver sleepiness and individual differences in preferences for countermeasures,* Journal of Sleep Research 17, Issue 1:16–22.

auto.de, 2009: auto.de 2009 *IAA 2009 Rundgang: Mercedes-Benz SLS AMG Flügeltürer* http://www.auto.de/magazin/IAA-2009-Rundgang-Mercedes-Benz-SLS-AMG-Fluegeltuerer (last visited: May 11, 2020).

Autokiste.de, 2007: Autokiste.de 2007 *Volvo Driver Alert: Zeit für eine Pause* http://www.autokiste.de/psg/index/show.htm?id=6679&bild=5 (last visited: May 11, 2020).

Brown et al., 2006: Malcolm Brown, Michael Marmor Vaegan, Eberhard Zrenner, Mitchell Brigell and Michael Bach 2006 *ISCEV Standard for Clinical Electro-oculography (EOG) ISCEV Standard for Clinical Electro-oculography (EOG),* Doc Ophthalmol, Volume: 113: pp. 205–212.

Baranski, 2007: Joseph V. Baranski 2007 *Fatigue, sleep loss and confidence in judgment,* Journal of Experimental Psychology, Volume: 13(4): pp. 182–196.

Barényi, 1951: Béla Barényi 1952, Patent number: (DBP 854 15) *Motor vehicles especially for the transportation of people*. https://www.mercedes-benz.com/de/mercedes-benz/classic/bela-barenyi-der-lebensretter/ (last visited: May 11, 2020).

Barr and Howarth, 2006: Lawrence Barr and Heidi Howarth 2006 *A Review And Evaluation of Emerging Driver Fatigue Detection Measures and Technologies*.

Batavia, 1999: Parag Batavia 1999 *Driver-Adaptive Lane Departure Warning Systems,* PhD thesis The Robotics Institute Carnegie Mellon University Pittsburgh, Pennsylvania, 15213.

Batista, 2007: **Jorge Batista** 2007 *A Drowsiness and Point of Attention Monitoring System for Driver Vigilance,* Proceedings of the IEEE Intelligent Transportation Systems Conference, Volume: 4(4): pp. 702–708.

Becker, 2008: **Ruth Becker** 2008 *Interindividuelle Auswirkungen von Schlafentzug,* PhD thesis Fachbereich Erziehungswissenschaft und Psychologie der freien Universität Berlin.

Belz et al., 2004: **S. M. Belz, G.S. Robinson and J.G. Casali** 2004 *Temporal Separation and Self-rating of Alertness as Indicators of Driver Fatigue in Commercial Motor Vehicle Operators,* Human Factors, Volume: 46 (1): pp. 154–69.

Belz, 2000: **Steven Mark Belz** 2000 *An On-road Investigation of Self-rating of Alertness and Temporal Separation as Indicators of Driver Fatigue in Commercial Motor Vehicle Operators,* PhD thesis Doctor of Philosophy in Industrial and Systems Engineering.

Benz & Co, 1886: **Benz & Co** 1886, Patent number: (DE 37435) *Fahrzeug mit Gasmotorantrieb.* http://upload.wikimedia.org/wikipedia/commons/3/37/Patentschrift_37435_Benz_Patent-Motorwagen.pdf (last visited: May 11, 2020).

Berger and Rumpe, 2008: **Christian Berger and Bernhard Rumpe** 2008 *Autonomes Fahren - Erkenntnisse aus der Darpa Challenge,* it, Volume: 4: pp. 258–264.

Berglund, 2007: **Jens Berglund** 2007 *In-Vehicle Prediction of Truck Driver Sleepiness - Steering Related Variables,* Master's thesis, Lulea University of Technology.

Berka et al., 2005: **Chris Berka, Daniel J. Levendowski and Philip Westbrook** 2005 *Implementation of a Closed-Loop Real-Time EEG-Based Drowsiness Detection System: Effects of Feedback Alarms on Performance in a Driving Simulator,* Proceedings of the International Conference on Human Computer Interaction, July 2005, Las Vegas, Nevada.

Bittner and Hana, 2000: **Roman Bittner and Karel Hana** 2000 *Detecting of Fatigue States of a Car Driver.*

Blanco and Bocanegra, 2009: **Myra Blanco and Joseph L. Bocanegra** 2009 *Assessment of a Drowsy Driver Warning System for Heavy-Vehicle Drivers,* Technical report National Highway Traffic Administration.

Bleich, 2009: **Nils Bleich** 2009 *Deutsche Automobilzulieferer in China: Chancen und Risiken der Erschließung des Chinesischen Automobilmarktes,* Diplomica Verlag Hamburg.

Bleymüller and Gehlert, 2012: **Josef Bleymüller and Günther Gehlert** 2012 *Statistik für Wirtschaftswissenschaftler,* Volume: 16 Franz Vahlen München.

BMW, 2011: **Media Information BMW** 2011 *The future of intelligent networking: The BMW Vision ConnectedDrive.*

Bohlin, 1959: **Nils Ivar Bohlin** 1961, Patent number: (DE 1101987a) *Sicherheitsgurt fuer Fahrzeuge insbesondere Kraftfahrzeuge.* https://www.dpma.de/english/our_office/publications/milestones/60jahredreipunktegurt/index.html (last visited: May 11, 2020).

Boyraz et al., 2007: **Pinar Boyraz, Memis Acar and David Kerr** 2007 *Signal Modelling and Hidden Markov Models for Driving Manoeuvre Recognition and Driver Fault Diagnosis in an urban road scenario,* Proceedings of the 2007 IEEE Intelligent Vehicles Symposium, Pages: 13–15.

Brainard and Hanifin, 2001: **G. C. Brainard and J. P. Hanifin** 2001 *Action spectrum for melatonin regulation in humans: evidence for a novel circadian photoreceptor,* The Journal of Neuroscience: the official journal of the Society for Neuroscience, Volume: 21: pp. 6405–6412.

Brown, 1994: **Ivan D. Brown** 1994 *Driver Fatigue,* Human Factors: The Journal of the Human Factors and Ergonomics Society, Volume: 36(2): pp. 298–314(17).

Buehren, 2008: **Markus Buehren** 2008 *Simulation und Verarbeitung von Radartiellisten im Automobil,* PhD thesis Chair of System Theory and Signal Processing.

BGH, 1969: **Bundesgerichtshof** 1969 *Court decision from 18.11.1969: Perceptibility of fatigue signs by the driver ("Zur Wahrnehmbarkeit der Ermüdungszeichen durch einen Kraftfahrer"),* AZ 4 StR 66/69.

BGH, 2002: **Bundesgerichtshof** 2002 *Court decision from 04.12.2002, Stendal,* AZ.: 23 O 67/02.

Burgess et al., 2002: **Helen Burgess, Katie Sharkey and Charmane Eastman** 2002 *Bright light, dark and Melatonin can promote circadian adaptation in night shift workers,* Sleep Medicine Reviews 6(5):407–420.

Carlson and Gerdes, 2002: **Christopher R. Carlson and Christian Gerdes** 2002 *Identifying tire pressure variation by nonlinear estimation of longitudinal stiffness and effective radius,* In *Proceedings of AVEC 2002 6th International Symposium of Advanced Vehicle Control,*.

Chawla et al., 2008: **M. P. Chawla, H. K. Verma and V. Kumar** 2008 *Artifacts and noise removal in electrocardiograms using independent component analysis,* International Journal on Cardiology, Volume: 129(2): pp. 278–281.

Clayton, 2006: **Clayton** 2006 *Klothoide*
http://ww3.cad.de/foren/ubb/uploads/Clayton/Klothoide-Formeln.pdf
(last visited: May 11, 2020).

Comon, 1994: **P. Comon** 1994 *Independent component analysis, a new concept?,* Signal Processing Volume: 36(3):287–314.

Costa, 2005: **Joaquim Costa and Jaime Cardoso** 2005 *Classification of Ordinal Data Using Neural Networks,* Machine Learning: 16th European Conference on Machine Learning (ECML), Porto, Portugal, Proceedings 10:690–697.

Cui, 2016: **Zhicheng Cui, Wenlin Chen and Yixin Chen** 2016 *Multi-Scale Convolutional Neural Networks for Time Series Classification,* CoRR, DBLP Computer Science Volume: abs/1603.06995.

Czupalla, 2007: **Stephan Czupalla** 2007 *Messfahrtenauswertung zur Erkennung von positions- und tageszeitabhängigen Ereignishäufungen für die Optimierung eines Fahrerzustandsbeobachters,* Master's thesis, Berufsakademie Horb.

Daimler, 2008: **Daimler** *HighTech Report 2/2008 - Feature Attention Assist*
http://www.worldcat.org/title/daimler-hightech-report/oclc/769131108
(last visited: May 11, 2020).

Daimler COM/M, 2009: **Daimler COM/M** *Meilensteine der Fahrzeugsicherheit. Die Vision vom unfallfreien Fahren.*
https://docplayer.org/5414305-Meilensteine-der-fahrzeugsicherheit-die-vision-vom-unfallfreien-fahren.html
(last visited: May 11, 2020).

de Mattos Pimenta, 2011: **Pedro A. de Mattos Pimenta** 2011 *Driver Drowsiness Classification Based on Lane and Steering Behavior,* Master's thesis, University of Stuttgart, Chair of System Theory and Signal Processing.

Delphi, 2006: **Delphi** 2006, Patent number: (US 7,021,161) *Gear Bearing for a Steering Wheel Position Sensor.*

Desai and Haque, 2006: **A.V. Desai and M.A. Haque** 2006 *Vigilance monitoring for operator safety: A simulation study on highway driving,* Journal of Safety Research 37:139–147.

DESTATIS, 2011a: **Statistisches Bundesamt DESTATIS** 2011a *Unfallentwicklung auf deutschen Strassen 2010*.

DESTATIS, 2011b: **Statistisches Bundesamt DESTATIS** 2011b *Verkehrsunfälle Zahlenreihen 2010*.

DESTATIS, 2013b: **Statistisches Bundesamt DESTATIS** 2013a *Unfallentwicklung auf deutschen Strassen 2012,* Begleitmaterial zur Pressekonferenz am 10. Juli 2013 in Berlin.

DESTATIS, 2013b: **Statistisches Bundesamt DESTATIS** 2013b *Verkehrsunfälle - Unfälle unter dem Einfluss von Alkohol oder anderen berauschenden Mitteln im Strassenverkehr*.

Die Welt.de, 2008: **Die Welt.de** *2010 fahren weltweit eine Milliarde Autos*
http://www.welt.de/welt_print/article1561636/2010-fahren-weltweit-eine-Milliarde-Autos.html
(last visited: May 11, 2020) a.

Dietmayer, 2008: **Klaus C.J. Dietmayer** 2008 *Lecture Script for the Lecture Messtechnik II,* University of Ulm.

Dietsche and Jäger, 2003: **Karl-Heinz Dietsche and Thomas Jäger** 2003 *Kraftfahrtechnisches Taschenbuch,* Volume 25 of *ISBN 3-528-23876-3,* Friedrich Vieweg & Sohn Verlag, Wiesbaden.

Dinges et al., 1987: **David F. Dinges, M. T. Orne, W. G. Whitehouse and E. C. Orne** *Temporal Placement of a Nap for Alertness: Contributions of Circadian Phase and Prior Wakefulness,* Sleep, Volume: August 10(4): pp. 313–29
http://www.ncbi.nlm.nih.gov/pubmed/3659730
(last visited: May 11, 2020)

Doppelklicker, 2011: **Doppelklicker** 2011 *Kfz-Versicherung: Beifahrer erhalten keinen Schadenersatz, wenn Müdigkeit des Fahrers bekannt war*.

Drory, 1985: **Amos Drory** 1985 *Effects of Rest and Secondary Task on Simulated Truck-Driving Task Performance,* Human Factors, Volume: 27(7): pp. 201–207.

Duda et al., 2001: **Richard O. Duda, Peter E. Hart and David G. Stork** 2001 *Pattern Classification,* Wiley-Interscience.

Duncker, 2007: **Gernot I. W. Duncker** 2007 *Jeder vierte Autofahrer sitzt übermüdet am Steuer,* Technical report Deutsche Ophthalmologische Gesellschaft e.V.

Anthony Best Dynamics, 2012: **Anthony Best Dynamics** 2012 *Steering robots SP6020 Outline specification,* 2012.

Elango, 2002: **Vetri Venthan Elango** 2002 *Safety Evaluation of Centerline Rumble Strips,* Master's thesis, University of Massachusetts.

Eskandarian and Mortazavi, 2007: **Azim Eskandarian and Ali Mortazavi** 2007 *Evaluation of a Smart Algorithm for Commercial Vehicle Driver Drowsiness Detection,* In *Proceedings of the IEEE Intelligent Vehicles Symposium, Istanbul, Turkey*.

Fagerberg, 2004: **Kalle Fagerberg** 2004 *Vehicle-Based Detection of Inattentive Driving for Integratin in an Adaptive Lane Departure Warning System - Drowsiness Detection,* Master's thesis, KTH Vetenskap Och Konst.

Fahrmeir et al. 2003: **Ludwig Fahrmeir, Rita Künstler, Iris Pigeot and Gerhard Tutz** 2003 *Statistik. Der Weg zur Datenanalyse,* Springer.

Fairbanks et al. 1995: **Rollin J. Fairbanks, Sarah E. Fahey and Walter W. Wierwille** 1995 *Research on Vehicle-Based Driver Status/Performance Monitoring: Seventh Semi-Annual Research Report,* Technical report National Highway Traffic Safety Administration.

Fawcett, 2004: **Tom Fawcett** 2004 *ROC Graphs: Notes and Practical Considerations for Researchers*, Pattern Recognition Letters, Volume: 27(8): pp. 882–891.

Fertner, 2009: **Maria-Luise Fertner** 2009 *Sekundenschlaf & Ablenkung*, Technical report ÖAMTC - Der Österreichische Automobil-, Motorrad- und Touring Club.

FHWA, 2012: **Federal Highway Administration FHWA** 2012 *Roadway Departure Safety - Pavement Safety - Rumble Strips and Stripes - Effectiveness*
http://safety.fhwa.dot.gov/roadway_dept/pavement/rumble_strips/effectiveness/
(last visited: May 11, 2020).

Forsman and Vilaa, 2012: **Pia M. Forsman and Bryan J. Vilaa** 2012 *Efficient driver drowsiness detection at moderate levels of drowsiness*, Accident Analysis and Prevention, Volume: May: pp. 10.

Friedrichs, 2006: **Fabian Friedrichs** 2006 *Schätzung von prosodischen Features zur Emotionsdetektion*, Master's thesis, University of Stuttgart, Chair of System Theory and Signal Processing.

Friedrichs et al. 2012: **Fabian Friedrichs, Werner Bernzen, Frauke Driewer and Wiebke Müller** 2012, Patent number: (DE 201,110,012,967) *Method for identifying or issuance of travel time of driver, involves determining travel time of driver, where travel time is continuously identified and optionally displayed during ignition of barrel of vehicle.*
http://www.google.com/patents/DE102011012967A1?cl=en
(last visited: May 11, 2020).

Friedrichs and Yang, 2010a: **Fabian Friedrichs and Bin Yang** 2010 *Camera-based Drowsiness Reference for Driver State Classification under Real Driving Conditions*, IEEE Intelligent Vehicles Symposium.

Friedrichs and Yang, 2010b: **Fabian Friedrichs and Bin Yang** 2010 *Drowsiness Monitoring by Steering and Lane Data based Features under Real Driving Conditions*, EUSIPCO.

Friedrichs and Yang, 2011: **Fabian Friedrichs and Bin Yang** 2011 *Consideration of Influences on Driver State Classification from External Factors*, Driver Distraction and Inattention (DDI) Conference.

Fuersich, 2009: **Alexander Fuersich** 2009 *Driver State Classification using Expert Knowledge in Hiddden Markov Models and Bayes Networks*, Master's thesis, University of Stuttgart, Chair of System Theory and Signal Processing.

Furtwängler, 2013: **Sara Furtwängler** 2013 *Bewährungsstrafe nach tödlichem Unfall auf A81*, Heilbronner Stimme
https://www.saechsische.de/bewaehrungsstrafe-nach-toedlichem-unfall-3842144.html
(last visited: May 11, 2020).

Gallay and Schleicher, 2002: **N. Gallay and R. Schleicher** 2002 *Fatigue indicators from Electroencephalogram - A Reasearch Report*.

Galley et al., 2005: **Lars Galley, Elisabeth Hentschel, Klaus-Peter Kuhn and Wolfgang Stolzmann** 2006, Patent number: (WO 2006131254 A1) *Method and Control Device Recognising, Specific to a Driver, Inattentiveness of a Driver of a Vehicle.*

Gärtner, 2009: **Christiane Gärtner** 2009 *Driving Style Classification for DriverMonitoring*, Master's thesis, University of Stuttgart, Chair of System Theory and Signal Processing.

Gärtner, 2017: **Jonas Gehring, Michael Auli, David Grangier, Denis Yarats and Yann N. Dauphin** 2017 *Convolutional Sequence to Sequence Learning*, PLMR, Proceedings of the 34th International Conference on Machine Learning, Volume: 70(06–11)(7): pp. 1243–1252.

Gutierrez, 2016: **P.A. Gutiérrez and M. Pérez-Ortiz and J. Sánchez-Monedero and F. Fernandez-Navarro and C. Hervás-Martínez** 2016 *Ordinal regression methods: survey and experimental study,* IEEE Transactions on Knowledge and Data Engineering, Volume: 28(1): pp. 127–146.

Gillberg et al., 1996: **Mats Gillberg, Göran Kecklund, John Axxelsson and Torbjörn Åkerstedt** 1996 *The Effects of a Short Daytime Nap After Restricted Night Sleep,* Sleep, Volume: 19(7): pp. 570–575.

Glaser and Mammar, 2005: **Sebastien Glaser and Saïd Mammar** 2005 *Experimental Time to Line Crossing Validation,* IEEE Conference on Intelligent Transportation Systems, Volume: 8: pp. 791–796.

Goodfellow et al., 2017: **Ian Goodfellow, Yoshua Bengio and Aaron Courville** 2017 *Deep Learning (Adaptive Computation and Machine Learning),* The MIT Press, Massachusetts
https://www.deeplearningbook.org/
(last visited: May 11, 2020).

Government of India, 2011: **Government of India** 2011 *Road Accidents in India 2011*
http://www.indiaenvironmentportal.org.in/files/file/road%20accidents%20in%20India%202017.pdf
(last visited: May 11, 2020).

Grace, 2001: **Richard Grace and Sonya Steward** 2001 *Drowsy Driver Monitor and Warning System,* First International Driving Symposium on Human Factors in Driver Assessment, Training and Vehicle Design page 5.

Greschner, 2011: **Uwe Markus Greschner** 2011 *Experimentelle Untersuchung von Maßnahmen gegen Schläfrigkeit beim Führen von Kraftfahrzeugen,* PhD thesis Von der Fakultät Konstruktions-, Produktions- und Fahrzeugtechnik der Universität Stuttgart.

Guan, 2008: **Tianyi Guan** 2008 *Modellierung der Fahrzeugdynamik zur Einschätzung der Perspektivenänderung einer Kamera anhand von CAN Bus Daten,* Master's thesis, Universität Stuttgart.

Han et al., 2017: **Young-Joo Han, Wooseong Kim and Joon-Sang Park** 2017 *Eye-tracking on smartphones using regression-based prediction,* Hindawi, Mobile Information Systems, Pages: 990–992.

Han et al., 2018: **Young-Joo Han, Wooseong Kim and Joon-Sang Park** 2018 *Efficient Eye-Blinking Detection on Smartphones: A Hybrid Approach Based on Deep Learning,* Hindawi, Mobile Information Systems, Volume: 2018: pp. 1–8.

Hargutt, 2001: **Volker Hargutt** 2001 *Das Liedschlussverhalten als Indikator für Aufmerksamkeits- und Müdigkeitsprozesse bei Arbeitshandlungen,* PhD thesis University of Würzburg.

Hargutt and Krüger, 2000: **Volker Hargutt and H.-P. Krüger** 2000 *Eyelid movements and their predictive value for fatigue stages.,* International Conference of Traffic and Transport Psychology (ICTTP).

Hargutt et al., 2005: **Volker Hargutt, H. Tietze and Hans-Peter Krüger** 2005 *Auto an Fahrer: "Sie sind müde!" - Wirkung verschiedener Strategien zur Rückmeldung des Fahrerzustands,* VDI-Gesellschaft Fahrzeug- und Verkehrstechnik (Hrsg.), Fahrer im 21. Jahrhundert. Der Mensch als Fahrer und seine Interaktion mit dem Fahrzeug (Tagung Braunschweig), Pages: 95–101.

Hartley, 1995: **Laurence Hartley** 1995 *Fatigue & Driving: driver Impairment, driver fatigue and driving simulation,* Taylor&Francis.

Hasberg and Hensel, 2009: **Carsten Hasberg and Stefan Hensel** 2009 *Online-Estimation of Road Map Elements using Spline Curves,* 12th International Conference on Information Fusion.

Heißing, 2011: Bernd Heißing 2011 *Chassis Handbook,* Springer
http://books.google.de/books?id=NSlSJtEy-NIC&q=antilock%20braking%20system
(last visited: May 11, 2020).

Hell, 2001: W. Hell 2001 *Verkannte Unfallursache.,* Kolloquium des DVR 2001.

Hell, 2010: Wolfram Hell *Fahrzeuginsassen richtig sichern,* ADAC e.V. and Ludwig-Maximilians-Universität München, Institut für Rechtsmedizin, Medizinisch-Biomechanische Unfallanalyse.

Hentschel et al., 2005: Elisabeth Hentschel, Dietmar Neumerkel, Lars Galley and Klaus-Peter Kuhn 2005, Patent number: (DE 103 55 221 A1) *Verfahren und Computerprogramm zum Erkennen von Unaufmerksamkeiten des Fahrers eines Fahrzeugs.*

Hermannstädter and Yang, 2013a: Peter Hermannstädter and Bin Yang 2013 *Driver Distraction Assessment Using Driver Modeling,* Proceedings of the IEEE International Conference on Systems, Man, and Cybernetics, Volume: October: pp. 13–16 Manchester, UK.

Hermannstädter and Yang, 2013b: Peter Hermannstädter and Bin Yang 2013 *Erkennung veränderten Fahrerverhaltens mit einem Fahrermodell mit Vorausschau und Motorikkomponente,* VDI-Bericht 4. Berliner Fachtagung Fahrermodellierung. Berlin, Germany, 13./14. Juni.

Herslund and Jorgensen, 2003: M.-B. Herslund and N. O. Jorgensen 2003 *Looked-but-failed-to-see-errors in traffic,* Accident Analysis & Prevention. Volume: 35(6): pp. 885–891.

Heuer, 2013: Steffan Heuer 2013 *Autonomous driving - The triumph of the assistance systems.*

Hochreiter, 1991: Josef Hochreiter 1991 *Untersuchungen zu dynamischen neuronalen Netzen,* Master's thesis, Institut für Informatik, Technische Universität München.

Hochreiter and Schmidhuber, 1997: Sepp Hochreiter and Jürgen Schmidhuber 1997 *Long Short-term Memory,* Neural Computation, Volume: 9(8): pp. 1735-80.

Horne and Reyner, 1995: J. A. Horne and L. A. Reyner 1995 *Sleep related vehicle accidents,* BMJ, Volume: 310: pp. 565–567.

Horne and Baulk, 2004: James A. Horne and Stuart D. Baulk 2004 *Awareness of sleepiness when driving,* Psychophysiology, Volume: 41(1): pp. 161–165.

Horne and Reyner, 1999: Jim Horne and Louise Reyner 1999 *Vehicle accidents related to sleep: a review,* Occup Environ Med, Volume: 56: pp. 289–294.

Houben et al., 1982: H. Houben, T. Thien, G. Wijnands and A. Van t Laar 1982 *Effects of cold exposure on blood pressure, heart rate and forearm blood flow in normotensives during selective and non-selective beta-adrenoceptor blockade,* British Journal of Clinical Pharmacology, Volume: 14(6): pp. 867–870.

Hutter et al., 2019: Frank Hutter, Lars Kotthoff and Joaquin Vanschoren 2019 *Automated Machine Learning - Methods, Systems, Challenges,* Springer Series on Challenges in Machine-Learning (Open).

Hyvärinen and Oja, 2000: Aapo Hyvärinen and Erkki Oja 2000 *Independent Component Analysis: Algorithms and Applications,* Neural Networks, Volume: 13(4-5): pp. 411–430.

Ibrahim, 2009: Mohamed Abolfadl Ibrahim 2009 *Global Parameter Optimization of Driver State Monitoring System,* Master's thesis, University of Stuttgart, ISS.

Idiada, 2012: Idiada *Vehicle proving ground test track, Spain,*
http://www.idiada.es
(last visited: May 11, 2020).

Iizuka and Obara, 1986: **Haruhiko Iizuka and Hideo Obara** 1986, Patent number: (4,594,583) *Method and system for detection of driver drowsiness by an abrupt steering change following no steering movement.*

Janos, 2018: **Nathan Janos and Jeff Roach** *1D Convolutional Neural Networks for Time Series Modeling*, 2018
https://pydata.org/la2018/schedule/presentation/14/
(last visited: May 11, 2020).

Jap2009: **Budi Thomas Jap, Sara Lal, Peter Fischer and Evangelos Bekiaris** 2009 *Using EEG spectral components to assess algorithms for detecting fatigue,* Expert Systems with Applications, Volume: 36: pp. 2352–2359.

Jellentrup et al., 2009: **Nina Jellentrup, Klaus-Peter Kuhn, Katja Nagel and Siegfried Rothe** 2009, Patent number: (DE 102008035217 A1) *Vorrichtung in einem Kraftfahrzeug zur Ermöglichung eines leistungsfördernden Kurzschlafes.*
http://www.patent-de.com/20090402/DE102008035217A1.html
(last visited: May 11, 2020).

Jellentrup and Rothe, 2009: **Nina Jellentrup and Siegfried Rothe** 2009, Patent number: (DE 102009009468 A1) *Vorrichtung zur Erzeugung eines Warn- oder Wecksignals für einen Fahrer.*
http://www.patent-de.com/20091029/DE102009009468A1.html
(last visited: May 11, 2020).

Jung and Makeig, 2000: **T. P. Jung and S. Makeig** 2000 *Removing electroencephalographic artifacts by blind source separation,* Psychophysiology, Volume: 37(2): pp. 163–178.

Kanstrup, 2006: **Lena Kanstrup** 2006 *Method for detection of sleepiness - Measurement of interaction between driver and vehicle,* Master's thesis, University of Linköping.

Karim et al., 2018: **F. Karim and S. Majumdar and H. Darabi and S. Chen** 2018 *LSTM Fully Convolutional Networks for Time Series Classification,* IEEE Access, Volume: 6: pp. 1662–1669.

Katz et al., 2004: **Egon Katz, Klaus-Peter Kuhn, Jürgen Schrader and Wolfram Schröder** 2004, Patent number: (DE 1192061 B1) *Verfahren zur fahrdynamischen Adaption der Körperabstützung einer Sitzenden in einem Fahrzeugsitz und Fahrzeugsitz hierzu.*

Kecklund and Åkerstedt, 1993: **Göran Kecklund and Torbj örn Åkerstedt** 1993 *Sleepiness In Long Distance Druck Driving: an Ambulatory EEG Study of Night Driving,* Ergonomics, Volume: 36.9: pp. 1007–1017.

King et al., 1999: **David J. King, David K. Mumford, and Gunter P. Siegmund** 1999 *An Algorithm for Detecting Heavy-Truck Driver Fatigue from Steering Wheel Motion,* National Highway Traffic Safety Administration (NHTSA).

Kircher et al., 2002: **Albert Kircher, Marcus Uddmann and Jesper Sandin** 2002 *Vehicle Control and Drowsiness,* Swedisch National Road Transport Research Institute.

Kirschstein, 2008: **Timo Kirchstein** 2008 *How is the EEG generated?,* Neurophysiologie-Labor, Volume: 30: pp. 29–37.

Knipling, 1998: **Ron Knipling** 1998 *PERCLOS: A Valid Psychophysiological Measure of Alertness As Assessed by Psychomotor Vigilance,* Technical report Federal Highway Administration.

Knipling and Wang, 1994: **Ronald R. Knipling and Jing-Shiam Wang** 1994 *Crashes and Fatalities Related to Driver Drowsiness/Fatigue,* Technical report National Highway Traffic Safety Administration.

Knipling1995: Ronald R. Knipling and Jing Shiam Wang 1995 *Revised Estimates of the U.S. Drowsy Driver Crash Problem Size Based on General Estimates System Case Reviews,* 39th Annual Proc., Association for the Adv. of Automotive Medicine, Chicago October.

Knipling and Wierwille, 1994: Ronald R. Knipling and Walter W. Wierwille 1994 *Vehicle-Based Drowsy Driver Detection: Current Status and Future Prospects*.

Kostal, 2012: Leopold Kostal 2012 *Steering Column Modules,* https://www.kostal-automobil-elektrik.com/en-gb/produkte/mechatronik-module/lenksaeulenmodule (last visited: May 11, 2020) last accessed: 27 November, 2012.

Kozak and Pohl, 2006: Ksenia Kozak and Jochen Pohl 2006 *Evaluation of Lane Departure Warnings for Drowsy Drivers,* In *Proceedings of the Human Factors And Ergonomics Society 50th Annual Meeting,* Page: 5.

Krizhevsky et al., 2012: Alex Krizhevsky, Ilya Sutskever and Geoffrey E Hinton 2012 *ImageNet Classification with Deep Convolutional Neural Networks,* Pages: 1097–1105 http://papers.nips.cc/paper/4824-imagenet-classification-with-deep-convolutional-neural-networks.pdf (last visited: May 11, 2020).

Kuhn and Heidinger, 1997: Klaus-Peter Kuhn and A. Heidinger 1997 *On-line driver type classification,* International journal of vehicle design, Volume: 18(6): pp. 616–625.

Künzel, 2008: Daniela Künzel 2008 *Die Rolle von Ablenkung und Müdigkeit bei Verkehrsunfällen: Nationale und internationale Statistiken,* Kuratorium für Verkehrssicherheit 2008.

Lagarias and Reeds, 1996: Jeffrey C. Lagarias and James A. Reeds 1996 *Convergence Properties of the Nelder-Mead Simplex Method in Low Dimensions,* SIAM Journal of Optimization, Volume: 9: pp. 112–147.

Lal and Craig, 2002: Sarkoj K. L. Lal and Ashley Craig 2002 *Driver fatigue: Electroencephalography and psychological assessment,* Psychophysiology, Volume: 39: pp. 313–321.

Lenne et al., 1998: Michael G. Lenne, Thomas J. Triggs and Jennifer R. Redman 1998 *Interactive Effects of Sleep Deprivation, Time of Day and Driving Experience on a Driving Task,* Sleep, Volume: 21(1): pp. 38–44.

Leveau, 1903: Gustave-Désiré Leveau 1903, Patent number: (FR 331926) *Bretelles protectrices pour voitures automobiles et autres.*

Liu, 2005: Chang Liu 2005 *Foundations of MEMS,* Illinois ECE Series.

Liu et al., 2009: Charles C. Liu, Simon G. Hosking and Michael G. Lenne 2009 *Predicting driver drowsiness using vehicle measures: Recent insights and future challenges,* Journal of Safety Research, Volume: 40: pp. 239–245.

Löfgren, 2007: Pär Löfgren 2007 *Identification of Driver Unawareness based on User Interaction,* Master's thesis, Institutionen för Systemteknik, Department of Electrical Engineering.

Lundquist and Schön, 2010: Christian Lundquist and Thomas B. Schön 2010 *Joint Ego-Motion and Road Geometry Estimation,* Information Fusion, Pages: 253–263.

LVGB, 2009: LVGB 2009 *UTM - Abbildung und UTM - Koordinaten,* Landesamt für Vermessung und Geoinformation Bayern.

Lyznicki et al., 1998: J. M. Lyznicki, T. C. Doege, R. M. Davis and M. A Williams 1998 *Sleepiness, driving and motor vehicle crashes,* JAMA: Journal of the American Medical Association, Volume: 279 (23): pp. 1908–1913.

Mahler, 2005: Michael Norbert Mahler 2005 *Radar-basierte Sensorkonzepte für den Kfz-Innenraum,* Cuvillier Verlag Göttingen.

Mammarand et al., 2006: **Saïd Mammarand, Sébastien Glaser and Mariana Netto** 2006 *Time to Line Crossing for Lane Departure Avoidance: A Theoretical Study and an Experimental Setting,* IEEE Transactions on Intelligent Transportation Systems, Volume: 7 No. 2, June: pp. 226–241.

Mara, 1999: **Joy Mara** 1999 *Drowsy Driving and Automobile Crashes,* National Highway Traffic Safety Administration (NHTSC).

Martin, 2006: **Elly Martin** 2006 *Breakthrough Research on Real-World Driver Behavior Released,* National Highway Traffic Safety Administration

MathWorks, 2007: **MathWorks** 2007 *MATLAB Documentation Center - Version 7.5.0.342 (R2007b),* The MathWorks Inc. Natick, Massachusetts.

Mattsson, 2007: **Kristina Mattsson** 2007 *In-vehicle prediction of truck driver sleepiness: lane position variables,* Master's thesis, Lulea University of Technology.

Mercedes-Benz MBRSA, 2013: **Mercedes-Benz MBRSA** 2013 *S-Class Sedan Attention Assist Manual.*

Mercedes-Benz, 2012: **Mercedes-Benz** 2012 *Techcenter Kneebag,*
http://m.mercedes-benz.de/techcenter/kneebag/detail.html
(last visited: May 11, 2020).

Mercedes-Benz, 2008: **E. Philips Mercedes-Benz** 2008 *Mercedes-Benz To Introduce Attention Assist Into Series Production In Spring 2009 .*

Mercedes-Benz USA, 2012: **Mercedes-Benz USA** 2012 *mbrace*
http://www.mbusa.com/mercedes/mbrace
(last visited: May 11, 2020).

Mets et al., 2011: **Monique A. J. Mets, Sander Ketzer and Camilla Blom** 2011 *Positive effects of Red Bull(R) Energy Drink on driving performance during prolonged driving,* Psychopharmacology, Volume: 214: pp. 737–745.

Miksch, 2010: **Michael Miksch** 2010 *Motion Compensation for Obstacle Detection based on Homography and Odometric Data with Virtual Camera Perspectives,* Proceedings of the IEEE Conference on Intelligent Vehicles Volume: 4: pp. 1152–1158.

Mitschke and Wallentowitz, 2004: **Manfred Mitschke and Henning Wallentowitz** 2004 *Dynamik der Kraftfahrzeuge,* Springer DE.

Mitsubishi, 2002: **Mitsubishi** 2012 *Driver's Attention Monitoring System MDAS*
http://www.jsae.or.jp/autotech/data_e/13-5e.html
(last visited: May 11, 2020).

Mitsubishi-Fuso, 2012: **Mitsubishi-Fuso** 2012 *Mitsubishi's Driver's Attention monitoring system (MDAS-III)*
https://www.mitsubishi-fuso.com/oa/en/press/121211/121211.html
(last visited: May 11, 2020).

Monk, 1991: **Timothy H. Monk** 1991 *Circadian aspects of subjective sleepiness: A behavioral messenger,* Sleep, sleepiness and performance, Pages: 39–63.

Moussa, 2009: **Wafik Moussa** 2009 *Designing a Driver Vigilance Monitoring Device: Application Driven Development of an FPGA Based Multiprocessor System,* LAP Lambert Academic Publishing.

Mukherjee and Robertson, 2015: **Sankha Subhra Mukherjee and Neil Robertson** 2015 *Deep Head Pose: Gaze-Direction Estimation in Multimodal Video,* IEEE Transactions on Multimedia, Volume: 17(11): pp. 2094–2107

Munzig, 2008: **Thorsten Munzig** 2008 *Positionserfassung mit PLCD-Sensoren - Berührungslose Weg- und Winkelemessung im Antriebsstrang und Chassis*
http://www.elektronikpraxis.vogel.de/hardwareentwicklung/articles/140953/
(last visited: May 11, 2020) last accessed: 27 November, 2012.

Nodine, 2008: **Emily Nodine** 2008 *The Detection of Drowsy Drivers Through Driver Performance Indicators,* PhD thesis TUFTS.

Nordbakke and Sagberg, 2007: **S. Nordbakke and F. Sagberg** 2007 *Sleepy at the wheel: Knowledge, symptoms and behaviour among car drivers,* Transportation Research Part F: Traffic Psychology and Behaviour, Volume: 10, Issue 1: pp. 1–10.

NOVA, 2002: **Australian Academy of Science NOVA** 2002 *Driver fatigue - an accident waiting to happen*.

NPC China, 2010: **National People's Congress NPC China** 2010 *Six years, the National Traffic Police sacrifice 435 thousand vehicles mortality decreased to 3.6*
http://npc.people.com.cn/GB/11474924.html
(last visited: May 11, 2020).

Oberman, 2006: **Lawrence Taylor and Steven Oberman** 2006 *Drunk driving defens,* Aspen Publishers.

Olabe, 2008: **Irati Markuerkiaga Olabe** 2008 *Driver-Fatigue Detection Based on Lane Data,* Master's thesis, University of Stuttgart, Chair of System Theory and Signal Processing.

onstar.com, 2013: **onstar.com** 2013 *mbrace*
https://www.onstar.com
(last visited: May 11, 2020).

Oord et al., 2016: **Aäron van den Oord, Sander Dieleman and Heiga Zen** 2016 *WaveNet: A Generative Model for Raw Audio*.

OpenStreetMaps.org, 2020: **OpenStreetMaps** *The Free Wiki World Map*
https://www.openstreetmap.org
(last visited: May 11, 2020).

Orfanidis, 1995: **J. Orfanidis** 1995 *Introduction to Signal Processing,* Prentice-Hall.

Oron-Gilad et al., 2007: **Tal Oron-Gilad, Adi Ronen and David Shinar** 2007 *Alertness maintaining tasks (AMTs) while driving,* Accident Analysis and Prevention, Volume: 3: pp. 851–860.

Pal and Chuang, 2008: **Nikhil R. Pal and Chien-Yao Chuang** 2008 *EEG-Based Subject- and Session-independent Drowsiness Detection: An Unsupervised Approach,* EURASIP Journal on Advances in Signal Processing, 519480:11.

Pander et al., 2008: **Tomasz Pander, Tomasz Przybyla and Robert Czabanski** 2008 *An Application of Detection Function for the Eye Blinking Detection,* HSI.

Pape, 2008: **Michael Pape** 2008 *Erkennung von Lenkereignissen anhand Fusion softer und adaptiver Schwellwertfunktionen und Fuzzy-Logik,* Master's thesis, Berufsakademie Stuttgart Horb.

ATP Papenburg, 2012: **ATP Papenburg**
http://www.atp-papenburg.de
(last visited: May 11, 2020).

Park et al., 2018: **Seonwook Park, Adrian Spurr and Otmar Hilliges** 2018 *Deep Pictorial Gaze Estimation*.

Parkhi et al., 2015: **Omkar M. Parkhi, Andrea Vedaldi and Andrew Zisserman** 2015 *Deep Face Recognition,* Pages: 41.1–41.12
https://dx.doi.org/10.5244/C.29.41
(last visited: May 11, 2020).

Patterson and Gibson, 2017: **Josh Patterson and Adam Gibson** 2017 *Deep Learning: A Practitioner's Approach,* O'Reilly, Beijing, ISBN 978-1-4919-1425-0.

Petit and Chaput, 1990: **Claire Petit and D. Chaput** 1990 *Research to prevent the driver from falling asleep behind the wheel,* Proceedings: Association for the Advancement of Automotive Medicine Annual Conference, Volume: 34: pp. 505–522.

Philip and Sagaspe, 2005: **Pierre Philip and Patricia Sagaspe** 2005 *Fatigue, Sleepiness and Performance in Simulated Versus Real Driving Conditions,* SLEEP, Volume: 28, No. 12: pp. 1511–1516.

Philip and Taillard, 2006: **Pierre Philip and J. Taillard** 2006 *The effects of coffee and napping on nighttime highway driving: a randomized trial,* Annals of Internal Medicine, Volume: 144 pp. (785-91):11.

Picot, 2010: **Antoine Picot** 2010 *Drowsiness detection based on visual signs: blinking analysis based on high frame rate video,* International Instrumentation and Measurement Technology Conference, Volume: 1:hal–00449307.

Pilutti and Ulsoy, 1999: **Tom Pilutti and A. Galip Ulsoy** 1999 *Identification of Driver State for Lane-Keeping Tasks,* IEEE Transactions on Systems, Man and Cybernetics - Part A. Systems and Humans 29(5):486.

Pilutti and Ulsoy, 1995: **Tom Pilutti and Galip Ulsoy** 1995 *On-Line Identification of Driver State for Lane-Keeping Tasks,* Proceedings of the American Control Conference Seattle, Washington June 1995.

Platt, 1962: **Fletcher N. Platt** 1966, Patent number: (3227998) *Automobile Driver Attention Indicator.*

Poh and McDuff, 2010: **Ming-Zher Poh and Daniel J. McDuff** 2010 *Non-contact, automated cardiac pulse measurements using video imaging and blind source separation,* OPTICS EXPRESS, Volume: 18, No. 10.

Pudil et al., 1994: **P. Pudil, F. J. Ferrii, J. Novovicova and J. Kittler** 1994a *Floating Search Methods for Feature Selection with Nonmonotonic Criterion Functions,* In Proceedings of the Twelveth International Conference on Pattern Recognition, IAPR. Conference B: Computer Vision & Image Processing, Volume: 2: pp. 279–283.

Pudil et al., 1994: **P. Pudil, J. Novovičová and J. Kittler** 1994b *Floating Search Methods for Feature Selection,* Pattern Recognition Letters 15(11):1119–1125
http://dx.doi.org/10.1016/0167-8655(94)90127-9
(last visited: May 11, 2020).

Reichert, 2008: **Andreas Reichert** 2008, Patent number: (DE 10 2007 001 362 A1) *Verfahren und Vorrichtung zur Fahrerermüdungserkennung mittels Drehmomentsensorik.*

Reyner and Horne, 2000: **Louise Reyner and James Horne** 2000 *Early morning driver sleepiness Effectiveness of 200 mg caffeine,* Psychophysiology, Volume: 37: pp. 251–256.

Reyner and Horne, 1998: **Louise A. Reyner and J. A. Horne** 1998 *Evaluation "in-car" countermeasures to sleepiness: cold air and radio,* Sleep, Volume: 21(1): pp. 46–50.

Reyner, 2005: **P. R. Barrett, J. A. Horne and Louise A. Reyner** 2005 *Early evening low alcohol intake also worsens sleepiness-related driving impairment,* Human psychopharmacology, Volume: 20(4): pp. 287–90.

Rieckmann, 2010: **Tanja Rieckmann** 2010 *Unfallschwerpunkt Autobahn: Rütteln für mehr Sicherheit*
http://www.spiegel.de/auto/aktuell/0,1518,722490,00.html
(last visited: May 11, 2020).

Riekert and Schunck, 1940: **P. Riekert and T. E. Schunck** 1940 *Zur Fahrmechanik des gummibereiften Kraftfahrzeugs,* Ingenieur-Archiv.

Ritter, 2007: **Hanno S. Ritter** 2007 *Volvo Driver Alert: Zeit für eine Pause*
http://www.autokiste.de/psg/archiv/a.htm?id=6679
(last visited: May 11, 2020).

Sagaspe et al., 2007: **Patricia Sagaspe, Jacques Taillard and Guillaume Chaumet** 2007 *Aging and Nocturnal Driving: Better with Coffee or a Nap? A Randomized Study,* Sleep, Volume: 30 (1808-1813): pp. 12.

Saul and Berger, 1991: **J. Saul and R. Berger** 1991 *Transfer function analysis of the circulation: unique insights into cardiovascular regulation,* American Journal of Physiology-Heart and Circulatory Physiology, Volume: 261(4):H1231–H1245.

Savitzky and Golay, 1964: **Abraham Savitzky and Marcel J. E. Golay** 1964 *Smoothing and Differentiation of Data by Simplified LS Procedure,* Anal. Chemistry, Volume: 36: pp. 1627.

Sayed, 2001: **R. Sayed and A. Eskandarian** 2001 *Unobtrusive drowsiness detection by neural network learning of driver steering,* Proceeding Institution of Mechanical Engineers, Volume: 215 D: pp. 969–975.

Schafer, 2011: **Ronald W. Schafer** 2011 *What is a Savitzky-Golay Filter?,* IEEE Signal Processing Magazine, Volume: July: pp. 111–117.

Schindler, 2007: **Erich Schindler** 2007 *Fahrdynamik - Grundlagen des Lenkverhaltens und ihre Anwendung für Fahrzeugreglersysteme,* TAE Expert Verlag
https://books.google.de/books?id=N4I8btNjDI4C
(last visited: May 11, 2020).

Schmidt, 2009: **Eike Schmidt** 2009 *Drivers Misjudgement Of Vigilance State During Prolonged Monotonous Daytime Driving,* Accident Analysis & Prevention, Volume: 41(5): pp. 1087–1093.

Schmidt, 2010: **Eike Schmidt** 2010 *Die objektive Erfassung von Muedigkeit waehrend monotoner Tagfahrten und deren verbale Selbsteinschaetzung durch den Fahrer,* PhD thesis Mathematisch-Naturwissenschaftliche Fakultät, Heinrich-Heine-Universität Düsseldorf.

Schmitz, 2004: **Carsten Helmut Schmitz** 2004 *Adaptiver Spurverlassenswarner mit Fahrerabsichts- und fahrerzustandsabhängiger Warnstrategie,* PhD thesis University Karlsruhe.

Schnabel, 2012: **Patrick Schnabel** 2012 *Elektronik Fibel Kompendium: MEMS - Micro-Electro-Mechanical Systems,*
http://www.elektronik-kompendium.de/sites/bau/1503041.htm
(last visited: May 11, 2020).

Schneider2006: **Kristina Schneider** 2006 *SPECTARIS: Müdigkeit ist Hauptursache für Verkehrsunfälle .*

Schramm and Hiller, 2014: **Dieter Schramm and Manfred Hiller** 2014 *Vehicle Dynamics,* Springer.

Scott, 2009: **Joanna Scott** 2009 *Coffee and Safer Driving,* Technical report International Coffee Organization.

SeeingMachines, 2007: **SeeingMachines** 2007 *Driver State Sensor - User Manual 2.0,* Seeing Machines.

Seko and et. al., 1986: **Yokohama Yasutoshi Seko and Takayuki Huruhiko Iizuka et. al.** 1986, Patent number: (4,611,199) *Alarm System and Method for Sensing a Stand-by State in a Driver Drowsiness Detection System.*

Sherry, 2000: **Patrick Sherry** 2000 *Fatigue Countermeasures in the Railroad Industry: Past and Current Developments,* PhD thesis Intermodal Transportation Institute, University of Denver.

Shi, 2015: **Xingjian Shi, Zhourong, Chen, Hao Wang, Dit-Yan Yeung, Wai-Kin Wong and Wang-chun Woo** 2015 *Convolutional LSTM Network: A Machine Learning Approach for Precipitation Nowcasting,* CoRR, DBLP Computer Science, Volume: abs/1506.04214.

Siegmund, 1996: **G. P. Siegmund, D. J. King and D. K. Mumford** 1996 *Correlation of Heavy-Truck Driver Fatique with Vehicle-Based Control Measures,* SAE Report 952594 ISSN 0148-7191.

Simon, 2012: **Michael Simon** 2012 *EEG measures as indicators of driver fatigue,* PhD thesis University of Ulm.

Simon and Schmidt, 2011: **Michael Simon and Eike A. Schmidt** 2011 *EEG alpha spindle measures as indicators of driver fatigue under real traffic conditions,* Clinical Neurophysiology, Volume: 112(6): pp. 1168–1178.

Sonnleitner, 2012: **Andreas Sonnleitner** 2012 *Die physiologische Erfassung des Fahrerzustandes: Der Einfluss von Unaufmerksamkeit des Fahrers auf EEG Parameter und Verhaltensdaten,* PhD thesis Heinrich-Heine Universität Düsseldorf.

Sonnleitner and Simon, 2012: **Andreas Sonnleitner and Michael Simon** 2012 *Alpha spindles as neurophysiological correlates indicating attentional shift in a simulated driving task,* International Journal of Psychophysiology, Volume: 83: pp. 110–118.

Stolzmann et al., 2002: **Wolfgang Stolzmann, Dietmar Neumerkel, Patrick Rammelt, Dirk Reichardt, and Axel Vogler** 2002 *Fahrermodelle - Ein Schlüssel für Unfallfreies Fahren?,* Kuenstliche Intelligenz, Volume: 03: pp. 34–36.

Svensson, 2004: **Ulrika Svensson** 2004 *Blinking Behaviour based drowsiness detection - method development and validation,* Master's thesis, Linköping University.

Tyco, 2010a: **Tyco MISCs TE** 2010 *Multi Coil Resolver*
https://www.te.com/usa-en/product-CAT-ATS0024.html
(last visited: May 11, 2020).

Tyco, 2010b: **Tyco MISCs TE** 2010 *Steering Position Sensor for Driver Attention Assistance*
http://www.te.com/aboutus/news/prodinnov.aspx?id=1841
(last visited: May 11, 2020)

Teofilov, 2009: **Angel Teofilov** 2009 *Kamerabasierte Müdigkeits- und Ablenkungserkennung,* Technical report University of Stuttgart.

Thiffault and Bergeron, 2003: **Pierre Thiffault and Jacques Bergeron** 2003 *Monotony of road environment and driver fatigue: A simulator study,* Accident Analysis and Prevention, Volume: 35(3): pp. 381–391.

Thorslund, 2003: **Birgitta Thorslund** 2003 *Electrooculogram Analysis and Development of a System for Defining Stages of Drowsiness,* Master's thesis, Linköping University.

Tietze and Hargutt, 2001: **Heiko Tietze and Volker Hargutt** 2001 *Zweidimensionale Analyse zur Beurteilung des Verlaufs von Ermüdung,* Technical report Interdisziplinäres Zentrum für Verkehrswissenschaften an der Universität Würzburg.

Tijerina et al., 1998: **Louis Tijerina, Walter W. Wierwille, Michael J. Goodman, S. Johnston, D. Stoltzfus and M. Gleckler** 1998 *A Preliminary Assessment of Algorithms for Drowsy and Inattentive Driver Detection on the Road,* Technical report U.S. Department of Transportation, National Highway Safety Administration.

TRUEcar, 2010: **TRUEcar** 2010 *Spotlight on Safety: Drowsy Driving Just as Risky as Drunk Driving*
http://blog.truecar.com/2010/12/22/spotlight-on-safety-drowsy-driving-just-as-risky-as-drunk-driving
(last visited: May 11, 2020).

Ueno et al., 1994: **Hiroshi Ueno, Masayuki Kaneda and Masataki Tsukino** 1994 *Development of drowsiness detection system,* Vehicle Navigation and Information Systems Conference, Proceedings.

Uhlich, 2006: **Stefan Uhlich** 2006 *Emotion recognition of speech signals,* Master's thesis, University of Stuttgart, Chair of System Theory and Signal Processing.

van Wees et al., 2004: **Kiliaan van Wees, Karel Brookhuis and D. De Waard** 2004 *Recommendations to Authorities and the Industry,* 2004 Awake EU Project.

Vector, 2012: **Vector** 2012 *CANape 11.0 Measuring, Calibrating, Diagnosing and Flashing ECUs,*
http://www.vector.com/vi_canape_de.html
(last visited: May 11, 2020).

Volvo Cars, 2007a: **Volvo Cars** 2007 *Blind Spot Information System BLIS*
http://www.volvocars.com/de/sales-services/service/specialsales/Pages/techniklexikon-b.aspx
(last visited: May 11, 2020).

Volvo Cars, 2007b: **Volvo Cars** 2007 *Volvo Cars introduces new systems for alerting tired and distracted drivers*
https://www.media.volvocars.com/at/de-at/media/photos/204608/blind-spot-information-blis-mit-lenkassistent
(last visited: May 11, 2020).

Volvo Cars, 2012: **Volvo Cars** 2012 *Driver Alert*
https://www.volvocars.com/de/support/manuals/s60/2019/fahrerunterstutzung/driver-alert-control/driver-alert-control
(last visited: May 11, 2020).

von Jan et al., 2010: **T. von Jan, T. Karnahl, K. Seifert, J. Hilgenstock and R. Zobel** 2005 *Don't sleep and drive - VW's fatigue detection technology,* National Highway Traffic Safety Administration (NHTSA) ESV 19
http://www-nrd.nhtsa.dot.gov/pdf/esv/esv19/Other/Print%2007.pdf
(last visited: May 11, 2020).

Wagoner, 2008: **Rick Wagoner** 2008 *CES 2008: Wagoner expected to announce driverless cars within a decade,* CNN Money/Autos
http://www.autoblog.com/2008/01/07/ces-2008-wagoner-expected-to-announce-driverless-cars-within-a/
(last visited: May 11, 2020).

Wang and Knipling, 1996: **J. S. Wang and R. R. Knipling** 1996 *The role of driver inattention in crashes: New statistics from the 1995 Crashworthiness Data System,* 40th An. Proc. Assoc. for the Adv. of Automotive Med. Volume: IA: pp. 377–392.

Wang et al., 2016: Xingyou Wang, Weijie Jiang and Zhiyong Luo 2016 *Combination of Convolutional and Recurrent Neural Network for Sentiment Analysis of Short Texts,* Proceedings of COLING 2016, the 26th International Conference on Computational Linguistics: Technical Papers, Osaka, Japan, Volume: 16: pp. 2428–2437.

Weiss, 2011: Thorsten-Tobias Weiss 2011 *Hochgenaue Positionierung und Kartographie mit Laserscannern für Fahrerassistenzsysteme,* PhD thesis University of Ulm.

Welch and Bishop, 2006: Greg Welch and Gary Bishop 2006 *An Introduction to the Kalman Filter,* University of North Carolina at Chapel Hill, Department of Computer Science.

Welling, 2005: Max Welling 2005 *Fisher Linear Discriminant Analysis,* Technical report University of Toronto, Department of Computer Science.

Wierwille, 1996a: Walter W. Wierwille 1996 *Research of vehicle-based driver Status/Performance monitoring - Part I,* Technical report.

Wierwille, 1996b: Walter W. Wierwille 1996 *Research of vehicle-based driver Status/Performance monitoring - Part III,* Technical report.

Wierwille and Ellsworth 1994: Walter W. Wierwille and Lynne A. Ellsworth 1994 *Research on Vehicle-Based Driver Status/Performance Monitoring; Development, Validation and Refinement of Algorithms For Detection of Driver Drowsiness,* Technical report U.S. Department of Transportation National Highway Traffic Safety Administratlon.

Wierwille et al. 1996: Walter W. Wierwille, Rollin J. Fairbanks, I. Mark G. Lewin and L. Mark G. Lewin 1996 *Research of vehicle-based driver Status/Performance monitoring - Part II,* Technical report.

Wigh, 2007: Frederik Wigh 2007 *Detection of Driver Unawareness Based on Long- and Short-Therm Analysis of Driver Lane Keeping,* Master's thesis, Linköpings Universitet.

Yang, 2011: Bin Yang 2011 *Digital Signal Processing,* University of Stuttgart, Chair of System Theory and Signal Processing.

Yang, 2013: Bin Yang and Stefan Uhlich 2013 *Pattern Recognition and Detection,* University of Stuttgart, Chair of System Theory and Signal Processing.

Yang, 2018: Bin Yang 2018 *Lectur Detection and Pattern Recognition,* University of Stuttgart, Institute of Signal Processing and System Theory.

Yeo, 2009: Mervyn V. M. Yeo, Xiaoping Li, Kaiquan Shen and Einar P. V. Wilder-Smith 2009 *Can SVM be used for automatic EEG detection of drowsiness during car driving?,* Safety Science, Volume: 47: pp. 115–124.

Zomotor, 1987: Adam Zomotor and Walter Klinkner 1987 *Fahrwerktechnik: Fahrverhalten,* Vogel Buchverlag, Würzburg.

Zulley, 1995: Jürgen Zulley 1995 *Chronobiologie, Bedeutung der biologischen Rhythmen,* Weißbuch Schlafmedizin, Pages: 41–43.

Zulley, 2006: Jürgen Zulley 2006 *Der Schlaf: Notwendig oder Zeitverschwendung,* University of Regensburg.

Index